Boundary-layer Flows in non-Newtonian Fluids

Paul Peter Dabrowski

B.Ed, B.AppSc, B.Sc(Hons) (Adel.)

Thesis submitted for the Degree of
Doctor of Philosophy
in
Applied Mathematics
at
The University of Adelaide
(School of Mathematical Sciences)

June 2009

Contents

List of Figures

List of Tables

Abstract

We examine the boundary-layer flow of generalised Newtonian fluids. A specific member of this class of non-Newtonian fluids, namely the Ostwald-de Waele or power-law fluid, is studied in some detail. We show, through the numerical solution of the governing equations, that this empirical model of fluids encountered in physical and industrial situations is of limited benefit when considering the boundary-layer flow of such a fluid. We then develop and employ a Carreau viscosity model in the same context and show that the numerical marching scheme has better convergence behaviour than was the case for power-law fluids. We also investigate the boundary-layer flow of a Newtonian fluid over a thin film of non-Newtonian fluid, described by a Carreau fluid model, by focusing specifically on similarity-type solutions.

Signed Declaration

This work contains no material which has been accepted for the award of any other degree or diploma in any university or other tertiary institution to Paul Peter Dabrowski and, to the best of my knowledge and belief, contains no material previously published or written by another person, except where due reference has been made in the text.

I give consent to this copy of my thesis, when deposited in the University Library, being made available for loan and photocopying, subject to the provisions of the Copyright Act 1968.

I also give permission for the digital version of my thesis to be made available on the web, via the University's digital research repository, the Library catalogue, the Australasian Digital Thesis Program (ADTP) and also through web search engines, unless permission has been granted by the University to restrict access for a period of time.

SIGNED: ....
DATE : ....

Acknowledgments

I would like to express my appreciation and thanks to all those who provided me with help and encouragement throughout my candidature.

To Associate Professor Jim Denier, of the School of Mathematical Sciences at the University of Adelaide, for providing objective and constructive guidance, demanding a high standard of research and encouraging a broad base of learning beyond the narrow scope of the research problem.

To the School of Mathematical Sciences at the University of Adelaide for providing me with the facilities and the resources necessary to undertake the work, an environment of academic excellence and the opportunity to meet researchers of international standing.

To my wife Elisabeth and daughters Chantelle and Grace, I would like to express my deepest thanks for their support and encouragement over the long period that it took me to complete this work. On numerous occasions when I questioned my resolve to continue with this undertaking, I found that their unflagging belief, along with occasional strong words of motivation, helped lift my failing spirits. For that I am eternally grateful.

To my many work colleagues and friends whose curiosity and interest in what I was pursuing was also a source of motivation.

List of Publications

Publications in Refereed Journals

1. Denier, J. P. & **Dabrowski, P. P.** 2004 On the boundary-layer equations for power-law fluids. *Proc. R. Soc. Lond. A* **460**, 3143–3158.

Publications in Refereed Conference Proceedings

- **P.P. Dabrowski** and J.P. Denier, *Blowing-induced boundary-layer separation of shear-thinning fluids*
  14th Australasian Fluid Mechanics Conference (14AFMC), December 10–14, 2001, University of Adelaide, Australia.

Abstracts in Conference Proceedings

- **P P. Dabrowski** and J P. Denier, *Separation of non-Newtonian boundary layer flows*
  The 37th Applied Mathematics Conference (ANZIAM 2001), February 3–7, 2001, Barossa Valley, South Australia.

Chapter 1

Introduction

Water and air, the most important fluids for life, are Newtonian fluids. The everyday familiarity that we have with water and air has caused us to regard the flow of Newtonian fluids as normal. Newtonian fluid flows have been studied extensively and the behaviours of the many different flow regimes are quite well understood. However, there are many fluids of importance in nature and technology that do not behave like a Newtonian fluid. Various aspects of the flow behaviour of these non-Newtonian fluids are markedly different from the flow of Newtonian fluids and, when seen for the first time, appear abnormal or even paradoxical. Walker (1978) describes some experiments, easily performed by a layperson, that show clearly and strikingly some of the unusual behaviours of non-Newtonian fluid flow.

The amount of apparent effort devoted to the study of the flow of Newtonian fluids, as evidenced by the number of past and present publications, should not suggest that research of non-Newtonian fluids has languished. There has been an immense amount of study performed on non-Newtonian fluids in a number of areas. Some of the topics covered in the literature are: agitation and mixing, boundary-layer theory, entrance effects, fibre spinning, instability, mould filling, pressure dependence of viscosity, turbulent flow, and withdrawal of plates from fluids.

There are many different characteristics that affect the behaviour of a fluid and that may also be used to provide a categorisation of all these fluids. Of primary importance in determining the flow behaviour of a fluid is the viscosity. On the basis of viscosity, fluids can be roughly subdivided into Newtonian and non-Newtonian. For Newtonian fluids the viscosity is taken to be constant over some range of shear rate (though it may vary slightly with temperature and pressure). For non-Newtonian fluids the viscosity varies with the shear rate and may be dependent on the shear rate itself. There are many viscosity models, or constitutive relations, to choose from and they vary in their complexity. A good overview of some of the more widely used viscosity models can be found in Barnes et al. (1989) or Bird et al. (1977).

1.1 Previous Research

The idea of boundary layers within the flow of real fluids was introduced by Ludwig Prandtl in 1904. Since then boundary-layer theory has been developed to a sophisticated level and it has enjoyed success in providing a better understanding of many flow phenomena. Many texts in the area of fluid dynamics also address the elements of boundary-layer theory; a comprehensive treatment is to be found in Rosenhead (1963) and Schlichting (1979).

The application of boundary-layer theory to an Ostwald-de Waele, or power-law[1], fluid was first described by Schowalter (1960) and Acrivos et al. (1960), where it was shown that self-similar solutions exist for the boundary-layer flow of a power-law fluid when the flow is of the Falkner-Skan type. Specifically, Schowalter (1960) examined the boundary-layer equations of a power-law fluid in the absence of body forces and showed the existence of self-similar solutions when the external velocity $U_e(x)$ is of the form x^m, where x is the distance along the surface of the body. Acrivos et al. (1960) considered the boundary-layer flow of a power-law fluid for the case $m = 0$, which corresponds to flow along a flat plate.

Lee and Ames (1966) describe the derivation of similarity transformations for the boundary-layer flow of power-law and Eyring[2] viscous fluids using group theoretic methods. The similar differential equations for a number of different flow systems are presented. Self-similar solutions

---

[1] A power-law fluid has a non-constant viscosity described by $\mu = K\left|\dot{\gamma}\right|^{n-1}$, where K is the consistency of the fluid, n is the fluid index and $\dot{\gamma}$ is the rate-of-deformation.

[2] The Eyring model is expressed in terms of three independent fluid properties: the zero-shear-rate viscosity, the elastic shear modulus and a reference stress.

for the flow of a power-law fluid in a number of flow systems are discussed.

Thompson and Snyder (1968) examined the boundary-layer flow of a power-law fluid in the presence of fluid injection at the surface with the aim of determining the drag reduction potential of such non-Newtonian fluids. The governing equations are formulated so as to yield similarity solutions, which are admissible when the injection velocity varies with longitudinal distance along the flat plate as $x^{-n/n+1}$, where n is the fluid index and x the distance along the plate from the leading edge. Solutions were found for a range of mass injection rates, the results indicate that the skin-friction coefficient decreases monotonically as the fluid index increases. For a fixed rate of fluid injection it is shown that the percentage reduction in the skin-friction coefficient is greater for smaller values of the fluid index. Results for the variation of displacement thickness and momentum thickness for various rates of fluid injection and fluid index value are also briefly presented.

Nachman and Taliaferro (1979) describe the steady boundary-layer flow of a power-law fluid over a permeable, semi-infinite flat plate in the special case of similarity preserving mass transfer. They employ Crocco variables (see Young (1989)) to express the non-linear parabolic partial differential equation governing the flow as a non-linear singular two point boundary value problem for a shear function. It is deduced that the initial condition for the shear function becomes infinite for fluid index values less than 1/2. This result indicates that the shear stress along the plate cannot be reduced to zero with any finite injection rate for these fluids. This result arises from the use of the Crocco formulation and would not be available from an analysis of the corresponding Blasius-like equation. Nachman and Callegari (1980) considered the boundary-layer flow of a pseudoplastic (shear-thinning) power-law fluid. Use is made of Crocco variables to express the governing equation in a form that resembles the generalised Emden-Fowler equation (see Bellman (1953)). They establish the existence of a power series representation for the solution of the Emden-Fowler equation.

Andersson and Toften (1989) discuss aspects of obtaining a numerical solution to the laminar boundary-layer equations for a power-law fluid. They provide a concise review of various techniques for finding solutions for laminar boundary-layer flow of power-law fluids and some shortcomings of these techniques. The system of partial differential equations for a power-law fluid is transformed into a non-linear third order ordinary differential equation. This equation is then solved using the Keller Box scheme where the resemblance between the turbulent eddy viscosity and the effective viscosity of the non-Newtonian fluid has been taken into account. The momentum equation is linearised using the standard incomplete linearisation and an alternative full scheme. It is suggested that the solution method presented is applicable to other inelastic 'generalised Newtonian fluids'. Application of the full linearisation method is more involved, whereas the incomplete linearisation method is more straightforward and provides noticeable computational savings, except for self-similar boundary layers of some pseudoplastic fluids. The main outcome of the investigation is that the Keller Box scheme can be used to solve boundary-layer flow problems for non-Newtonian fluids rather than establishing the correctness of the power-law viscosity model.

Both an experimental and numerical investigation into the effects of Reynolds number, along with other characteristics, on the drag and lift of a flat plate in the flow of shear-thinning power-law fluids is discussed by Wu and Thompson (1996). Predicted lift and drag coefficients from simulations with a FEM code were found to be in good agreement with the experimental results obtained using a force balance. The drag experienced by a fluid flowing along a surface is associated with the development of a boundary layer. The accuracy of the boundary-layer assumptions at lower Reynolds numbers is often questioned. Their work provides minimum Reynolds number values that are a function of the shear-thinning fluid index and below which the boundary-layer approximation may be considered inadequate. This outcome is of particular relevance to the investigations being undertaken in this study as it lends credence to our use of the boundary-layer approximation for the high Reynolds number flows that are of interest to us.

As far as the boundary-layer flow of a two fluid system involving non-Newtonian fluids is concerned, an early investigation of such problems is that described by Thompson and Snyder (1969). They consider the boundary-layer flow of a Newtonian fluid along a flat plate through which a non-Newtonian fluid (a power-law fluid) is being injected. A similarity transformation is applied to the pair of governing partial differential equations to yield a coupled pair of ordinary differential equations. The approach employed is closer to the concept of local similarity rather than being self-similar in the strictest sense. Suitable boundary and interfacial conditions are also derived. A shooting method is used to solve this set of equations. The results obtained indicate that the lower non-Newtonian region of the boundary layer increases in thickness as the mass injection rate increases while the fluid index is kept constant. With the mass injection held constant and increasing the fluid index, it was found that the lower region becomes thinner. The outer Newtonian region became thinner for both cases.

Two-fluid systems, along with the boundary-layer approximation, have been used to model the behaviour of de/anti-icing fluid on aircraft wings. Özgen (1995) and Özgen et al. (1998) describe a two-fluid system where the lower de/anti-icing fluid is modelled by a power-law fluid with a Newtonian fluid representing air flowing over a surface. The pair of partial differential equations are used to obtained the corresponding Orr-Sommerfeld equations so as to investigate the stability properties of the two-fluid system. Though our investigations are not directed at the issue of hydrodynamic stability of such flow systems, we note that a linear velocity profile is used for the lower fluid in the analysis performed by Özgen (1995) and Özgen et al. (1998).

Timoshin (1997) considered the stability of the boundary-layer flow of a Newtonian fluid over a thin film composed of a different fluid. However, the lower fluid is not explicitly identified as being non-Newtonian in character. The analysis performed on this two-fluid system made use of triple-deck theory. We note again that the velocity profile in the lower thin film is assumed to be linear. Nonetheless, this work provides some insights into the instability mechanisms that operate in two-fluid flow systems and the approach used could be employed to undertake a similar study involving a non-Newtonian fluid in the thin film.

1.2 Motivation

Water and air, being the fluids most frequently encountered in everyday life, are examples of Newtonian fluids. However, there are many other fluids that are less frequently noticed on, say, a daily basis, but are commonly encountered both in nature and industry, that are classified as non-Newtonian fluids. It would therefore be natural to investigate the flow behaviour of non-Newtonian fluids. A considerable amount of effort has been directed to the study of non-Newtonian fluids. This effort has been in both the experimental and mathematical/physical modelling domains. A major portion of these studies have been directed toward gaining a better understanding of the bulk flow of various non-Newtonian fluids. The study of the behaviour of the boundary-layer flow of non-Newtonian fluids has not been undertaken as extensively and has often been performed on relatively 'simple' non-Newtonian fluids. These studies have employed the concept of self-similarity which provides some valuable insights into the behaviour of the boundary layer. The use of other approaches based on numerical schemes may, however, unveil other aspects of the boundary-layer flow of a non-Newtonian fluid.

Our initial interest was in the boundary-layer flow of a non-Newtonian fluid in the presence of mass transfer through a surface. Catherall et al. (1965) presents a similar analysis of the boundary-layer flow of a Newtonian fluid with injection through a flat plate. That study was particularly concerned with the structure of the boundary-layer when detachment was deemed to be occurring. Consequently, an additional interest for us was whether detachment of the boundary-layer occurs in the flow of non-Newtonian fluids and how the location of the point of detachment was affected by some of the fluid's properties. Since there are a large number of different type of non-Newtonian fluids, it would not be convenient or possible to examine all of them. Hence, a fluid that is frequently encountered in natural and industrial setting, as well as being amenable to mathematical treatment, will be selected as a prototypal non-Newtonian fluid.

There has also been considerable interest and research activity in the area of boundary-layer control using mechanisms such as fluid injection or suction through the surface. Gaining a better understanding of the boundary-layer flow of a non-Newtonian fluid in the presence of mass transfer through the surface will provide insights into methods that will allow better control of such flow situations.

Non-Newtonian fluids are also found in two-fluid systems, where a non-Newtonian thin film acts as a lubricating layer over which a Newtonian fluid may be flowing. Such a model has been, and continues to be, used to model the flow of air over an aircraft coated with an anti/de-icing solution. The study of the boundary layer within such two-fluid systems will enhance our current understanding of the behaviour of these flows.

1.3 Goals of this Work

The intent of this work is to provide a better understanding of the structure of two-dimensional boundary-layer flows of generalised[3] Newtonian fluids. Such an understanding is a prerequisite for the prediction and control of the mechanism of boundary-layer separation in flows involving fluids of this type. We start this investigation of the boundary-layer flow of generalised Newtonian fluids by considering those fluids that are described by one of the simplest viscosity models, viz. the Ostwald-de Waele, or power-law, fluids. The description of generalised Newtonian fluids and the derivation of the governing equations for the boundary-layer flow of a power-law fluid are presented in Chapter 2.

As the system of partial differential equations governing the boundary-layer flow of a generalised Newtonian fluid is non-linear, a numerical scheme needs to be used to find solutions. A suitable numerical scheme has been developed for solving the governing equations for a power-law fluid and is described in Chapter 3. This numerical scheme is used to investigate the development of the boundary-layer flow in the presence of mass transfer (fluid injection) through the surface. The investigations presented in Chapter 3 are directed by the following questions: Does the numerical scheme required to solve the governing equations for an Ostwald-de Waele model fluid apply over the full range of values that the underlying parameter(s) can take? In the presence of fluid injection through the surface, does the boundary layer eventually separate? If so, what effect does the fluid index have on the location of the point of separation? What effect does the form of the external flow have on the tendency of the boundary layer to separate in the presence of mass transfer through the surface?

---

[3] This term is used to describe the class of fluids where the form of the relationship between the stress and rate-of-deformation is the same as for Newtonian fluids, while the viscosity is non-constant and is a function of the rate-of-deformation.

In Chapter 4 we consider whether similarity-type solutions that exist can provide any insights into the nature of the boundary layer of a power-law fluid that were not provided by the numerical solutions. Firstly, the ordinary differential equation from which self-similar solutions are obtained is derived and some aspects of the numerical techniques for solving it are discussed. Next, a far-field asymptotic analysis of the Blasius-like differential equation is carried out for the purpose of checking the validity of the numerically obtained solutions. The investigations presented in this chapter are guided by the following questions: To what extent does the fluid index affect both the nature and number of similarity-type solutions of the Blasius-like (or Falkner-Skan-like) non-linear ordinary differential equation? What is the asymptotic form of the self-similarity solutions in the far-field and how do these solutions match onto the free-stream?

The Ostwald-de Waele model for viscosity is relatively simple, though quite extensively employed, but may be of limited usefulness in some situations. An alternative model for viscosity, the Carreau model, is presented in Chapter 5. The Carreau viscosity model is briefly described and the system of partial differential equations governing the boundary-layer flow is derived. We show that a self-similar solution exists for a specific external flow. A numerical scheme for obtaining a solution to these equations is developed and used to investigate the development of the boundary-layer flow. Finally we discuss the existence and structure of the flow far down-stream in the boundary layer of a Carreau fluid. This chapter is guided by the following questions: What is the form of the system of equations governing the boundary-layer flow of a Carreau fluid? Is a family of self-similar solutions available? Does the numerical scheme required to solve the governing equation for a Carreau fluid apply over the full range of values that the underlying model parameter(s) can take? Does the velocity profile within the boundary-layer flow of a Carreau fluid converge to an asymptotic, or limiting, form at a large distance down-stream from the leading edge of a flat plate?

Flows involving two fluids present many interesting mathematical issues, as well as being important from a practical viewpoint in various industrial and technological settings. The boundary-layer flow of a Newtonian fluid along a thin film of non-Newtonian fluid over a flat plate, with fluid being injected into the thin film, is examined in Chapter 6. The coupled system of partial differential equations is derived along with the appropriate boundary and interfacial conditions. Self-similar velocity profiles are obtained from the numerical solution of the corresponding pair of coupled ordinary differential equations. A small injection velocity analysis is carried out to determine the form of the velocity profile in the thin film when the fluid injection rate is very low. The investigations presented in this chapter are guided by the following questions: What form the kinematic and dynamic conditions at the material interface between the two fluids take? How is the self-similar velocity profile, particularly the location of the fluid interface, affected by changes of the parameters in the viscosity model for the fluid in the thin film? How is the self-similar velocity profile, particularly the location of the fluid interface, affected by the rate of fluid injection into the thin film? What is the form of the velocity profile in the thin film when the fluid injection velocity is very small?

Lastly, in Chapter 7 some further directions that may be pursued as a result of this research are discussed briefly.

Chapter 2

Derivation of the Governing Equations

There are many different phenomena that can be encountered while studying the flow of various fluids. Not only is there diversity in the phenomena themselves, but there is considerable diversity in the structure of the fluids being investigated. The structure of a fluid may be described from a continuum or a molecular viewpoint. There exist a number of theories of varying degrees of generalisation that are capable of describing most of the phenomena likely to be seen.

The physical geometry along which the fluid flow occurs, as well as the accompanying boundary conditions, play the most important role in determining how a fluid flow develops. Various physical properties of the fluid also influence the nature of the fluid flow. The viscosity is a fundamental property of a fluid that accounts for a wide variety of the flow phenomena that occur. The fluid viscosity is known to be temperature and pressure dependent, however, for the majority of everyday flows taking place under so-called ‘standard’ temperature and pressure conditions, there is only a negligible effect on the viscosity that is due to variations in these physical quantities. This does not necessarily mean that the viscosity of the fluids involved in such flows remains constant. For some fluids the viscosity exhibits a dependence on the shear rate that is applied to the fluid.

The shear rate dependence of the viscosity can be described by the generalised Newtonian model. In this model there are several empiricisms for specifying the non-Newtonian viscosity.

The *Ostwald-de Waele* or 'power-law' model for the non-Newtonian viscosity is one such empiricism that will be investigated in detail here. The flow being considered here is presumed to be isothermal, hence energy equations do not appear in subsequent discussions. However, it is noted that many important industrial processes are non-isothermal in practice.

The specific aspects of the viscosity model used to describe the nature of a fluid are contained in an appropriate constitutive relation for the fluid. The constitutive relations for non-Newtonian fluids possess varying degrees of complexity. A description of how non-Newtonian fluids can be categorised is given in Barnes et al. (1989). Considerable effort continues to be directed to the study of constitutive relations. Some constitutive relations arise from empirically derived observations, while others are obtained from physical and theoretical considerations.

In this chapter the governing equations for the boundary-layer flow of a non-Newtonian fluid described by the power-law model are derived. In Section 2.1 the class of fluids known as Generalised Newtonian fluids are discussed. There the power-law fluid model is also briefly described. The boundary-layer equations for such a fluid are derived from the Cauchy equations of motion.

2.1 The Generalised Newtonian Fluid

In many industrial processes it is observed that the viscosity of a fluid changes with the shear rate, i.e. the viscosity is non-Newtonian. A change in viscosity by two or three orders of magnitude for some fluids is possible. A large variation in viscosity such as this cannot be ignored when flow problems involving lubrication and polymer processing, to mention only two, are investigated. Hence, one of the first empirically derived modifications to Newton's law of viscosity was to allow the viscosity to vary with shear rate (or with shear stress). This class of fluids is commonly referred to as *generalised Newtonian fluids* and is described in Bird et al. (1977).

The constitutive relation for a Newtonian fluid in a simple flow with velocity $\boldsymbol{u} = (u(y), 0, 0)$

is given by

$$\tau_{yx} = -\mu \frac{\mathrm{d}u}{\mathrm{d}y},$$

where τ is the shear stress and the parameter μ, the viscosity of the fluid, is dependent on the local fluid properties such as temperature, pressure and material composition. The viscosity of a Newtonian fluid is assumed to be constant. This simple constitutive relation describes common fluids such as air and water.

For a generalised Newtonian fluid in the same simple flow, the constitutive relation is given by

$$\tau_{yx} = -\eta \frac{\mathrm{d}u}{\mathrm{d}y}.$$

Here we follow the convention used in the rheological literature of representing the non-Newtonian viscosity of the fluid by η, which is a function of $|\mathrm{d}u/\mathrm{d}y|$ (or$|\tau_{yx}|$). Occasionally we will make use of μ when referring to the non-Newtonian viscosity, such a change of notation will be indicated as needed. The change in viscosity is expected to depend on the magnitude rather than the sign of the shear rate (or shear stress), hence the use of the absolute value signs in the above expressions. Various empirical relations can be tried for the function η so as to fit non-Newtonian viscosity curves obtained from experiments or other measurements.

The constitutive relations given above can be readily extended to any arbitrary flow field $\boldsymbol{v} = \boldsymbol{v}(x, y, z, t)$. For an incompressible Newtonian fluid the constitutive relation is

$$\boldsymbol{\tau} = -\mu \dot{\boldsymbol{\gamma}},$$

in which $\dot{\boldsymbol{\gamma}}$ is the rate-of-deformation tensor $\boldsymbol{\nabla v} + (\boldsymbol{\nabla v})^T$. For a generalised Newtonian fluid the constitutive relation is

$$\boldsymbol{\tau} = -\eta \dot{\boldsymbol{\gamma}}, \tag{2.1}$$

where the non-Newtonian viscosity η, a scalar, is a function of $\dot{\boldsymbol{\gamma}}$ (or $\boldsymbol{\tau}$) as well as of temperature and pressure. For η to be a scalar function of the tensor $\dot{\boldsymbol{\gamma}}$, it must be a function of the 'invariants' of $\dot{\boldsymbol{\gamma}}$. The invariants of a tensor are those combinations of the components of $\dot{\boldsymbol{\gamma}}$ that transform as scalars under a rotation of the co-ordinate system. Three invariants are defined by selecting the following independent tensor component combinations:

$$\begin{aligned}
I_1 &= \sum\nolimits_i \dot{\gamma}_{ii}, \\
I_2 &= \sum\nolimits_i \sum\nolimits_j \dot{\gamma}_{ij}\dot{\gamma}_{ji}, \\
I_3 &= \sum\nolimits_i \sum\nolimits_j \sum\nolimits_k \dot{\gamma}_{ij}\dot{\gamma}_{jk}\dot{\gamma}_{ki}.
\end{aligned}$$

The first invariant I_1 can be expressed as $2(\boldsymbol{\nabla} \cdot \boldsymbol{v})$, which for incompressible fluids is identically zero. For flows that are dominated by shearing — axial flow in pipes, thin-film flow — the third invariant I_3 vanishes identically. A common assumption is that I_3 does not play an important role in other flows as well, thus excluding I_3 from further consideration does not impose a severe restriction on the functional form of η. Thus in what follows, without loss of generality, η is assumed to be a function of I_2 only. Now the second invariant I_2 can be expressed in terms of $\dot{\gamma}$, the magnitude of $\dot{\boldsymbol{\gamma}}$, via

$$\dot{\gamma} = \sqrt{\frac{1}{2}\sum\nolimits_i \sum\nolimits_j \dot{\gamma}_{ij}\dot{\gamma}_{ji}} = \sqrt{\frac{1}{2} I_2},$$

where the proper sign is affixed to the square root to ensure that $\dot{\gamma}$ is positive. Hence the non-Newtonian viscosity is commonly written as $\eta = \eta(\dot{\gamma})$. The viscosity may in some instances be a function of the shear stress, so we write $\eta = \eta(\tau)$ where τ, the magnitude of $\boldsymbol{\tau}$, is the independent variable.

A number of empirical relations for $\eta(\dot{\gamma})$ have been derived from raw data. It is more convenient and useful to make use of analytical expressions of $\eta(\dot{\gamma})$ that have been found to 'fit' the experimental data with sufficient accuracy. Some of the more popular and commonly used empirical relations are:

$$\begin{aligned}
\text{Ostwald-de Waele model} \quad & \boldsymbol{\tau} = -\left\{K\left|\dot{\gamma}\right|^{n-1}\right\}\dot{\boldsymbol{\gamma}}, \\
\text{Carreau model} \quad & \boldsymbol{\tau} = -\left\{\eta_\infty + (\eta_0 - \eta_\infty)[1 + (\lambda\dot{\gamma})^2]^{\frac{n-1}{2}}\right\}\dot{\boldsymbol{\gamma}}, \\
\text{Eyring model} \quad & \boldsymbol{\tau} = -\left\{t_0\tau_0\left(\frac{\sin^{-1}(t_0\dot{\gamma})}{t_0\dot{\gamma}}\right)\right\}\dot{\boldsymbol{\gamma}}, \\
\text{Ellis model} \quad & \boldsymbol{\tau} = -\left\{\frac{\eta_0}{1 + \left(\frac{\tau}{\tau_{1/2}}\right)^{\alpha-1}}\right\}\dot{\boldsymbol{\gamma}}.
\end{aligned}$$

While the generalised Newtonian fluid model is often used for some fluids of importance in industry, it must be emphasised that it does have severe limitations. This fluid model cannot account for phenomena involving normal forces, viscoelastic time-dependent effects, or flows that are not dominated by steady shear. Even though the development of the generalised Newtonian fluid was presented as an extension of the Newtonian fluid supported by experimental data, an argument based on continuum mechanics shows that $\eta = \eta(\dot{\gamma})$ is the first term of a general expression for steady-state shear flows. The higher order terms provide detail related to the normal stresses in such flows, see Bird et al. (1977). We see that although the generalised Newtonian fluid model has its origins in empirical data, it has acquired a legitimate basis from recent continuum mechanics theories. Despite some of the limitations of the generalised Newtonian fluid model, industrial engineers are not averse to applying this model to flow systems that are more complicated and which may vary with time.

We should take note of several points in concluding this brief discussion on generalised Newtonian fluids. Firstly, the assumption that equation (2.1) is of a form suitable for describing non-Newtonian behaviour may not be correct. It may be the case that a different constitutive equation may be better suited to account for non-Newtonian effects, however, the merits of the wide range of competing constitutive relationships are not pursued any further here. Secondly, the effect that I_3 may play has been largely neglected and ignored. This viewpoint is held principally because of a lack of experimental support for the importance or utility of this invariant. Lastly, the majority of generalised fluid models are based on *empirical* data and so are only approximations to the actual behaviour of real fluids.

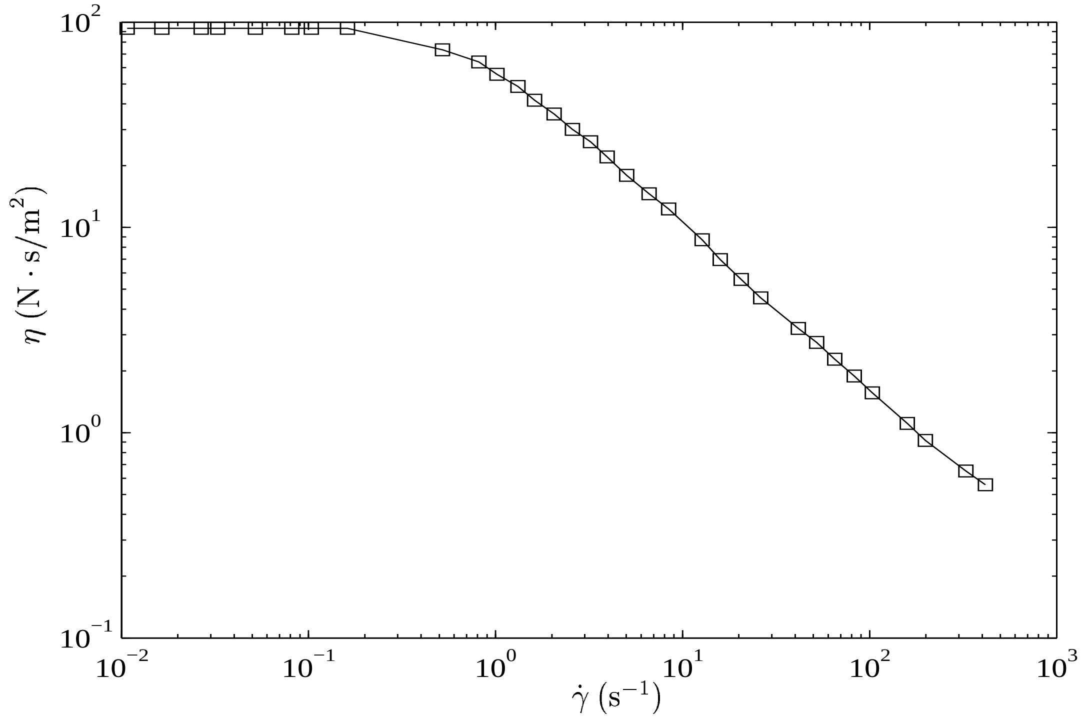

Figure 2.1: Dependence of viscosity on shear rate for a solution of 7% aluminium laurate in a mixture of decalin and $m-$cresol. [Derived from data of J.D. Huppler, E. Ashare, and L.A. Holmes, *Trans. Soc. Rheol., 11*, 159–179 (1967)]

2.1.1 Power-Law Fluids

Figure 2.1 shows the dependence of viscosity on shear rate for an aluminium soap solution which is an example of a generalised Newtonian fluid. The descending linear region of this graph of $\log \eta$ vs. $\log \dot{\gamma}$ is considered to be of most importance in industrial problems. This linear portion of the graph can be described by a 'power-law'

$$\eta = K \left| \dot{\gamma} \right|^{n-1} , \tag{2.2}$$

in which K, with units N · s^n/m^2, is referred to as the consistency of the fluid and the dimensionless quantity n is known as the fluid index. These constants characterise the fluids being modelled by this constitutive relation. A limitation of the power-law is that it does not adequately describe the portion of the graph near $\dot{\gamma} = 0$, however this region, though important, is often neglected in a flow engineer's considerations. Also it is not possible to use the fluid parameters K and n to construct a 'time constant' and this prohibits the tying together of steady-state flow phenomena with short-lived viscoelastic phenomena.

Power-law fluids are further categorised according to the fluid index n. If $n < 1$, the fluid is referred to as 'pseudoplastic' or 'shear-thinning', while if $n > 1$, the fluid is called 'dilatant' or 'shear-thickening'. If $n = 1$ and $K = \mu$ then the constitutive relation for a Newtonian fluid is recovered.

Equation (2.2) represents a constitutive relation that is one of the best-known and widely used in flow engineering work. As was mentioned for the generalised Newtonian fluid model, the power-law fluid model has been used to study more complicated flow systems than it is strictly applicable to. An assessment of the errors in the results of such calculations has often not been undertaken.

The simple form of the power-law fluid model, along with its wide-spread use, was a determining factor in choosing it for further study. A close study of this fluid model will, hopefully, provide a better understanding of its applicability, particularly, to boundary-layer flows.

2.2 Boundary-Layer Equations for Power-Law Fluids

In this section the equations governing the boundary-layer flow of a power-law fluid are obtained. The flow is assumed to be steady, incompressible and three dimensional with no external body forces. The surface over which the fluid flows is taken to be effectively flat. We start with the primitive variable form of the continuity and momentum transport equations, viz:

$$
\begin{aligned}
\frac{\partial u^*}{\partial x^*} + \frac{\partial v^*}{\partial y^*} + \frac{\partial w^*}{\partial z^*} &= 0, \\
\rho \left[u^* \frac{\partial u^*}{\partial x^*} + v^* \frac{\partial u^*}{\partial y^*} + w^* \frac{\partial u^*}{\partial z^*} \right] &= -\frac{\partial p^*}{\partial x^*} + \frac{\partial \tau^*_{x^*x^*}}{\partial x^*} + \frac{\partial \tau^*_{y^*x^*}}{\partial y^*} + \frac{\partial \tau^*_{z^*x^*}}{\partial z^*}, \\
\rho \left[u^* \frac{\partial v^*}{\partial x^*} + v^* \frac{\partial v^*}{\partial y^*} + w^* \frac{\partial v^*}{\partial z^*} \right] &= -\frac{\partial p^*}{\partial y^*} + \frac{\partial \tau^*_{x^*y^*}}{\partial x^*} + \frac{\partial \tau^*_{y^*y^*}}{\partial y^*} + \frac{\partial \tau^*_{z^*y^*}}{\partial z^*}, \\
\rho \left[u^* \frac{\partial w^*}{\partial x^*} + v^* \frac{\partial w^*}{\partial y^*} + w^* \frac{\partial w^*}{\partial z^*} \right] &= -\frac{\partial p^*}{\partial z^*} + \frac{\partial \tau^*_{x^*z^*}}{\partial x^*} + \frac{\partial \tau^*_{y^*z^*}}{\partial y^*} + \frac{\partial \tau^*_{z^*z^*}}{\partial z^*}.
\end{aligned}
$$

In the above equations a Cartesian co-ordinate system is assumed with (u^*, v^*, w^*) and p^* representing the components of the fluid velocity and the pressure inside the flow. The various components of the stress tensor are given by τ^*_{ij}. We proceed by putting these equations into non-dimensional form using the standard approach of taking L as a typical length, U as a typical speed and ϵ as a scale factor, of the order of the boundary-layer thickness, that rescales y^* and z^*. As such, we regard ϵ as being the non-dimensional boundary-layer 'thickness', the precise form of which is given later. The dimensionless variables are defined by

$$\begin{aligned} &x = \frac{x^*}{L}, \quad y = \frac{y^*}{\epsilon L}, \quad z = \frac{z^*}{\epsilon L} \\ &u = \frac{u^*}{U}, \quad v = \frac{v^*}{\epsilon U}, \quad w = \frac{w^*}{\epsilon U}, \quad p = \frac{p^*}{\rho U^2}. \end{aligned}$$

Making use of these non-dimensional variables allows us to write the continuity and momentum transport equations as:

$$\frac{\partial u}{\partial x} + \frac{\partial v}{\partial y} + \frac{\partial w}{\partial z} = 0, \tag{2.3a}$$

$$u\frac{\partial u}{\partial x} + v\frac{\partial u}{\partial y} + w\frac{\partial u}{\partial z} = -\frac{\partial p}{\partial x} + \frac{1}{\rho U^2}\left[\frac{\partial \tau_{xx}}{\partial x} + \frac{\partial \tau_{yx}}{\partial y} + \frac{\partial \tau_{zx}}{\partial z}\right], \tag{2.3b}$$

$$\epsilon\left[u\frac{\partial v}{\partial x} + v\frac{\partial v}{\partial y} + w\frac{\partial v}{\partial z}\right] = -\frac{1}{\epsilon}\frac{\partial p}{\partial y} + \frac{1}{\rho U^2}\left[\frac{\partial \tau_{xy}}{\partial x} + \frac{\partial \tau_{yy}}{\partial y} + \frac{\partial \tau_{zy}}{\partial z}\right], \tag{2.3c}$$

$$\epsilon\left[u\frac{\partial w}{\partial x} + v\frac{\partial w}{\partial y} + w\frac{\partial w}{\partial z}\right] = -\frac{1}{\epsilon}\frac{\partial p}{\partial z} + \frac{1}{\rho U^2}\left[\frac{\partial \tau_{xz}}{\partial x} + \frac{\partial \tau_{yz}}{\partial y} + \frac{\partial \tau_{zz}}{\partial z}\right]. \tag{2.3d}$$

The stress versus rate-of-strain relationship for a power-law fluid is obtained by making use of equation (2.2) for the non-Newtonian viscosity in equation (2.1). This gives, in primitive variable form,

$$\boldsymbol{\tau}^* = -\left\{K\left|\dot{\gamma}^*\right|^{n-1}\right\}\dot{\boldsymbol{\gamma}}^*. \tag{2.4}$$

It is not uncommon for the non-Newtonian viscosity η to be referred to as the 'apparent viscosity' and we make use of μ_{app} to denote it. With this notation the components of the stress tensor can be expressed as

$$\tau^*_{ij} = \mu^*_{app}\left(\frac{\partial u^*_i}{\partial x^*_j} + \frac{\partial u^*_j}{\partial x^*_i}\right). \tag{2.5}$$

After changing to non-dimensional variables the components of the stress tensor are given by

$$\begin{aligned}
\tau_{xx} &= 2\left(\frac{U}{L}\right)\mu_{app}\frac{\partial u}{\partial x},\\
\tau_{yy} &= 2\left(\frac{U}{L}\right)\mu_{app}\frac{\partial v}{\partial y},\\
\tau_{zz} &= 2\left(\frac{U}{L}\right)\mu_{app}\frac{\partial w}{\partial z},\\
\tau_{yx} = \tau_{xy} &= \left(\frac{U}{L}\right)\mu_{app}\left(\frac{1}{\epsilon}\frac{\partial u}{\partial y}+\epsilon\frac{\partial v}{\partial x}\right),\\
\tau_{zx} = \tau_{xz} &= \left(\frac{U}{L}\right)\mu_{app}\left(\frac{1}{\epsilon}\frac{\partial u}{\partial z}+\epsilon\frac{\partial w}{\partial x}\right),\\
\tau_{zy} = \tau_{yz} &= \left(\frac{U}{L}\right)\mu_{app}\left(\frac{\partial w}{\partial y}+\frac{\partial v}{\partial z}\right).
\end{aligned}$$

The apparent viscosity μ_{app} for a power-law fluid is not constant and, as noted previously, is a function of the second scalar invariant of the rate-of-strain tensor, i.e. $\mu_{app} = f(I_2)$. Making use of the definition for the second invariant I_2, the apparent viscosity can be expressed in non-dimensional form as

$$\begin{aligned}
\mu_{app} = K\left(\frac{U}{L}\right)^{n-1}\Bigg|\Bigg[&2\left(\frac{\partial u}{\partial x}\right)^2+2\left(\frac{\partial v}{\partial y}\right)^2+2\left(\frac{\partial w}{\partial z}\right)^2+\left(\frac{1}{\epsilon}\frac{\partial u}{\partial y}+\epsilon\frac{\partial v}{\partial x}\right)^2\\
&+\left(\frac{1}{\epsilon}\frac{\partial u}{\partial z}+\epsilon\frac{\partial w}{\partial x}\right)^2+\left(\frac{\partial w}{\partial y}+\frac{\partial v}{\partial z}\right)^2\Bigg]^{\frac{1}{2}}\Bigg|^{n-1}.
\end{aligned}$$

This form for the apparent viscosity can be simplified by noting that as the boundary-layer thickness ϵ is small ($\ll 1$), the $O(\epsilon^{-1})$ terms will be dominant. Hence, by retaining the dominant terms, the expression for μ_{app} can to be written as

$$\mu_{app} \approx K\left(\frac{U}{\epsilon L}\right)^{n-1}\left\{\left[\left(\frac{\partial u}{\partial y}\right)^2+\left(\frac{\partial u}{\partial z}\right)^2\right]^{\frac{n-1}{2}}+O(\epsilon)\right\}.$$

For ease of notation we define

$$\kappa = \left(\frac{\partial u}{\partial y}\right)^2+\left(\frac{\partial u}{\partial z}\right)^2.$$

With this simplified form for μ_{app}, the derivatives of the apparent viscosity are written as

$$\begin{aligned}
\frac{\partial \mu_{app}}{\partial x} &= (n-1)K\left(\frac{U}{\epsilon L}\right)^{n-1}\kappa^{\frac{n-3}{2}}\left\{\frac{\partial u}{\partial y}\frac{\partial^2 u}{\partial x \partial y}+\frac{\partial u}{\partial z}\frac{\partial^2 u}{\partial x \partial z}\right\},\\
\frac{\partial \mu_{app}}{\partial y} &= (n-1)K\left(\frac{U}{\epsilon L}\right)^{n-1}\kappa^{\frac{n-3}{2}}\left\{\frac{\partial u}{\partial y}\frac{\partial^2 u}{\partial y^2}+\frac{\partial u}{\partial z}\frac{\partial^2 u}{\partial y \partial z}\right\},\\
\frac{\partial \mu_{app}}{\partial z} &= (n-1)K\left(\frac{U}{\epsilon L}\right)^{n-1}\kappa^{\frac{n-3}{2}}\left\{\frac{\partial u}{\partial y}\frac{\partial^2 u}{\partial z \partial y}+\frac{\partial u}{\partial z}\frac{\partial^2 u}{\partial z^2}\right\}.
\end{aligned}$$

Next we obtain expressions for the derivatives of the stress terms appearing in the x-momentum transport equation. These derivatives are

$$\begin{aligned}
\frac{\partial \tau_{xx}}{\partial x} &= \left(\frac{2U}{L}\right)\left[\frac{\partial \mu_{app}}{\partial x}\frac{\partial u}{\partial x}+\mu_{app}\frac{\partial^2 u}{\partial x^2}\right]\\
&= \left(\frac{KU}{L}\right)\left(\frac{U}{\epsilon L}\right)^{n-1}\kappa^{\frac{n-3}{2}}\left[2(n-1)\left\{\frac{\partial u}{\partial y}\frac{\partial^2 u}{\partial x \partial y}+\frac{\partial u}{\partial z}\frac{\partial^2 u}{\partial x \partial z}\right\}\frac{\partial u}{\partial x}+2\kappa\frac{\partial^2 u}{\partial x^2}\right], \qquad (2.6)\\
\frac{\partial \tau_{yx}}{\partial y} &= \left(\frac{U}{L}\right)\left[\frac{\partial \mu_{app}}{\partial y}\left(\frac{1}{\epsilon}\frac{\partial u}{\partial y}+\epsilon\frac{\partial v}{\partial x}\right)+\mu_{app}\left(\frac{1}{\epsilon}\frac{\partial^2 u}{\partial y^2}+\epsilon\frac{\partial^2 v}{\partial y \partial x}\right)\right]\\
&= \left(\frac{KU}{L}\right)\left(\frac{U}{\epsilon L}\right)^{n-1}\kappa^{\frac{n-3}{2}}\left[(n-1)\left\{\frac{\partial u}{\partial y}\frac{\partial^2 u}{\partial y^2}+\frac{\partial u}{\partial z}\frac{\partial^2 u}{\partial y \partial z}\right\}\left(\frac{1}{\epsilon}\frac{\partial u}{\partial y}+\epsilon\frac{\partial v}{\partial x}\right)\right.\\
&\qquad \left.+\kappa\left(\frac{1}{\epsilon}\frac{\partial^2 u}{\partial y^2}+\epsilon\frac{\partial^2 v}{\partial y \partial x}\right)\right], \qquad (2.7)\\
\frac{\partial \tau_{zx}}{\partial z} &= \left(\frac{U}{L}\right)\left[\frac{\partial \mu_{app}}{\partial z}\left(\frac{1}{\epsilon}\frac{\partial u}{\partial z}+\epsilon\frac{\partial w}{\partial x}\right)+\mu_{app}\left(\frac{1}{\epsilon}\frac{\partial^2 u}{\partial z^2}+\epsilon\frac{\partial^2 w}{\partial z \partial x}\right)\right]\\
&= \left(\frac{KU}{L}\right)\left(\frac{U}{\epsilon L}\right)^{n-1}\kappa^{\frac{n-3}{2}}\left[(n-1)\left\{\frac{\partial u}{\partial y}\frac{\partial^2 u}{\partial z \partial y}+\frac{\partial u}{\partial z}\frac{\partial^2 u}{\partial z^2}\right\}\left(\frac{1}{\epsilon}\frac{\partial u}{\partial z}+\epsilon\frac{\partial w}{\partial x}\right)\right.\\
&\qquad \left.+\kappa\left(\frac{1}{\epsilon}\frac{\partial^2 u}{\partial z^2}+\epsilon\frac{\partial^2 w}{\partial z \partial x}\right)\right]. \qquad (2.8)
\end{aligned}$$

These expressions for the derivatives of the stress components are substituted into the right-hand-side of the x-momentum transport equation (2.3b) to yield

$$\begin{aligned}
RHS = \frac{1}{\rho U^2}&\left(\frac{KU}{L}\right)\left(\frac{U}{\epsilon L}\right)^{n-1}\kappa^{\frac{n-3}{2}}\left[2(n-1)\left\{\frac{\partial u}{\partial y}\frac{\partial^2 u}{\partial x \partial y}+\frac{\partial u}{\partial z}\frac{\partial^2 u}{\partial x \partial z}\right\}\frac{\partial u}{\partial x}\right.\\
&+2\kappa\frac{\partial^2 u}{\partial x^2}+(n-1)\left\{\frac{\partial u}{\partial y}\frac{\partial^2 u}{\partial y^2}+\frac{\partial u}{\partial z}\frac{\partial^2 u}{\partial y \partial z}\right\}\left(\frac{1}{\epsilon^2}\frac{\partial u}{\partial y}+\frac{\partial v}{\partial x}\right)\\
&+\kappa\left(\frac{1}{\epsilon^2}\frac{\partial^2 u}{\partial y^2}+\frac{\partial^2 v}{\partial y \partial x}\right)+(n-1)\left\{\frac{\partial u}{\partial y}\frac{\partial^2 u}{\partial z \partial y}+\frac{\partial u}{\partial z}\frac{\partial^2 u}{\partial z^2}\right\}\left(\frac{1}{\epsilon^2}\frac{\partial u}{\partial z}+\frac{\partial w}{\partial x}\right)
\end{aligned}$$

$$\begin{aligned}
&+\kappa\left(\frac{1}{\epsilon^2}\frac{\partial^2 u}{\partial z^2}+\frac{\partial^2 w}{\partial z\partial x}\right)\Bigg]\\
&=\left(\frac{K}{\rho UL}\right)\left(\frac{U}{\epsilon L}\right)^{n-1}\kappa^{\frac{n-3}{2}}\left[\frac{(n-1)}{\epsilon^2}\left\{\frac{\partial u}{\partial y}\frac{\partial^2 u}{\partial y^2}+\frac{\partial u}{\partial z}\frac{\partial^2 u}{\partial y\partial z}\right\}\frac{\partial u}{\partial y}\right.\\
&+\frac{(n-1)}{\epsilon^2}\left\{\frac{\partial u}{\partial y}\frac{\partial^2 u}{\partial z\partial y}+\frac{\partial u}{\partial z}\frac{\partial^2 u}{\partial z^2}\right\}\frac{\partial u}{\partial z}+\frac{\kappa}{\epsilon^2}\left(\frac{\partial^2 u}{\partial y^2}+\frac{\partial^2 u}{\partial z^2}\right)\\
&+(n-1)\left(2\left\{\frac{\partial u}{\partial y}\frac{\partial^2 u}{\partial x\partial y}+\frac{\partial u}{\partial z}\frac{\partial^2 u}{\partial x\partial z}\right\}\frac{\partial u}{\partial x}+\left\{\frac{\partial u}{\partial y}\frac{\partial^2 u}{\partial y^2}+\frac{\partial u}{\partial z}\frac{\partial^2 u}{\partial y\partial z}\right\}\frac{\partial v}{\partial x}\right.\\
&\left.\left.+\left\{\frac{\partial u}{\partial y}\frac{\partial^2 u}{\partial z\partial y}+\frac{\partial u}{\partial z}\frac{\partial^2 u}{\partial z^2}\right\}\frac{\partial w}{\partial x}\right)+\kappa\left(2\frac{\partial^2 u}{\partial x^2}+\frac{\partial^2 v}{\partial y\partial x}+\frac{\partial^2 w}{\partial z\partial x}\right)\right].
\end{aligned}\tag{2.9}$$

A further simplification can be made by differentiating the continuity equation (2.3a) with respect to x to give

$$\frac{\partial^2 u}{\partial x^2}+\frac{\partial^2 v}{\partial x\partial y}+\frac{\partial^2 w}{\partial x\partial z}=0.\tag{2.10}$$

Making use of this identity along with factoring out the $\frac{1}{\epsilon^2}$ yields the following expression for the right-hand-side of equation (2.3b)

$$\begin{aligned}
RHS=&\left(\frac{K}{\rho UL}\right)\left(\frac{U}{\epsilon L}\right)^{n-1}\frac{1}{\epsilon^2}\kappa^{\frac{n-3}{2}}\left[(n-1)\left\{\frac{\partial u}{\partial y}\frac{\partial^2 u}{\partial y^2}+\frac{\partial u}{\partial z}\frac{\partial^2 u}{\partial y\partial z}\right\}\frac{\partial u}{\partial y}\right.\\
&\left.+(n-1)\left\{\frac{\partial u}{\partial y}\frac{\partial^2 u}{\partial z\partial y}+\frac{\partial u}{\partial z}\frac{\partial^2 u}{\partial z^2}\right\}\frac{\partial u}{\partial z}+\kappa\left(\frac{\partial^2 u}{\partial y^2}+\frac{\partial^2 u}{\partial z^2}\right)+O(\epsilon^2)\right],
\end{aligned}\tag{2.11}$$

where the $O(\epsilon^2)$ term has the form

$$\begin{aligned}
\epsilon^2&\left[2(n-1)\left\{\frac{\partial u}{\partial y}\frac{\partial^2 u}{\partial x\partial y}+\frac{\partial u}{\partial z}\frac{\partial^2 u}{\partial x\partial z}\right\}\frac{\partial u}{\partial x}+(n-1)\left\{\frac{\partial u}{\partial y}\frac{\partial^2 u}{\partial y^2}+\frac{\partial u}{\partial z}\frac{\partial^2 u}{\partial y\partial z}\right\}\frac{\partial v}{\partial x}\right.\\
&\left.+(n-1)\left\{\frac{\partial u}{\partial y}\frac{\partial^2 u}{\partial z\partial y}+\frac{\partial u}{\partial z}\frac{\partial^2 u}{\partial z^2}\right\}\frac{\partial w}{\partial x}+\kappa\frac{\partial^2 u}{\partial x^2}\right].
\end{aligned}$$

In equation (2.11) we want the combination of scaling quantities along with the boundary-layer thickness ϵ to be an $O(1)$ quantity. To facilitate this, we introduce the dimensionless parameter, commonly referred to as the non-Newtonian or ‘apparent’ Reynolds number, that is defined by

$$Re=\frac{\rho U^{2-n}L^n}{K}.\tag{2.12}$$

Applying a simple dominant balance between the apparent Reynolds number and the boundary-layer thickness results in

$$\left(\frac{1}{Re}\right)\left(\frac{1}{\epsilon^{n+1}}\right) = O(1).$$

The form of this relationship indicates that the boundary-layer thickness is determined by the apparent Reynolds number and is given by

$$\epsilon = O(Re^{-\frac{1}{n+1}}). \tag{2.13}$$

We note that these expressions for the apparent Reynolds number and the boundary-layer thickness for a power-law fluid readily reduce to the familiar Newtonian fluid counterparts upon setting $n = 1$ and $K = \mu$.

Hence, making use of the relationship between the apparent Reynolds number and the boundary-layer thickness allows the x-momentum transport equation to be written as

$$\begin{aligned} u\frac{\partial u}{\partial x} + v\frac{\partial u}{\partial y} + w\frac{\partial u}{\partial z} = -\frac{\partial p}{\partial x} + \kappa^{\frac{n-3}{2}} \Bigg[&(n-1)\left\{\frac{\partial u}{\partial y}\frac{\partial^2 u}{\partial y^2} + \frac{\partial u}{\partial z}\frac{\partial^2 u}{\partial y \partial z}\right\}\frac{\partial u}{\partial y} \\ &+ (n-1)\left\{\frac{\partial u}{\partial y}\frac{\partial^2 u}{\partial z \partial y} + \frac{\partial u}{\partial z}\frac{\partial^2 u}{\partial z^2}\right\}\frac{\partial u}{\partial z} \\ &+ \kappa\left(\frac{\partial^2 u}{\partial y^2} + \frac{\partial^2 u}{\partial z^2}\right) + O(\epsilon^2)\Bigg]. \end{aligned} \tag{2.14}$$

Proceeding in a similar manner, we derive the y-momentum transport equation for a power-law fluid. The derivatives of the stress terms appearing in equation (2.3c) are given by the following expressions

$$\begin{aligned} \frac{\partial \tau_{xy}}{\partial x} &= \left(\frac{U}{L}\right)\left[\frac{\partial \mu_{app}}{\partial x}\left(\frac{1}{\epsilon}\frac{\partial u}{\partial y} + \epsilon\frac{\partial v}{\partial x}\right) + \mu_{app}\left(\frac{1}{\epsilon}\frac{\partial^2 u}{\partial x \partial y} + \epsilon\frac{\partial^2 v}{\partial x^2}\right)\right] \\ &= \left(\frac{KU}{L}\right)\left(\frac{U}{\epsilon L}\right)^{n-1}\kappa^{\frac{n-3}{2}}\Bigg[(n-1)\left\{\frac{\partial u}{\partial y}\frac{\partial^2 u}{\partial x \partial y} + \frac{\partial u}{\partial z}\frac{\partial^2 u}{\partial x \partial z}\right\}\left(\frac{1}{\epsilon}\frac{\partial u}{\partial y} + \epsilon\frac{\partial v}{\partial x}\right) \\ &\qquad + \kappa\left(\frac{1}{\epsilon}\frac{\partial^2 u}{\partial x \partial y} + \epsilon\frac{\partial^2 v}{\partial x^2}\right)\Bigg], \end{aligned} \tag{2.15}$$

$$\frac{\partial \tau_{yy}}{\partial y} = \left(\frac{2U}{L}\right)\left[\frac{\partial \mu_{app}}{\partial y}\frac{\partial v}{\partial y} + \mu_{app}\frac{\partial^2 v}{\partial y^2}\right]$$

$$\begin{aligned}
&= \left(\frac{KU}{L}\right)\left(\frac{U}{\epsilon L}\right)^{n-1} \kappa^{\frac{n-3}{2}} \left[2(n-1)\left\{\frac{\partial u}{\partial y}\frac{\partial^2 u}{\partial y^2} + \frac{\partial u}{\partial z}\frac{\partial^2 u}{\partial y \partial z}\right\}\frac{\partial v}{\partial y}\right. \\
&\qquad \left. + 2\kappa \frac{\partial^2 v}{\partial y^2}\right],
\end{aligned} \tag{2.16}$$

$$\begin{aligned}
\frac{\partial \tau_{zy}}{\partial z} &= \left(\frac{U}{L}\right)\left[\frac{\partial \mu_{app}}{\partial z}\left(\frac{\partial w}{\partial y} + \frac{\partial v}{\partial z}\right) + \mu_{app}\left(\frac{\partial^2 w}{\partial z \partial y} + \frac{\partial^2 v}{\partial z^2}\right)\right] \\
&= \left(\frac{KU}{L}\right)\left(\frac{U}{\epsilon L}\right)^{n-1} \kappa^{\frac{n-3}{2}} \left[(n-1)\left\{\frac{\partial u}{\partial y}\frac{\partial^2 u}{\partial z \partial y} + \frac{\partial u}{\partial z}\frac{\partial^2 u}{\partial z^2}\right\}\left(\frac{\partial w}{\partial y} + \frac{\partial v}{\partial z}\right)\right. \\
&\qquad \left. + \kappa\left(\frac{\partial^2 w}{\partial z \partial y} + \frac{\partial^2 v}{\partial z^2}\right)\right].
\end{aligned} \tag{2.17}$$

Substituting these expressions into the viscous stress term appearing in the right-hand-side of the y-momentum transport equation (2.3c) gives

$$\begin{aligned}
RHS &= \frac{1}{\rho U^2}\left(\frac{KU}{L}\right)\left(\frac{U}{\epsilon L}\right)^{n-1} \kappa^{\frac{n-3}{2}} \times \\
&\quad \left[(n-1)\left\{\frac{\partial u}{\partial y}\frac{\partial^2 u}{\partial x \partial y} + \frac{\partial u}{\partial z}\frac{\partial^2 u}{\partial x \partial z}\right\}\left(\frac{1}{\epsilon}\frac{\partial u}{\partial y} + \epsilon\frac{\partial v}{\partial x}\right) + \kappa\left(\frac{1}{\epsilon}\frac{\partial^2 u}{\partial x \partial y} + \epsilon\frac{\partial^2 v}{\partial x^2}\right)\right. \\
&\quad + \frac{2(n-1)}{\epsilon}\left\{\frac{\partial u}{\partial y}\frac{\partial^2 u}{\partial y^2} + \frac{\partial u}{\partial z}\frac{\partial^2 u}{\partial y \partial z}\right\}\frac{\partial v}{\partial y} + \frac{2\kappa}{\epsilon}\frac{\partial^2 v}{\partial y^2} \\
&\quad \left. + \frac{(n-1)}{\epsilon}\left\{\frac{\partial u}{\partial y}\frac{\partial^2 u}{\partial z \partial y} + \frac{\partial u}{\partial z}\frac{\partial^2 u}{\partial z^2}\right\}\left(\frac{\partial w}{\partial y} + \frac{\partial v}{\partial z}\right) + \frac{\kappa}{\epsilon}\left(\frac{\partial^2 w}{\partial z \partial y} + \frac{\partial^2 v}{\partial z^2}\right)\right] \\
&= \frac{1}{Re}\left(\frac{1}{\epsilon}\right)^{n-1} \kappa^{\frac{n-3}{2}} \left[\frac{(n-1)}{\epsilon}\left\{\frac{\partial u}{\partial y}\frac{\partial^2 u}{\partial x \partial y} + \frac{\partial u}{\partial z}\frac{\partial^2 u}{\partial x \partial z}\right\}\frac{\partial u}{\partial y}\right. \\
&\quad + \frac{2(n-1)}{\epsilon}\left\{\frac{\partial u}{\partial y}\frac{\partial^2 u}{\partial y^2} + \frac{\partial u}{\partial z}\frac{\partial^2 u}{\partial y \partial z}\right\}\frac{\partial v}{\partial y} \\
&\quad + \frac{(n-1)}{\epsilon}\left\{\frac{\partial u}{\partial y}\frac{\partial^2 u}{\partial z \partial y} + \frac{\partial u}{\partial z}\frac{\partial^2 u}{\partial z^2}\right\}\left(\frac{\partial w}{\partial y} + \frac{\partial v}{\partial z}\right) \\
&\quad + \frac{\kappa}{\epsilon}\left(\frac{\partial^2 u}{\partial x \partial y} + 2\frac{\partial^2 v}{\partial y^2} + \frac{\partial^2 w}{\partial z \partial y} + \frac{\partial^2 v}{\partial z^2}\right) \\
&\quad \left. + \epsilon(n-1)\left\{\frac{\partial u}{\partial y}\frac{\partial^2 u}{\partial x \partial y} + \frac{\partial u}{\partial z}\frac{\partial^2 u}{\partial x \partial z}\right\}\frac{\partial v}{\partial x} + \kappa\epsilon\frac{\partial^2 v}{\partial x^2}\right].
\end{aligned} \tag{2.18}$$

Differentiation of the continuity equation (2.3a) with respect to y results in

$$\frac{\partial^2 u}{\partial y \partial x} + \frac{\partial^2 v}{\partial y^2} + \frac{\partial^2 w}{\partial y \partial z} = 0. \tag{2.19}$$

Making use of this identity along with factoring out the $\frac{1}{\epsilon^2}$ term allows the above expression for the viscous stress to be expressed in the following simplified form

$$\begin{aligned} RHS = \frac{1}{Re}\left(\frac{1}{\epsilon}\right)^n \kappa^{\frac{n-3}{2}} \Bigg[&(n-1)\left\{\frac{\partial u}{\partial y}\frac{\partial^2 u}{\partial x \partial y} + \frac{\partial u}{\partial z}\frac{\partial^2 u}{\partial x \partial z}\right\}\frac{\partial u}{\partial y} \\ &+ 2(n-1)\left\{\frac{\partial u}{\partial y}\frac{\partial^2 u}{\partial y^2} + \frac{\partial u}{\partial z}\frac{\partial^2 u}{\partial y \partial z}\right\}\frac{\partial v}{\partial y} \\ &+ (n-1)\left\{\frac{\partial u}{\partial y}\frac{\partial^2 u}{\partial z \partial y} + \frac{\partial u}{\partial z}\frac{\partial^2 u}{\partial z^2}\right\}\left(\frac{\partial w}{\partial y} + \frac{\partial v}{\partial z}\right) \\ &+ \kappa\left(\frac{\partial^2 v}{\partial y^2} + \frac{\partial^2 v}{\partial z^2}\right) + O(\epsilon^2)\Bigg], \end{aligned} \tag{2.20}$$

where the $O(\epsilon^2)$ term has the form

$$\epsilon^2\left[(n-1)\left\{\frac{\partial u}{\partial y}\frac{\partial^2 u}{\partial x \partial y} + \frac{\partial u}{\partial z}\frac{\partial^2 u}{\partial x \partial z}\right\}\frac{\partial v}{\partial x} + \kappa\frac{\partial^2 v}{\partial x^2}\right]. \tag{2.21}$$

Making use of the relationship between Re and ϵ, we arrive at the following form for the y-momentum transport equation

$$\begin{aligned} \epsilon\left[u\frac{\partial v}{\partial x} + v\frac{\partial v}{\partial y} + w\frac{\partial v}{\partial z}\right] = -\frac{1}{\epsilon}\frac{\partial p}{\partial y} + \epsilon\kappa^{\frac{n-3}{2}}\Bigg[&(n-1)\left\{\frac{\partial u}{\partial y}\frac{\partial^2 u}{\partial x \partial y} + \frac{\partial u}{\partial z}\frac{\partial^2 u}{\partial x \partial z}\right\}\frac{\partial u}{\partial y} \\ &+ 2(n-1)\left\{\frac{\partial u}{\partial y}\frac{\partial^2 u}{\partial y^2} + \frac{\partial u}{\partial z}\frac{\partial^2 u}{\partial y \partial z}\right\}\frac{\partial v}{\partial y} \\ &+ (n-1)\left\{\frac{\partial u}{\partial y}\frac{\partial^2 u}{\partial z \partial y} + \frac{\partial u}{\partial z}\frac{\partial^2 u}{\partial z^2}\right\}\left(\frac{\partial w}{\partial y} + \frac{\partial v}{\partial z}\right) \\ &+ \kappa\left(\frac{\partial^2 v}{\partial y^2} + \frac{\partial^2 v}{\partial z^2}\right) + O(\epsilon^2)\Bigg]. \end{aligned} \tag{2.22}$$

Lastly we derive the z-momentum transport equation for a power-law fluid. The derivatives of the stress terms appearing in equation (2.3d) are given by the following expressions

$$\begin{aligned} \frac{\partial \tau_{xz}}{\partial x} &= \left(\frac{U}{L}\right)\left[\frac{\partial \mu_{app}}{\partial x}\left(\frac{1}{\epsilon}\frac{\partial u}{\partial z} + \epsilon\frac{\partial w}{\partial x}\right) + \mu_{app}\left(\frac{1}{\epsilon}\frac{\partial^2 u}{\partial x \partial z} + \epsilon\frac{\partial^2 w}{\partial x^2}\right)\right] \\ &= \left(\frac{KU}{L}\right)\left(\frac{U}{\epsilon L}\right)^{n-1}\kappa^{\frac{n-3}{2}}\Bigg[(n-1)\left\{\frac{\partial u}{\partial y}\frac{\partial^2 u}{\partial x \partial y} + \frac{\partial u}{\partial z}\frac{\partial^2 u}{\partial x \partial z}\right\}\left(\frac{1}{\epsilon}\frac{\partial u}{\partial z} + \epsilon\frac{\partial w}{\partial x}\right) \\ &\qquad + \kappa\left(\frac{1}{\epsilon}\frac{\partial^2 u}{\partial x \partial z} + \epsilon\frac{\partial^2 w}{\partial x^2}\right)\Bigg], \end{aligned} \tag{2.23}$$

$$\begin{aligned}
\frac{\partial \tau_{yz}}{\partial y} &= \left(\frac{U}{L}\right)\left[\frac{\partial \mu_{app}}{\partial y}\left(\frac{\partial v}{\partial z}+\frac{\partial w}{\partial y}\right)+\mu_{app}\left(\frac{\partial^2 v}{\partial y \partial z}+\frac{\partial^2 w}{\partial y^2}\right)\right] \\
&= \left(\frac{KU}{L}\right)\left(\frac{U}{\epsilon L}\right)^{n-1}\kappa^{\frac{n-3}{2}}\left[(n-1)\left\{\frac{\partial u}{\partial y}\frac{\partial^2 u}{\partial y^2}+\frac{\partial u}{\partial z}\frac{\partial^2 u}{\partial y \partial z}\right\}\left(\frac{\partial v}{\partial z}+\frac{\partial w}{\partial y}\right)\right. \\
&\qquad \left.+\,\kappa\left(\frac{\partial^2 v}{\partial y \partial z}+\frac{\partial^2 w}{\partial y^2}\right)\right], \qquad (2.24) \\
\frac{\partial \tau_{zz}}{\partial z} &= \left(\frac{2U}{L}\right)\left[\frac{\partial \mu_{app}}{\partial z}\frac{\partial w}{\partial z}+\mu_{app}\frac{\partial^2 w}{\partial z^2}\right] \\
&= \left(\frac{KU}{L}\right)\left(\frac{U}{\epsilon L}\right)^{n-1}\kappa^{\frac{n-3}{2}}\left[2(n-1)\left\{\frac{\partial u}{\partial y}\frac{\partial^2 u}{\partial z \partial y}+\frac{\partial u}{\partial z}\frac{\partial^2 u}{\partial z^2}\right\}\frac{\partial w}{\partial z}\right. \\
&\qquad \left.+\,2\kappa\frac{\partial^2 w}{\partial z^2}\right]. \qquad (2.25)
\end{aligned}$$

Substituting these expressions into the viscous stress term appearing in the right-hand-side of the z-momentum transport equation (2.3d) gives

$$\begin{aligned}
RHS &= \frac{1}{\rho U^2}\left(\frac{KU}{L}\right)\left(\frac{U}{\epsilon L}\right)^{n-1}\kappa^{\frac{n-3}{2}}\times \\
&\quad \left[(n-1)\left\{\frac{\partial u}{\partial y}\frac{\partial^2 u}{\partial x \partial y}+\frac{\partial u}{\partial z}\frac{\partial^2 u}{\partial x \partial z}\right\}\left(\frac{1}{\epsilon}\frac{\partial u}{\partial z}+\epsilon\frac{\partial w}{\partial x}\right)+\kappa\left(\frac{1}{\epsilon}\frac{\partial^2 u}{\partial x \partial z}+\epsilon\frac{\partial^2 w}{\partial x^2}\right)\right. \\
&\quad +\frac{(n-1)}{\epsilon}\left\{\frac{\partial u}{\partial y}\frac{\partial^2 u}{\partial y^2}+\frac{\partial u}{\partial z}\frac{\partial^2 u}{\partial y \partial z}\right\}\left(\frac{\partial v}{\partial z}+\frac{\partial w}{\partial y}\right)+\frac{\kappa}{\epsilon}\left(\frac{\partial^2 v}{\partial y \partial z}+\frac{\partial^2 w}{\partial y^2}\right) \\
&\quad \left.+\frac{2(n-1)}{\epsilon}\left\{\frac{\partial u}{\partial y}\frac{\partial^2 u}{\partial z \partial y}+\frac{\partial u}{\partial z}\frac{\partial^2 u}{\partial z^2}\right\}\frac{\partial w}{\partial z}+\frac{2\kappa}{\epsilon}\frac{\partial^2 w}{\partial z^2}\right] \\
&= \frac{1}{Re}\left(\frac{1}{\epsilon}\right)^{n-1}\kappa^{\frac{n-3}{2}}\left[\frac{(n-1)}{\epsilon}\left\{\frac{\partial u}{\partial y}\frac{\partial^2 u}{\partial x \partial y}+\frac{\partial u}{\partial z}\frac{\partial^2 u}{\partial x \partial z}\right\}\frac{\partial u}{\partial z}\right. \\
&\quad +\frac{(n-1)}{\epsilon}\left\{\frac{\partial u}{\partial y}\frac{\partial^2 u}{\partial y^2}+\frac{\partial u}{\partial z}\frac{\partial^2 u}{\partial y \partial z}\right\}\left(\frac{\partial v}{\partial z}+\frac{\partial w}{\partial y}\right) \\
&\quad +\frac{2(n-1)}{\epsilon}\left\{\frac{\partial u}{\partial y}\frac{\partial^2 u}{\partial z \partial y}+\frac{\partial u}{\partial z}\frac{\partial^2 u}{\partial z^2}\right\}\frac{\partial w}{\partial z} \\
&\quad +\frac{\kappa}{\epsilon}\left(\frac{\partial^2 u}{\partial x \partial z}+\frac{\partial^2 v}{\partial y \partial z}+\frac{\partial^2 w}{\partial y^2}+2\frac{\partial^2 w}{\partial z^2}\right) \\
&\quad \left.+\,\epsilon(n-1)\left\{\frac{\partial u}{\partial y}\frac{\partial^2 u}{\partial x \partial y}+\frac{\partial u}{\partial z}\frac{\partial^2 u}{\partial x \partial z}\right\}\frac{\partial w}{\partial x}+\kappa\epsilon\frac{\partial^2 w}{\partial x^2}\right]. \qquad (2.26)
\end{aligned}$$

Differentiation of the continuity equation (2.3a) with respect to z results in

$$\frac{\partial^2 u}{\partial z \partial x} + \frac{\partial^2 v}{\partial z \partial y} + \frac{\partial^2 w}{\partial z^2} = 0. \tag{2.27}$$

Making use of this identity along with factoring out the $\frac{1}{\epsilon^2}$ term allows the above expression for the viscous stress to be expressed in the following simplified form

$$\begin{aligned} RHS = \frac{1}{Re}\left(\frac{1}{\epsilon}\right)^n \kappa^{\frac{n-3}{2}} \Bigg[& (n-1)\left\{\frac{\partial u}{\partial y}\frac{\partial^2 u}{\partial x \partial y} + \frac{\partial u}{\partial z}\frac{\partial^2 u}{\partial x \partial z}\right\}\frac{\partial u}{\partial z} \\ & + (n-1)\left\{\frac{\partial u}{\partial y}\frac{\partial^2 u}{\partial y^2} + \frac{\partial u}{\partial z}\frac{\partial^2 u}{\partial y \partial z}\right\}\left(\frac{\partial v}{\partial z} + \frac{\partial w}{\partial y}\right) \\ & + 2(n-1)\left\{\frac{\partial u}{\partial y}\frac{\partial^2 u}{\partial z \partial y} + \frac{\partial u}{\partial z}\frac{\partial^2 u}{\partial z^2}\right\}\frac{\partial w}{\partial z} + \kappa\left(\frac{\partial^2 w}{\partial y^2} + \frac{\partial^2 w}{\partial z^2}\right) + O\left(\epsilon^2\right)\Bigg], \end{aligned} \tag{2.28}$$

where the $O\left(\epsilon^2\right)$ term has the following form

$$\epsilon^2\left[(n-1)\left\{\frac{\partial u}{\partial y}\frac{\partial^2 u}{\partial x \partial y} + \frac{\partial u}{\partial z}\frac{\partial^2 u}{\partial x \partial z}\right\}\frac{\partial w}{\partial x} + \kappa\frac{\partial^2 w}{\partial x^2}\right]. \tag{2.29}$$

Making use of the relationship between Re and ϵ, we arrive at the following form for the z-momentum transport equation

$$\begin{aligned} \epsilon\left[u\frac{\partial w}{\partial x} + v\frac{\partial w}{\partial y} + w\frac{\partial w}{\partial z}\right] = -\frac{1}{\epsilon}\frac{\partial p}{\partial z} + \epsilon\kappa^{\frac{n-3}{2}} \Bigg[& (n-1)\left\{\frac{\partial u}{\partial y}\frac{\partial^2 u}{\partial x \partial y} + \frac{\partial u}{\partial z}\frac{\partial^2 u}{\partial x \partial z}\right\}\frac{\partial u}{\partial z} \\ & + (n-1)\left\{\frac{\partial u}{\partial y}\frac{\partial^2 u}{\partial y^2} + \frac{\partial u}{\partial z}\frac{\partial^2 u}{\partial y \partial z}\right\}\left(\frac{\partial v}{\partial z} + \frac{\partial w}{\partial y}\right) \\ & + 2(n-1)\left\{\frac{\partial u}{\partial y}\frac{\partial^2 u}{\partial z \partial y} + \frac{\partial u}{\partial z}\frac{\partial^2 u}{\partial z^2}\right\}\frac{\partial w}{\partial z} \\ & + \kappa\left(\frac{\partial^2 w}{\partial y^2} + \frac{\partial^2 w}{\partial z^2}\right) + O\left(\epsilon^2\right)\Bigg]. \end{aligned} \tag{2.30}$$

From the foregoing derivation of the boundary-layer equations for a power-law fluid, the coordinate transformation from physical variables to non-dimensional variables scaled on the boundary-layer thickness is described by

$$x \to \frac{x^*}{L}, \quad y \to \frac{y^*}{Re^{-\frac{1}{n+1}}L}, \quad z \to \frac{z^*}{Re^{-\frac{1}{n+1}}L}$$
$$u \to \frac{u^*}{U}, \quad v \to \frac{v^*}{Re^{-\frac{1}{n+1}}U}, \quad w \to \frac{w^*}{Re^{-\frac{1}{n+1}}U}, \quad P \to \frac{P^*}{\rho U^2}.$$

Equations (2.14), (2.22) and (2.30) are the non-dimensionalised and boundary-layer thickness scaled versions of the Cauchy momentum transport equations for a power-law fluid. These equations become a valid approximation of the fluid flow within the boundary layer when the Reynolds number *Re* is large. Applying this limiting process gives the following set of equations to describe the boundary-layer flow of a power-law fluid

$$\frac{\partial u}{\partial x} + \frac{\partial v}{\partial y} + \frac{\partial w}{\partial z} = 0, \tag{2.31a}$$

$$\begin{aligned} u\frac{\partial u}{\partial x} + v\frac{\partial u}{\partial y} + w\frac{\partial u}{\partial z} = -\frac{\partial p}{\partial x} + \kappa^{\frac{n-3}{2}}\Bigg[(n-1)\left\{\frac{\partial u}{\partial y}\frac{\partial^2 u}{\partial y^2} + \frac{\partial u}{\partial z}\frac{\partial^2 u}{\partial y \partial z}\right\}\frac{\partial u}{\partial y} \\ +(n-1)\left\{\frac{\partial u}{\partial y}\frac{\partial^2 u}{\partial z \partial y} + \frac{\partial u}{\partial z}\frac{\partial^2 u}{\partial z^2}\right\}\frac{\partial u}{\partial z} + \kappa\left(\frac{\partial^2 u}{\partial y^2} + \frac{\partial^2 u}{\partial z^2}\right)\Bigg], \end{aligned} \tag{2.31b}$$

$$0 = -\frac{\partial p}{\partial y}, \tag{2.31c}$$

$$0 = -\frac{\partial p}{\partial z}. \tag{2.31d}$$

The boundary-layer equations (2.31) have been derived for a full three-dimensional flow geometry. However, the fluid flow that is considered and discussed in the following chapters is two dimensional. Such two dimensional flows are based on the assumption that the flow in the spanwise, i.e. z, direction is, to all intents, identical. This allows for the z dependence in the boundary-layer equations to be dropped so as to give

$$\frac{\partial u}{\partial x} + \frac{\partial v}{\partial y} = 0, \tag{2.32a}$$

$$u\frac{\partial u}{\partial x} + v\frac{\partial u}{\partial y} = -\frac{\partial p}{\partial x} + n\left|\frac{\partial u}{\partial y}\right|^{n-1}\frac{\partial^2 u}{\partial y^2}, \tag{2.32b}$$

$$0 = -\frac{\partial p}{\partial y}. \tag{2.32c}$$

To close this system of equations we impose the boundary conditions

$$u = 0, \quad v = v^* \quad \text{on} \quad y = 0, \tag{2.33a}$$

$$u \to U_e(x) \quad \text{as} \quad y \to \infty. \tag{2.33b}$$

These boundary conditions reflect the physical requirement that the fluid flow satisfies full viscous no-slip at the surface and also allows for mass transfer through the flat plate. The stream-wise velocity within the boundary layer must match smoothly onto the free-stream, $U_e(x)$, at a large distance from the surface.

2.2.1 Small Wall Curvature - Prandtl Transformation

The boundary-layer equations that have been derived above are for the flow of a power-law fluid over a flat plate. The Cartesian coordinate system used was tacitly assumed to have the abscissa parallel to, and the ordinate normal to the flat plate. It is quite feasible and practical for the flow to be over a surface exhibiting variable curvature. The surface curvature is assumed to be small when considered on the boundary-layer scale.

The curved surface is defined by

$$y_s = g(x),$$

where y_s represents the height, or y value, of the surface at streamwise location x. We note that (x, y_s) have been non-dimensionalised and scaled to the boundary-layer thickness using the coordinate transformation described in Section 2.2.

Now the effect of the small wall curvature on the boundary-layer equations describing the flow can be accounted for via the Prandtl transformation, see Rosenhead (1963). This involves firstly defining $\tilde{y} = y - y_s$, where this variable represents the vertical distance above the curved surface at a given streamwise location x. This new variable $\tilde{y}$ in the wall normal direction is a function of x and y, i.e. $\tilde{y}(x, y) = y - g(x)$. Next, all the dependent variables that are functions of (x, y) need to be expressed in terms of the new variables $(x, \tilde{y})$. For example, taking $u(x, \tilde{y})$ we find that

$$\begin{aligned} \frac{\partial u}{\partial x} &= \frac{\partial u}{\partial x} - g_x \frac{\partial u}{\partial \tilde{y}}, \\ \frac{\partial u}{\partial y} &= \frac{\partial u}{\partial \tilde{y}}. \end{aligned}$$

Making use of the new coordinates we find that the continuity equation (2.32a) becomes

$$\frac{\partial u}{\partial x} - g_x \frac{\partial u}{\partial \tilde{y}} + \frac{\partial v}{\partial \tilde{y}} = 0,$$

which can be re-arranged as

$$\frac{\partial u}{\partial x} + \frac{\partial}{\partial \tilde{y}} (v - g_x u) = 0.$$

By defining the wall-normal velocity component $\tilde{v} = v - g_x u$, we are able to express the continuity equation in the more familiar form

$$\frac{\partial u}{\partial x} + \frac{\partial \tilde{v}}{\partial \tilde{y}} = 0.$$

The remaining variables in the x and y momentum equations are unaffected by this transformation. With the newly defined variables $\tilde{y}$ and $\tilde{v}$, we are able to write the boundary-layer equations as

$$\begin{aligned} \frac{\partial u}{\partial x} + \frac{\partial \tilde{v}}{\partial \tilde{y}} &= 0, \\ u \frac{\partial u}{\partial x} + \tilde{v} \frac{\partial u}{\partial \tilde{y}} &= -\frac{\partial p}{\partial x} + n \left| \frac{\partial u}{\partial \tilde{y}} \right|^{n-1} \frac{\partial^2 u}{\partial \tilde{y}^2}, \\ 0 &= \frac{\partial p}{\partial \tilde{y}}. \end{aligned}$$

The accompanying boundary conditions required to close this system of equations now become

$$u = 0, \quad \tilde{v} = \tilde{v}^* \qquad \text{on} \qquad \tilde{y} = 0,$$

$$u \to U_e(x) \qquad \text{as} \qquad \tilde{y} \to \infty.$$

We note that for the boundary-layer flow over a lightly curved surface, the governing equations are identical in form to those corresponding to the boundary-layer flow over a flat plate.

2.3 Chapter Summary

In this chapter we have given a brief overview of Generalised Newtonian Fluids. This class of fluids is one of many classes of non-Newtonian fluids. A specific example of a generalised Newtonian fluid is the power-law, or Ostwald-de Waele, fluid that has been selected for further study. The power-law constitutive relation is amongst the most 'popular' in many commercial Computational Fluid Dynamics (CFD) packages and is also frequently used to describe fluids encountered in industry and flow engineering.

For a power-law fluid, the governing boundary-layer equations (2.32) and accompanying boundary conditions (2.33) have been derived in a formal manner. The effect of small wall curvature has also been considered and it has been found that the form of the governing equations remains unaffected apart from a redefinition of the transverse coordinate and velocity component.

In the following chapters we will be concerned with examining the solution of this system of partial differential equations.

Chapter 3

Boundary-layer Flow of a Power-law Fluid

Self-similar solutions for the boundary-layer equations of non-Newtonian, and Newtonian, fluids provide valuable insights into the behaviour of the fluid flow. However, the conditions under which self-similar solutions are obtained may be either too restrictive, or only applicable over a limited range of relevant parameters. To obtain a fuller understanding of the fluid flow it is necessary to treat the boundary-layer equations as a system of parabolic partial differential equations. Furthermore, as the boundary-layer equations are nonlinear in character they must in general be solved numerically.

Various techniques for the numerical solution of the boundary-layer equations for Newtonian fluids have been developed over many years. An early method for the solution of the boundary-layer equations was described by Hartree and Womersley (1937), in which the x derivatives are replaced by finite-differences so as to approximate the partial differential equation by an ordinary differential equation. This ordinary differential equation is then solved using a technique based on finite-differences. This method has been employed by others such as Leigh (1955) and Smith and Clutter (1963) to produce quite satisfactory solutions to the boundary-layer equations for a number of flow regimes. Blottner (1975) has compared the use of other finite-difference methods such as the Crank-Nicolson scheme and the Keller box scheme for the numerical solution of the boundary-layer equations.

Any of these techniques should, in principle, be suitable for finding a numerical solution to the boundary-layer equations governing the base flow of a non-Newtonian fluid modelled by a power-law relationship. Andersson and Toften (1989) describe the use of the Keller-box scheme to obtain solutions to the Falkner-Skan-type equation for a power-law fluid. Though the numerical scheme was applied to a linearised form of the boundary-layer equations, rather than the complete nonlinear version of the boundary-layer equations, the results presented indicate that modern finite-difference techniques can be successfully applied to find solutions to non-Newtonian fluid flows.

In this chapter we look at the effect that mass transfer through the surface has on the boundary-layer flow of a power-law fluid. The corresponding problem for Newtonian fluids, though with zero pressure gradient in the external flow, has been considered by Catherall et al. (1965). They found that fluid injection reduces the skin friction which subsequently approaches zero and the boundary layer separates from the surface.

We formulate the boundary-layer equations for a power-law fluid with an arbitrary external flow. A numerical scheme, based on that used by Catherall et al. (1965), is developed and used to obtain solutions to the governing equations. This numerical scheme facilitates an investigation into the effect that the fluid index, n, has on the location of the separation point subject to a uniform rate of fluid injection through the flat plate. We investigate the effect that an adverse or favourable pressure gradient, in both the presence and absence of mass transfer through the surface, has on the point at which the boundary-layer separates.

3.1 Equations of Motion

In this section we consider the laminar boundary-layer flow of a non-Newtonian fluid that is modelled by a power-law constitutive relation along a semi-infinite horizontal flat plate. The plate is permeable and permits the same non-Newtonian fluid to be injected into the boundary layer; Figure 3.1 shows the flow geometry along with the co-ordinate system that is used. All

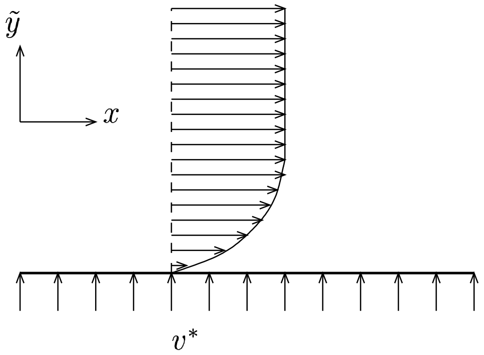

Figure 3.1: Representation of flow geometry and co-ordinate system.

variables are in non-dimensional form and have been rescaled to a suitable boundary-layer thickness.

For the flow depicted in Figure 3.1 the origin for the co-ordinate system used is assumed to be at the leading edge of the flat plate. Although the fluid injection rate is shown as being constant along the entire length of the semi-infinite plate, the injection rate may vary with distance along the plate. The boundary-layer approximation is known to have limited applicability at or near the leading edge, and the effect of this limitation on the proposed numerical scheme will be considered briefly in due course.

The equations governing the flow are

$$\frac{\partial u}{\partial x}+\frac{\partial v}{\partial y}=0, \tag{3.1a}$$

$$u\frac{\partial u}{\partial x}+v\frac{\partial u}{\partial y}=-\frac{\mathrm{d}p}{\mathrm{d}x}+n\left|\frac{\partial u}{\partial y}\right|^{n-1}\frac{\partial^2 u}{\partial y^2}. \tag{3.1b}$$

To close the system we impose the boundary conditions

$$u=0, \quad v=V(x) \quad \text{on} \quad y=0, \tag{3.1c}$$

$$u\to U_e(x) \quad \text{as} \quad y\to\infty. \tag{3.1d}$$

These boundary conditions reflect the prescribed physical requirement that the fluid flow satisfies full viscous no-slip at the surface and normal flow through the surface. The streamwise velocity within the boundary layer is required to match smoothly onto the free-stream,

$U_e(x)$, at a large distance from the surface. The mass transfer, denoted by $V(x)$, may be either suction of fluid from or injection of fluid into the boundary layer. While the mass transfer may depend on the streamwise location x, we will be concerned mainly with injection of fluid through the surface at a constant rate.

In the free-stream $u(x,y) \to U_e(x)$, where $U_e(x)$ is the external free-stream velocity. Using this far-field behaviour of the streamwise velocity, the x-momentum equation (3.1b) allows the pressure gradient to be expressed as

$$-\frac{\mathrm{d}p}{\mathrm{d}x} = U_e(x)\frac{\mathrm{d}U_e}{\mathrm{d}x}.$$

The form of the free-stream velocity, $U_e(x)$, can be used to set up various flow types of interest, such as the flow under a zero, adverse or favourable pressure gradient.

For most types of boundary-layer flow the velocity component aligned with the main flow direction, u, shows very rapid changes across the boundary layer. Additionally, a boundary-layer flow involving an adverse pressure gradient shows rapid growth of the boundary-layer thickness with streamwise distance. Hence it is common practice to employ new independent variables that are less sensitive to these effects.

We introduce new independent variables (ξ, η) for the streamwise and wall-normal directions respectively. The new variables are given by

$$\xi = A_1 x^{\alpha_1} \quad \text{and} \quad \eta = y\frac{A_2 U_e^{\alpha_2}}{x^{\frac{1}{n+1}}},$$

where the scaling constants A_1, A_2 and the exponents α_1, α_2 are to be determined. The partial derivatives with respect to the original co-ordinates can be expressed as

$$\begin{aligned}\frac{\partial}{\partial x} &= \alpha_1 A_1 x^{\alpha_1 - 1}\frac{\partial}{\partial \xi} + \eta\left(\alpha_2\frac{\frac{\mathrm{d}U_e}{\mathrm{d}x}}{U_e} - \frac{1}{(n+1)x}\right)\frac{\partial}{\partial \eta},\\ \frac{\partial}{\partial y} &= \frac{A_2 U_e^{\alpha_2}}{x^{\frac{1}{n+1}}}\frac{\partial}{\partial \eta}.\end{aligned}$$

Any occurrences of the variable x are replaced accordingly by ξ to give

$$\begin{aligned}
\frac{\partial}{\partial x} &= \alpha_1 A_1 \left(\frac{\xi}{A_1}\right)^{\frac{\alpha_1-1}{\alpha_1}} \frac{\partial}{\partial \xi} + \eta \left(\alpha_1 \alpha_2 A_1 \left(\frac{\xi}{A_1}\right)^{\frac{\alpha_1-1}{\alpha_1}} \frac{\frac{\mathrm{d}U_e}{\mathrm{d}\xi}}{U_e} - \frac{1}{n+1}\left(\frac{\xi}{A_1}\right)^{-\frac{1}{\alpha_1}}\right) \frac{\partial}{\partial \eta}, \\
\frac{\partial}{\partial y} &= A_2 U_e^{\alpha_2} \left(\frac{\xi}{A_1}\right)^{-\frac{1}{\alpha_1(n+1)}} \frac{\partial}{\partial \eta}.
\end{aligned}$$

We note that U_e is now a function of ξ.

Under these transformations the x-momentum equation (3.1b) becomes

$$\begin{aligned}
& n \left| A_2 U_e^{\alpha_2} \left(\frac{\xi}{A_1}\right)^{-\frac{1}{\alpha_1(n+1)}} \frac{\partial u}{\partial \eta} \right|^{n-1} \left[A_2 U_e^{\alpha_2} \left(\frac{\xi}{A_1}\right)^{-\frac{1}{\alpha_1(n+1)}} \right]^2 \frac{\partial^2 u}{\partial \eta^2} + \alpha_1 A_1 \left(\frac{\xi}{A_1}\right)^{\frac{\alpha_1-1}{\alpha_1}} U_e \frac{\mathrm{d}U_e}{\mathrm{d}\xi} = \\
& u \left[\alpha_1 A_1 \left(\frac{\xi}{A_1}\right)^{\frac{\alpha_1-1}{\alpha_1}} \frac{\partial u}{\partial \xi} + \eta \left(\alpha_1 \alpha_2 A_1 \left(\frac{\xi}{A_1}\right)^{\frac{\alpha_1-1}{\alpha_1}} \frac{\frac{\mathrm{d}U_e}{\mathrm{d}\xi}}{U_e} - \frac{1}{n+1}\left(\frac{\xi}{A_1}\right)^{-\frac{1}{\alpha_1}} \right) \frac{\partial u}{\partial \eta} \right] \\
& + v A_2 U_e^{\alpha_2} \left(\frac{\xi}{A_1}\right)^{-\frac{1}{\alpha_1(n+1)}} \frac{\partial u}{\partial \eta},
\end{aligned}$$

which after some simplification gives

$$\begin{aligned}
& n A_2^{n+1} U_e^{\alpha_2(n+1)} \frac{\partial^2 u}{\partial \eta^2} \left| \frac{\partial u}{\partial \eta} \right|^{n-1} + \alpha_1 \xi U_e \frac{\mathrm{d}U_e}{\mathrm{d}\xi} = \\
& \qquad u \left[\alpha_1 \xi \frac{\partial u}{\partial \xi} + \eta \left(\alpha_1 \alpha_2 \xi \frac{\frac{\mathrm{d}U_e}{\mathrm{d}\xi}}{U_e} - \frac{1}{n+1} \right) \frac{\partial u}{\partial \eta} \right] + v A_2 U_e^{\alpha_2} \left(\frac{\xi}{A_1}\right)^{\frac{n}{\alpha_1(n+1)}} \frac{\partial u}{\partial \eta}. \qquad (3.2)
\end{aligned}$$

Equation (3.2) allows us to determine the form of α_1, A_1 and A_2 in the following manner. Requiring that the exponent of the streamwise variable, ξ, be equal to unity wherever it occurs in the right-hand side of equation (3.2) results in $\alpha_1 = \frac{n}{n+1}$. Similarly, requiring that the coefficient of the highest derivative term in the left-hand side of (3.2) is equal to unity results in $A_2 = \left(\frac{1}{n}\right)^{\frac{1}{n+1}}$. Lastly, by setting $\frac{A_2}{A_1} = \frac{1}{n}$ we obtain $A_1 = n^{\frac{n}{n+1}}$. The appropriate form of α_2 is still to be determined.

Making use of these values for α_1, A_1 and A_2, the x-momentum equation (3.2) becomes

$$U_e^{\alpha_2(n+1)}\frac{\partial^2 u}{\partial \eta^2}\left|\frac{\partial u}{\partial \eta}\right|^{n-1}+\frac{n}{n+1}\xi U_e\frac{\mathrm{d}U_e}{\mathrm{d}\xi}=\frac{u}{n+1}\left[n\xi\frac{\partial u}{\partial \xi}+\eta\left(\alpha_2 n\xi\frac{\frac{\mathrm{d}U_e}{\mathrm{d}\xi}}{U_e}-1\right)\frac{\partial u}{\partial \eta}\right] \\ +\frac{1}{n}U_e^{\alpha_2}\xi v\frac{\partial u}{\partial \eta}, \qquad (3.3)$$

and the continuity equation (3.1a) becomes

$$\frac{1}{n}U_e^{\alpha_2}\xi\frac{\partial v}{\partial \eta}=\frac{\eta}{n+1}\left(1-\alpha_2 n\xi\frac{\frac{\mathrm{d}U_e}{\mathrm{d}\xi}}{U_e}\right)\frac{\partial u}{\partial \eta}-\frac{n}{n+1}\xi\frac{\partial u}{\partial \xi}.$$

Integrating the continuity equation with respect to η gives

$$\frac{1}{n}U_e^{\alpha_2}\xi v=\frac{1}{n+1}\int_0^\eta\left[\eta\left(1-\alpha_2 n\xi\frac{\frac{\mathrm{d}U_e}{\mathrm{d}\xi}}{U_e}\right)\frac{\partial u}{\partial \eta}-n\xi\frac{\partial u}{\partial \xi}\right]\mathrm{d}\eta+G(\xi).$$

Making use of the boundary condition on $\eta=0$, i.e. $v=V(\xi)$, gives

$$G(\xi)=\frac{U_e^{\alpha_2}\xi V}{n},$$

so that the integrated form of the continuity equation is given by

$$\frac{1}{n}U_e^{\alpha_2}\xi v=\frac{1}{n+1}\left(1-\alpha_2 n\xi\frac{\frac{\mathrm{d}U_e}{\mathrm{d}\xi}}{U_e}\right)\left[\eta u-\int_0^\eta u\,\mathrm{d}\eta\right]-\frac{n}{n+1}\int_0^\eta\xi\frac{\partial u}{\partial \xi}\,\mathrm{d}\eta+\frac{U_e^{\alpha_2}\xi V}{n}. \qquad (3.4)$$

By substituting (3.4) into (3.3) and rearranging terms we obtain the following integro-differential equation

$$U_e^{\alpha_2(n+1)}\frac{\partial^2 u}{\partial \eta^2}\left|\frac{\partial u}{\partial \eta}\right|^{n-1}+\left\{\frac{1}{n+1}\int_0^\eta\left[\left(1-\alpha_2 n\xi\frac{\frac{\mathrm{d}U_e}{\mathrm{d}\xi}}{U_e}\right)u+n\xi\frac{\partial u}{\partial \xi}\right]\mathrm{d}\eta-\frac{U_e^{\alpha_2}\xi V}{n}\right\}\frac{\partial u}{\partial \eta} \\ +\frac{n}{n+1}\xi U_e\frac{\mathrm{d}U_e}{\mathrm{d}\xi}-\frac{n}{n+1}\xi u\frac{\partial u}{\partial \xi}=0. \qquad (3.5a)$$

The corresponding boundary conditions expressed in the new variables are

$$u = 0, \quad v = V(\xi) \quad \text{on} \quad \eta = 0, \tag{3.5b}$$

$$u \to U_e(\xi) \quad \text{as} \quad \eta \to \infty. \tag{3.5c}$$

We note that equation (3.5a) along with the boundary conditions (3.5b,c) provides a concise description of the fluid flow being considered.

By defining $u = U_e q$ where $q = \frac{\partial f}{\partial \eta}$ and f is the dimensionless stream function, equation (3.5a) becomes

$$\begin{aligned} &U_e^{\alpha_2(n+1)+n} \frac{\partial^2 q}{\partial \eta^2} \left| \frac{\partial q}{\partial \eta} \right|^{n-1} \\ &+ U_e^2 \left\{ \frac{1}{n+1} \int_0^\eta \left[\left(1 - \alpha_2 n \xi \frac{\frac{\mathrm{d}U_e}{\mathrm{d}\xi}}{U_e} \right) q + n\xi \frac{\frac{\mathrm{d}U_e}{\mathrm{d}\xi}}{U_e} + n\xi \frac{\partial q}{\partial \xi} \right] \mathrm{d}\eta - \frac{U_e^{\alpha_2 - 1} \xi V}{n} \right\} \frac{\partial q}{\partial \eta} \\ &+ \frac{n}{n+1} \xi U_e \frac{\mathrm{d}U_e}{\mathrm{d}\xi} (1 - q^2) - \frac{n}{n+1} \xi U_e^2 q \frac{\partial q}{\partial \xi} = 0. \end{aligned}$$

We can now determine the form of α_2 by requiring that $\alpha_2(n+1) + n = 2$ to give $\alpha_2 = \frac{2-n}{n+1}$. Additionally, we define the pressure gradient function

$$\beta(\xi) = \frac{n}{n+1} \xi \frac{\frac{dU_e}{d\xi}}{U_e},$$

to give

$$\begin{aligned} \frac{\partial^2 q}{\partial \eta^2} \left| \frac{\partial q}{\partial \eta} \right|^{n-1} + \left\{ \frac{1}{n+1} \int_0^\eta \left[\left((2n-1)\beta + 1 \right) q + n\xi \frac{\partial q}{\partial \xi} \right] \mathrm{d}\eta - \frac{\xi V}{n\, U_e^{\frac{2n-1}{n+1}}} \right\} \frac{\partial q}{\partial \eta} \\ + \beta(1 - q^2) - \frac{n}{n+1} \xi q \frac{\partial q}{\partial \xi} = 0. \end{aligned} \tag{3.6a}$$

The boundary conditions now take the form

$$q = 0, \quad v = V(\xi) \quad \text{on} \quad \eta = 0, \tag{3.6b}$$

$$q \to 1 \quad \text{as} \quad \eta \to \infty. \tag{3.6c}$$

The solution of equation (3.6a) subject to the boundary conditions (3.6b,c) can be used to determine u at any streamwise location using $u = U_e(\xi)q$. Note that in the case of a power-of-x free-stream, i.e. $U_e \propto x^m$, the pressure gradient function $\beta(\xi)$ becomes a constant.

The final form for the transformation of independent variables is

$$\xi = (nx)^{\frac{n}{n+1}}, \tag{3.7a}$$

$$\eta = y\left(\frac{U_e^{2-n}}{nx}\right)^{\frac{1}{n+1}}, \tag{3.7b}$$

and we note that η has the form of a Falkner-Skan-like similarity variable that has the effect of compensating for the growth of the boundary layer. The solution grid in the transformed domain can use a uniform step-size for ξ and η so that errors introduced during discretisation will be smaller than if a non-uniform grid had been used.

3.2 Numerical Method

The existence of a closed-form solution to equation (3.6a) is very unlikely due to the non-linear terms appearing in the equation. We can gain some understanding about the nature of the solutions to this problem through the use of numerical simulations. A number of numerical methods that are available for solving partial differential equations, such as finite elements and spectral methods, may also be applicable to this class of problem. The numerical method that was chosen for solving equation (3.6a) is based on finite differences.

The boundary-layer equations are a system of parabolic partial differential equations and are commonly solved by numerical schemes that march along in the streamwise direction. The numerical scheme developed to solve equation (3.6a) is very similar to that used by Catherall et al. (1965). This technique was described by Hartree and Womersley (1937) in the context of solving the classical boundary-layer equations and is conceptually related to the Method of Lines.

We begin by replacing the variables q, ξ and β by averages, and ξ-derivatives are replaced by finite-differences. Let

$$\widehat{q} = \frac{q_1 + q_2}{2}, \qquad \widehat{\xi} = \frac{\xi_1 + \xi_2}{2}, \qquad \frac{\partial q}{\partial \xi} = \frac{q_2 - q_1}{\Delta\xi} \qquad \text{where} \qquad \Delta\xi = \xi_2 - \xi_1.$$

The subscripts denote two closely spaced locations along the streamwise direction. The integro-differential equation (3.6a) was derived from a set of partial differential equations with two independent variables, however, the use of these discretised variables changes the governing equation to an ordinary differential equation that is dependent on only one independent variable, η. The integro-differential equation (3.6a) now becomes

$$\begin{aligned} \frac{\mathrm{d}^2\widehat{q}}{\mathrm{d}\eta^2}\left|\frac{\mathrm{d}\widehat{q}}{\mathrm{d}\eta}\right|^{n-1} &+ \left\{\int_0^\eta \left[\frac{((2n-1)\beta_1+1)q_1 + ((2n-1)\beta_2+1)q_2}{2(n+1)} + \frac{n\widehat{\xi}(q_2-q_1)}{(n+1)\Delta\xi}\right] \mathrm{d}\eta \right. \\ &\left. - \frac{\widehat{\xi}V}{n\,\widehat{U_e^{\frac{2n-1}{n+1}}}}\right\}\frac{\mathrm{d}\widehat{q}}{\mathrm{d}\eta} + \frac{\beta_1(1-q_1^2)+\beta_2(1-q_2^2)}{2} - \frac{n}{n+1}\widehat{\xi}\widehat{q}\frac{(q_2-q_1)}{\Delta\xi} = 0. \end{aligned} \tag{3.8}$$

Note that the term $\widehat{U_e^{\frac{2n-1}{n+1}}}$ indicates the average after the exponentiation of U_e has been carried out.

The solution to equation (3.6a) is the streamwise velocity for any value of the fluid index n in the range $0 < n < 2$. The far-field boundary condition, requiring that the streamwise velocity matches onto the free-stream velocity, manifests itself as $\frac{\mathrm{d}\widehat{q}}{\mathrm{d}\eta}$ becoming vanishingly small. For shear-thickening fluids, with the fluid index in the range $1 < n < 2$, the numerical scheme that is suggested by the partly discretised equation (3.8) should work well. However, for shear-thinning fluids with the fluid index in the range $0 < n < 1$ this far-field matching requirement results in vanishingly small numbers being raised to a negative exponent along with the associated computer arithmetic problems that follow. Hence, we choose to develop and describe a numerical scheme that will solve equation (3.6a) specifically for shear-thinning fluids. A variant of this numerical scheme that is appropriate for dealing with the boundary-layer flow of a shear-thickening power-law fluid will be discussed later.

We proceed by multiplying equation (3.8) throughout by $\left(\frac{\mathrm{d}\widehat{q}}{\mathrm{d}\eta}\right)^{1-n}$, then replacing all appearances of q_2 by $2\widehat{q}-q_1$, or equivalently with $q_2-q_1=2(\widehat{q}-q_1)$, to give

$$\frac{\mathrm{d}^2\widehat{q}}{\mathrm{d}\eta^2}+\left\{\int_0^\eta\left[\frac{(2n-1)(\beta_1-\beta_2)q_1+2((2n-1)\beta_2+1)\widehat{q}}{2(n+1)}+\frac{n\theta(\widehat{q}-q_1)}{n+1}\right]\mathrm{d}\eta-K_{in}\right\}\left(\frac{\mathrm{d}\widehat{q}}{\mathrm{d}\eta}\right)^{2-n}$$
$$+\left\{\widehat{\beta}(1-q_1^2)-2\beta_2\widehat{q}(\widehat{q}-q_1)-\frac{n\theta}{n+1}\widehat{q}(\widehat{q}-q_1)\right\}\left(\frac{\mathrm{d}\widehat{q}}{\mathrm{d}\eta}\right)^{1-n}=0,$$

where $K_{in}=\frac{\widehat{\xi}V}{n\,U_e^{\widehat{\frac{2n-1}{n+1}}}}$, $\theta=\frac{\xi_1+\xi_2}{\Delta\xi}$, and $\widehat{\beta}=\frac{\beta_1+\beta_2}{2}$. Further regrouping of the terms in the above equation gives

$$\frac{\mathrm{d}^2\widehat{q}}{\mathrm{d}\eta^2}+\left\{\int_0^\eta\left[\left(\frac{(2n-1)(\beta_1-\beta_2)-2n\theta}{2(n+1)}\right)q_1+\left(\frac{(2n-1)\beta_2+n\theta+1}{n+1}\right)\widehat{q}\right]\mathrm{d}\eta-K_{in}\right\}\left(\frac{\mathrm{d}\widehat{q}}{\mathrm{d}\eta}\right)^{2-n}$$
$$+\left\{\widehat{\beta}(1-q_1^2)-\left(2\beta_2+\frac{n\theta}{n+1}\right)\widehat{q}(\widehat{q}-q_1)\right\}\left(\frac{\mathrm{d}\widehat{q}}{\mathrm{d}\eta}\right)^{1-n}=0. \tag{3.9}$$

Next the derivatives with respect to η are discretised using second-order accurate finite-difference approximations:

$$\left.\frac{\mathrm{d}^2\widehat{q}}{\mathrm{d}\eta^2}\right|_j=\frac{\widehat{q}_{j+1}-2\widehat{q}_j+\widehat{q}_{j-1}}{h^2},$$
$$\left.\frac{\mathrm{d}\widehat{q}}{\mathrm{d}\eta}\right|_j=\frac{\widehat{q}_{j+1}-\widehat{q}_{j-1}}{2h}.$$

The suffix j is the index to the mesh points and h is the step-size in the η direction. After making these substitutions and multiplying through by h^2, equation (3.9) takes the following discretised form

$$(\widehat{q}_{j+1}-2\widehat{q}_j+\widehat{q}_{j-1})+\left\{h^2\int_0^{\eta_j}\left[\left(\frac{(2n-1)(\beta_1-\beta_2)-2n\theta}{2(n+1)}\right)q_1\right.\right.$$
$$\left.\left.+\left(\frac{(2n-1)\beta_2+n\theta+1}{n+1}\right)\widehat{q}\right]\mathrm{d}\eta-K_{in}^*\right\}\left(\frac{\widehat{q}_{j+1}-\widehat{q}_{j-1}}{2h}\right)^{2-n}$$
$$+h^2\left\{\widehat{\beta}(1-q_1^2)_j-\left(2\beta_2+\frac{n\theta}{n+1}\right)\widehat{q}_j(\widehat{q}-q_1)_j\right\}\left(\frac{\widehat{q}_{j+1}-\widehat{q}_{j-1}}{2h}\right)^{1-n}=0,$$

where $K_{in}^*=h^2K_{in}$. The definite integral in the above expression is evaluated by the trapezoidal rule, which is denoted by $\sum''$, with the first and last terms halved. Hence, the above equation takes the following form

$$\begin{aligned}(\widehat{q}_{j+1} - 2\widehat{q}_j + \widehat{q}_{j-1}) + \Bigg\{ h^3 {\sum_{r=0}^{j}}'' \Bigg[\left(\frac{(2n-1)(\beta_1 - \beta_2) - 2n\theta}{2(n+1)} \right) q_{1r} \\ + \left(\frac{(2n-1)\beta_2 + n\theta + 1}{n+1} \right) \widehat{q}_r \Bigg] - K^*_{in} \Bigg\} \left(\frac{\widehat{q}_{j+1} - \widehat{q}_{j-1}}{2h} \right)^{2-n} \\ + h^2 \left\{ \widehat{\beta}(1 - q_1^2)_j - \left(2\beta_2 + \frac{n\theta}{n+1} \right) \widehat{q}_j (\widehat{q} - q_1)_j \right\} \left(\frac{\widehat{q}_{j+1} - \widehat{q}_{j-1}}{2h} \right)^{1-n} = 0. \quad (3.10)\end{aligned}$$

Equation (3.10) needs to be solved at the uniformly spaced mesh points $j = 1, \ldots, J$, with $j = 0$ corresponding to the flat plate and $j = J + 1$ to the free-stream. The solution of this equation at the j^{th} mesh point involves the unknowns $\widehat{q}_1, \ldots, \widehat{q}_{j+1}$. At the J^{th} mesh point use is made of the far-field boundary condition, viz. the given streamwise velocity, by setting the $J + 1^{th}$ mesh point to the given value. The velocity in the far-field may be normalised, hence allowing the velocity at the final mesh point to be given by $\widehat{q}_{J+1} = 1$. This system of non-linear algebraic equations requires a solution to be found at each streamwise location of the marching scheme being used to solve the governing parabolic partial differential equation.

Let the vector $\widehat{\mathbf{q}} = (\widehat{q}_1, \widehat{q}_2, \ldots, \widehat{q}_J)^T$ and define a function $\mathbf{F}$ by

$$\mathbf{F}(\widehat{\mathbf{q}}) = (f_1(\widehat{\mathbf{q}}), \ldots, f_j(\widehat{\mathbf{q}}), \ldots, f_J(\widehat{\mathbf{q}})),$$

where $f_j(\widehat{\mathbf{q}})$ is given by the left hand side of equation (3.10). We note that at mesh point j the unknowns $\widehat{q}_{j+2}, \ldots, \widehat{q}_J$ are understood to have coefficients identically equal to zero in the function $f_j(\widehat{\mathbf{q}})$. Using vector notation the system of non-linear equations assumes the form

$$\mathbf{F}(\widehat{\mathbf{q}}) = \mathbf{0}. \quad (3.11)$$

This system of non-linear algebraic equations will need to be solved by an iterative process. An iteration scheme similar to that used by Terrill (1960) that results in a set of simultaneous linear equations expressed in matrix form as $\mathbf{A}\widehat{\mathbf{q}} = \mathbf{b}$ could be implemented. However, equation (3.11) lends itself to solution more directly using Newton's iterative method for non-linear systems. The iteration procedure is based upon the ansatz

$$\widehat{\mathbf{q}}^{(k)} = \widehat{\mathbf{q}}^{(k-1)} - J(\widehat{\mathbf{q}}^{(k-1)})^{-1}\mathbf{F}(\widehat{\mathbf{q}}^{(k-1)}),$$

where $J(\widehat{\mathbf{q}})$ is the Jacobian matrix and k is the iteration index. Expanding the trapezoidal sum and applying the no-slip condition at $j = 0$ gives the following form for the function $f_j(\widehat{\mathbf{q}})$ at mesh point j

$$\begin{aligned} f_j\left(\widehat{\mathbf{q}}^{(k)}\right) = {} & \left(\widehat{q}_{j+1}^{(k)} - 2\widehat{q}_j^{(k)} + \widehat{q}_{j-1}^{(k)}\right) \\ & + \left\{h^3\left[\left(\frac{(2n-1)(\beta_1-\beta_2) - 2n\theta}{2(n+1)}\right)\left(q_{1,1} + \ldots + q_{1,j-1} + \frac{1}{2}q_{1,j}\right) + \right.\right. \\ & \left.\left.\left(\frac{(2n-1)\beta_2 + n\theta + 1}{n+1}\right)\left(\widehat{q}_1^{(k)} + \ldots + \widehat{q}_{j-1}^{(k)} + \frac{1}{2}\widehat{q}_j^{(k)}\right)\right] - K_{in}^*\right\}\left(\frac{\widehat{q}_{j+1}^{(k)} - \widehat{q}_{j-1}^{(k)}}{2h}\right)^{2-n} \\ & + h^2\left\{\widehat{\beta}(1-q_1^2)_j - \left(2\beta_2 + \frac{n\theta}{n+1}\right)\widehat{q}_j^{(k)}(\widehat{q}^{(k)} - q_1)_j\right\}\left(\frac{\widehat{q}_{j+1}^{(k-1)} - \widehat{q}_{j-1}^{(k-1)}}{2h}\right)^{1-n}. \end{aligned} \tag{3.12}$$

In equation (3.12) the superscript k is used to indicate both the iteration step and which variables are being solved for at the current step of the iterative procedure. We also note that the finite-difference approximation for $\left(\frac{\mathrm{d}\widehat{q}}{\mathrm{d}\eta}\right)^{1-n}$ is calculated using values of $\widehat{q}$ from the previous iteration step. The Jacobian matrix that is required to solve this system of equations using a Newton iteration procedure is sparse with all elements above the super-diagonal being zero. The detailed structure of the Jacobian matrix is given in Appendix A.

Falkner-Skan flows are defined by a free-stream potential flow with a streamwise velocity given by $U_e(\xi) \propto \xi^m$. The pressure gradient parameter β for Falkner-Skan flows is constant, i.e. $\beta = m$. Hence, setting $\beta_1 = \beta_2 = \beta$ allows equation (3.12) to take the following simplified form

$$\begin{aligned}
f_j\left(\widehat{\mathbf{q}}^{(k)}\right) = {} & \left(\widehat{q}_{j+1}^{(k)} - 2\widehat{q}_j^{(k)} + \widehat{q}_{j-1}^{(k)}\right) \\
& + \left\{ h^3 \left[\left(\frac{(2n-1)\beta + n\theta + 1}{n+1} \right) \left(\widehat{q}_1^{(k)} + \ldots + \widehat{q}_{j-1}^{(k)} + \frac{1}{2}\widehat{q}_j^{(k)} \right) - \right.\right. \\
& \left.\left. \frac{n\theta}{n+1} \left(q_{1,1} + \ldots + q_{1,j-1} + \frac{1}{2} q_{1,j} \right) \right] - K_{in}^* \right\} \left(\frac{\widehat{q}_{j+1}^{(k)} - \widehat{q}_{j-1}^{(k)}}{2h} \right)^{2-n} \\
& + h^2 \left\{ \beta(1 - q_1^2)_j - \left(2\beta + \frac{n\theta}{n+1} \right) \widehat{q}_j^{(k)} (\widehat{q}^{(k)} - q_1)_j \right\} \left(\frac{\widehat{q}_{j+1}^{(k-1)} - \widehat{q}_{j-1}^{(k-1)}}{2h} \right)^{1-n} . \qquad (3.13)
\end{aligned}$$

Equation (3.13) generates a system of non-linear algebraic equations that are specific for a Falkner-Skan flow. The Jacobian matrix needed to solve this non-linear system is slightly simpler than was needed for solving equation (3.12). The structure of the simpler Jacobian matrix is given in Appendix A. The solution of this non-linear system via a Newton iteration procedure yields the streamwise velocity profile at a given down-stream location. The numerical marching scheme is simply the application of this sequence of calculations along the length of the flat plate.

The set of equations (3.1) governing the boundary-layer flow of a power-law fluid are parabolic partial differential equations. The accompanying boundary conditions have been accounted for in the design of the numerical marching scheme described in this section. However, the numerical marching scheme will require an essential additional condition to work as expected. That extra condition is a prescribed velocity profile at an initial station ξ_0.

3.2.1 Initial Velocity Profile

The marching based numerical scheme described in Section 3.2 needs an initial condition to start the iteration process at the first streamwise location. Such an initial condition is given by a streamwise velocity profile appropriate for the class of flow being considered.

The velocity profile at the leading edge $\xi = 0$ is given by the solution of the Falkner-Skan-like equation for power-law fluids. The appropriate form of this equation is obtained by substituting $\xi = 0$ into equation (3.6a) to give

$$\frac{\partial^2 q}{\partial \eta^2}\left|\frac{\partial q}{\partial \eta}\right|^{n-1} + \left\{\frac{1}{n+1}\int_0^\eta \left[\left((2n-1)\beta + 1\right) q\right] \,\mathrm{d}\eta\right\}\frac{\partial q}{\partial \eta} + \beta(1-q^2) = 0. \tag{3.14}$$

Equation (3.14) can be expressed in a more familiar form by letting $q = \frac{\mathrm{d}f}{\mathrm{d}\eta}$, where f is the normalised stream function and ordinary derivatives are used to indicate that q and f are independent of ξ, viz.

$$\frac{\mathrm{d}^3 f}{\mathrm{d}\eta^3}\left|\frac{\mathrm{d}^2 f}{\mathrm{d}\eta^2}\right|^{n-1} + \left\{\frac{1}{n+1}\int_0^\eta \left[\left((2n-1)\beta + 1\right)\frac{\mathrm{d}f}{\mathrm{d}\eta}\right] \mathrm{d}\eta\right\}\frac{\mathrm{d}^2 f}{\mathrm{d}\eta^2} + \beta\left(1 - \left(\frac{\mathrm{d}f}{\mathrm{d}\eta}\right)^2\right) = 0.$$

We recall that β is constant when the free-stream potential flow is of Falkner-Skan-type and is referred to as the pressure gradient parameter.

Re-arranging and simplifying some of the terms finally gives

$$f''' + \frac{(2n-1)\beta + 1}{n+1}(f'')^{2-n} f + \beta\left(1 - (f')^2\right)(f'')^{1-n} = 0. \tag{3.15a}$$

The boundary conditions for this third-order non-linear ODE are

$$f = 0, \quad f' = 0, \quad \text{on} \quad \eta = 0, \tag{3.15b}$$

$$f' \to 1 \quad \text{as} \quad \eta \to \infty. \tag{3.15c}$$

Equation (3.15a) is a generalised version of the classical Falkner-Skan equation for power-law fluids and it can readily be seen that setting $n = 1$ results in equation (3.15a) taking the form of the standard Falkner-Skan equation.

Equation (3.15a) and the boundary conditions (3.15b,c) form a two-point boundary-value problem that can be solved numerically using a shooting method based around a fourth order Runge-Kutta quadrature scheme. The solution obtained is then used as the initial guess for the iteration procedure that begins at the first streamwise location and marches along the length of the plate until a suitable termination condition is satisfied.

3.3 Numerical Results: Shear-thinning Fluids

The numerical method described above for solving the equation governing the boundary-layer flow of a power-law fluid was implemented in Fortran. Use was made of subroutine libraries such as LAPACK to solve the system of equations at each streamwise location.

Before the program could be used to investigate the solutions of equation (3.6a) it was considered necessary to validate it. By setting $n = 1$ in equation (3.6a) we recover the equation describing the boundary-layer flow of a Newtonian fluid. The solution obtained for this case can then be compared with the results provided by Catherall et al. (1965).

To validate the computer program the step size, h, in the η-direction was set to 1.0×10^{-2} and the far-field, η_∞, was set to 20. The marching step-size, $\Delta\xi$, in the ξ-direction was set to 1.0×10^{-4}. A stopping location, ξ_{end}, was set to 2 to halt the marching scheme if the stopping condition based on the reduced skin friction was not satisfied. The iteration stopping criterion at each marching location, $\Delta\widehat{\mathbf{q}}^{(k)}$, was set to 1.0×10^{-5}. Fluid injection at the surface, V, was set to unity and the external flow was uniform, i.e. $\beta = 0$. For this value of β the Falkner-Skan equation reduces to the classical Blasius equation. The solution of the Blasius equation provides the initial velocity profile at $\xi = 0$.

The injection of fluid through the surface is expected to result in the separation of the boundary layer away from the surface. The reduced skin friction at the surface was used to monitor whether separation of the boundary layer was imminent. A reduced skin friction value was calculated at each ξ location and compared with a threshold value of 1.0×10^{-4}. When the value of the reduced skin friction fell below this threshold the boundary-layer was deemed to be at the point of separation and the program halted.

When the program was run with these parameters the separation point was found to be located at $\xi_s = 0.8596$. Making use of equation (3.7a) gives the separation point as $x_s = 0.7389$. Catherall et al. (1965) report the position of separation as $x_s \approx 0.7456$. The small difference in x_s may be attributed to different processing parameters along with using a marching scheme at three different step sizes h followed by Richardson extrapolation. Also the calculation of reduced skin friction at the surface was done using central differences rather than forward differences. The stopping criteria are also likely to have been different. Thus exact replication of their results was not possible. Nonetheless, the closeness of the reported values of x_s was taken as an indication that the implementation of the numerical scheme was correct. With this value of $\Delta\xi$, the location of the separation point is accurate to 4 decimal points and so facilitates a fairer comparison with the results reported by Catherall et al. (1965). Since this marching step-size did not impose too severe a load on computational resources, it was retained for subsequent numerical work.

Calculations could now be undertaken for a number of different flow regimes. The flow regimes studied and the results obtained are described in the following sections.

3.3.1 Zero Pressure Gradient

Even though the numerical scheme is, in principle, intended to be capable of accepting an arbitrary external flow, the numerical scheme that was implemented was specifically for Falkner-Skan flows. For this class of flows the external flow velocity is given by $U_e(x) \propto x^m$ and the pressure gradient parameter β is constant, i.e. $\beta = m$. The first flow regime that we consider has a zero pressure gradient, which corresponds to an external flow velocity that is constant. The pressure gradient parameter β takes the value 0 in this case. The fluid injection rate was kept fixed at a value of 1.0 along the entire length of the plate. This flow configuration parallels the flow geometry considered by Catherall et al. (1965) for a Newtonian fluid.

Solutions were obtained for shear-thinning fluids for a number of different values of the fluid index n in the range $0 < n < 1$. Streamwise velocity profiles were recorded at regular ξ locations as well as ξ_s, the location where the boundary layer was deemed to have 'separated' from the flat plate.

A selection of the streamwise velocity profiles for $n = 0.95$ are shown in Figure 3.2, starting with the initial Blasius-like velocity profile. From these velocity profiles we can see how the boundary layer develops with distance along the flat plate. Differences between the velocity

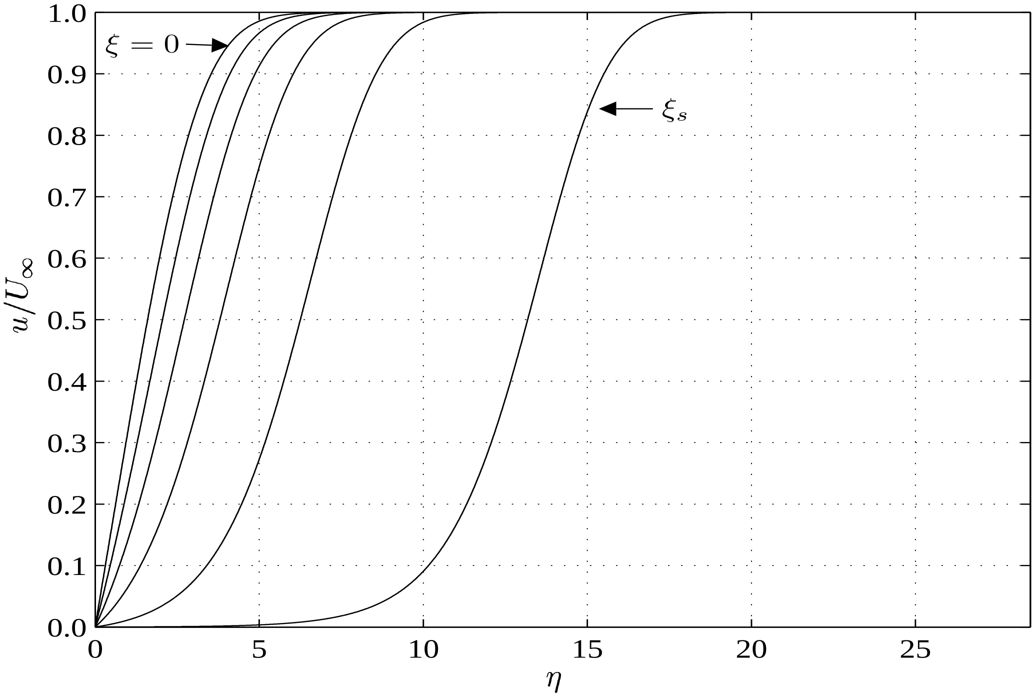

Figure 3.2: Velocity profiles for fluid index $n = 0.95$ at $\xi = 0.0, 0.2, \ldots, 0.8$ and the separation point ξ_s.

profiles taken at the sample points $\xi = 0.2, 0.4$ are relatively small, indicating a gradual change in the boundary layer with distance from the leading edge of the plate. However, with increasing distance along the surface the differences between consecutive sampled velocity profiles are more evident and there is a rapid transition to the final velocity profile at the point of separation. A comparison of the velocity profiles indicates that the boundary-layer thickness is increasing with distance from the leading-edge of the plate. The boundary-layer thickness is taken to be 0.99 of the normalised free-stream velocity. We also see that the velocity gradient, or velocity shear, in the vicinity of the plate surface decreases with distance along the plate. The reduced skin friction τ_0, used to determine whether separation of the boundary layer has occurred, is related to the velocity gradient by $\tau_0 = \left.\frac{\mathrm{d}u}{\mathrm{d}\eta}\right|_{\eta=0}$. Further away from the surface the boundary-layer velocity increases and matches with the free-stream velocity.

The streamwise velocity profiles for $n = 0.90, 0.85, 0.80, 0.75, 0.70$ are shown in Figures 3.3, 3.4, 3.5, 3.6, 3.7 respectively. The gradual variation away from the initial velocity profile with distance down-stream from the leading edge can also be seen in these velocity profiles. As the

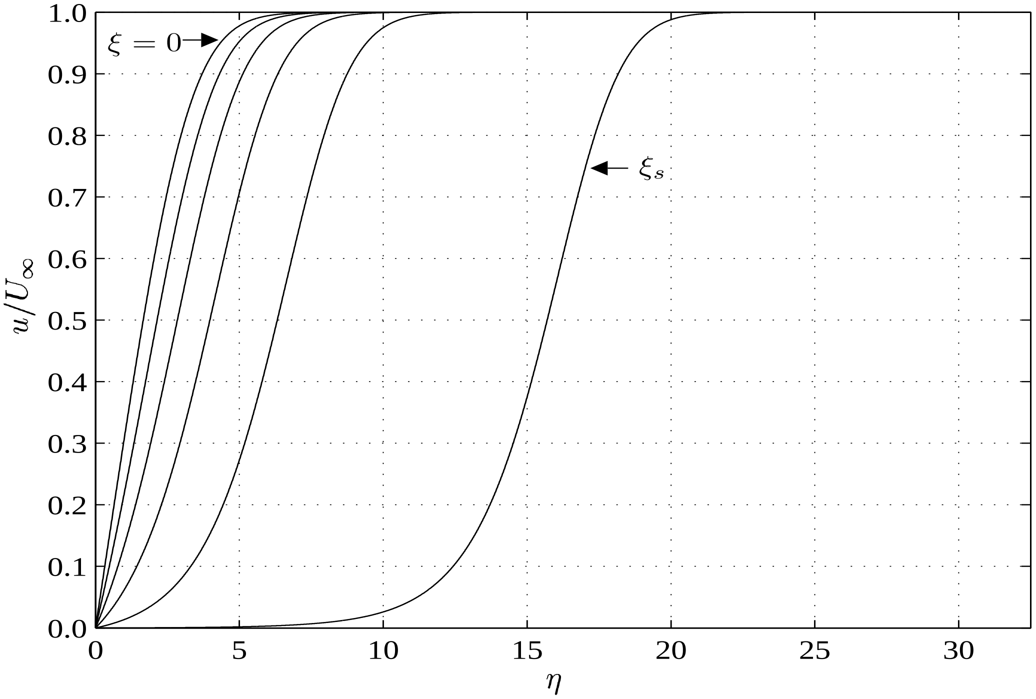

Figure 3.3: Velocity profiles for fluid index $n = 0.90$ at $\xi = 0.0, 0.2, \ldots, 0.8$ and the separation point ξ_s.

flow develops along the plate the velocity profiles display the characteristic ‘blowing off’ of the boundary layer as the separation point is approached.

It was noticed during the running of the computer program that this numerical scheme is very sensitive to the initial velocity profile. For example, using the classical Blasius velocity profile that is suitable for $n = 1$ to start the marching scheme for $n = 0.95$ would result in the numerical scheme not being able to meet convergence conditions at the first few streamwise locations. Thus it was necessary to solve equation (3.15a) for the required value of n to ensure that the correct initial velocity profile was used to start the marching scheme.

For shear-thinning fluids the solution of equation (3.15a) is known to have algebraic decay in the far-field. The nature of the solution to equation (3.15a), for power-law fluids in general, in the far-field is discussed in more detail in Chapter 4 and in Denier and Dabrowski (2004). Hence, to match onto the far-field boundary condition with a reasonably high accuracy it is necessary for η_∞, the distance from the surface where the asymptotic boundary condition is applied, to be quite large. The impact of this on the numerical marching scheme is that

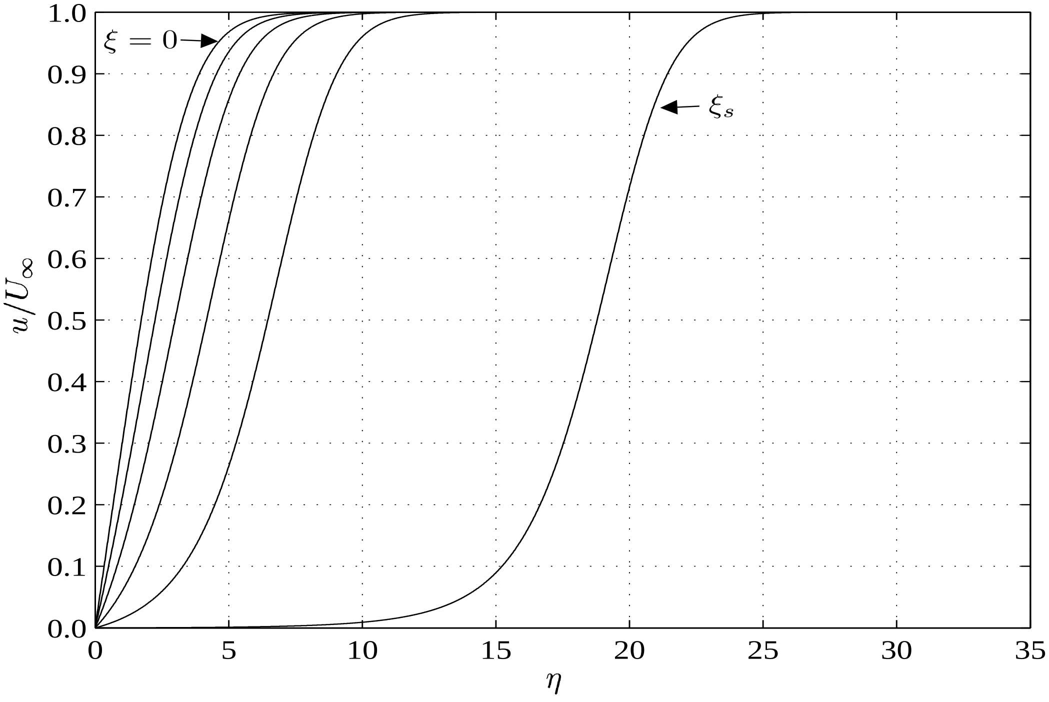

Figure 3.4: Velocity profiles for fluid index $n = 0.85$ at $\xi = 0.0, 0.2, \ldots, 0.8$ and the separation point ξ_s.

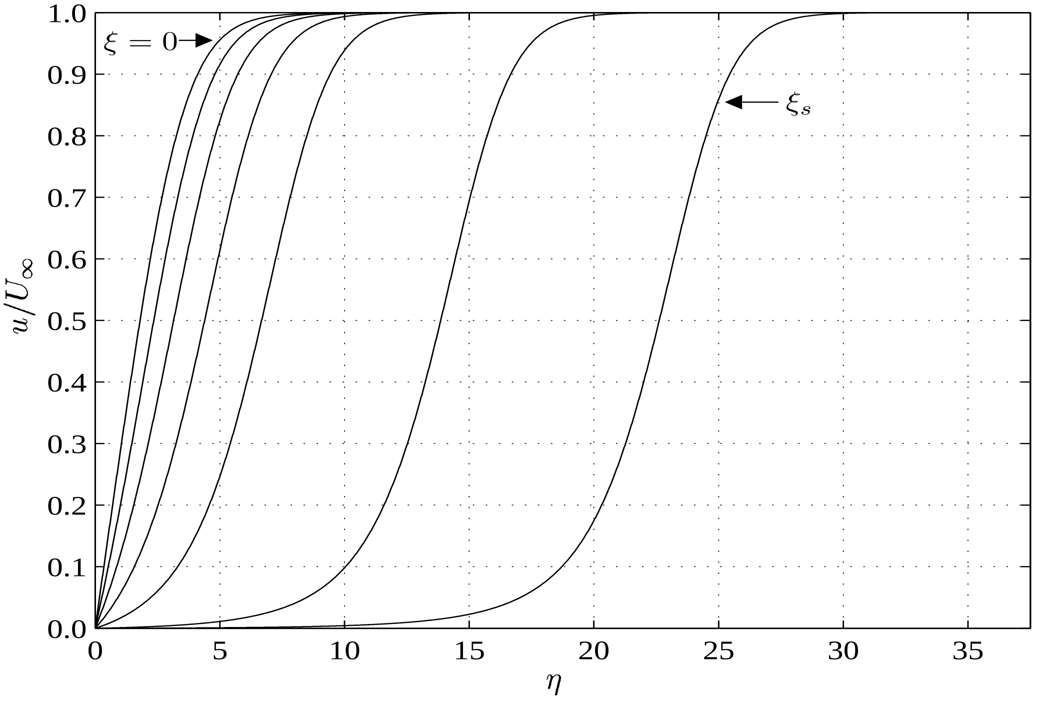

Figure 3.5: Velocity profiles for fluid index $n = 0.80$ at $\xi = 0.0, 0.2, \ldots, 1.0$ and the separation point ξ_s.

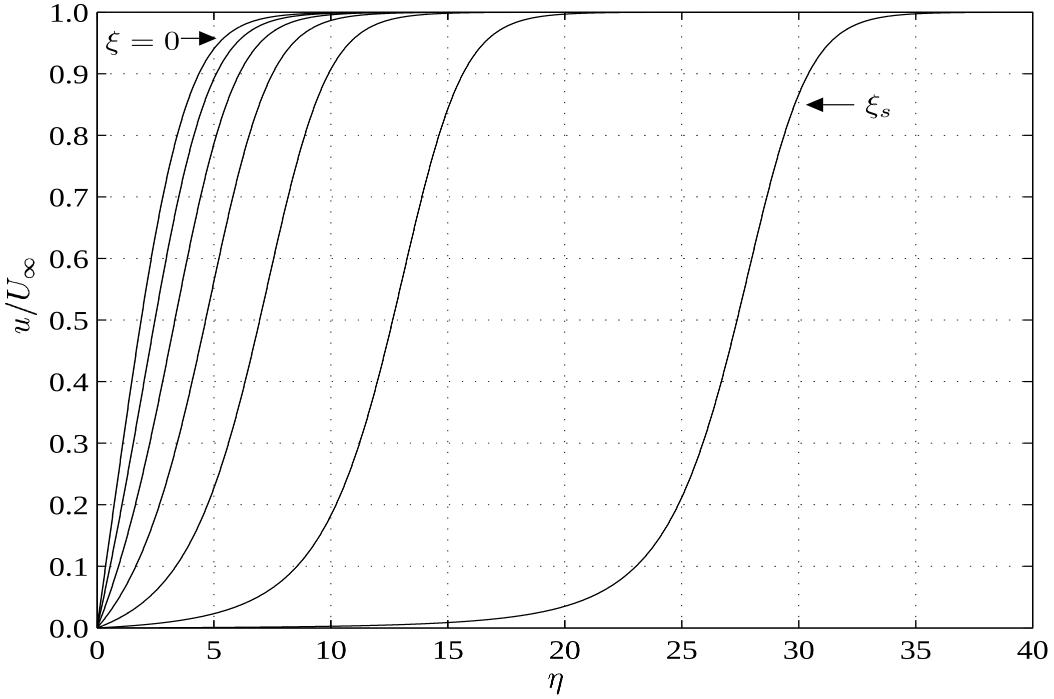

Figure 3.6: Velocity profiles for fluid index $n = 0.75$ at $\xi = 0.0, 0.2, \ldots, 1.0$ and the separation point ξ_s.

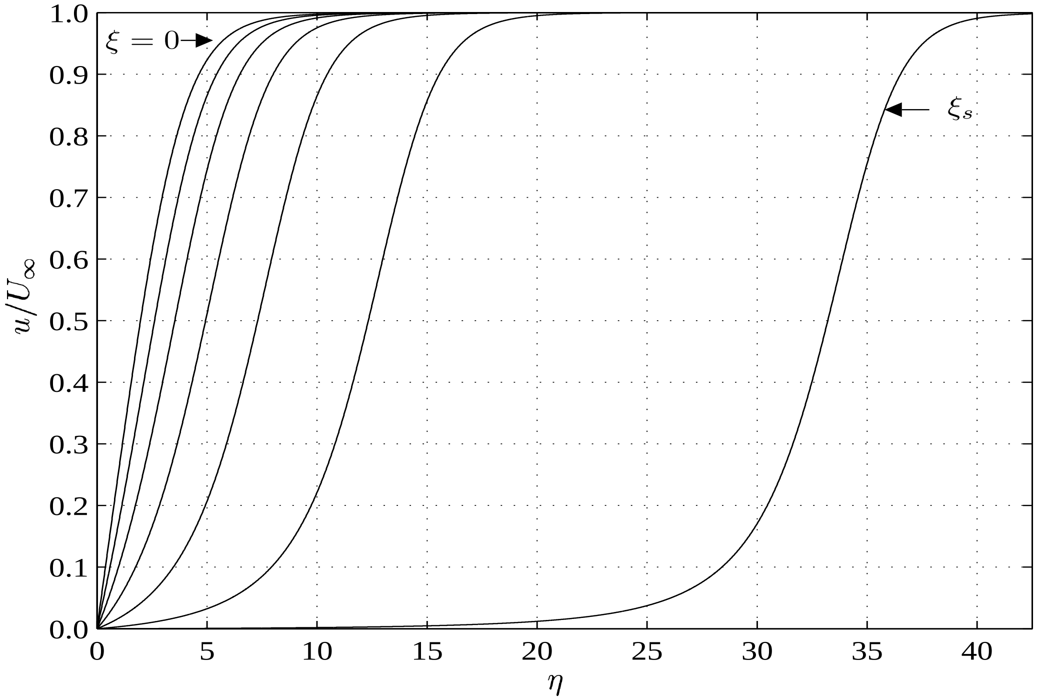

Figure 3.7: Velocity profiles for fluid index $n = 0.70$ at $\xi = 0.0, 0.2, \ldots, 1.0$ and the separation point ξ_s.

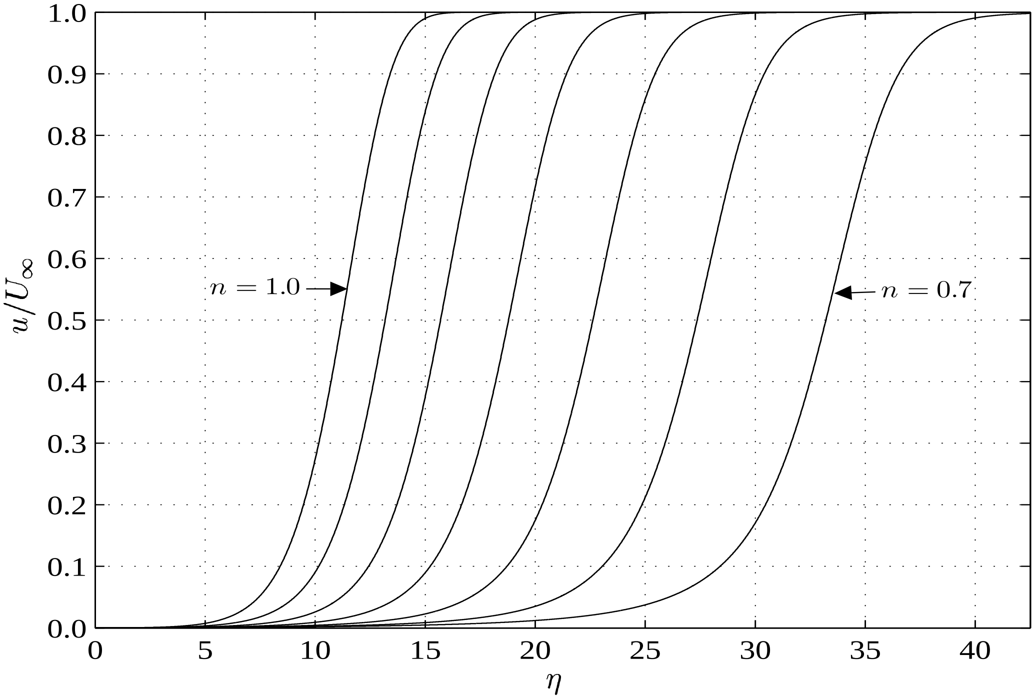

Figure 3.8: Velocity profiles for $n = 1.00, 0.95, \ldots, 0.70$ at the separation point ξ_s.

as the fluid index n is decreased, the size of the computational domain in the wall-normal direction is increased. An appropriate far-field value, η_∞, for each value of the fluid index n was determined via some experimentation.

A single, suitably large value for η_∞, for example 50.0, could have been used for all the numerical calculations performed. During early trials with the numerical marching scheme using different values of η_∞ it was found that if the far-field position, η_∞, was not sufficiently large then the numerical marching scheme would terminate prematurely. The velocity profile at this false 'separation' point exhibited a sharp, and physically unrealistic, transition to the free-stream velocity value. It was also found that an excessively large value of η_∞ did not change the location of the separation point nor the corresponding velocity profile. Hence, the value of η_∞ was selected in a manner that kept the running time of the numerical marching scheme to a minimum without compromising the results.

Figure 3.8 shows the velocity profiles at the point of 'separation' for the values of the fluid index n for which calculations have been carried out. This figure shows the importance of the correct selection of η_∞ for a given fluid index to allow the velocity profile to develop and

Fluid Index n	1.00	0.95	0.90	0.85	0.80	0.75	0.70
ξ_s	0.8596	0.8992	0.9444	0.9959	1.0548	1.1222	1.1992
x_s	0.7389	0.8464	0.9847	1.1660	1.4094	1.7449	2.2207

Table 3.1: Separation point for different fluid index values

converge properly as the point of separation is approached. We also see that for values of n close to unity, the velocity profile matches onto the free-stream for a relatively low value of η_∞ and using a larger value would not alter the results. The velocity profiles at the separation point also show a non-uniform spacing between each other. As the fluid index n decreases the spacing between velocity profiles at the point of separation increases. This indicates a non-linear relationship between the location of the separation point, ξ_s, and the fluid index n.

The location of the separation point in the computational co-ordinate, ξ_s, and the non-dimensionalised physical co-ordinate, x_s, for different values of the fluid index n is summarised in Table 3.1. A plot of the separation points, ξ_s, over the range of fluid index values n for which calculations were performed is shown in Figure 3.9.

We can see from Figure 3.9 that as the fluid index decreases the location of the separation point, in computational co-ordinates, moves further along the flat plate. A curve may be fitted through the points in Table 3.1, which would then allow the location of the separation point to be calculated for different values of the fluid index. Performing such a curve-fit results in $\xi_s = 0.8572n^{-0.9356}$ and a R^2 value of 0.9998, R^2 is the ‘coefficient of determination’. A more detailed analysis of the relationship between ξ_s and n would need to be performed to determine whether this empirical result is indeed correct; we do not pursue this here.

The reduced skin friction, τ_0, was calculated and monitored as the velocity profile was calculated at each streamwise location. The reduced skin friction has been plotted for $n = 1.00, 0.95, \ldots, 0.70$ and is shown in Figure 3.10. The calculation of the reduced skin friction at the wall is found to be equal to the initial condition $f''(0)$ used to find the solution of equation (3.15a) for different values of the fluid index. Hence for a given fluid index the reduced skin friction curve starts at the appropriate value of $f''(0)$ and then decreases smoothly toward zero at the separation point.

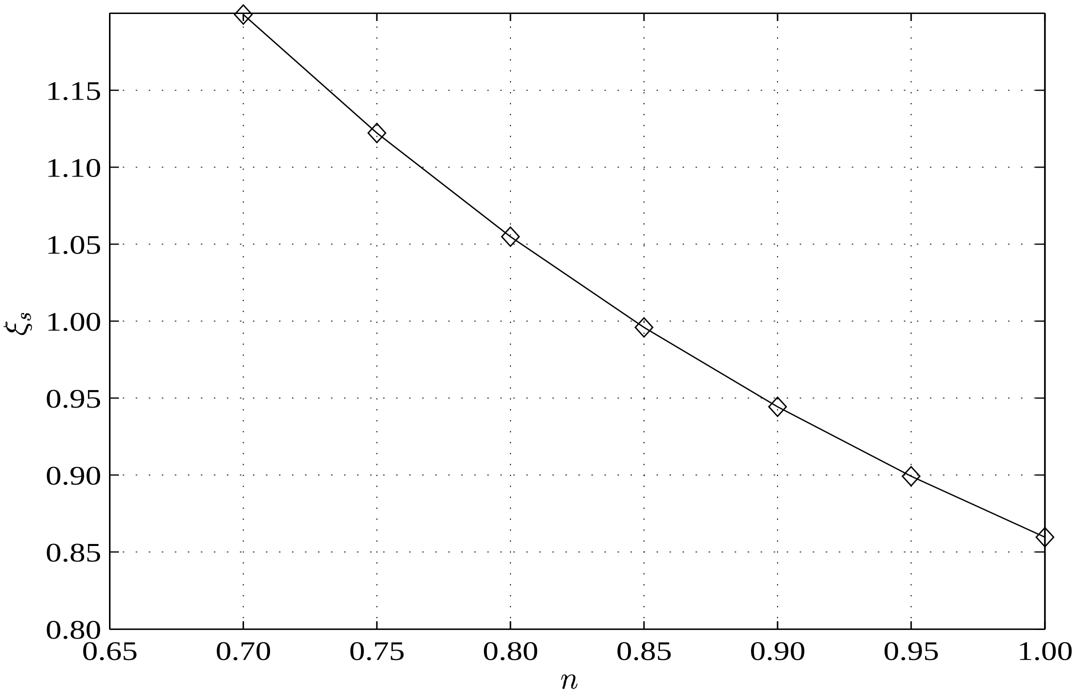

Figure 3.9: Separation point location, x_s, for different values of the fluid index n.

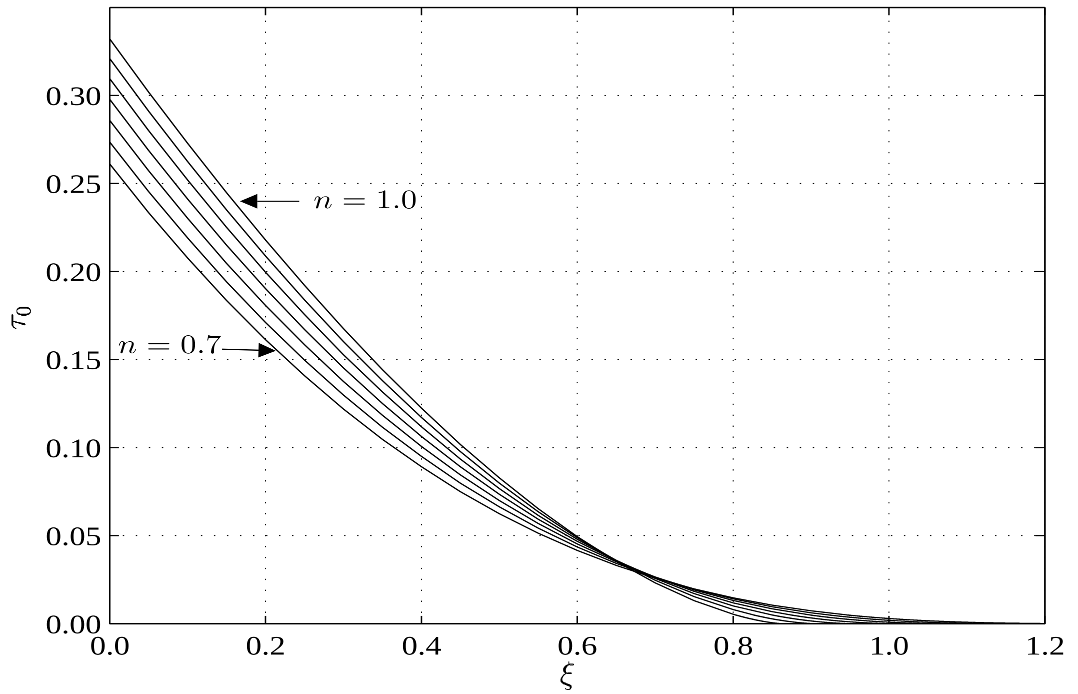

Figure 3.10: Reduced skin friction, τ_0, at different streamwise locations ξ down to the separation point for $n = 1.00, 0.95, \ldots, 0.70$.

The non-Newtonian, or apparent, viscosity in the Ostwald-de Waele fluid model is expressed as

$$\mu_{app} = K \left| \frac{\mathrm{d}u}{\mathrm{d}y} \right|^{n-1},$$

for the two-dimensional flow that is being considered. A commonly used definition for the fluid viscosity μ is that it is a measure of the internal friction, or resistance, that opposes the deformation, or flow, of the fluid. Hence, for a shear-thinning fluid with $0 < n < 1$, we see that when the velocity shear is large then the apparent viscosity decreases asymptotically to a constant value. As the velocity shear tends to a small value, then the apparent viscosity increases without bound. We note that this behaviour is a short-coming of the power-law viscosity model. Nonetheless, in the near neighbourhood of the flat plate where the velocity shear is relatively large, the apparent viscosity of a shear-thinning fluid is smaller than would be the viscosity of a Newtonian fluid in the presence of the same velocity shear. The shear-thinning fluid is, in effect, experiencing less friction (resistance) near the flat plate and is able to flow more freely along the surface. Though fluid is entering through the surface so as to induce boundary-layer separation, the point at which separation occurs is delayed due to the more freely flowing fluid in the streamwise direction.

3.3.2 Adverse Pressure Gradient

In Section 3.3.1 we have described how the boundary-layer flow of a shear-thinning power-law fluid will eventually undergo separation in the presence of mass transfer, specifically fluid injection, through the plate surface in conjunction with a uniform external flow. However, separation of a boundary-layer flow may also be induced by an external flow with a non-zero pressure gradient. For Newtonian fluids it is known that an adverse pressure gradient alone, with zero mass transfer through the surface, will eventually cause the boundary layer to become detached from the surface, as is described in Schlichting (1979). In this section we examine the effect that an external potential flow driven by an adverse pressure gradient, as well as mass transfer through the surface, has on the boundary-layer flow of a shear-thinning power-law fluid.

m	0.00	-0.01	-0.02	-0.03	-0.04	-0.05	-0.06	-0.07	-0.08
τ_0	0.3209	0.3009	0.2799	0.2575	0.2335	0.2073	0.1782	0.1450	0.1047

Table 3.2: Reduced skin friction for $n = 0.95$ and $m = -0.01, -0.02, \ldots, -0.08$, with zero mass transfer through the surface.

The form of the governing equation (3.6a) and boundary conditions (3.6b), as well as the numerical marching scheme, allows for a general external potential flow to be specified for the boundary-layer flow of a power-law fluid. Hence, for the shear-thinning fluids being considered here, we wish to determine the effect that the fluid index n has on the tendency of the boundary layer to separate from the flat plate for different values of the pressure gradient exponent m. In the Falkner-Skan class of flows, an adverse pressure gradient corresponds to negative values of m or β.

Firstly we examine the effect that an adverse pressure gradient alone will have on the boundary-layer flow of a shear-thinning fluid. The relevant parameters for the numerical marching scheme have been set as follows. The mass transfer rate (fluid injection velocity) at the surface was set to zero, the η step-size, h, for the uniform mesh in the wall-normal direction was set to 0.01, and the marching step-size, $\Delta\xi$, was set to 1.0×10^{-4}. The far-field boundary, η_∞, was set to 22.5. The fluid index was kept fixed at $n = 0.95$, while the pressure gradient exponent m was varied from $-0.1, \ldots, -0.9$ in steps of -0.1. As the pressure gradient parameter m, and hence β, is non-zero the initial velocity profile is given by the solution of the generalised Falkner-Skan equation (3.15a). The numerical marching scheme was, somewhat arbitrarily, stopped at the location $\xi = 2.0$ along the flat plate.

The numerical marching scheme was used to obtain solutions for this flow configuration. The reduced skin friction, τ_0, was calculated along the length of the plate and velocity profiles were sampled from selected ξ locations. For each of the pressure gradient exponents the reduced skin friction was found to be constant along the flat plate. The reduced skin friction values obtained are summarised in Table 3.2. For each value of m, the streamwise velocity profiles from the sampled ξ locations were compared and found to be identical (insofar as the accuracy of the numerical scheme is concerned) to each other. This indicated the existence of self-similar solutions for this flow regime.

From the results in Table 3.2, it can also be seen that the reduced skin friction decreases in a non-linear manner as the pressure gradient exponent m is made more negative. This behaviour indicates that at a critical value of m the initial velocity profile would correspond to that of a detached flow. When the numerical marching scheme was used with $m = -0.09$, the reduced skin friction along the flat plate varied about a value of 0.04. For this value of m, the boundary-layer flow was considered to be almost fully detached. A more accurate estimate for this critical value of m could not be determined here due to some numerical stability issues with the calculation of the initial velocity profile.

Additional calculations for other values of the fluid index n over a similar range of values of pressure gradient parameter m were also carried out. The results obtained were found to possess the same behaviour as what was observed and described for $n = 0.95$, but are not shown here. These results indicate that self-similar solutions exist for the boundary-layer flow of a shear-thinning power-law fluid with an adverse pressure gradient in the free-stream. Such self-similar solutions can be used to determine the critical value of m, see Chapter 4 and Denier and Dabrowski (2004).

Next we consider the effect that mass transfer through the surface has on the boundary-layer flow of a shear-thinning power-law fluid driven by an adverse pressure gradient. Mass transfer may involve either the injection or removal, via suction, of fluid through the surface. The effect of fluid removal, or suction, through the surface was investigated first. The control parameters for the numerical marching scheme were initially set to $\eta_\infty = 25$ with the η step-size h set to 0.025 for a power-law fluid with $n = 0.95$. A trial run of the numerical marching scheme indicated that the streamwise velocity profiles had matched onto the free-stream velocity well before $\eta_\infty = 25$. So for subsequent values of n the control parameters were reset to $\eta_\infty = 10$ with $h = 0.01$, primarily to lower the total execution time of the numerical marching scheme. The results obtained are summarised in Table 3.3.

In Table 3.3 there are two values for each combination of fluid index n and pressure gradient exponent m. The first value indicates the reduced skin friction at the leading edge, $\xi = 0$, of the flat plate and is obtained from the initial velocity profile. This value is purely for

	$n = 0.95$	$n = 0.90$	$n = 0.85$	$n = 0.80$	$n = 0.75$	$n = 0.70$
$m = -0.01$	0.300991	0.290256	0.279302	0.268206	0.257083	0.246066
	2.100628	2.194297	2.302853	2.432330	2.589363	2.783608
$m = -0.02$	0.279936	0.269991	0.259845	0.249685	0.239338	0.229243
	2.104100	2.198292	2.307241	2.436920	2.593833	2.787418
$m = -0.03$	0.257526	0.248513	0.239312	0.230025	0.220787	0.211744
	2.107526	2.202244	2.311587	2.441463	2.598249	2.791156
$m = -0.04$	0.233453	0.225563	0.218479	0.209350	0.201291	0.193464
	2.110890	2.206140	2.315878	2.445950	2.602599	2.794813
$m = -0.05$	0.207260	0.200764	0.194070	0.187317	0.180666	0.174270
	2.114175	2.209963	2.320099	2.450366	2.606873	2.798379
$m = -0.06$	0.178222	0.173532	0.168593	0.163573	0.158650	0.153978
	2.117361	2.213695	2.324235	2.454697	2.611057	2.801842
$m = -0.07$	0.145023	0.142856	0.140292	0.137556	0.134849	0.132328
	2.120422	2.217314	2.328264	2.458925	2.615137	2.805190
$m = -0.08$	0.104690	0.106623	0.107686	0.108258	0.108608	0.108916
	2.123330	2.220794	2.332165	2.463033	2.619097	2.808411
$m = -0.09$	0.044950	0.058118	0.066871	0.073408	0.078642	0.083054
	2.126046	2.224103	2.335913	2.467000	2.622922	2.811491

Table 3.3: Reduced skin friction at $\xi = 0.0$ and $\xi = 2.0$ for different fluid index values n and adverse pressure gradient m with suction.

reference, since the boundary-layer approximation is not strictly applicable at the leading edge. The second value is the reduced skin friction at $\xi = 2.0$, the end-point for the numerical marching scheme. These results indicate that suction through the surface has the effect of increasing the reduced skin friction with distance along the flat plate.

This set of results suggest some strategies for controlling the development of the boundary-layer flow of a shear-thinning fluid. For instance, starting with a fixed value of the fluid index n and with a boundary-layer flow that is almost detached, the mechanism of fluid suction through the surface can be used to control the manner in which the boundary layer develops and overcome its initial tendency to detach fully. Likewise, if the pressure gradient exponent m is prescribed and required to remain fixed, then selecting a suitable shear-thinning fluid in conjunction with fluid suction along the surface provides a means for controlling both the skin friction and the boundary-layer flow along the flat plate.

Lastly, we consider the effect that fluid injection, or blowing, through the surface in the presence of an adverse pressure gradient has on the boundary layer of a shear-thinning power-

m	0.00	-0.01	-0.02	-0.03	-0.04	-0.05
ξ_s	0.9444	0.6920	0.5747	0.4819	0.4010	0.3269

Table 3.4: Location of separation point for fluid index $n = 0.90$ for various pressure gradient values m with fluid injection.

m	0.00	-0.01	-0.02	-0.03	-0.04	-0.05
τ_0	0.1528	0.1340	0.1337	0.0907	0.0641	0.0287

Table 3.5: Reduced skin friction at $\xi = 0.3$ for fluid index $n = 0.90$ for various pressure gradient values m with fluid injection.

law fluid. We have seen that a boundary-layer flow driven by an adverse pressure gradient along with zero mass transfer through the surface experiences a decreasing skin friction as the value of m is made more negative. The boundary-layer flow may be described as tending to a state of detachment from the surface. Also recall that fluid injection alone, along with a zero pressure gradient, results in separation of the boundary layer from the surface. Hence, we expect that a combination of fluid injection along with an adverse pressure gradient should result in the boundary layer detaching, or separating, from the surface at a shorter distance from the leading edge of the plate than was observed before. A set of calculations were performed for a fluid index value of $n = 0.90$ to verify this. The far-field was set to $\eta_\infty = 32.5$, the η step-size h was set to 0.01 and mass transfer was switched to a constant rate of injection. Other control parameters for the numerical marching scheme were kept as for previous calculations.

The results obtained confirm that an adverse pressure gradient along with fluid injection will cause the boundary-layer flow to separate from the surface at a smaller distance from the leading edge of the plate than was found for a zero pressure gradient with fluid injection. The location of the point of separation for the values of the pressure gradient exponent m considered is summarised in Table 3.4.

A different way of gauging the effect of fluid injection in conjunction with an adverse pressure gradient is to select a reference location along the flat plate and compare the reduced skin friction at that point for various values of m. The values of the reduced skin friction taken at $\xi = 0.3$ along the flat plate are presented in Table 3.5. We see in Table 3.5 that the reduced skin friction is steadily decreasing as the external flow becomes more adverse or unfavourable along with constant fluid injection through the surface.

In this section we have seen that an adverse pressure gradient acting alone, i.e. with zero mass transfer through the surface, has the effect of decreasing the skin friction as the pressure gradient parameter m takes a more negative value. The boundary-layer flow of a shear-thinning power-law fluid eventually becomes detached from the surface at a critical value of m. Switching on fluid suction through the surface in the presence of an adverse pressure gradient causes the skin friction to increase with distance along the plate. The boundary-layer flow can be described as remaining attached to the plate. Fluid injection along with an adverse pressure gradient has the effect of advancing the onset of detachment of the boundary-layer flow.

3.3.3 Favourable Pressure Gradient

In this section we examine the effect that an external potential flow driven by a favourable pressure gradient has on the boundary-layer flow of a shear-thinning power-law fluid. A favourable pressure gradient occurs when the pressure gradient exponent m in the equation for the external velocity, given by $U_e(\xi) = C\xi^m$, takes positive values. For a Newtonian fluid ($n = 1$) driven by a favourable pressure gradient it is known that the boundary layer does not detach from the surface, see Schlichting (1979).

Calculations for $m = 0.01, 0.02, \ldots, 0.05$, with zero mass transfer rate at the surface, were carried out using the numerical marching scheme. The far-field was set to $\eta_\infty = 25.0$ and the η step-size was 0.025. The marching scheme started at $\xi = 0.0$ and stopped at $\xi = 1.0$, using a step-size $\Delta\xi = 1.0 \times 10^{-4}$. The fluid index used for these calculations was $n = 0.90$. The reduced skin friction values were found to be constant along the length of the flat plate for each value of m considered and are summarised in Table 3.6. These results confirm that the boundary-layer flow is self-similar and serve as a reference for later comparisons.

We also compared the streamwise velocity profiles at a fixed ξ station for the pressure gradient exponents m used in the calculations. Adopting a definition for the boundary-layer thickness

m	0.00	0.01	0.02	0.03	0.04	0.05
τ_0	0.30949	0.32786	0.34546	0.36238	0.37871	0.39448

Table 3.6: Reduced skin friction for fluid index $n = 0.90$ for various pressure gradient values m with zero mass transfer.

to be the value of η at which the streamwise velocity is 0.99 of the normalised free-stream velocity, it was found that the boundary-layer thickness decreases as the pressure gradient becomes more favourable, i.e. as m increases. Though calculations for other values of the fluid index n have not been carried out, this observation along with the values of the reduced skin friction in Table 3.6 can be taken to indicate that the boundary-layer flow of a shear-thinning power-law fluid remains attached to the surface while being driven by a favourable pressure gradient only.

In Section 3.3.2 the presence of fluid suction through the surface was shown to have the effect of increasing the skin friction. An increase in skin friction can be equated to a reduction of the boundary-layer thickness, as defined above, since both indicate that the boundary-layer flow is ‘hugging’ the surface. The combination of a favourable pressure gradient along with fluid suction is intuitively expected to produce a reduction of the boundary-layer thickness. Hence, the boundary-layer flow will ‘hug’ or adhere to the surface rather than separate away from the flat plate. Calculations for a boundary-layer flow driven by a favourable pressure gradient in combination with fluid suction through the surface were not undertaken. This was due to the expectation that the results produced by the numerical scheme would not differ significantly from the predicted outcome.

We can now consider the effect that a favourable pressure gradient along with fluid injection through the surface will have on the boundary-layer flow of a shear-thinning power-law fluid. The important question being whether the boundary-layer flow will eventually detach from the surface. For this set of calculations the mass transfer rate was 1.0 along the length of the plate. The numerical marching scheme started from $\xi = 0.0$ and stopped at $\xi = 2.0$, using a step-size of $\Delta\xi = 1.0 \times 10^{-4}$. The η step-size h was set to 0.01, but the far-field, η_∞, needed to be set to a value that depended on the fluid index, n, and the pressure gradient parameter m. The reason for using different values of η_∞ was to save on computation time by defining a

	$n = 0.95$	$n = 0.90$	$n = 0.85$	$n = 0.80$
$m = 0.01$	0.339869	0.327895	0.315554	0.302957
	0.004786	0.004535	0.004284	0.004033
$m = 0.02$	0.357988	0.345459	0.332619	0.319467
	0.009646	0.009139	0.008633	0.008127
$m = 0.03$	0.375371	0.362383	0.349094	0.335415
	0.014580	0.013813	0.013048	0.012278
$m = 0.04$	0.392100	0.378705	0.364982	0.350858
	0.019589	0.018558	0.017524	0.016487
$m = 0.05$	0.408245	0.394483	0.380371	0.365844
	0.024675	0.023373	0.022067	0.020755

Table 3.7: Reduced skin friction at $\xi = 0.0$ and $\xi = 2.0$ for different fluid index values n and favourable pressure gradient m with fluid injection.

solution domain so as to cover the region of the boundary layer where the flow was developing and was of interest. The reduced skin friction was calculated at each ξ location and the results are summarised in Table 3.7.

The results shown previously in Table 3.1 indicate that a boundary-layer flow driven by a zero pressure gradient external flow along with fluid injection will separate well before $\xi = 2.0$. For $n = 0.80$ the boundary layer was deemed to be separated at $\xi = 1.0548$. The results in Table 3.7 indicate that even a small favourable pressure gradient has the effect of delaying the separation of the boundary-layer flow from the surface. For $n = 0.80$, even though the reduced skin friction is very small at $\xi = 2.0$ the boundary layer is still considered to be attached to the surface. As the value of m increases, the values of the reduced skin friction at $\xi = 2.0$ also increases. These results are in agreement with the earlier observation that a favourable pressure gradient appears to cause the boundary layer to 'adhere' to the surface, while fluid injection is having the opposite effect by causing the boundary layer to detach from the surface. Whether the boundary layer remains attached to the surface or separates is determined by the interplay between a favourable pressure gradient and fluid injection through the surface. When the favourable pressure gradient dominates then the boundary-layer flow will remain attached to the surface, otherwise separation of the boundary layer will occur.

3.4 Numerical Results: Shear-thickening Fluids

The discussion in Section 3.3 addressed the nature of the boundary-layer flow of a shear-thinning power-law fluid. The numerical marching scheme used to find numerical solutions of the governing equations was tailored specifically for such fluids. We next consider the boundary-layer flow of shear-thickening power-law fluids.

The boundary-layer flow of a power-law fluid, either shear-thinning or shear-thickening, is governed by equation (3.6a). Applying the first step of the discretisation process gives us equation (3.8) which is valid for a power-law fluid in general. Multiplication of equation (3.8) by $\left(\frac{\mathrm{d}\widehat{q}}{\mathrm{d}\eta}\right)^{1-n}$ is not required for shear-thickening fluids. Proceeding with the discretisation process as was done in Section 3.2, the resulting form of the equation governing the boundary-layer flow of a shear-thickening fluid is

$$\begin{aligned}(\widehat{q}_{j+1} - 2\widehat{q}_j + \widehat{q}_{j-1}) \left|\frac{\widehat{q}_{j+1}-\widehat{q}_{j-1}}{2h}\right|^{n-1} &+ \left\{ h^3 \sum_{r=0}^{j}{}'' \left[\left(\frac{(2n-1)(\beta_1-\beta_2)-2n\theta}{2(n+1)}\right) q_{1r} \right.\right. \\ &+ \left.\left. \left(\frac{(2n-1)\beta_2+n\theta+1}{n+1}\right)\widehat{q}_r \right] - K^*_{in} \right\} \left(\frac{\widehat{q}_{j+1}-\widehat{q}_{j-1}}{2h}\right) \\ &+ h^2 \left\{ \widehat{\beta}(1-q_1^2)_j - \left(2\beta_2 + \frac{n\theta}{n+1}\right)\widehat{q}_j(\widehat{q}-q_1)_j \right\} = 0.\end{aligned}$$

The resulting system of non-linear algebraic equations will need to be solved by an iterative procedure very similar to that used for shear-thinning fluids. The function $f_j(\widehat{\mathbf{q}})$ that defines the non-linear algebraic equation at mesh point j in the presence of a Falkner-Skan flow in the free-stream is given by

$$\begin{aligned}f_j\left(\widehat{\mathbf{q}}^{(k)}\right) = &\left(\widehat{q}_{j+1}^{(k)} - 2\widehat{q}_j^{(k)} + \widehat{q}_{j-1}^{(k)}\right) \left|\frac{\widehat{q}_{j+1}^{(k-1)} - \widehat{q}_{j-1}^{(k-1)}}{2h}\right|^{n-1} \\ &+ \left\{ h^3 \left[\left(\frac{(2n-1)\beta+n\theta+1}{n+1}\right)\left(\widehat{q}_1^{(k)} + \ldots + \widehat{q}_{j-1}^{(k)} + \frac{1}{2}\widehat{q}_j^{(k)}\right) - \right.\right. \\ &\left.\left. \frac{n\theta}{n+1}\left(q_{1,1} + \ldots + q_{1,j-1} + \frac{1}{2}q_{1,j}\right)\right] - K^*_{in}\right\} \left(\frac{\widehat{q}_{j+1}^{(k)} - \widehat{q}_{j-1}^{(k)}}{2h}\right) \\ &+ h^2 \left\{ \beta(1-q_1^2)_j - \left(2\beta + \frac{n\theta}{n+1}\right)\widehat{q}_j^{(k)}(\widehat{q}^{(k)} - q_1)_j \right\}. \end{aligned} \tag{3.16}$$

Equation (3.16) generates a system of non-linear algebraic equations that are solved over the same uniformly spaced mesh as was used for shear-thinning fluids. The Jacobian matrix required by the Newton iteration procedure is slightly different to that used for shear-thinning fluids. The specific form of the Jacobian matrix can be derived from the above equation and is given in Appendix A.

The numerical scheme defined by equation (3.16) was implemented as a Fortran computer program. As the form of the governing equation for a shear-thickening fluid is different to that for a shear-thinning fluid, the implemented computer code was put through a validation check. Setting $n = 1$ in equation (3.16) yields the flow of a Newtonian fluid as was considered by Catherall et al. (1965). Hence, the parameter settings used to validate the numerical scheme for shear-thinning fluids were used to validate the numerical scheme for shear-thickening fluids. The separation point was found to be located at $\xi_s = 0.8596$, or $x_s = 0.7389$, and this was taken as confirmation that the implementation of the numerical scheme was correct.

Just as was the case for shear-thinning fluids, an initial velocity profile is required to start the numerical marching scheme for shear-thickening fluids. Such an initial velocity profile is provided by the solution of equation (3.15a) with the fluid index in the range $1 < n < 2$. However, it is found that the solution 'hits' unity at a finite value of η rather than asymptotically approaching the free-stream value. The common practice is to then 'pad' the remainder of the initial velocity profile with 1's out to η_∞. Since the width of the boundary layer decreases as $n \to 2$, the solution domain for the numerical scheme can also be decreased rather than needing to be extended as was needed for shear-thinning fluids. Difficulties with finding the solution to equation (3.15a) when $1 < n < 2$ are discussed in more detail in Chapter 4 as well as in Denier and Dabrowski (2004).

The numerical scheme could now be used to investigate the behaviour of the boundary-layer flow of a shear-thickening fluid under different free-stream flow conditions along with injection through the flat plate.

3.4.1 Zero Pressure Gradient

The numerical scheme has been designed to handle the Falkner-Skan class of flows, where the external flow is described by $U_e(x) \propto x^m$. We first consider the boundary-layer flow of a shear-thickening fluid driven by an external flow with a zero pressure gradient. Such a flow regime is obtained by setting $m = 0$ so that the external flow has constant velocity and pressure gradient parameter β is zero.

The numerical marching scheme was then used to investigate shear-thickening fluids with $n = 1.05, 1.10, \ldots, 1.30, 1.40, 1.50$. The far-field η_∞ was set to 20 and all other parameters for the numerical marching scheme were the same as was used for the shear-thinning fluids. This choice for η_∞ was dictated by the finite width of the boundary layer observed during the calculation of the initial velocity profile.

It was found that the numerical marching scheme failed to progress along the flat plate to a point of separation for all the values of n considered apart from $n = 1.10$. The numerical scheme would start at $\xi = 0$ and progress to a ξ location at which convergence to a solution could not be achieved because either the maximum number of iterations was exceeded or numerical overflow occurred. The ξ location at which the numerical scheme stopped varied with the value of n being considered. As the value of n increased it was noted that the stopping location for the numerical scheme was closer to the leading edge of the flat plate. For $n = 1.10$ the numerical scheme progressed along the flat plate to a separation point at $\xi_s = 0.7935$.

This behaviour of the numerical scheme for shear-thickening fluids was both unexpected and puzzling. We considered the possibility that the choice of η_∞ was inappropriate, so a set of calculations was performed with $\eta_\infty = 25$ using the same set of fluid index values. It was found that the numerical scheme produced essentially the same results as were obtained previously with $\eta_\infty = 20$. A third set of calculations was carried out with $\eta_\infty = 15$. For this value of η_∞ it was found that the numerical scheme marched to a point of separation for $n = 1.05$ and 1.10. The separation point was located at $\xi_s = 0.8246$ and 0.7935 respectively. For the remaining values of n considered the numerical scheme failed to converge to a solution.

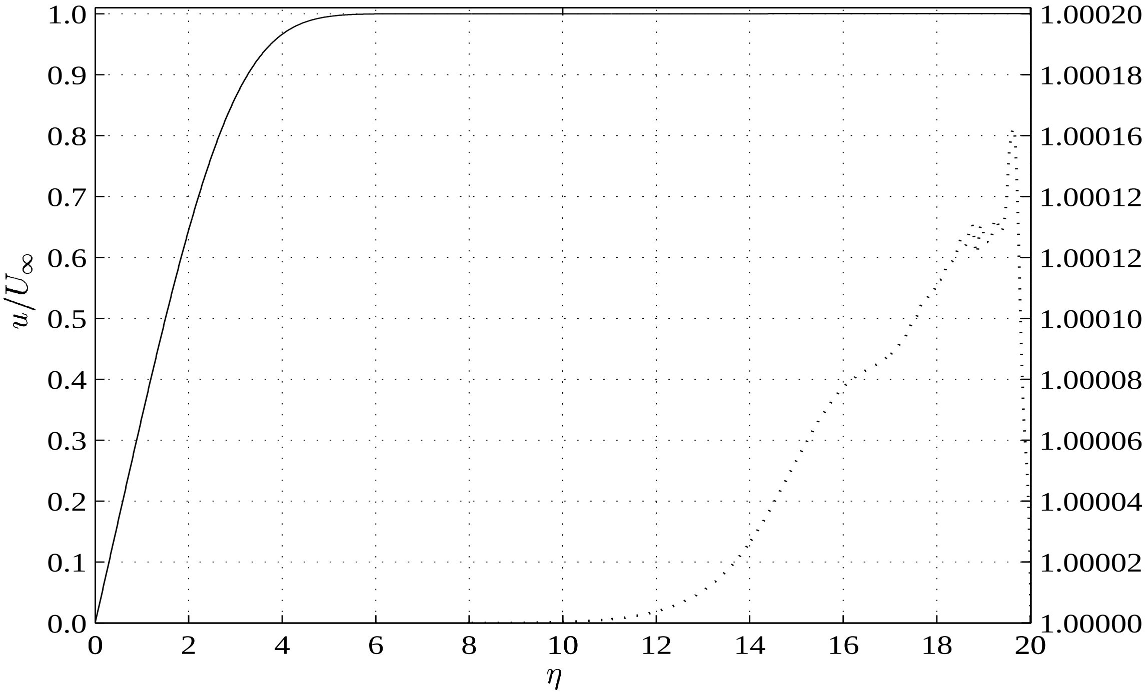

Figure 3.11: Streamwise velocity profile for a shear-thickening fluid ($n = 1.05$) at $\xi = 0.006$ (solid line). Overshooting of the solution and 'jittery' behaviour indicated by dashed line.

In Figure 3.11 the streamwise velocity profile for $n = 1.05$ and $\eta_\infty = 20$ at $\xi = 0.006$, the location where the numerical marching scheme stopped, is shown. This velocity profile appears to satisfy the asymptotic far-field condition of matching onto the free-stream. However, a closer examination reveals the presence of overshoot, albeit a rather small one, in the calculated velocity profile. For $\eta_\infty = 25$ the numerical marching scheme stopped at $\xi = 0.0051$ and an examination of the resulting velocity profile reveals the presence of overshoot over a finite range of η values. The velocity profiles for $n = 1.15$ and 1.20 were also checked and velocity overshoot was observed for the different far-field values of η_∞, except when numerical overflow occurred.

The velocity profiles produced by the numerical marching scheme for $n = 1.10$, and 1.05 with $\eta_\infty = 15$, were also examined for evidence of overshoot. The velocity profiles converged to the far-field boundary condition and showed no graphical evidence of overshoot. For shear-thinning fluids we observed that as n took values smaller than unity, the location of the point of separation moved progressively further away from the leading edge of the flat plate. Hence, for shear-thickening fluids we would expect that the point of separation should occur nearer to the leading edge as n takes values greater than unity. The partial set of results obtained for $n = 1.05$ and 1.10 appear, though tentatively, to support this expectation.

The reason as to why this numerical scheme for shear-thickening fluids does not, in general, converge to a solution needs to be considered. One potential explanation arises from the fact that the numerical scheme is represented by equation (3.16) which is a discretised approximation to equation (3.6a). Thus the numerical scheme may converge to a solution of the discretised equation, though this solution is not guaranteed to be valid for the original continuous form of the governing equation. A more detailed examination of the velocity profile at the separation point for $n = 1.10$ reveals very small variations about unity in the far-field. Even though these variations are smaller than the inherent accuracy of the numerical scheme, their presence suggests that this numerical scheme may possess some poor convergence properties and may be very sensitive to the solution mesh and/or initial conditions. An examination of corresponding velocity profiles for shear-thinning fluids reveals a monotonic approach to unity in the far-field. This suggests that the numerical scheme for shear-thinning fluids has better behaved convergence properties. A different possibility is that the power-law viscosity model, and the solution resulting from the governing equation, is not entirely applicable to the boundary-layer flow of shear-thickening fluids. We will consider this question further in Chapter 4.

3.5 Chapter Summary

In this chapter the set of partial differential equations governing the boundary-layer flow of a generalised Newtonian fluid were introduced. Then a co-ordinate transformation was applied to yield a corresponding integro-differential equation. A general numerical marching scheme was developed to solve this integro-differential equation which was subsequently adapted to deal with shear-thinning power-law fluids.

The numerical marching scheme was used to investigate the effect of the fluid index n on the point of separation of a boundary-layer flow under the influence of a zero pressure gradient with a constant rate of fluid injection. It was found that as the fluid index n was made smaller the point of separation ξ_s was located at larger distances from the leading edge of the flat plate.

When the boundary-layer flow was being driven by an adverse pressure gradient with zero mass transfer the reduced skin friction was constant along the flat plate, though it did decrease as the value of m was made more negative. The existence of a critical value of m for each fluid index n was apparent, but it could could not be determined using the extant numerical method. The boundary-layer flow driven by an adverse pressure gradient only is self-similar. The effect of fluid suction through the surface along with the adverse pressure gradient was to cause the reduced skin friction to increase with distance along the plate, thus decreasing its susceptibility to separate. Fluid injection through the surface in the presence of an adverse pressure gradient was seen to have the effect of causing the point of separation of the boundary layer to be located at shorter distances from the leading edge of the flat plate.

When a favourable pressure gradient with zero mass transfer was driving the boundary-layer flow the reduced skin friction remained constant along the flat plate, but its value increased as the value of m increased. The results indicate that self-similar solutions exist for the boundary-layer flow when the pressure gradient is favourable. The effect of the favourable pressure gradient can be described as causing the boundary-layer thickness to decrease as the value of m increases. The introduction of fluid injection through the surface, along with a favourable pressure gradient, has the effect of causing the skin friction to decrease with distance along the surface. Though not verified with numerical calculations, the results suggest that eventually a point of separation would occur at a sufficient distance down-stream from the leading edge. The location of the separation point is likely to be determined by the relative dominance of either the favourable pressure gradient or the rate of fluid injection.

The results obtained indicate that the boundary-layer flow of a shear-thinning power-law fluid is qualitatively similar to that of a Newtonian fluid. The fluid index n provides an additional ‘degree of freedom’ that can be used in conjunction with mass transfer through the surface and the external pressure gradient to provide a means for control of the boundary layer.

The numerical marching scheme was modified to investigate the boundary-layer flow of shear-thickening fluids. However, it was found that the numerical scheme failed to converge to a solution at a ξ location that was a very short distance past the leading edge of the flat plate for most values of n considered. Some results support the intuitive expectation that the boundary layer separation point for shear-thickening fluids should move toward the leading edge. While an alternate formulation of the marching scheme could possibly provide better results, the underlying power-law viscosity model may itself be inappropriate for shear-thickening fluids. We investigate this matter further in Chapter 4.

Chapter 4

Similarity-type Solutions for a Power-law Fluid

The equations describing the boundary-layer flow of a power-law fluid along a flat plate are non-linear in character. An exact solution cannot be easily found and numerical methods, as described in Chapter 3, are used to provide approximate solutions. However, important insights into the main physical features that may exist within the boundary layer are provided by self-similar solutions to the boundary-layer equations. Similarity-type solutions are known, and have been extensively studied, for flows such as the flat plate, Falkner-Skan, converging channel and Goldstein. Additionally, self-similar solutions often serve as the basis for other methods that are used to study more complex non-similar flows.

Investigations into self-similar solutions of the boundary-layer flow of power-law fluids can be considered to have started with the work of Schowalter (1960) and Acrivos et al. (1960). Both investigators looked at flow along a flat plate and give the form of the similarity transformation as well as the ordinary differential equation from which a self-similar solution is obtained. Acrivos et al. (1960) presented some solutions to the governing Blasius-like differential equation for the case of zero mass transfer through the surface of the plate. The external flow is assumed to be uniform in these investigations.

Lee and Ames (1966) consider the form of the similarity transformation for a number of different non-Newtonian fluids. For power-law fluids they considered various external flow regimes and gave the form of the ordinary differential equations governing these flows. A Falkner-Skan-type equation for power-law fluids is derived therein using group-theoretic methods. Self-similar velocity profiles are provided by the solutions of these differential equations.

A self-similar solution for the boundary-layer flow of a power-law fluid with mass transfer through the surface is discussed by Nachman and Taliaferro (1979). They show that similarity is preserved when the function describing mass transfer through the surface is of a specific form that depends on the streamwise location. They also show that the fluid injection rates need to lie in a critical range to ensure self-similar velocity profiles.

In this chapter we derive a version of the Falkner-Skan-type equation for power-law fluids that is used in subsequent discussions. The derivation is in the style presented by Schlichting (1979) rather than the group-theoretic approach used by Lee and Ames (1966). In Section 4.2 we focus specifically on the case of an external flow with a zero pressure gradient so that the Falkner-Skan-type differential equation reduces to a Blasius-like form. We also look at the asymptotic form of the solution in the far-field. Some techniques for obtaining a numerical solution of the Blasius-like differential equation are discussed and the solutions found are shown. In Section 4.3 we look at solutions of the Falkner-Skan-type differential equation for various non-zero values of the pressure gradient parameter.

4.1 Derivation of Governing Equation

The equations governing the boundary-layer flow of a power-law fluid, as derived in Chapter 2, are

$$\frac{\partial u}{\partial x}+\frac{\partial v}{\partial y}=0, \tag{4.1a}$$

$$u\frac{\partial u}{\partial x}+v\frac{\partial u}{\partial y}=-\frac{\mathrm{d}p}{\mathrm{d}x}+n\left|\frac{\partial u}{\partial y}\right|^{n-1}\frac{\partial^2 u}{\partial y^2}, \tag{4.1b}$$

and the corresponding boundary conditions are

$$u = 0, \quad v = V(x) \quad \text{on} \quad y = 0, \tag{4.1c}$$

$$u \to U_e(x) \quad \text{as} \quad y \to \infty. \tag{4.1d}$$

These boundary conditions reflect the physical requirement that the fluid flow satisfies full viscous no-slip at the surface and mass transfer rate through the surface that may vary with streamwise distance. We will take the normal flow through the surface to be constant, possibly zero. The streamwise velocity within the boundary layer is required to match smoothly onto the free-stream at a large distance from the surface. The mass transfer taking place through the surface may be constant along the entire length being considered or it may vary with streamwise location along the surface. Furthermore, this mass transfer may be either injection of fluid into, or suction of fluid from, the boundary layer.

By considering the behaviour of the x-momentum equation at a large distance from the surface, or alternatively by making use of Bernoulli's equation, it is found that $-\frac{\mathrm{d}p}{\mathrm{d}x} = U_e(x)\frac{\mathrm{d}U_e}{\mathrm{d}x}$, where $U_e(x)$ describes the external flow as a function of distance along the surface.

Prescribing a particular form for the external flow, $U_e(x)$, results in a specific type of self-similar solution for the boundary-layer flow. If the external flow is of the form $U_e(x) = Cx^m$ then the self-similar solutions are referred to as being of Falkner-Skan-type. Flows over a flat plate are included in the family of Falkner-Skan solutions and are recovered by letting $m = 0$. For Newtonian fluids the constant C depends only on the parameter m, while for the class of non-Newtonian fluids being considered here C will also depend on the fluid index n.

We proceed to derive the differential equation governing the boundary-layer flow of a power-law fluid for which self-similar solutions are to be found by introducing a similarity variable defined by

$$s(x, y) = y\left\{\frac{(2n-1)m+1}{n+1}\,\frac{U_e^{2-n}}{x}\right\}^{\frac{1}{n+1}}. \tag{4.2}$$

We also make use of the stream function ψ defined by

$$\psi(x,y) = f(s)\left\{\frac{n+1}{(2n-1)m+1}\,U_e^{2n-1}x\right\}^{\frac{1}{n+1}}, \tag{4.3}$$

where $f(s)$ is a dimensionless stream function. A more detailed description of the derivation of this specific form of the similarity variable s and stream function ψ is given in Appendix B.

The stream function ψ identically satisfies the continuity equation (4.1a), while the $x-$momentum equation (4.1b) is transformed into the Falkner-Skan-like ordinary differential equation

$$nf'''|f''|^{n-1} + f''f + \beta(1-(f')^2) = 0, \tag{4.4}$$

where primes denote differentiation with respect to the similarity variable s. The quantity β, referred to as the pressure gradient parameter, is given by

$$\beta = \frac{(n+1)m}{(2n-1)m+1},$$

and the velocity components u and v are given by

$$u = U_e f', \tag{4.5a}$$

$$v = -\left\{\left(\frac{(2n-1)m+1}{n+1}\right)^n C^{2n-1}x^{(2n-1)m-n}\right\}^{\frac{1}{n+1}}\left[f - \frac{(n-2)m+1}{(2n-1)m+1}\,sf'\right]. \tag{4.5b}$$

We observe that setting $n = 1$ for the fluid index, which corresponds to a Newtonian fluid, results in the similarity variable s, the stream function ψ, as well as equation (4.4) being reduced to the well-known forms associated with Falkner-Skan flows; see Schlichting (1979). We also note that this form of equation (4.4) is equivalent to that given by Lee and Ames (1966), the main difference being in the choice of coefficients of the corresponding terms in the Falkner-Skan-like differential equation.

The boundary conditions (4.1c) and (4.1d) are transformed into

$$f(0) = -V(x)\left\{\left(\frac{(2n-1)m+1}{n+1}\right)^{n} C^{2n-1}x^{(2n-1)m-n}\right\}^{-\frac{1}{n+1}}, \tag{4.6a}$$

$$f'(0) = 0, \tag{4.6b}$$

$$f'(s) \to 1 \quad \text{as} \quad s \to \infty. \tag{4.6c}$$

To find self-similar solutions we require that equation (4.4) and the accompanying boundary conditions are independent of the original variables x and y. The boundary condition (4.1c) that permits mass transfer through the surface has become (4.6a) as a result of introducing the similarity variable s. The presence of x in this boundary condition means that a self-similar solution for equation (4.4) cannot be obtained. However, the form of the function $V(x)$ describing the mass transfer through the surface may be chosen so to ensure the existence of a self-similar solution. Letting $V(x) = V_0 x^{\frac{(2n-1)m-n}{n+1}}$ allows the boundary condition (4.6a) to be expressed as

$$f'(0) = -V_0\hat{C}(m,n), \tag{4.7}$$

where both V_0 and $\hat{C}(m,n)$ are constants. This form for $V(x)$ is not unlike that used by Nachman and Taliaferro (1979) in their discussion of the boundary-layer flow of a power-law fluid along a flat plate in the presence of similarity-preserving mass transfer. Hence, a self-similar solution can be sought for equation (4.4) subject to boundary conditions (4.6b), (4.6c) and (4.7).

The nature of the flow being considered determines the form that the boundary conditions that accompany equation (4.4) ultimately take. Even though the boundary-layer flow discussed in Chapter 3 involved fluid injection at the surface, we will focus on flows with zero mass transfer through the surface as this case still provides useful insights into the structure of the boundary layer. Hence, self-similar solutions to equation (4.4) will be sought subject to the following boundary conditions

$$f = f' = 0 \quad \text{on} \quad s = 0, \tag{4.8a}$$

$$f' \to 1 \quad \text{as} \quad s \to \infty. \tag{4.8b}$$

Equation (4.4) and the boundary conditions (4.8) constitute a third-order non-linear two-point boundary value problem that has no known analytic solutions (except in the degenerate case when $n = 2$) and needs to be solved by a numerical scheme. Techniques for obtaining solutions to such boundary value problems are often based on simple shooting, finite-differences or collocation. The method of simple shooting is used to obtain solutions to equation (4.4), these solutions are discussed in the following sections.

We proceed by firstly finding solutions to equation(4.4) when $\beta = 0$, which describes the boundary-layer flow along a flat plate. These solutions will, hopefully, provide an intuitive understanding of the structure in the boundary-layer for this simple flow geometry. Solutions for non-zero values of β are subsequently discussed in Section 4.3.

4.2 Zero Pressure Gradient($\beta = 0$)

The choice of $\beta = 0$ has the geometric interpretation of corresponding to a potential flow over a flat plate, for which $u \to U_e$ (constant) as $s \to \infty$. Hence, without loss of generality, we set $U_e(x) = 1$. For this choice of β, equation (4.4) simplifies to the following form

$$f''' + \frac{1}{n} f (f'')^{2-n} = 0, \tag{4.9}$$

subject to the boundary conditions (4.8).

We note that equation (4.9) is essentially of the same form as that given by Acrivos et al. (1960), where a different coefficient appears due to a slight difference in the choice of the similarity variable. This equation is a third-order non-linear two-point boundary value problem that can only be solved by a suitable numerical method. A number of different numerical methods are available for finding the numerical solution of equation (4.9) and we next provide a description of one such method. After the numerical method has been used to find solutions of equation (4.9), we shall also discuss the asymptotic behaviour of these solutions in the far-field.

4.2.1 Numerical Solution

As indicated previously, the non-linear form of equation (4.9) means that a numerical technique needs to be employed to find a solution. Boundary value problems must be solved at all points in the solution domain simultaneously, oftem using methods based on finite-difference approximations. The presence of the $(f'')^{2-n}$ term in equation (4.9) would make a method based on finite-differences somewhat awkward, quite apart from the matter of the semi-infinite solution domain. In contrast, initial value problems can be solved by a stepwise, or 'marching', procedure. In this sense, initial value problems are easier to solve. This marching method for solving initial value problems may be adapted and used to solve boundary value problems. The resulting technique is known as the 'shooting' method and we use this method to numerically solve equation (4.9).

The shooting method is based on the idea of converting a boundary value problem into an equivalent initial value problem and integrating by marching from the initial point to the terminal point. As part of the conversion step, it is necessary to specify extra initial conditions and iteratively adjust them until the required conditions at the terminal point are satisfied. To solve equation (4.9) with the shooting method, the asymptotic boundary condition is replaced by an initial condition for $f''(0)$ and integrated from $s = 0$ to a large value of s where $f'(\infty) = 1$ is deemed to be satisfied. The selection of the correct value for $f''(0)$ may be done with a trial-and-error approach or, as is more common, a Newton iteration scheme that converges to the correct value of $f''(0)$ is used.

Acrivos et al. (1960) indicate, but give no details, that a method originally devised by Töepfer for the Blasius equation that requires no guessing for $f''(0)$ can also be used for solving equation (4.9). Rosenhead (1963) provides details of how this method is used to solve the Blasius equation. Here we give a brief description of the method and discuss its suitability for finding numerical solutions to equation (4.9).

It can be verified that equation (4.9) is scale-invariant to the transformation defined by

$$\overline{s} = a^{2-n} s$$

$$\overline{f}(\overline{s}) = a^{1-2n} f,$$

where a is an arbitrary 'constant of homology'. When this transformation is applied to equation (4.9) the following associated ordinary differential equation is obtained

$$\overline{f}''' + \frac{1}{n}\overline{f}(\overline{f}'')^{2-n} = 0, \tag{4.10}$$

where the prime indicates differentiation with respect to $\overline{s}$. The boundary conditions given at $s = 0$ become $\overline{f}(0) = \overline{f}'(0) = 0$, while the asymptotic boundary condition becomes

$$\lim_{s\to\infty} f'(s) = a^{n+1} \lim_{\overline{s}\to\infty} \overline{f}'(\overline{s}).$$

Since $f'(\infty) = 1$, the far-field boundary condition for equation (4.10) takes the form

$$\lim_{\overline{s}\to\infty} \overline{f}'(\overline{s}) = \frac{1}{a^{n+1}}.$$

Hence, the associated differential equation (4.10) has the same initial conditions as equation (4.9), but the asymptotic boundary condition requires the solution to converge to a different and unknown value, viz. $\frac{1}{a^{n+1}}$.

It would seem that little benefit has been gained from the use of this transformation, as it is still necessary to specify either $f''(0)$ or $\overline{f}''(0)$ to solve equation (4.9) or equation (4.10) respectively. However, we note that $f''(0) = a^3\overline{f}''(0)$, where with a specified $\overline{f}''(0)$ and a known value of a we can calculate the required $f''(0)$. Since $\overline{f}''(0)$ is completely arbitrary we set it equal to unity. The value of a is determined from the far-field solution of equation

(4.10). Hence, the additional initial condition for $f''(0)$ needed to solve equation (4.9) is given by

$$f''(0) = \left\{ \lim_{\overline{s} \to \infty} \overline{f}'(\overline{s}) \right\}^{-\frac{3}{n+1}} . \tag{4.11}$$

The numerical method for finding the solution to equation (4.9) consists of two stages. First, solve the initial value problem posed by equation (4.10) for $\overline{f}(\overline{s})$ subject to the initial conditions $\overline{f}(0) = \overline{f}'(0) = 0$ and $\overline{f}''(0) = 1$. The integration is carried out to a suitably large $\overline{s}_\infty$ at which the value of $\overline{f}'$ is considered to have satisfied the asymptotic boundary condition. This is indicated by a plateau on the plot of $\overline{f}'$, as well by meeting an appropriate stopping condition. The value of $f''(0)$ is then calculated with sufficient accuracy according to equation (4.11). Secondly, solve equation (4.9) for $f(s)$ starting with initial values $f(0) = f'(0) = 0$, and the newly found value of $f''(0)$. This two stage numerical process eliminates the iterative search for $f''(0)$ that is common in standard shooting methods. It is also described as being quite stable and as having no significant build-up of error.

This numerical method was implemented as a Matlab script employing the Runge-Kutta solver `ode45`, essentially to rapidly prototype the method and check its effectiveness. It was also implemented as a Fortran program based on a standard fourth order Runge-Kutta single-step integrator. The method was tried for various values of n and far-field locations $\overline{s}_\infty$ to check the behaviour of the value of $\overline{f}'$ in the far-field. The values of $\overline{f}'(\overline{s}_\infty)$ obtained are shown in Table 4.1.

The results in Table 4.1 indicate that for values of the fluid index slightly less than unity the solution to equation (4.10) in the far-field, $\overline{f}'(\overline{s}_\infty)$, has converged to a constant value. For fluid index values below 0.7 there is still some variability in the values of $\overline{f}'(\overline{s}_\infty)$. However, as $\overline{s}_\infty$ takes progressively larger values it is seen that more digits in the value of $\overline{f}'(\overline{s}_\infty)$ remain unchanged. For example, for $n = 0.4$ we have $\overline{f}'(\overline{s}_\infty = 50) - \overline{f}'(\overline{s}_\infty = 25) = 0.000179$, whereas $\overline{f}'(\overline{s}_\infty = 150) - \overline{f}'(\overline{s}_\infty = 125) = 0.0000017$. Hence, for small values of n we can ensure that $\overline{f}'(\overline{s}_\infty)$ has converged to an appropriate accuracy by choosing a sufficiently large value of $\overline{s}_\infty$. By calculating $\overline{f}'(\overline{s}_\infty)$ to a high level of accuracy, we are then able to ensure that the initial condition $f''(0)$ for the solution of equation (4.9) is also known to a high accuracy.

n	$\overline{s}_\infty = 25$	$\overline{s}_\infty = 50$	$\overline{s}_\infty = 75$	$\overline{s}_\infty = 100$	$\overline{s}_\infty = 125$	$\overline{s}_\infty = 150$
0.1	1.0460786	1.0478182	1.0483143	1.0485413	1.0486691	1.0487502
0.2	1.2581674	1.2593406	1.2596233	1.2597402	1.2598014	1.2598381
0.3	1.3803195	1.3808658	1.3809717	1.3810102	1.3810286	1.3810388
0.4	1.4609016	1.4610806	1.4611066	1.4611145	1.4611179	1.4611196
0.5	1.5178824	1.5179191	1.5179227	1.5179236	1.5179240	1.5179242
0.6	1.5600880	1.5600917	1.5600919	1.5600920	1.5600920	1.5600920
0.7	1.5924359	1.5924360	1.5924360	1.5924360	1.5924360	1.5924360
0.8	1.6179111	1.6179111	1.6179111	1.6179111	1.6179111	1.6179111
0.9	1.6384072	1.6384072	1.6384072	1.6384072	1.6384072	1.6384072
1.0	1.6552030	1.6552030	1.6552030	1.6552030	1.6552030	1.6552030
1.1	1.6691869	1.6691869	1.6691869	1.6692706	1.6692722	1.6692737
1.2	1.6809933	1.6809935	1.6809936	1.6810992	1.6811097	1.6811202
1.3	1.6910838	1.6910839	1.6910840	1.6911653	1.6911753	1.6911852

Table 4.1: Far-field convergence values for solutions to equation (4.10) for a selection of fluid index values n and 'infinity' $\overline{s}_\infty$.

Alternatively, the solution of equation (4.10) can be found at a moderate value of $\overline{s}_\infty$ and the initial condition $f''(0)$ used in the second stage of the solution procedure can be refined by a Newton-Raphson iteration (akin to the usual shooting method). The slow convergence of $\overline{f}'$ in the far-field for small values of n is attributable to the asymptotic form of the solution in the far-field.

Figure 4.1 shows the solution $\overline{f}'(\overline{s})$ to equation (4.10) for $n = 0.50$. This curve displays the qualitative behaviour that is expected of a boundary layer, such as the gradual approach to a limiting value.

For fluid index values greater than unity the results in Table 4.1 indicate a lack of convergence in the values of $\overline{f}'(\overline{s}_\infty)$ as the value of $\overline{s}_\infty$ is progressively increased. For example, for $n = 1.3$ we have $\overline{f}'(\overline{s}_\infty = 50) - \overline{f}'(\overline{s}_\infty = 25) = 0.0000001$, whereas $\overline{f}'(\overline{s}_\infty = 150) - \overline{f}'(\overline{s}_\infty = 125) = 0.0000099$. Also, for $n = 1.40$ and $\overline{s}_\infty = 150$ it was noticed that the maximum value for $\overline{f}'(\overline{s})$ did not occur at the terminal point. Solutions to equation (4.10) for $n = 1.40$ and 1.50 are shown in Figure 4.1. The solution for $n = 1.40$ consists of an essentially flat plateau region that is characteristic of a boundary layer. The solution for $n = 1.50$ shows dramatically how the solution 'dips' down after the plateau region and how using the value of $\overline{f}'(\overline{s}_\infty)$ to calculate the initial condition $f''(0)$ would be quite erroneous.

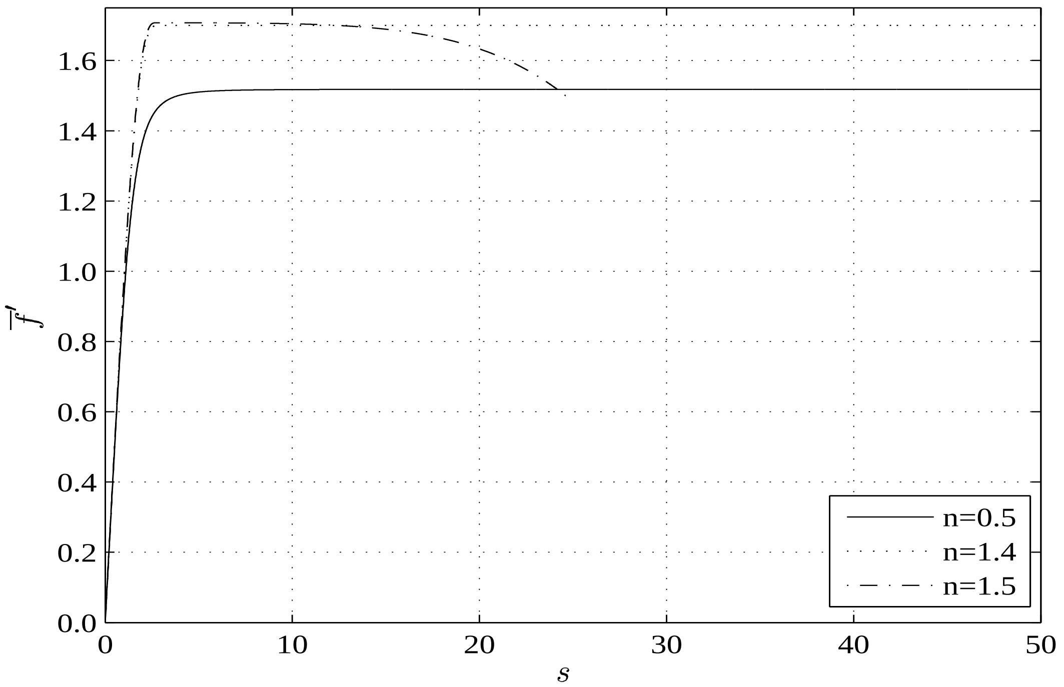

Figure 4.1: Solutions of Eqn (4.10) for fluid index values $n = 0.50, 1.4, 1.5$.

The two-stage numerical method described here is quite useful for solving equation (4.9) when the fluid index is in the range $0 < n < 1$ provided $\overline{s}_\infty$ is chosen appropriately to ensure the desired accuracy during the first stage of the calculation. The results obtained indicate that this method may also be used when the fluid index is greater than 1, up to $n \approx 1.40$. However, for $n \geq 1.50$ this method is entirely unsuitable and should not be used.

We note that the numerical solution found during each stage of the numerical method must satisfy the asymptotic boundary condition that accompanies both equations (4.9) and (4.10). However, as equation (4.10) is identical in form to equation (4.9), we expect that any non-convergent asymptotic behaviour in the solution to equation (4.9) will be replicated in the asymptotic behaviour of the solution to equation (4.9).

In the following two sections we discuss in more detail the solution of equation (4.9) for shear-thinning and shear-thickening power-law fluids.

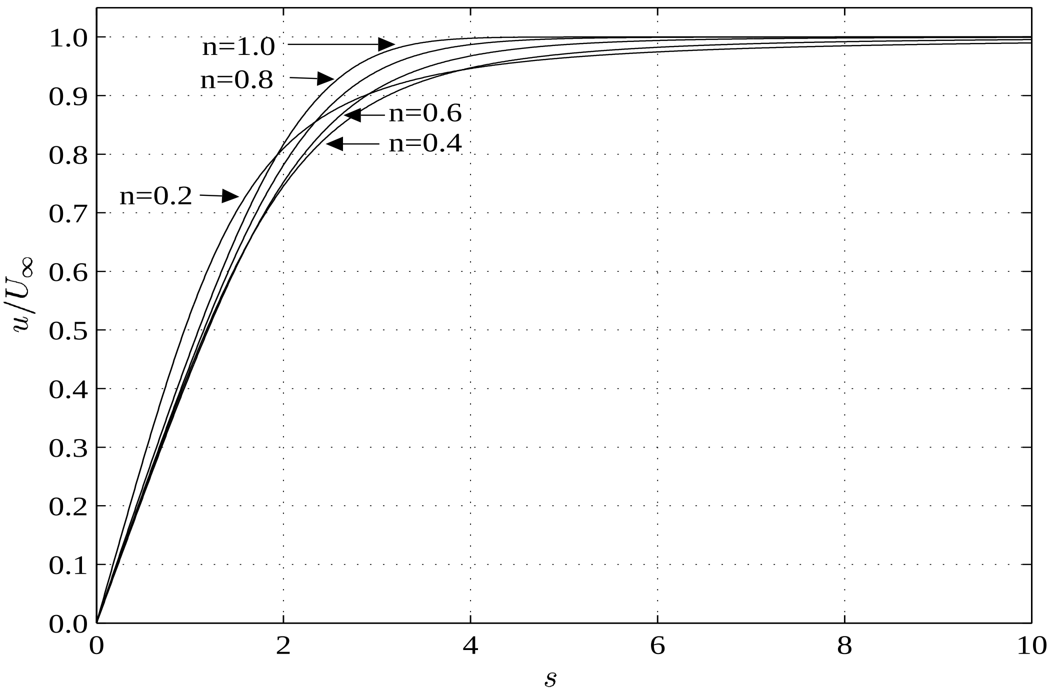

Figure 4.2: Self-similar velocity profiles for fluid index values $n = 1.0, 0.8, \ldots, 0.2$ showing thickening of the boundary-layer.

4.2.2 Shear-thinning Fluids

Power-law fluids having the fluid index in the range $0 < n < 1$ are often referred to as shear-thinning or pseudoplastic. The numerical method described in Section 4.2.1 was used to find solutions to equation (4.9) for this class of fluids. The fluid index values considered was $n = 1.0, 0.8, \ldots, 0.2$. The results given in Table 4.1 were used to properly select values for $\overline{s}_\infty$. The value $n = 1$ corresponds to a Newtonian fluid for which the solution is obtained from the classical Blasius equation. This case served as a confidence check that the numerical technique being used was performing correctly.

The self-similar solutions to equation (4.9) for different values of n represent the streamwise velocity in the boundary-layer flow of a shear-thinning fluid. Velocity profiles for the values of n considered are shown in Figure 4.2. When compared with the Blasius solution, we see that for values of n down to approximately 0.6 the velocity profiles do not show much variability in appearance. In the next section we will show that the solution to equation (4.9) possesses algebraic decay in the far-field and this can be observed for the velocity profiles plotted. This effect becomes more noticeable for lower values of n where the velocity profiles exhibit a more gentle 'shoulder'. These velocity profiles confirm that matching of the boundary-layer velocity with the far-field uniform free-stream takes place at greater distances from the surface as the fluid index n decreases, corresponding to thickening of the boundary-layer.

The two-stage numerical method for solving the two-point boundary value problem (4.9) along with boundary conditions (4.8) was modified to use a Newton-Raphson iteration to refine the value of $f''(0)$. For shear-thinning fluids this numerical method was found to be generally quite robust and efficient. However, in using this numerical method some care must be taken to ensure that the solutions obtained exhibit the correct form of asymptotic decay in the far-field. Furthermore, by examining the nature of the asymptotic form of the numerical solutions in the far field we will gain a better understanding of the behaviour of the self-similar solutions of the boundary-layer flow of power-law fluids. We will next examine the asymptotic form of the velocity profile for shear-thinning fluids in the far-field.

Asymptotic form for Shear-thinning fluids

We proceed by noting that the asymptotic boundary condition (4.8b) allows us to write the solution $f(s)$ in the far-field as

$$f(s) = s + a + \varphi(s) \quad \text{as} \quad s \to \infty,$$

where a is a constant and $\varphi(s) \ll 1$. To determine the large s structure we define $\zeta = s + a$ so that the form for $f(s)$ becomes

$$f(\zeta) = \zeta + \varphi(\zeta), \tag{4.12}$$

with $\varphi(\zeta) \ll 1$ as $\zeta \to \infty$. Substituting this expression into equation (4.9), and neglecting products of φ with its derivatives, yields, to leading order,

$$n\varphi''' + \zeta(\varphi'')^{2-n} \sim 0,$$

where the primes denote differentiation with respect to ζ. Integrating this equation gives the large ζ behaviour of φ as

$$\varphi(\zeta) \sim \alpha_1 \zeta^{\frac{2n}{n-1}},$$

where $\alpha_1 = \left[\frac{1-n}{2n}\right]^{\frac{n}{n-1}} \left(\frac{1-n}{n+1}\right)$. Substituting this expression into equation (4.12) and differentiating with respect to ζ gives in the limit $\zeta \to \infty$ (or equivalently $s \to \infty$)

$$f'(\zeta) \sim 1 + \alpha_2 \zeta^{\frac{n+1}{n-1}} + \ldots, \tag{4.13}$$

where the ellipsis denote lower-order terms and $\alpha_2 = -\left[\frac{1-n}{2n}\right]^{\frac{n}{n-1}} \left(\frac{2n}{n+1}\right)$.

Hence, equation (4.13) is a first-order approximation to the solution of equation (4.9) in the far-field and its form predicts that the solution in the far-field will display algebraic decay, provided $n < 1$. We note that for $n = 1$ the exponent in (4.13) possesses a singularity that indicates faster than algebraic decay in the far-field. However, the velocity in the far-field of the boundary layer of a Newtonian fluid is known to display exponential decay as it approaches the free-stream velocity; see Rosenhead (1963) for details.

For shear-thinning fluids, with $0 < n < 1$, equation (4.13) predicts algebraic decay toward the free-stream velocity value from below. Letting $n = 1 - \delta$, so that δ represents the degree of shear-thinning in the fluid with $0 < \delta < 1$, we can express the exponent in equation (4.13) as $1 - \frac{2}{\delta}$. For slightly shear-thinning fluids with small values of δ, this exponent will be negative and of large magnitude. The velocity profile for such fluids will have very rapid algebraic decay in the far-field. For values of δ closer to unity, corresponding to a more shear-thinning fluid, this exponent is smaller in magnitude and is negative. Hence the velocity profile of power-law fluids with a higher degree of shear-thinning will exhibit slower algebraic decay in the far-field.

The algebraic decay of the velocity field for shear-thinning fluids poses some concerns with regard to matching such a solution to an inviscid outer (potential) flow. It is implicitly assumed that such matching is possible when the large Reynolds number limit is applied to the Cauchy equations. However, there is a parallel for this algebraic decay that occurs for Newtonian fluids. General similarity solutions of the Falkner-Skan equation possessing algebraic decay are known to exist. Brown and Stewartson (1965) considered the conditions under which such solutions can match onto an outer potential flow and whether they are of relevance in the context of such solutions being an asymptotic description of a real boundary layer. They demonstrated that solutions showing algebraic decay are not appropriate if such solutions are to be matched onto an outer potential flow and, consequently, should be disregarded.

The boundary-layer flow being considered here is somewhat complicated by the additional non-linearity in the apparent viscosity. We will show that this term plays a crucial role in correctly describing the correct matching of the inner boundary layer with an outer potential flow. Now we turn to the matter of matching the boundary-layer solutions of equation (4.9) to an outer flow for fluid index values $0 < n < 1$.

The solutions presented above were derived from the boundary-layer equations on the assumption that they match smoothly onto an outer inviscid (i.e. potential) flow. To ensure that this is the case we first note that combining equations (4.5) and (4.13), when $m = 0$, gives

$$u = 1 + \hat{\alpha}_2 x^{-\frac{1}{n+1}} y^{\frac{n+1}{n-1}} + \dots, \tag{4.14a}$$

$$v = \gamma x^{-\frac{n}{n+1}} + \alpha_2 \left(\frac{1}{n+1}\right)^{\frac{n}{n-1}} x^{-\frac{n}{n-1}} y^{\frac{2n}{n-1}} + \dots, \qquad \text{as} \qquad y \to \infty, \tag{4.14b}$$

where $\hat{\alpha}_2$ and γ are constants. Next, we recall that under the boundary-layer approximation the apparent viscosity μ_{app} can be expressed as

$$\begin{aligned} \mu_{app} &= Re^{\frac{n-1}{n+1}} \tilde{\mu} \\ &= Re^{\frac{n-1}{n+1}} \left[\left(\frac{\partial u}{\partial y}\right)^2 + 2\epsilon^2 \left(\frac{\partial u}{\partial y}\frac{\partial v}{\partial x} + \left(\frac{\partial u}{\partial x}\right)^2 + \left(\frac{\partial v}{\partial y}\right)^2 \right) + \epsilon^4 \left(\frac{\partial v}{\partial x}\right)^2 \right]^{\frac{n-1}{2}}, \end{aligned} \tag{4.15}$$

where $\epsilon = Re^{-\frac{1}{n+1}}$ is the boundary-layer thickness. Thus, to leading order in powers of ϵ, the apparent viscosity depends solely upon the horizontal shear within the boundary-layer flow. Referring to equation (4.15) for the apparent viscosity, we find that for large y (i.e. in the outer region of the boundary layer) the terms that were previously excluded from our boundary-layer analysis now become important. A simple dominant balance of the terms in equation

(4.15) indicates that our boundary-layer expansion breaks down when $y = O(Re^{\frac{1-n}{n+1}})$. We also note that, on the boundary-layer scale, the outer potential flow occurs when $y = O(Re^{\frac{1}{n+1}}) \gg O(Re^{\frac{1-n}{n+1}})$ (since $0 < n < 1$). Therefore, we define a new stretched co-ordinate by

$$\begin{aligned} Y &= Re^{\frac{n-1}{n+1}} y \\ &= Re^{\frac{n}{n+1}} \hat{y}, \end{aligned}$$

where $\hat{y}$ is the non-dimensional form of the vertical co-ordinate. The co-ordinate Y is large on the boundary-layer scale y but still small on the physical length-scale.

The asymptotic form for the velocity components given by equation (4.14) now suggests that in the new outer, or viscous, region we write

$$\begin{aligned} U &= 1 + Re^{-1} U_1(x, Y) + \ldots, \\ V &= Re^{-\frac{1}{n+1}} (V_0(x) + Re^{-\frac{2n}{n+1}} V_1(x, Y) + \ldots). \end{aligned}$$

Substituting these expansions into the Cauchy equations (2.3) gives, at leading order,

$$\frac{\partial U_1}{\partial x} + \frac{\partial V_1}{\partial Y} = 0, \tag{4.16a}$$

$$\frac{\partial U_1}{\partial x} = n \left| \frac{\partial U_1}{\partial Y} + \frac{\partial V_0}{\partial x} \right|^{n-1} \frac{\partial^2 U_1}{\partial Y^2}, \tag{4.16b}$$

where $V_0(x)$ is determined by matching with the inner boundary-layer solution. From equation (4.14) this gives

$$V_0(x) = \gamma x^{-\frac{n}{n+1}}.$$

Equation (4.16b) needs to be solved subject to the matching of U_1 with the inner boundary-layer solution, which from equation (4.14b) is

$$U_1(x, Y) = \hat{\alpha}_2 x^{-\frac{1}{n+1}} Y^{\frac{n+1}{n-1}} \qquad \text{as} \qquad Y \to 0, \tag{4.17}$$

and exponential decay as $Y \to \infty$ which ensures a smooth transition between the new outer viscous layer and the uniform flow in the free stream. Having determined the form of U_1, equation (4.14a) can now be integrated to give V_1. However, the exact form of V_1 is not needed in the subsequent analysis and so is not pursued here. The boundary condition (4.17) on U_1 at $Y = 0$, together with the form for V_0, precludes any similarity type solutions of the non-linear diffusion equation (4.14b). Nonetheless, it can readily be shown that this equation admits solutions that satisfy the prescribed (matching) boundary conditions. We proceed by noting that the singular nature of equation (4.17) gives $U_{1Y} \gg V_{0x}$ in the limit $Y \to 0$. Hence, letting $U_1 = x^{-\frac{1}{n+1}}\tilde{U}(Y)$ and ignoring the V_{0x} term in equation (4.16b) gives, to leading order,

$$-\frac{1}{n+1}\tilde{U} = n\left|\frac{\mathrm{d}\tilde{U}}{\mathrm{d}Y}\right|^{n-1}\frac{\mathrm{d}^2\tilde{U}}{\mathrm{d}Y^2}.$$

The solution of this equations gives the correct asymptotic form $\tilde{U}(Y) \sim Y^{\frac{n+1}{n-1}}$ as $Y \to 0$.

Next we examine the form of U_1 in the limit $Y \to \infty$. If we assume that $U_1 \to 0$ then, upon retaining the dominant terms in equation (4.16b), we find that U_1, which by assumption is much smaller than unity, is governed by

$$\frac{\partial U_1}{\partial x} = n\left|\frac{\mathrm{d}V_0}{\mathrm{d}x}\right|^{n-1}\frac{\partial^2 U_1}{\partial Y^2}.$$

Making the substitution $\xi = \frac{Y}{\sigma}$, where

$$\sigma^2 = 2n\int\left|\frac{\mathrm{d}V_0}{\mathrm{d}x}\right|^{n-1}\mathrm{d}x.$$

gives

$$\frac{\mathrm{d}^2U_1}{\mathrm{d}\xi^2} = -\xi\frac{\mathrm{d}U_1}{\mathrm{d}\xi}.$$

The solution of this equation has the asymptotic form

$$U_1 \sim \frac{1}{\xi}(1+\ldots)\,\mathrm{e}^{-\frac{\xi^2}{2}},$$

as $\xi \to \infty$. Hence, we see that equation (4.16b) has solutions that provide a smooth match between the outer viscous layer and the free-stream potential flow.

The analysis performed above demonstrates that equation (4.16b) possesses a solution that satisfies the appropriate matching conditions at $Y = 0$ and as $Y \to \infty$. Though we have not provided numerical solutions of equation (4.16b), we note that since it is a parabolic partial differential equation in x it should, in principle, be possible to develop a numerical scheme to march an initial velocity profile forward in x. However, to provide an appropriate initial velocity profile for such a procedure, we note that $V_0(x)$ becomes unbounded as $x \to 0$ and this would require us to perform a small-x asymptotic analysis of the full Cauchy equations. As $x = 0$ corresponds to the leading edge of the flat plate, the small-x analysis would need to take account of leading-edge effects. Such a study is outside the scope of the current work and will not be pursued further.

4.2.3 Shear-thickening Fluids

Power-law fluids having the fluid index in the range $1 < n < 2$ are referred to as shear-thickening or dilatant. The set of fluid index values n considered for dilatant fluids was $n = 1.0, 1.1, \dots, 1.4$. The numerical method described in Section 4.2.1 is not readily applicable to this class of fluids. However, the results from Table 4.1 were used to determine an initial guess for $f''(0)$ and then a standard shooting method was used to find solutions to equation (4.9).

Velocity profiles for the values of n considered are plotted in Figure 4.3. The features displayed by these velocity profiles are in agreement with profiles reported by Acrivos et al. (1960) and Lee and Ames (1966). From the velocity profiles in Figure 4.3 it can be seen that as the fluid index n increases, the velocity profile matches onto the free-stream velocity at progressively smaller values of s. Such thinning of the boundary-layer is common among shear-thickening fluids.

During the numerical solution of equation (4.9) for values of $n > 1$ it was found that manual intervention was often required to monitor the convergence criteria, whereas for shear-thinning fluids the numerical scheme converged onto the solution quite readily.

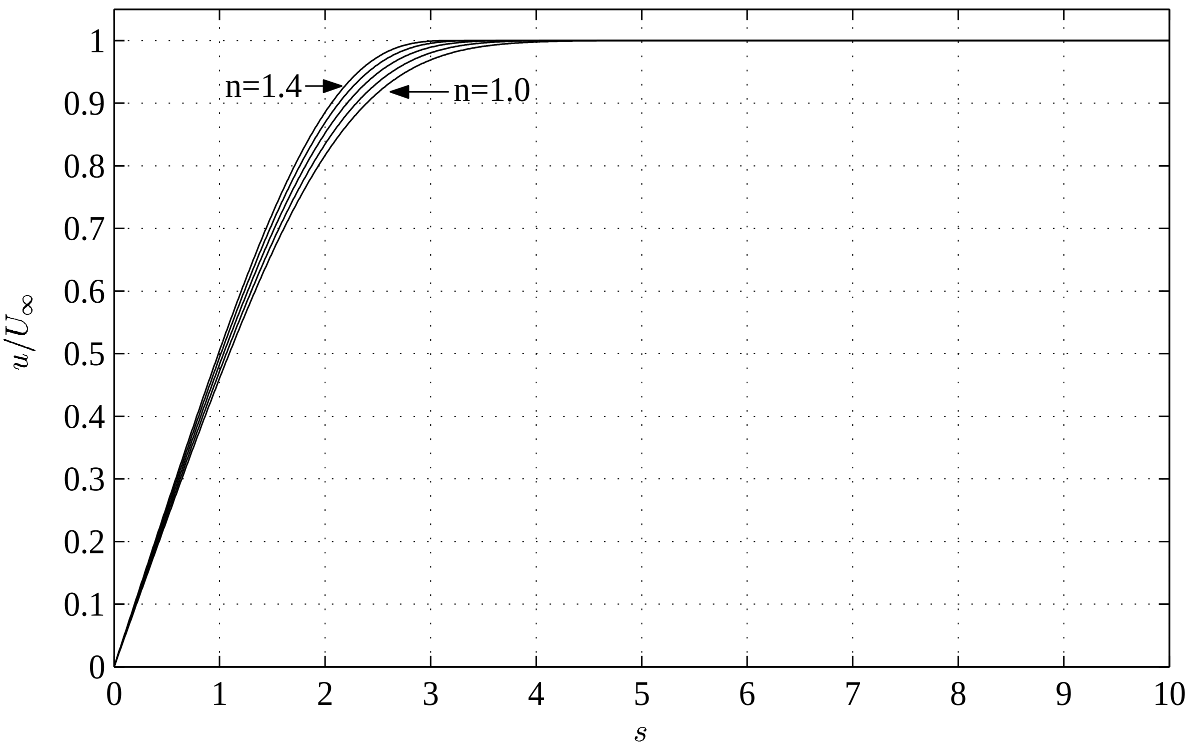

Figure 4.3: Self-similar velocity profiles for fluid index values $n = 1.0, 1.1, \ldots, 1.4$ showing thinning of the boundary-layer.

For shear-thickening fluids we note that equation (4.13) does not provide a valid asymptotic description for the approach of the streamwise velocity to the potential flow in the far-field. The exponent in equation (4.13) will take positive values when the fluid index is greater than unity, so using this asymptotic form for shear-thickening fluids indicates that the solution will exhibit algebraic growth rather than decay, thus invalidating the assumption used in its derivation. Additionally, the coefficient α_2 does not admit real values for n in the nominated range. This indicates that equation (4.13), obtained by taking a dominant balance from equation (4.9), does not have any real solutions that exhibit algebraic decay for $1 < n < 2$. It would therefore seem that there is some type of breakdown in the solution of equation (4.9) for $n > 1$. Furthermore, no other dominant balance is available within equation (4.4) which produces far-field decay for $n > 1$. It is this fact that suggests that the shear-thickening boundary layer must be of ‘finite width’, as first alluded to by Acrivos et al. (1960).

The indication that solutions to equation (4.9) for $n > 1$ may not exist suggests that some care needs to be exercised when trying to obtained solutions to equation (4.9) by numerical schemes of the variety discussed in Section 4.2.1.

Asymptotic form for Shear-thickening fluids

Using a numerical scheme based on the standard shooting method coupled with Newton-Raphson iteration to find the solution of equation (4.9) for shear-thickening fluids provides results of limited usefulness. However, a more promising approach that provides a better understanding of the nature of the boundary layer of a shear-thickening fluid is to regard the original problem as a free-boundary problem, where the outer limit of the 'boundary layer' now becomes an unknown of the system. Thus we pose the problem for non-zero m as

$$nf''' = \left[\frac{m(n+1)}{m(2n-1)+1}\right]\left[(f')^2 - 1\right]|f''|^{1-n} - f\,|f''|^{2-n}, \tag{4.18a}$$

to be solved subject to the usual no-slip conditions

$$f = f' = 0 \qquad \text{on} \qquad s = 0, \tag{4.18b}$$

and the new boundary conditions

$$f' = 1, \qquad f'' = 0 \qquad \text{on} \qquad s = s_c. \tag{4.18c}$$

We observe that equation (4.18a) is essentially identical to equation equation (4.4) along with the appropriate replacement for the pressure gradient parameter. Also the absolute value of f has been introduced in the terms involving exponents which take negative values when $n > 1$.

The boundary condition (4.18c) ensures that the streamwise velocity does not overshoot its far-field value of unity at the 'outer' edge of the boundary layer. Though this system appears to be over-specified, it can be seen that when s_c is treated as an unknown we then obtain an eigenvalue problem for s_c in the form of a two-point boundary-value problem which can be solved using standard methods.

To make the computation of solutions more convenient, it is useful to take advantage of the autonomous nature of the system (4.18) and to make a shift of coordinates so as to define the origin to be at the critical point $z = s_c - s$. Applying this shift of coordinates gives the transformed equation

$$n\frac{\mathrm{d}^3 f}{\mathrm{d}z^3} = \left[\frac{m(n+1)}{m(2n-1)+1}\right]\left[1 - \left(\frac{\mathrm{d}f}{\mathrm{d}z}\right)^2\right]\left|\frac{\mathrm{d}^2 f}{\mathrm{d}z^2}\right|^{1-n} + \left|\frac{\mathrm{d}^2 f}{\mathrm{d}z^2}\right|^{2-n} f,$$

along with the transformed boundary conditions

$$\begin{aligned} \frac{\mathrm{d}f}{\mathrm{d}z} = -1, \quad \frac{\mathrm{d}^2 f}{\mathrm{d}z^2} &= 0 \quad \text{on} \quad z = 0, \\ f = \frac{\mathrm{d}f}{\mathrm{d}z} &= 0 \quad \text{on} \quad z = s_c. \end{aligned}$$

In order to numerically integrate the transformed equation we employ the small-z asymptotic form for f to start the calculation at some suitably chosen $\Delta z \ll 1$. This is given by

$$f = \tilde{\beta} - z + \tilde{\gamma} z^{\alpha} + \cdots, \tag{4.19}$$

where $\tilde{\beta}$ is an unknown that is to be determined, with α and $\tilde{\gamma}$ being 'constants' that are dependent on the fluid and flow parameters. Making the appropriate substitutions into the transformed equation and simplifying results in

$$\begin{aligned} n\alpha(\alpha-1)(\alpha-2)\tilde{\gamma} z^{\alpha-3} &= \tilde{\beta}(\alpha(\alpha-1))^{2-n}\left|\tilde{\gamma}\right|^{2-n} z^{n(2-\alpha)+2\alpha-4} \\ &+ \left\{2\left[\frac{m(n+1)}{m(2n-1)+1}\right]\alpha\tilde{\gamma} - \alpha(\alpha-1)\left|\tilde{\gamma}\right|\right\}(\alpha(\alpha-1))^{1-n}\left|\tilde{\gamma}\right|^{1-n} z^{n(2-\alpha)+2\alpha-3} \\ &- \left\{\left[\frac{m(n+1)}{m(2n-1)+1}\right]\alpha^2\tilde{\gamma} - \alpha(\alpha-1)\left|\tilde{\gamma}\right|\right\}(\alpha(\alpha-1))^{1-n}\left|\tilde{\gamma}\right|^{1-n}\tilde{\gamma} z^{n(2-\alpha)+3\alpha-4}. \end{aligned}$$

Performing a balance of the leading terms, we find that $\alpha = \frac{2n-1}{n-1}$, while $\tilde{\gamma}$ is given by the solution of

$$\frac{\left|\tilde{\gamma}\right|^{2-n}}{\tilde{\gamma}} = \frac{n}{\tilde{\beta}}(\alpha(\alpha-1))^{n-1}(\alpha-2).$$

This asymptotic form allows us to apply boundary conditions at some suitably small Δz and then integrate out to the location at which the boundary condition $f = f_z = 0$ is satisfied. This was accomplished using a fourth-order Runge-Kutta quadrature routine coupled with Newton-Raphson iteration on the unknowns $\tilde{\beta}$ (or equivalently $\tilde{\gamma}$) and s_c.

It is worth noting at this point that equation (4.9) can be solved analytically when $n = 2$, with the pressure gradient parameter $\beta = 0$, for then the non-linear ordinary differential equation reduces to the linear third-order ordinary differential equation

$$f''' + \frac{1}{n} f = 0. \tag{4.20}$$

Equation (4.20) has the general solution

$$f(s) = C_1 e^{-2as} + C_2 e^{as} \sin(a\sqrt{3}s) + C_3 e^{as} \cos(a\sqrt{3}s),$$

where $a = (1/2)^{4/3}$ and C_i $(i = 1, 2, 3)$ are constants of integration. Imposing the boundary condition $f(0) = 0$ gives $C_3 = -C_1$, while $f'(0) = 0$ gives $C_2 = \sqrt{3}C_1$. Hence, the general solution simplifies to the following form

$$f(s) = C_1 e^{-2as} + C_1 e^{as} \left[\sqrt{3} \sin(a\sqrt{3}s) - \cos(a\sqrt{3}s)\right]. \tag{4.21}$$

The constant of integration C_1 and the critical position s_c are then determined from the 'far-field' boundary conditions, namely that $f' = 1$ and $f'' = 0$ on $s = s_c$. It is easiest to apply the second of these to first determine the position s_c, which is readily shown to satisfy the transcendental equation

$$\cos(a\sqrt{3}s_c) = -\frac{1}{2} \exp(-3as_c). \tag{4.22}$$

With s_c determined the value for the constant of integration C_1 appearing in equation (4.21) can finally be determined from the remaining boundary condition, namely $f' = 1$ on $s = s_c$. It is worth noting that the presence of the exponential terms in the general solution (4.21) indicates that it is not possible to satisfy the usual asymptotic boundary condition $f'(\infty) \to 1$. Hence, we conclude from this that a similarity-type solution with the required asymptotic behaviour in the far-field does not exist for $n = 2$.

We note that the form of the exponential term appearing on the right-hand side of equation

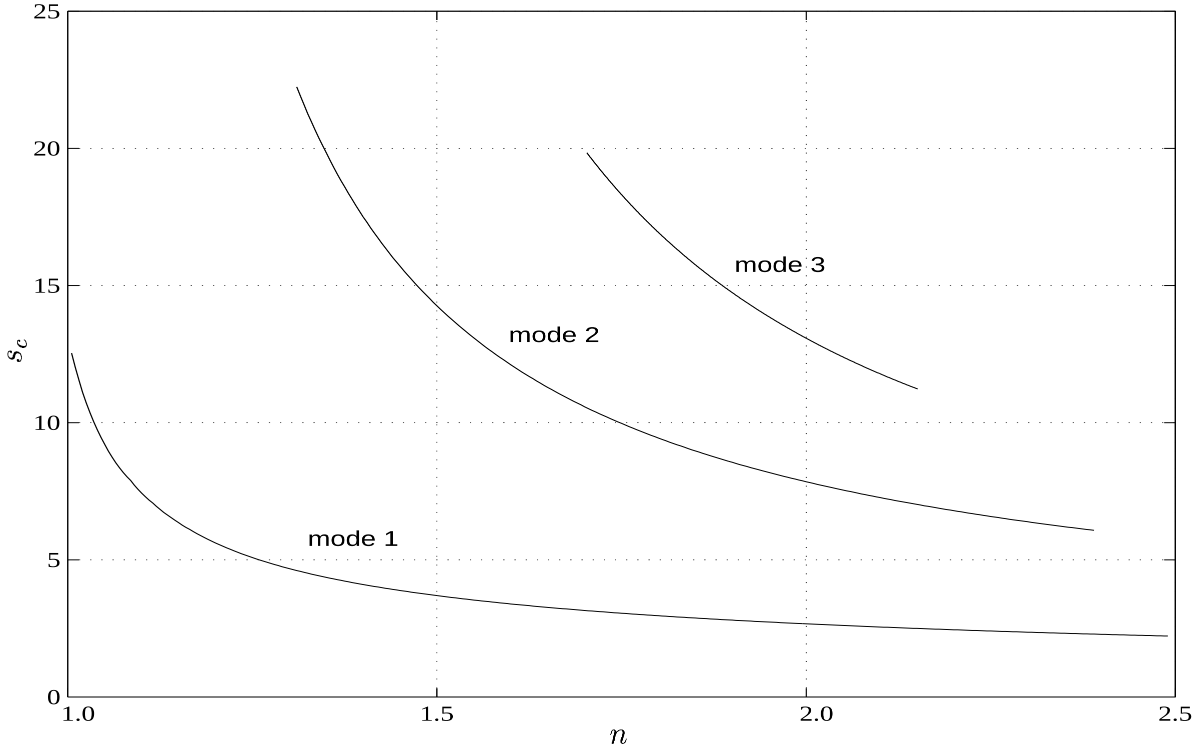

Figure 4.4: Plots of the location of the critical point for the first three eigenmodes of (4.20).

(4.22) allows us to obtain estimates for s_c by writing (4.22), to a first approximation, as

$$\cos(a\sqrt{3}s_c) \approx 0.$$

This gives $s_c \approx (1+2k)\frac{\pi}{2\sqrt{3}a}$ $(k = 0, 1, 2, \ldots)$. These approximate values were used as starting values for the numerical solution of the full system (4.20). The equations were solved using both a forward and backward shooting method. Typically, when the forward-shooting method failed to converge to a solution, the backward-shooting method was found to be successful. The results from both calculations are summarised in Figures 4.4 and 4.5. Figure 4.4 shows the position of s_c versus n. Only the first three modes are presented; however, the results for $n = 2$ confirm that there is an infinite number of modal solutions of the system (4.20). This is supported by the observation that the transcendental equation (4.22) possesses an infinite number of solutions for s_c. Referring to Figure 4.4, we note that for the first modal solution it appears that s_c is finite for $n = 1$. This is simply an artefact of our numerical scheme, which iterates on the values $f'(s_c) - 1$ and $f''(s_c)$ until these quantities are less than a predefined tolerance, which in obtaining these results was set to 10^{-12}. At this tolerance level

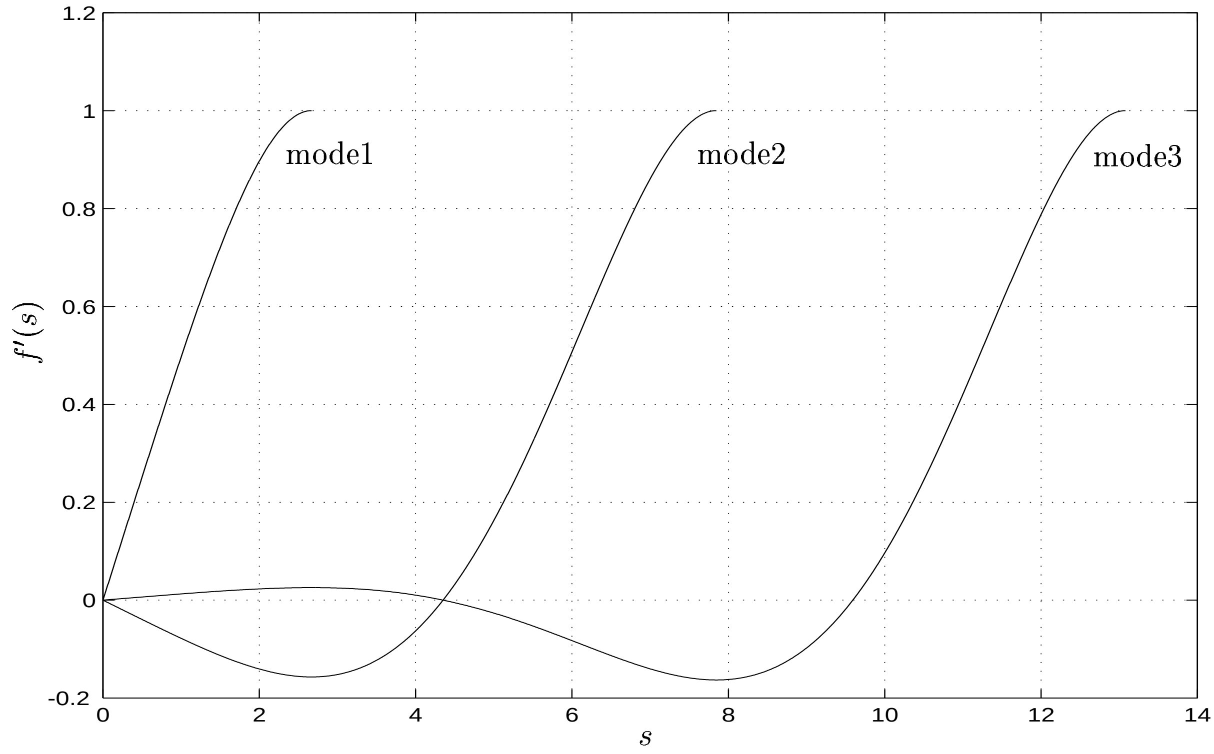

Figure 4.5: The first three eigenfunctions for fluid index $n = 2$.

the numerical scheme cannot distinguish between a converged solution and the true solution, which for $n = 1$ is known to have exponential decay to the free-stream value of unity.

The first three eigenfunctions, for a fluid index $n = 2$, are shown in Figure 4.5. Mode 1 appears to represent a 'boundary layer' with forward flow throughout the flow domain. However, this solution is non-physical as it lacks the asymptotic behaviour that is characteristic of boundary-layer flows. The higher modes exhibit regions with negative velocity, where $f' < 0$ for some range of s. The solutions for higher mode numbers become increasingly oscillatory with alternating regions of positive and negative velocity. However, there is no physical mechanism whereby the laminar flow over a flat plate can have a region with negative velocity. Consequently, those eigenfunctions which exhibit regions in which $f' < 0$ are not physically realisable and can be ignored.

We now turn our attention to the question of matching the inner solution described above with the outer flow solution.

The phenomenon of a finite-thickness boundary layer is also encountered in hypersonic boundary layers (see Bush (1966); Lee and Cheng (1969); Mikhailov et al. (1971)). In such flows the abrupt termination of the boundary layer arises due to the vanishing nature of the temperature, and consequently the fluid viscosity (which is a function of temperature), in the outer regions of a hypersonic boundary layer. For the case of a fluid whose viscosity-temperature relation is described by Sutherland's law (with a non-linear dependence of viscosity upon temperature), Bush (1966) demonstrated that this singularity is smoothed out in a thin viscous transition layer which allows uniform matching with an outer inviscid shock layer. Lee and Cheng (1969) extended this analysis to the case where the viscosity-temperature relation is given by Chapman's law (with a linear dependence of viscosity upon temperature). Although there are some subtle differences between the two cases, both result in the need for a viscous transition layer at the outer extent of the finite-width boundary layer. The parallels between the structure of the hypersonic boundary-layer and that of the shear-thickening boundary layer are obvious. In the latter case the underlying cause of the existence of the finite-width boundary layer is the vanishing of the leading-order viscosity as $s \to \infty$. The regularisation of the resulting singularity is accomplished through the re-introduction of lower-order terms in the viscosity function. A similar adjustment layer was also observed by Denier and Hewitt (2004) in their study of the flow of a power-law fluid above a rotating disk.

In order to determine the structure within this viscous adjustment layer, we first note that, as mentioned above, the underlying cause of the finite-width of the boundary layer is due to the vanishing of the leading-order viscosity as $s \to s_c$. From our original scalings, the terms that were ignored in our leading-order approximation for $\hat{\mu}$ in the boundary layer are of the form

$$Re^{-\frac{2}{n+1}} \left(\frac{\partial v}{\partial y} \right)^2 \qquad \text{and} \qquad Re^{-\frac{2}{n+1}} \frac{\partial u}{\partial y} \frac{\partial v}{\partial x}.$$

With the expansion given above for u as $s \to s_c$ we obtain

$$\left(\frac{\partial v}{\partial y} \right)^2 \sim x^{-\frac{2}{n+1}} (s - s_c)^{\frac{2}{n-1}} + \ldots, \qquad Re^{-\frac{2}{n+1}} \frac{\partial u}{\partial y} \frac{\partial v}{\partial x} \sim x^{-2} (s - s_c)^{\frac{1}{n-1}} + \ldots.$$

Thus our somewhat naive truncation of the viscosity function breaks down when

$$s - s_c = O(Re^{-\frac{2(n-1)}{n+1}}).$$

As a result of this observation, we define

$$y = y_c(x) - Re^{-\frac{2(n-1)}{n+1}}\xi,$$

and write

$$u = 1 + Re^{-\frac{2n}{n+1}}\hat{U}(x,\xi) + \dots, \qquad v = \hat{V}(x) + \dots,$$

where the ellipsis denote lower-order terms that do not enter into the subsequent analysis. The leading-order term for v is determined through a trivial match with the 'inner' solution. This gives

$$\hat{V}(x) = A_1 x^{A_2+m+1}\hat{\beta}\left[s_c - (m + A_2)\right],$$

where the constants $A_1 = \left(\frac{1}{n+1}\right)^{\frac{1}{n+1}}$, $A_2 = \frac{1-m(2-n)}{n+1}$ and $\hat{\beta}$ was defined in previously. From the streamwise momentum equation we obtain, after some simplifications,

$$-\hat{V}(x)\frac{\partial \hat{U}}{\partial \xi} = \frac{\partial}{\partial \xi}\left(\hat{\mu}\frac{\partial \hat{U}}{\partial \xi}\right), \tag{4.23}$$

where the viscosity function $\hat{\mu}$ is given by

$$\hat{\mu} = \left[\left(\frac{\partial \hat{U}}{\partial \xi}\right)^2 - 2\frac{\partial \hat{U}}{\partial \xi}\frac{\mathrm{d}\hat{V}}{\mathrm{d}x} + \left(\frac{\mathrm{d}\hat{V}}{\mathrm{d}x}\right)^2\right]^{\frac{n-1}{2}}.$$

The boundary conditions appropriate to equation (4.23) are

$$\hat{U} \to 0 \quad \text{as} \quad \xi \to -\infty, \qquad \hat{U} \sim A_2^{\frac{n}{n-1}} \quad \text{as} \quad \xi \to \infty.$$

These ensure correct asymptotic decay of the streamwise velocity in the far-field ($\xi \to -\infty$) and matching to the algebraic terms in the 'inner' region ($\xi \to \infty$). It proves useful to rescale equation (4.23) by writing $\hat{U} = \alpha_0 F, \xi = \alpha_1 \zeta$, where $\alpha_0 = \frac{(-\hat{V}_x)^{n-1}}{\hat{V}}$ and $\alpha_1 = \frac{(-\hat{V}_x)^n}{\hat{V}}$. The equation for $F(\zeta)$ is then

$$\frac{\partial}{\partial \zeta}\left[\left|F' - 1\right|^{n-1} F'\right] = -F'.$$

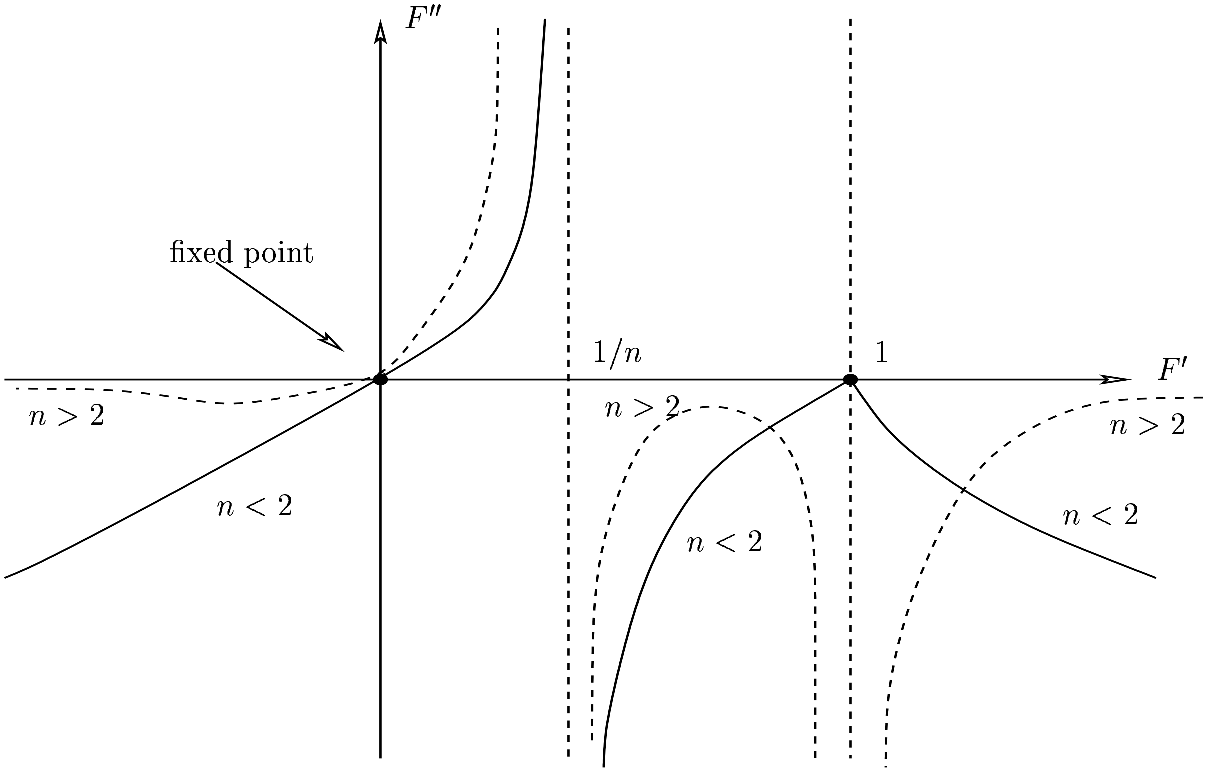

Figure 4.6: Schematic of the (F', F'') phase plane.

A schematic of the structure of the (F', F'') phase plane is given in Figure 4.6. The solutions which satisfy the asymptotic matching conditions are found in the lower-left quadrant, for which F'' is strictly negative. Plots of F versus ζ are given in Figure 4.7, from which we observe that the singularity which arises in the finite-width boundary layer can be smoothed out within the viscous adjustment layer.

4.3 Non-Zero Pressure Gradient($\beta \neq 0$)

Setting the fluid index n to 1 corresponds to a Newtonian fluid and equation (4.4) reduces to the classical Falkner-Skan equation which has been extensively studied. These studies indicate that for Newtonian fluids the boundary-layer velocity profile is affected by the pressure gradient parameter β. When the pressure gradient is favourable, corresponding to $\beta > 0$, the boundary-layer flow remains essentially laminar and the velocity profiles continue to be self-similar. As the value of β is increased the velocity profile exhibits a very steep initial portion which approaches the far-field velocity quite rapidly. Using the common definition for the boundary-

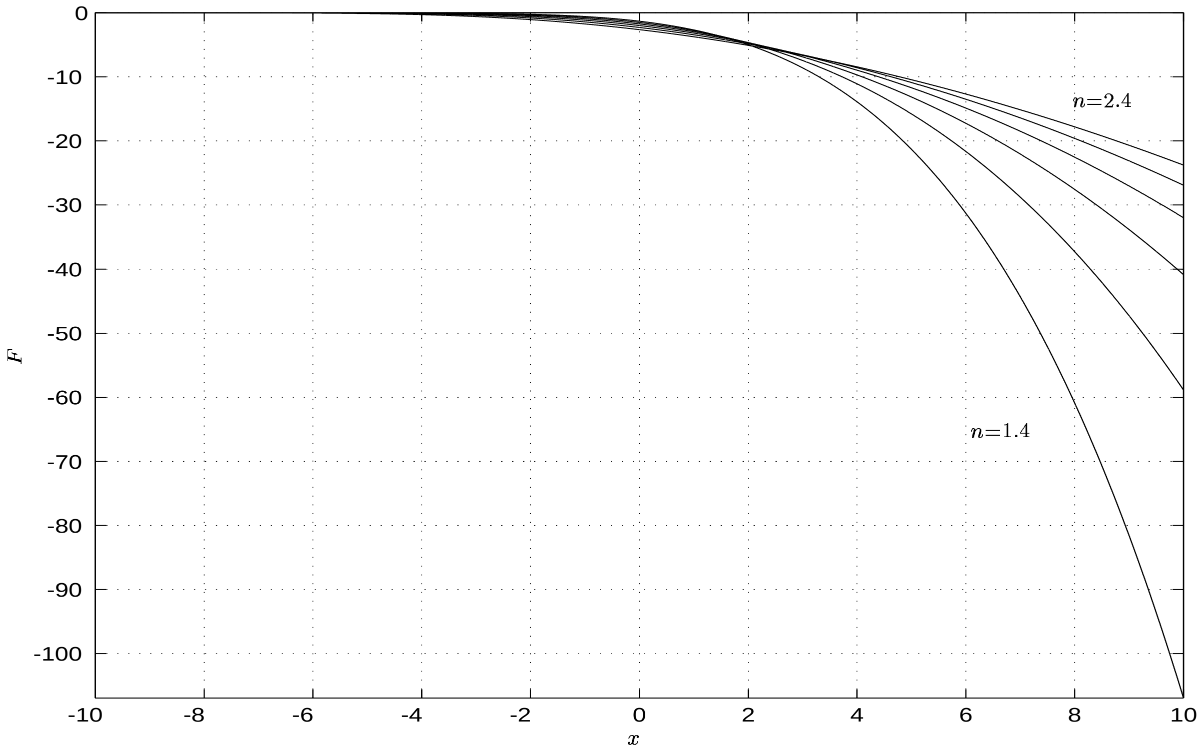

Figure 4.7: Plots of F versus x for $n = 1.4, 1.6, 1.8, \ldots, 2.4$.

layer thickness as the distance from the surface at which the streamwise velocity is 99% of the free-stream value, it is found that the boundary-layer thickness decreases as β increases. In the case of an adverse pressure gradient ($\beta < 0$), the velocity profiles are seen to retain their self-similar character. As the value of β is made progressively more negative the gradient of the initial portion of the velocity profile decreases and tends toward zero. The gradient of the velocity curve at $s = 0$ is referred to as the reduced skin friction and is given by $f''(0)$. When $\beta = -0.19884$ the reduced skin friction is effectively zero.

A separated flow typically exhibits a marked increase in drag and may indicate the onset of turbulence. In some flows, for instance where mixing is important, it may be highly desirable to achieve a non-laminar flow by firstly inducing separation, which may then progress to turbulence. If the fluid involved is of the power-law variety then the occurrence and corresponding location of the flow separation point can be known beforehand for the flow regime being considered. Alternatively, if a non-laminar flow is undesirable then being able to know the location along the surface where the flow separates is very useful. A fluid property, such as a non-constant viscosity, could be used to provide some 'localised' control for the onset of separation. Hence, the ability to determine when the reduced skin friction is almost zero has some potential practical benefit.

The boundary-layer flow of a Newtonian fluid is most easily influenced, or controlled, by the pressure gradient parameter β as the viscosity of this class of fluids is essentially constant. For non-Newtonian fluids of the power-law type, the fluid index n provides a mechanism for setting the viscosity of the fluid in the boundary layer. If it turns out that the point of separation is dependent on the value of n, then we have an additional means (i.e. the fluid viscosity), as well as the pressure gradient parameter β, with which to control the boundary-layer flow and the location of the point of separation. Hence, we performed a set of numerical investigations into the effect that both the fluid index n and the pressure gradient parameter β have on the velocity profile and on the reduced skin friction. The results obtained are described below.

Numerical calculations were performed to determine the velocity profile for a shear-thinning fluid with fluid index $n = 0.8$ subject to different positive values of the pressure gradient parameter β, that is, in the presence of a favourable pressure gradient. The values of β considered were $0.0, 0.05, 0.10$. The streamwise velocity profiles obtained are shown in Figure 4.8. The calculations were carried out to $s_\infty = 20$ though the plots display the portion of the velocity profiles that is relatively near to the flat plate.

The results obtained indicate that as β increases the reduced skin friction, given by the value of $f''(0)$, also increases. We also note that the boundary-layer thickness, as defined above, is showing a small decrease as β takes larger values. These observations are qualitatively similar to those for the boundary-layer flow of a Newtonian fluid under like conditions.

Next, we performed a similar set of numerical calculations to determine the streamwise velocity profile for a shear-thinning fluid with fluid index $n = 0.8$ subject to different negative values of the pressure gradient parameter β, that is, an adverse pressure gradient. The values of β considered were $0.0, -0.05, \ldots, -0.20$. The streamwise velocity profiles obtained are shown in Figure 4.9. The calculations were carried out to $s_\infty = 20$ though the plots display the portion of the velocity profiles that is relatively near to the flat plate.

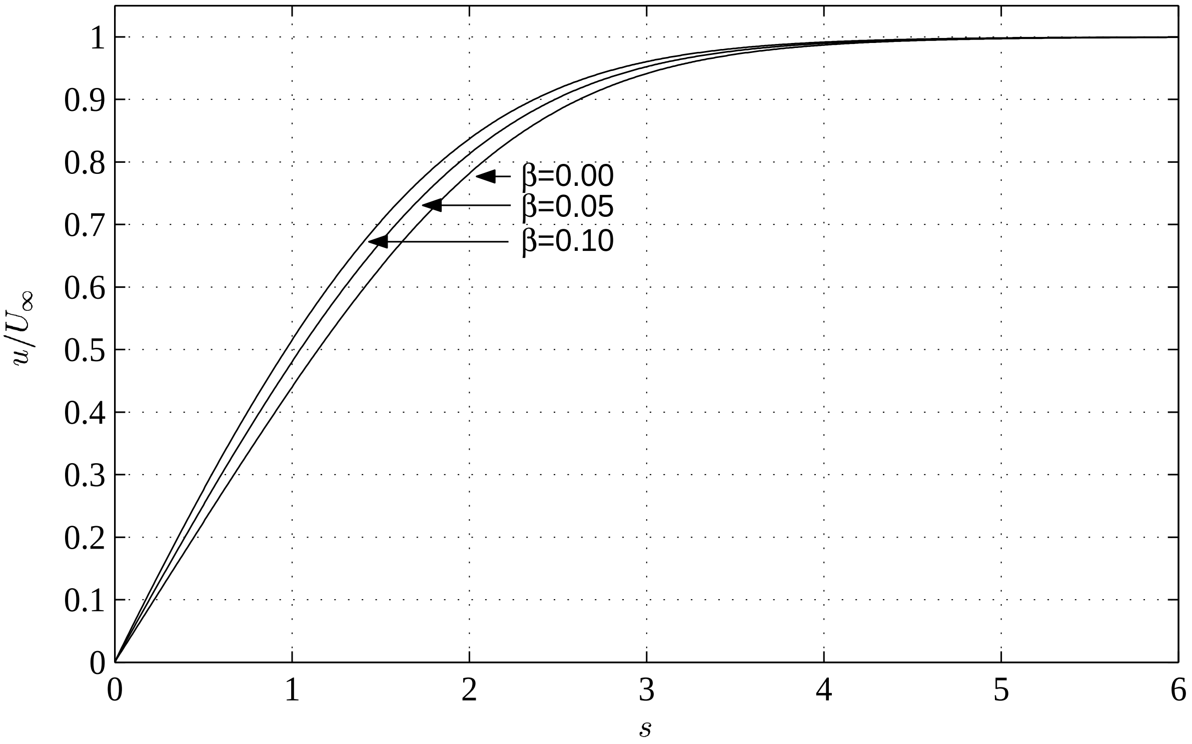

Figure 4.8: Streamwise velocity profiles for $\beta = 0.0, 0.05, 0.10$ and fluid index $n = 0.8$.

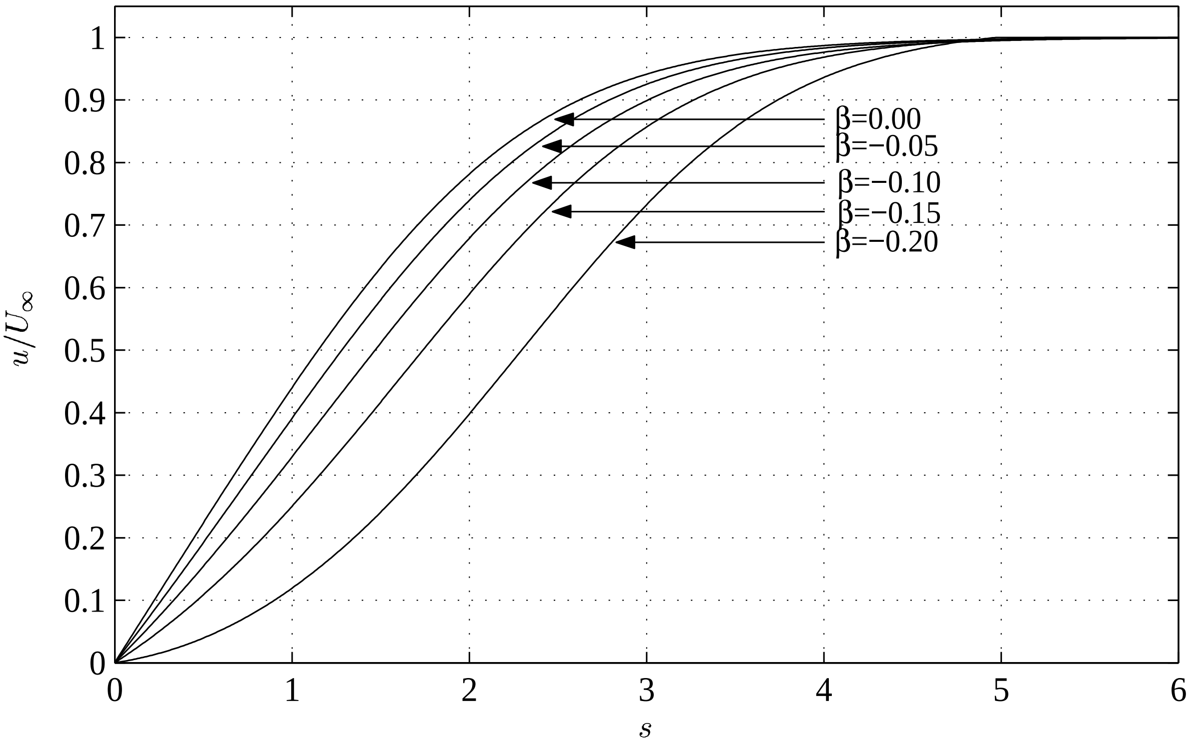

Figure 4.9: Streamwise velocity profiles for $\beta = 0.0, -0.05, \ldots, -0.20$ and fluid index $n = 0.8$.

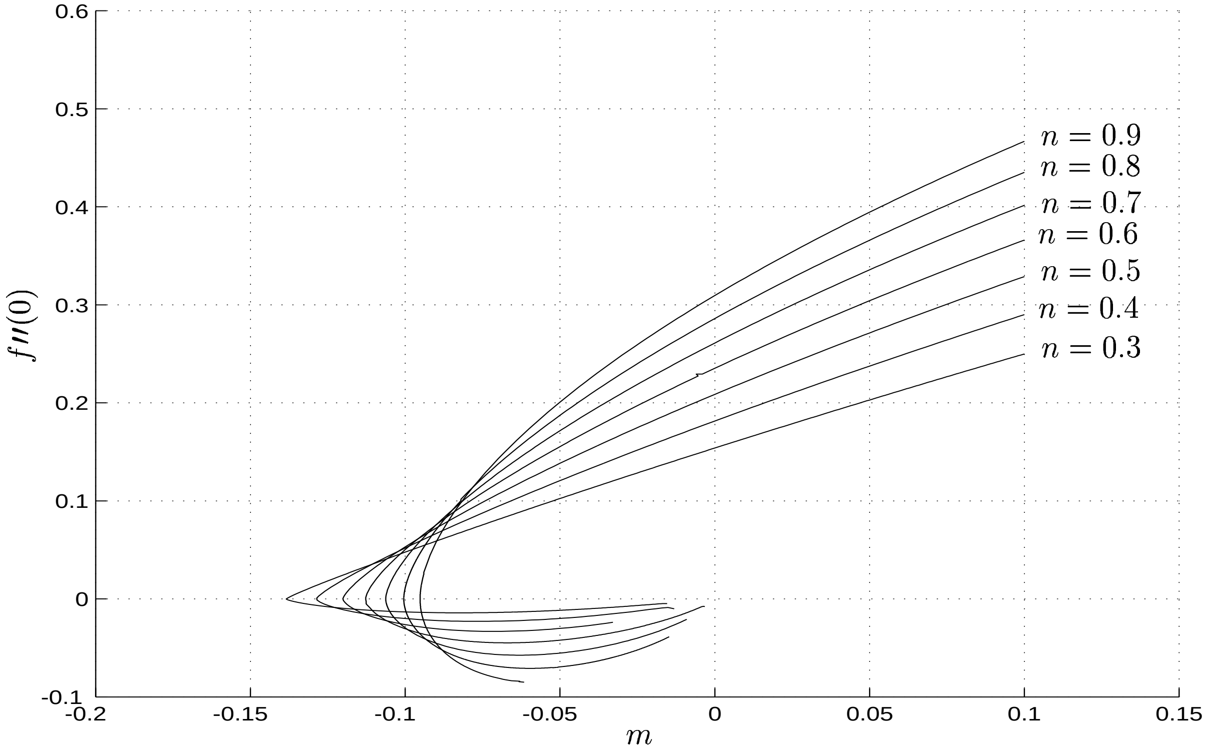

Figure 4.10: The variation of wall shear $f''(0)$ with m for a variety of shear-thinning values of n.

For the values of β depicted, the results obtained indicate that the reduced skin friction ($f''(0)$) is decreasing as β takes more negative values. The decrease in $f''(0)$ is more apparent as β becomes more negative and approaches a critical value β_{crit}, or equally m_{crit}. We also observe that there is a gradual thickening of the boundary layer as β becomes more negative.

The observations discussed above prompted a further series of calculations to determine the reduced skin friction $f''(0)$, or equivalently the wall shear, over a range of values of m for various shear-thinning fluids. For these calculations the value of $f''(0)$ was set and the appropriate value of β, or m, was found using Newton iteration. This numerical scheme was applied over a suitable range of reduced skin friction values. The numerical results obtained are summarised in Figure 4.10, where we present plots of wall shear versus the parameter m. These results are similar to the well-known Hartree (1937) distributions encountered in classical Falkner-Skan ($n = 1$) distributions of wall shear versus Hartree parameter (in effect, our parameter 'm'). From these plots we see the existence of a unique solution for positive values of the Hartree parameter for a given value of the fluid index n, while non-unique solutions are found at negative values of the Hartree parameter. The non-uniqueness manifests itself in a second

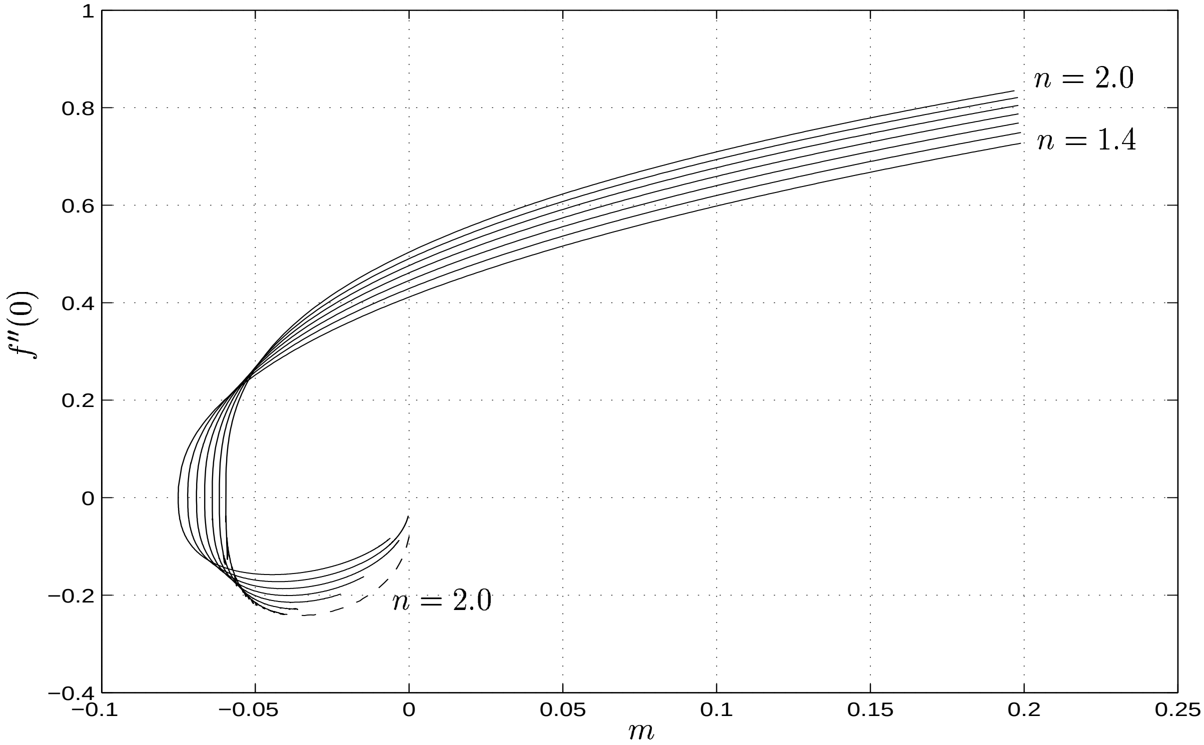

Figure 4.11: The variation of wall shear $f''(0)$ with m for a variety of shear-thickening values of n.

class of solutions with $f''(0) < 0$; though these solutions are of mathematical interest they do not represent any physically realisable flow.

This series of calculations to determine $f''(0)$ over a range of values of m was repeated for shear-thickening fluids. As was the case for shear-thinning fluids, we observe the typical curves of wall shear $f''(0)$ versus m in Figure 4.11. These curves confirm the presence of unique solutions for positive values of m and the non-uniqueness of the observed solutions for $m < 0$. Furthermore, these multiple solutions, though they appear disconnected when $m = 0$, are connected when considered as members of the family of solutions in (m, n)-space as is evidenced by the dashed curve appearing in Figures 4.11 and 4.12. The solid curves were obtained by numerically continuing the results for the first mode (starting with $m = 0$) into the m-plane, whereas the dashed curve (for $n = 2$) was obtained by numerical continuation of the results for the mode 2 solution (also starting with $m = 0$). These two curves meet, thus confirming that what we have referred to above as modes 1 and 2 are actually members of the same solution family. The results displayed in Figure 4.12 show the multiplicity of critical locations for negative m and that s_c is increasing with decreasing m.

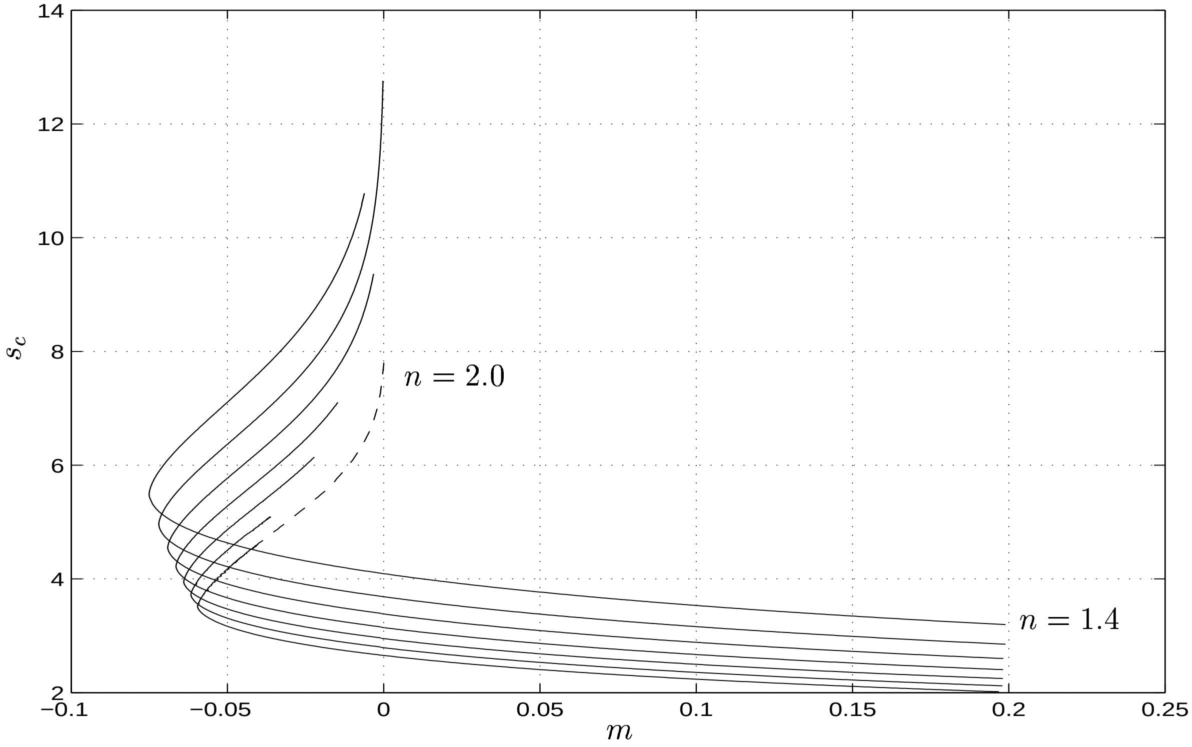

Figure 4.12: The variation of s_c with m for a variety of shear-thickening values of n.

4.4 Chapter Summary

In this chapter we have derived a similarity-type transformation that converts the partial differential equations governing the boundary-layer flow of a power-law fluid into an equivalent ordinary differential equation. The solution of the two-point boundary value problem was obtained by solving an equivalent initial value problem using a numerical scheme consisting of a standard shooting method and coupled with Newton iteration to find the unknown $f''(0)$. This numerical scheme was found to be satisfactory for shear-thinning fluids; however, for shear-thickening fluids the numerical scheme was less effective and the solutions needed to be interpreted with some care.

An asymptotic analysis of the behaviour of the solution in the far-field was also performed. It was shown that, under the original boundary-layer scaling, the solution for shear-thinning fluids exhibited algebraic decay. However, for shear-thickening fluids it was found that the derived asymptotic form did not predict decay in the far-field, hence, suggesting that the shear-thickening boundary layer is of ‘finite-width’. It was demonstrated for shear-thinning fluids that by introducing a transition layer between the boundary-layer and the free-stream, via an appropriate rescaling, that a composite solution which matches with the boundary-layer solution as well as exhibiting exponential decay as $s \to \infty$ exists. For shear-thickening fluids we identified an infinite family of solutions. As was the case for shear-thinning flows, shear-thickening fluids require the presence of a viscous transition layer in which the singularity that arises as a result of the abrupt termination of the boundary layer is smoothed out, hence allowing matching with the outer potential flow.

We also considered the relationship between the wall shear $f''(0)$ with the parameter m that influences the pressure gradient in the free-stream flow. The numerical results indicate that for positive values of m both shear-thinning and shear-thickening fluids possess a unique solution. When m takes negative values then both classes of fluid possess non-unique (or multiple) solutions. It was argued that the non-unique solutions are members of a single family of solutions for shear-thickening flows.

The similarity-type solutions described in this chapter cannot be directly compared with the numerical results presented in Chapter 3 due to differences in the underlying methods and flow scenarios as captured by the relevant boundary conditions. In particular, we focussed here on flows with sero mass transfer through the surface. Nonetheless, some qualitative agreement between the results obtained using similarity techniques with numerical results can be observed. This provides a limited degree of validation for the numerical method employed in Chapter 3.

The results presented here in this chapter clearly demonstrate the significant issues that arise when a simple constitutive relation based on the power-law rheology is used tp model the boundary-layer flow of either shear-thinning or shear-thickening fluids. That the problem for shear-thinning fluids can be made mathematically consistent is perhaps gratifying, however, this does not hide the fact that the underlying model is fundamentally flawed. Interestingly, the mathematical ‘fix’ described in this chapter (see also Denier and Dabrowski (2004)) has now been used in a wide variety of modelling problems, see Andersson (2006), Guedda and Kersner (2007), Bayada et al. (2007), Benlahsen et al. (2008), Molla and Yao (2008), Yao and

Molla (2008), Zhao and Khayat (2008), Molla and Yao (2009a), Molla and Yao (2009b), Molla and Yao (2009c), Prasad et al. (2009). These recent works do not, however, propose a suitable remedy to this problem, something that we consider in the next chapter.

Chapter 5

Boundary-layer Flow of a Carreau Fluid

The generalised Newtonian fluid, based on a power-law constitutive relation, has been used quite widely for modelling various industrial flows. This constitutive relation has also been investigated for boundary-layer flows. However, the power-law constitutive relation is considered to be applicable over a moderate range of shear-rate. It is generally accepted that its limitations become most apparent when the shear-rate is either very low or very high.

When the numerical marching scheme described in Chapter 3 was modified to investigate the boundary-layer flow of shear-thickening (dilatant) fluids, it was found that the scheme had difficulty converging to a solution. This failure to converge to a solution was determined to be partially due to the finite-width nature and non-exponential decay in the far-field of the initial velocity profile for a shear-thickening fluid; this has been discussed in Chapter 4 and in Denier and Dabrowski (2004). The other factor was identified as being the inappropriateness of the power-law constitutive relation particularly in regions of uniform flow where the shear-rate is very small.

In view of such inherent limitations of the power-law viscosity model, especially for very low and very high shear-rates, we now consider a different viscosity model from the category of generalised Newtonian fluids. The alternative constitutive relation selected is based on the Carreau viscosity model. This model overcomes the limitations of the classical power-law model identified above and appears to be gaining wider acceptance in industrial and technological flows.

This chapter is organised as follows. In Section 5.1 we present the Carreau viscosity model and then use it to obtain a formulation of the boundary-layer equations for a Carreau fluid. In Section 5.2 we describe a self-similar solution and discuss some of its properties. Section 5.3 explains the numerical scheme used for finding non-similar solutions to the boundary-layer equations for the Carreau fluid. Section 5.4 presents the results obtained with the numerical marching scheme for shear-thinning and shear-thickening fluids. The role of the Carreau viscosity model parameters on the solutions is also explained. In Section 5.5 the existence of an asymptotic form for the velocity profile at a large distance from the leading edge of a flat plate is described and compared with the numerical solutions. Finally in Section 5.6 some conclusions about the material in this chapter are presented.

5.1 Equations of Motion

The power-law viscosity model has the limitation that it cannot adequately predict the viscosity for very small or very large shear rates. Severe convergence difficulties can occur in regions of the flow field where the second invariant I_2 of $\dot{\boldsymbol{\gamma}}$, the rate-of-deformation tensor, is very small; for example, in regions representing a uniform flow. Numerical convergence problems were observed during the solution of the boundary-layer flow for a shear-thickening fluid. At large distances from the boundary surface the velocity shear rates become vanishingly small. A power-law viscosity model, when used to describe shear-thickening fluids, results in the 'apparent viscosity' being effectively zero for such small shear rates. Real fluids, however, possess a finite, though very small, viscosity even when the velocity shear is effectively zero in the far-field region of the flow. Hence, a viscosity model that gives a constant, albeit small, value for the 'apparent viscosity' when the shear rate tends toward zero would conform better with the behaviour of a real fluid. A model for the fluid viscosity which possesses such a property is the Carreau model.

The Carreau model for fluid viscosity μ^* is given by

$$\mu^* = \mu_\infty + (\mu_0 - \mu_\infty)\left\{1 + (K_1\dot{\gamma}^*)^2\right\}^{\frac{n-1}{2}},$$

where n is the fluid index, μ_0 is the zero-shear-rate viscosity, μ_∞ is the infinite-shear-rate viscosity and $\dot{\gamma}^*$ is the shear-rate. The parameter K_1 is a characteristic time constant (with τ being a corresponding characteristic stress) associated with the transition from low-shear Newtonian to non-Newtonian behaviour. These parameters are related by $K_1 = \mu_0/\tau$. By having the units of time, K_1 is sometimes referred to as a 'relaxation time', however this term is somewhat inappropriate as these fluids are not considered to possess any form of 'memory'. The above equation can be expressed as

$$\mu^* = \mu_\infty\left[1 + C_0\left\{1 + (K_1\dot{\gamma}^*)^2\right\}^{\frac{n-1}{2}}\right], \tag{5.1}$$

where $C_0 = \frac{\mu_0 - \mu_\infty}{\mu_\infty}$ is a viscosity ratio. We note that when $n = 1$, equation (5.1) reduces to $\mu^* = \mu_0$, which corresponds a Newtonian fluid with constant viscosity. The Carreau model for fluid viscosity is, in some regards, a generalisation of the power-law viscosity model.

The derivation of the boundary-layer equations for a Carreau-model fluid begins with the primitive variable form of the conservation of mass and momentum equations for a steady, incompressible, viscous flow in the absence of external body forces. The same non-dimensionalisation as was performed for the power-law fluid case is applied to the governing equations here.

The non-dimensionalised viscosity, denoted by μ, becomes

$$\mu = \mu_\infty\left[1 + C_0\left\{1 + \left(\frac{K_1 U}{\epsilon L}\right)^2\left(\frac{\partial u}{\partial y}\right)^2\right\}^{\frac{n-1}{2}}\right]. \tag{5.2}$$

The derivatives of the stress terms are substituted into the right-hand-side of the x-momentum equation to give

$$\text{rhs} = -\frac{\partial p}{\partial x} + \left(\frac{\mu_\infty}{\rho U L}\right)\frac{1}{\epsilon^2}\left[(n-1)C_0\left(\frac{K_1 U}{\epsilon L}\right)^2\left\{1+\left(\frac{K_1 U}{\epsilon L}\right)^2\left(\frac{\partial u}{\partial y}\right)^2\right\}^{\frac{n-3}{2}}\left(\frac{\partial u}{\partial y}\right)^2\frac{\partial^2 u}{\partial y^2}\right.$$
$$\left.+\left[1+C_0\left\{1+\left(\frac{K_1 U}{\epsilon L}\right)^2\left(\frac{\partial u}{\partial y}\right)^2\right\}^{\frac{n-1}{2}}\right]\frac{\partial^2 u}{\partial y^2}+O(\epsilon^2)\right], \quad (5.3)$$

where the $O(\epsilon^2)$ term takes the form

$$\epsilon^2\left[(n-1)C_0\left(\frac{K_1 U}{\epsilon L}\right)^2\left\{1+\left(\frac{K_1 U}{\epsilon L}\right)^2\left(\frac{\partial u}{\partial y}\right)^2\right\}^{\frac{n-3}{2}}\frac{\partial u}{\partial y}\left(2\frac{\partial u}{\partial x}\frac{\partial^2 u}{\partial x \partial y}+\frac{\partial v}{\partial x}\frac{\partial^2 u}{\partial y^2}\right)\right.$$
$$\left.+\left[1+C_0\left\{1+\left(\frac{K_1 U}{\epsilon L}\right)^2\left(\frac{\partial u}{\partial y}\right)^2\right\}^{\frac{n-1}{2}}\right]\frac{\partial^2 u}{\partial x^2}\right].$$

We define a ‘non-Newtonian’ Reynolds number

$$Re \equiv \frac{\rho U L}{\mu_\infty}, \quad (5.4)$$

and note that for a Carreau-model fluid the Reynolds number is independent of the fluid index n and is identical in form to the familiar definition of the Reynolds number for a Newtonian fluid.

In equation (5.3) we require that both the pressure term and the viscous term be $O(1)$, which results in

$$\left(\frac{1}{Re}\right)\left(\frac{1}{\epsilon^2}\right) = O(1),$$

from which we find that the boundary-layer thickness is given by

$$\epsilon = O(Re^{-\frac{1}{2}}). \quad (5.5)$$

We note here that the boundary-layer thickness for a Carreau-model fluid is independent of the fluid index n, as distinct from the boundary-layer thickness of power-law fluids which is dependent on the fluid index.

Analysis of the term $\left(\frac{K_1 U}{\epsilon L}\right)^2$ shows it to be a dimensionless quantity. We represent this dimensionless parameter as

$$\lambda^2 = \left(\frac{K_1 U}{\epsilon L}\right)^2 .$$

The parameter λ is taken to be an $O(1)$ quantity and can be considered to be a dimensionless equivalent of the constant K_1, which had units of time, in the Carreau model for viscosity.

With the previous assumption, the x-momentum equation in the boundary layer of a Carreau fluid is then given by

$$u\frac{\partial u}{\partial x} + v\frac{\partial u}{\partial y} = -\frac{\partial p}{\partial x} + \left[1 + C_0\left\{1 + n\left(\lambda\frac{\partial u}{\partial y}\right)^2\right\}\left\{1 + \left(\lambda\frac{\partial u}{\partial y}\right)^2\right\}^{\frac{n-3}{2}}\frac{\partial^2 u}{\partial y^2} + O(\epsilon^2)\right]. \quad (5.6)$$

The y-momentum equation in the boundary layer of a Carreau fluid is derived in a similar manner and is given by

$$\begin{aligned}\epsilon\left[u\frac{\partial v}{\partial x} + v\frac{\partial v}{\partial y}\right] = -\frac{1}{\epsilon}\frac{\partial p}{\partial y} + \epsilon\Bigg[(n-1)C_0\lambda^2\left\{1 + \left(\lambda\frac{\partial u}{\partial y}\right)^2\right\}^{\frac{n-3}{2}}\frac{\partial u}{\partial y}\left(\frac{\partial^2 u}{\partial x \partial y}\frac{\partial u}{\partial y} + 2\frac{\partial^2 u}{\partial y^2}\frac{\partial v}{\partial y}\right)\\ + \left[1 + C_0\left\{1 + \left(\lambda\frac{\partial u}{\partial y}\right)^2\right\}^{\frac{n-1}{2}}\right]\frac{\partial^2 v}{\partial y^2} + O(\epsilon^2)\Bigg]. \quad (5.7)\end{aligned}$$

The system of partial differential equations describing the boundary-layer flow of a fluid with viscosity governed by the Carreau model is obtained by letting $Re \to \infty$, i.e. $\epsilon \to 0$. When this limit is applied the governing equations reduce to

$$\frac{\partial u}{\partial x} + \frac{\partial v}{\partial y} = 0, \quad (5.8a)$$

$$u\frac{\partial u}{\partial x} + v\frac{\partial u}{\partial y} = -\frac{\partial p}{\partial x} + \left[1 + C_0\left\{1 + n\left(\lambda\frac{\partial u}{\partial y}\right)^2\right\}\left\{1 + \left(\lambda\frac{\partial u}{\partial y}\right)^2\right\}^{\frac{n-3}{2}}\right]\frac{\partial^2 u}{\partial y^2}, \quad (5.8b)$$

$$0 = -\frac{\partial p}{\partial y}. \quad (5.8c)$$

The boundary conditions that apply to the above system of equations are the same as those used for the power-law model fluid, viz.

$$u = 0, \quad v = V(x) \quad \text{on} \quad y = 0, \tag{5.9a}$$

$$u \to U_e(x) \quad \text{as} \quad y \to \infty. \tag{5.9b}$$

In Section 2.2.1 the effect of small wall curvature on the equations governing the boundary-layer flow of a power-law fluid was discussed. The Prandtl transformation was used to show that the form of the governing equations remained the same after the introduction of a new wall-normal coordinate $\tilde{y}$ and velocity component $\tilde{v}$. In an identical manner, the Prandtl transformation can be used to examine the effect of small wall curvature on the boundary-layer flow of a Carreau fluid. It is found that the form of equations (5.8) remains unaltered after the introduction of $\tilde{y}$ for the wall-normal coordinate and $\tilde{v}$ for the corresponding velocity component.

The boundary-layer flow of a Carreau fluid is described by the system of partial differential equations (5.8) along with boundary conditions (5.9). This system of equations is non-linear and a closed-form solution is not readily apparent. Hence we will need to solve this problem numerically. Following the usual practice for solving this class of problem, we proceed by transforming this system of equations into a form suitable for solution by numerical methods. The choice of transformation is guided by the observation that the Reynolds number is of the same form as encountered in the study of Newtonian fluids. Hence, we define

$$\xi = x, \qquad \eta = y\left(\frac{U_e}{x}\right)^{\frac{1}{2}},$$

and introduce the stream function

$$\psi(x, y) = (U_e x)^{\frac{1}{2}} f(\xi, \eta),$$

where $U_e(x)$ is the external velocity in the far-field of the flow and $f(\xi, \eta)$ is the dimensionless stream function. The general method used here for transforming the governing equations is based on a stream function formulation and differs slightly from that used in Section 3.1.

The velocity components are given by

$$u = U_e \frac{\partial f}{\partial \eta}, \qquad v = -\left[\frac{\left(\frac{dU_e}{dx} x + U_e\right)}{2(U_e x)^{\frac{1}{2}}} f + (U_e x)^{\frac{1}{2}} \left(\frac{\partial f}{\partial \xi} + \eta_x \frac{\partial f}{\partial \eta} \right) \right].$$

The stream function satisfies the continuity equation identically. When the above expressions for u, v and the derivatives of u are substituted into the x-momentum equation we obtain, after some simplification,

$$\frac{\partial^3 f}{\partial \eta^3} \left[1 + C_0 \left\{ 1 + n \frac{U_e^3}{\xi} \left(\lambda \frac{\partial^2 f}{\partial \eta^2} \right)^2 \right\} \left\{ 1 + \frac{U_e^3}{\xi} \left(\lambda \frac{\partial^2 f}{\partial \eta^2} \right)^2 \right\}^{\frac{n-3}{2}} \right]$$
$$+ \frac{\xi}{U_e} \frac{dU_e}{d\xi} \left[1 - \left(\frac{\partial f}{\partial \eta} \right)^2 \right] + \frac{1}{2} \left[\frac{\xi}{U_e} \frac{dU_e}{d\xi} + 1 \right] f \frac{\partial^2 f}{\partial \eta^2} = \xi \left[\frac{\partial^2 f}{\partial \xi \partial \eta} \frac{\partial f}{\partial \eta} - \frac{\partial^2 f}{\partial \eta^2} \frac{\partial f}{\partial \xi} \right].$$

We now introduce the external pressure gradient parameter β defined as

$$\beta(\xi) = \frac{\xi}{U_e} \frac{dU_e}{d\xi}. \tag{5.10}$$

The term $\frac{1}{\xi}$ can be seen to cause singular behaviour for very small values of ξ. This singularity can be removed by factoring out this term to give

$$\frac{\partial^3 f}{\partial \eta^3} \left[1 + C_0 \xi^{\frac{1-n}{2}} \left\{ \xi + n U_e^3 \left(\lambda \frac{\partial^2 f}{\partial \eta^2} \right)^2 \right\} \left\{ \xi + U_e^3 \left(\lambda \frac{\partial^2 f}{\partial \eta^2} \right)^2 \right\}^{\frac{n-3}{2}} \right]$$
$$+ \frac{1}{2} [\beta + 1] f \frac{\partial^2 f}{\partial \eta^2} + \beta \left[1 - \left(\frac{\partial f}{\partial \eta} \right)^2 \right] = \xi \left[\frac{\partial^2 f}{\partial \xi \partial \eta} \frac{\partial f}{\partial \eta} - \frac{\partial^2 f}{\partial \eta^2} \frac{\partial f}{\partial \xi} \right]. \tag{5.11}$$

Equation (5.11) is a third order non-linear partial differential equation and its numerical solution still requires some effort. We continue by reducing the third order derivative appearing in equation (5.11) to second order by letting $q = \frac{\partial f}{\partial \eta}$ as this allows for a simpler numerical scheme to be developed. Making this substitution gives

$$\frac{\partial^2 q}{\partial \eta^2}\left[1 + C_0 \xi^{\frac{1-n}{2}}\left\{\xi + nU_e^3\left(\lambda\frac{\partial q}{\partial \eta}\right)^2\right\}\left\{\xi + U_e^3\left(\lambda\frac{\partial q}{\partial \eta}\right)^2\right\}^{\frac{n-3}{2}}\right]$$
$$+\left[\frac{1}{2}(\beta+1) f + \xi\frac{\partial f}{\partial \xi}\right]\frac{\partial q}{\partial \eta} + \beta\left[1-q^2\right] - \xi q\frac{\partial q}{\partial \xi} = 0. \qquad (5.12)$$

Since $\frac{\partial f}{\partial \eta} = q(\xi, \eta)$, integrating once with respect to η gives

$$f(\xi, \eta) = \int_0^\eta q \, \mathrm{d}\eta + G(\xi).$$

Making use of the boundary condition at $\eta = 0$ we find that $f(\xi, 0) = G(\xi)$. Hence,

$$f(\xi, \eta) = \int_0^\eta q \, \mathrm{d}\eta + f(\xi, 0). \qquad (5.13)$$

Differentiating equation (5.13) with respect to ξ gives

$$\frac{\partial f(\xi, \eta)}{\partial \xi} = \int_0^\eta \frac{\partial q}{\partial \xi}\, d\eta + \frac{\partial f(\xi, 0)}{\partial \xi}.$$

Making use of these expressions for f and $\frac{\partial f}{\partial \xi}$ in equation (5.12) yields

$$\frac{\partial^2 q}{\partial \eta^2}\left[1 + C_0 \xi^{\frac{1-n}{2}}\left\{\xi + nU_e^3\left(\lambda\frac{\partial q}{\partial \eta}\right)^2\right\}\left\{\xi + U_e^3\left(\lambda\frac{\partial q}{\partial \eta}\right)^2\right\}^{\frac{n-3}{2}}\right]$$
$$+\left[\int_0^\eta \left\{\frac{1}{2}(\beta+1)q + \xi\frac{\partial q}{\partial \xi}\right\} \mathrm{d}\eta + \frac{1}{2}(\beta+1) f(\xi, 0) + \xi\frac{\partial f(\xi, 0)}{\partial \xi}\right]\frac{\partial q}{\partial \eta} + \beta\left[1-q^2\right] - \xi q\frac{\partial q}{\partial \xi} = 0. \qquad (5.14)$$

The boundary conditions (5.9 a,b) also need to be expressed in terms of the computational coordinates (ξ, η). When the appropriate change of variables is made the no-slip boundary condition at the surface, $u = 0$ on $\eta = 0$, becomes

$$\left.\frac{\partial f}{\partial \eta}\right|_{\eta=0} = 0, \quad \text{or} \quad q|_{\eta=0} = 0. \qquad (5.15)$$

The mass transfer at the surface, $v = V(\xi)$ on $\eta = 0$, becomes

$$V = -\left(\frac{U_e}{\xi}\right)^{\frac{1}{2}} \left[\frac{1}{2}(\beta+1)f(\xi,0) + \xi\left(\frac{\partial f(\xi,0)}{\partial \xi} + \eta_x \left.\frac{\partial f}{\partial \eta}\right|_{\eta=0}\right)\right],$$

which can be simplified to

$$-\left(\frac{\xi}{U_e}\right)^{\frac{1}{2}} V = \frac{1}{2}(\beta+1)f(\xi,0) + \xi\frac{\partial f(\xi,0)}{\partial \xi} \tag{5.16}$$

The far-field boundary condition, $u \to U_e$ as $\eta \to \infty$, becomes

$$\frac{\partial f}{\partial \eta} \to 1 \quad \text{as} \quad \eta \to \infty, \quad \text{or} \quad q \to 1. \tag{5.17}$$

The form of the mass transfer boundary condition (5.16) can be used to simplify equation (5.14) to give the following

$$\frac{\partial^2 q}{\partial \eta^2}\left[1 + C_0\xi^{\frac{1-n}{2}}\left\{\xi + nU_e^3\left(\lambda\frac{\partial q}{\partial \eta}\right)^2\right\}\left\{\xi + U_e^3\left(\lambda\frac{\partial q}{\partial \eta}\right)^2\right\}^{\frac{n-3}{2}}\right]$$
$$+\left[\int_0^\eta \left\{\frac{1}{2}(\beta+1)q + \xi\frac{\partial q}{\partial \xi}\right\} \mathrm{d}\eta - \left(\frac{\xi}{U_e}\right)^{\frac{1}{2}} V\right]\frac{\partial q}{\partial \eta} + \beta\left[1-q^2\right] - \xi q\frac{\partial q}{\partial \xi} = 0. \tag{5.18a}$$

The accompanying boundary conditions are

$$q = 0 \quad \text{on} \quad \eta = 0, \tag{5.18b}$$

$$q \to 1 \quad \text{as} \quad \eta \to \infty, \tag{5.18c}$$

as the mass transfer boundary condition appears implicitly in equation (5.18a).

The partial differential equation governing the boundary-layer flow of the Carreau fluid, viz. equation (5.18a), is an integro-differential equation which has a form not unlike that of equation (3.6a) which governs the boundary-layer flow of a power-law fluid. We recall that equation (3.6a) needed to be re-arranged slightly when the fluid index was in the range $0 < n < 1$. However, a key difference here is that equation (5.18) can be used in its current form, without the need for re-arrangement of terms, for both shear-thinning and shear-thickening fluids. We do need to be aware of the numerical singularity that exists at $\xi = 0$ for shear-thickening fluids ($n > 1$) as a result of the term $\xi^{\frac{1-n}{2}}$. This singular behaviour will manifest itself via the 'coefficient' term of $\frac{\partial^2 q}{\partial \eta^2}$, which will become large in magnitude at very small values of ξ. A convenient way of avoiding this problem is to start the numerical solution procedure at a location some distance down-stream from $\xi = 0$.

5.2 A Similarity-type Solution

As noted above, the non-linear nature of the partial differential equation governing the boundary-layer flow of a Carreau model fluid makes it quite formidable to solve, with an analytical solution not being readily apparent. The existence of a similarity-type solution would provide valuable insight into the behaviour of the flow. An examination of equation (5.11) tends to indicate that a general class of similarity-type solutions, akin to the Falkner-Skan solutions for Newtonian fluids, is not readily obvious, and may not, exist. However, equation (5.11) can be reduced to a form that allows a self-similar solution to be found if the external flow is given by $U_e(\xi) = \xi^{\frac{1}{3}}$. This specific external flow, from the Falkner-Skan family, corresponds to the potential flow over a wedge whose included angle is $\frac{\pi}{2}$.

Substituting this form of $U_e(\xi)$ into equation (5.11) and assuming that $f(\xi, \eta) = f(\eta)$ (i.e. the streamwise velocity field depends only upon the similarity variable η) we obtain

$$\left[1 + C_0 \left\{1 + n\left(\lambda f''\right)^2\right\} \left\{1 + \left(\lambda f''\right)^2\right\}^{\frac{n-3}{2}}\right] f''' + \frac{2}{3} f f'' + \frac{1}{3}\left[1 - \left(f'\right)^2\right] = 0, \qquad (5.19a)$$

where the prime denotes differentiation with respect to η. The associated boundary conditions are

$$f = f' = 0 \quad \text{on} \quad \eta = 0, \qquad (5.19b)$$

$$f' \to 1 \quad \text{as} \quad \eta \to \infty. \qquad (5.19c)$$

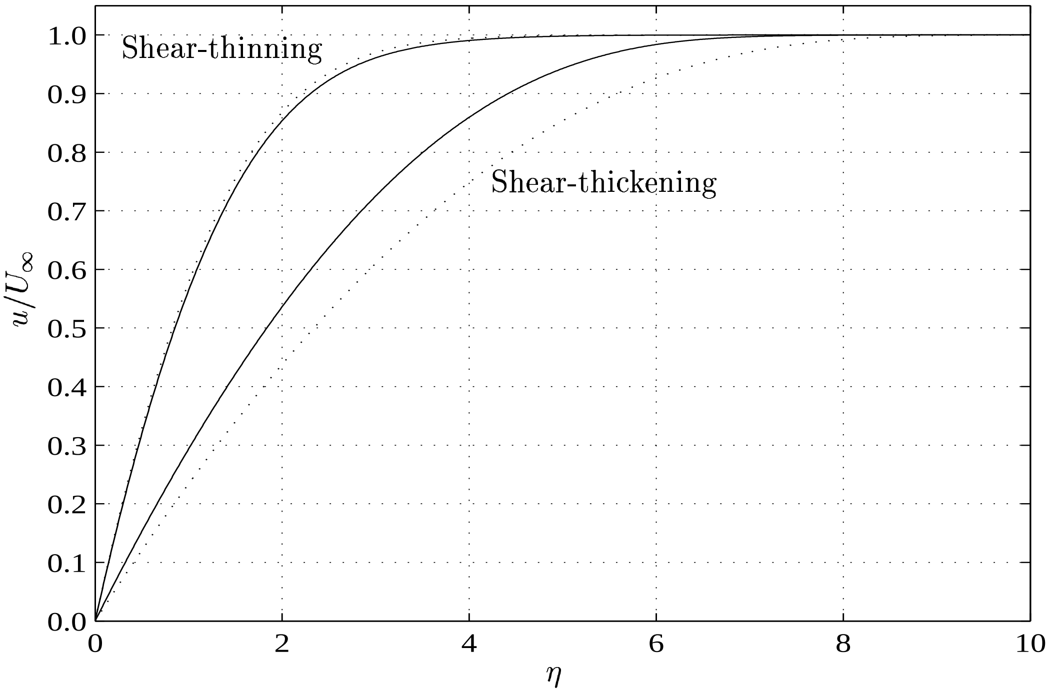

Figure 5.1: Self-similar velocity profiles for shear-thinning ($n = 0.5$) and shear-thickening ($n = 1.5$) Carreau fluids. Relaxation parameter values $\lambda = 50$ (solid line) and $\lambda = 200$ (dotted line); $C_0 = 1$.

Equation (5.19) was solved using a shooting method which employed a fourth-order Runge-Kutta quadrature scheme coupled to Newton iteration. As part of the solution process, both the self-similar velocity profile as well as the viscosity were obtained. The calculations had the far-field η_∞ set at 20 and the η step-size was set to 0.01.

Some representative streamwise velocity profiles for shear-thinning and shear-thickening Carreau fluids are shown in Figure 5.1, though the display range is limited to $\eta = 10$. The velocity profiles shown are for fluid index values $n = 0.5$ and $n = 1.5$. For each fluid index, the relaxation parameter λ takes the values 50 (solid line) and 200 (dotted line). The value of C_0 was held fixed at unity.

A comparison of these velocity profiles indicates that the boundary-layer thickness (based on the η value at which the streamwise velocity is 99% of the free-stream velocity) for shear-thinning fluids is smaller than for shear-thickening fluids. Also the reduced skin friction, given by the slope of the velocity profile at $\eta = 0$, is greater for shear-thinning fluids than it is for shear-thickening fluids. Figure 5.1 also shows the effect of the relaxation parameter λ

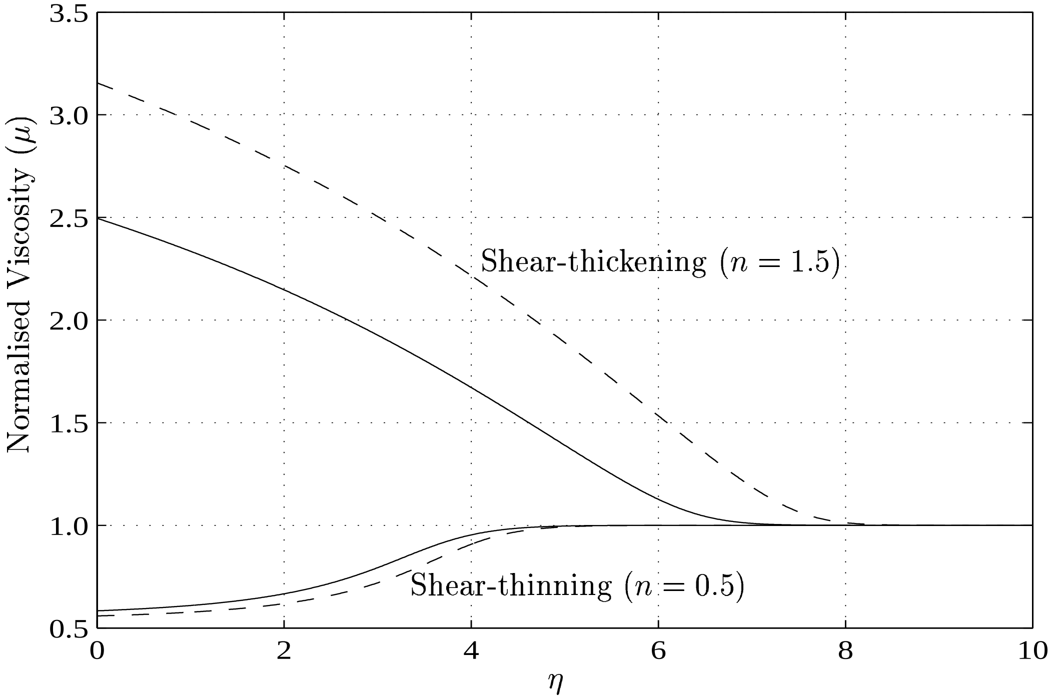

Figure 5.2: Normalised 'fluid viscosity' within the boundary layer of shear-thinning ($n = 0.5$) and shear-thickening ($n = 1.5$) Carreau fluids. Relaxation parameter values $\lambda = 50$ (solid line) and $\lambda = 100$ (dashed line); $C_0 = 1$.

on the streamwise velocity profiles. For shear-thinning fluids the variation of the relaxation parameter has a fairly minimal effect on the velocity profile, and hence the boundary-layer thickness and reduced skin friction. For shear-thickening fluids changing the value of the relaxation parameter has a more noticeable effect. With a larger value of λ the boundary-layer thickness increases while the skin friction is decreased.

The existence of self-similar solutions for a Carreau fluid helps us to gain an understanding of how the viscosity varies within the boundary-layer. The 'fluid viscosity' was calculated using

$$\mu = 1 + C_0 \left\{1 + (\lambda f'')^2\right\}^{\frac{n-1}{2}},$$

which was normalised so as to be equal to unity as $\eta \to \infty$. The results obtained, for the combinations of n and λ given above, are shown in Figure 5.2.

Figure 5.2 demonstrates that for shear-thinning and shear-thickening fluids the viscosity has a finite value on the flat plate surface ($\eta = 0$) and with increasing distance from the surface

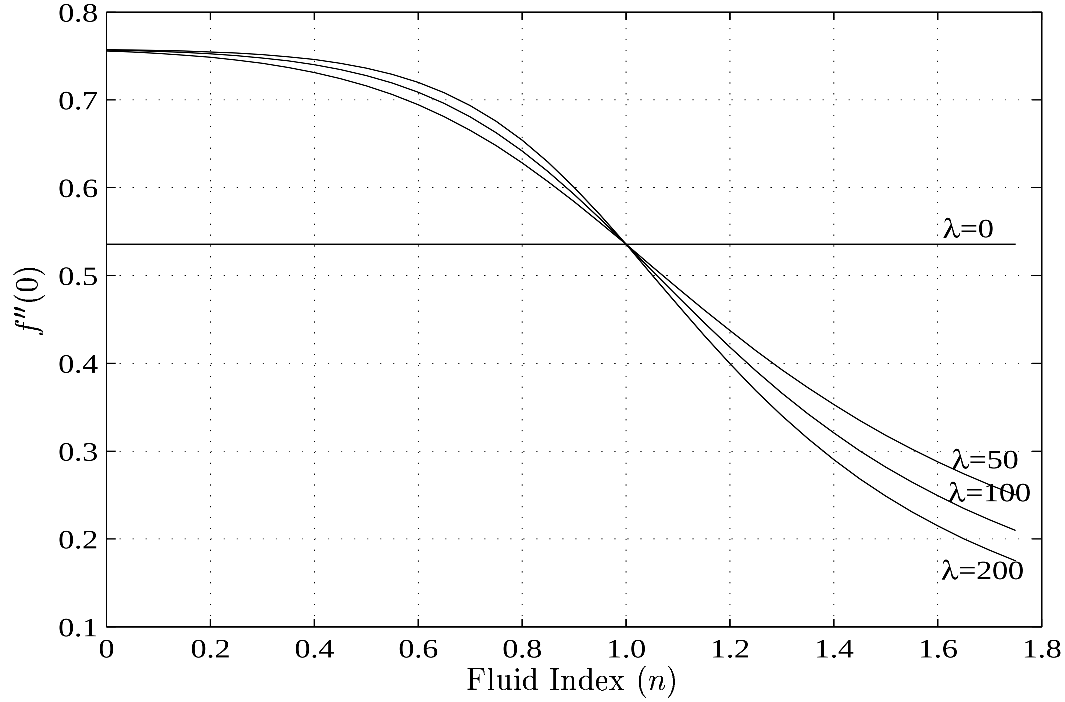

Figure 5.3: Plot of the reduced skin friction (velocity shear) at the wall for various values of λ with $C_0 = 1$.

the viscosity approaches a finite value. For shear-thinning Carreau fluids the finite value in the far-field is approached from below, while for shear-thickening fluids the approach is from above. The effect of the relaxation parameter λ on the viscosity is more noticeable for shear-thickening than shear-thinning Carreau fluids.

The main point to note from Figure 5.2 is that the Carreau viscosity model predicts a viscosity that is never zero or infinite over the extent of the boundary layer; this is in contrast to the simpler power-law rheological model. Hence, the Carreau viscosity model can be used to adequately capture the variation of viscosity within a boundary layer of a non-Newtonian fluid, without suffering from any of the non-physical crises that arise when the simpler power-law viscosity model is employed.

Some insight into the behaviour of the reduced skin friction (i.e. velocity shear) at the wall can also be gained from the self-similar solutions. Figure 5.3 shows a plot of the reduced skin friction versus fluid index n for values of $\lambda = 0, 50, 100, 200$ and $C_0 = 1$. For $\lambda = 0$ equation (5.19) reduces to a form that is independent of n, so the resulting self-similar solution and reduced skin friction (given by $f''(0)$) provides a baseline for comparison with other values of λ. For $n = 1$ equation (5.19) reduces to a form that is independent of λ and identical to the form for the $\lambda = 0$ case. Hence, all solutions for $n = 1$ and non-zero λ lie on the baseline given by $\lambda = 0$.

For the values of λ considered, the plots in Figure 5.3 show that the reduced skin friction decreases with increasing fluid index. The maximum value of the reduced skin friction occurs when the fluid index is zero and λ is non-zero. Setting $n = 0$ in equation (5.19) results in a final form that is dependent on λ; indicating that the reduced skin friction will vary with λ for $n = 0$ as the results show.

5.3 Numerical Method

The boundary-layer flow of a fluid with viscosity described by the Carreau model is governed by equation (5.18a) and boundary conditions (5.18b,c). We now turn our attention to other classes of free-stream velocity profiles for which the similarity solution given in Section 5.2 is not applicable.

As the parabolic partial differential equations governing the boundary-layer flow of a Carreau fluid have a structure that is not unlike the boundary-layer equations for a power-law fluid, the numerical method that will be used to solve them is essentially the same as was employed for the numerical solution of the power-law model fluid. The numerical method described below is intended to be quite general and applicable to a wide range of external flow regimes.

Proceeding as before, the derivatives in the ξ-direction are replaced by finite differences and all other quantities are replaced by averages. The subscripts denote two closely spaced locations in the stream-wise direction, i.e. at cross-sections $\xi = \xi_1$ and $\xi = \xi_2$ respectively. Let

$$\widehat{q} = \frac{q_1 + q_2}{2}, \quad \widehat{\xi} = \frac{\xi_1 + \xi_2}{2}, \quad \widehat{U}_e = \frac{U_{e_1} + U_{e_2}}{2}, \quad \frac{\partial q}{\partial \xi} = \frac{q_2 - q_1}{\Delta \xi},$$

where $\Delta\xi = \xi_2 - \xi_1$.

Hence, at any stage of the marching scheme that will be used to solve the parabolic partial differential equations the values q_1 are assumed to be known and the values q_2 are to be determined.

Making these substitutions in equation (5.18a) and simplifying some of the expressions results in

$$
\begin{aligned}
&\frac{d^2\widehat{q}}{d\eta^2}\left[1+C_0\widehat{\xi}^{\frac{1-n}{2}}\left\{\widehat{\xi}+n\widehat{U}_e^3\left(\lambda\frac{d\widehat{q}}{d\eta}\right)^2\right\}\left\{\widehat{\xi}+\widehat{U}_e^3\left(\lambda\frac{d\widehat{q}}{d\eta}\right)^2\right\}^{\frac{n-3}{2}}\right]\\
&\quad+\left[\frac{1}{2}\int_0^\eta\frac{(\beta_1+1)q_1+(\beta_2+1)q_2}{2}\,d\eta+\int_0^\eta\widehat{\xi}\left(\frac{q_2-q_1}{\Delta\xi}\right)\,d\eta-\left(\frac{\widehat{\xi}}{\widehat{U}_e}\right)^{\frac{1}{2}}V\right]\frac{d\widehat{q}}{d\eta}\\
&\quad+\frac{\beta_1\left(1-q_1^2\right)+\beta_2\left(1-q_2^2\right)}{2}-\widehat{\xi}\widehat{q}\left(\frac{q_2-q_1}{\Delta\xi}\right)=0.
\end{aligned}
$$

Next we replace all appearances of q_2 by $2\widehat{q}-q_1$, or equivalently with $q_2-q_1=2(\widehat{q}-q_1)$, to give

$$
\begin{aligned}
&\frac{d^2\widehat{q}}{d\eta^2}\left[1+C_0\widehat{\xi}^{\frac{1-n}{2}}\left\{\widehat{\xi}+n\widehat{U}_e^3\left(\lambda\frac{d\widehat{q}}{d\eta}\right)^2\right\}\left\{\widehat{\xi}+\widehat{U}_e^3\left(\lambda\frac{d\widehat{q}}{d\eta}\right)^2\right\}^{\frac{n-3}{2}}\right]\\
&\quad+\left[\frac{1}{2}(\beta_2+2\theta+1)\int_0^\eta\widehat{q}\,d\eta+\frac{1}{4}(\beta_1-\beta_2-4\theta)\int_0^\eta q_1\,d\eta-K_{in}\right]\frac{d\widehat{q}}{d\eta}\\
&\quad+\widehat{\beta}\left(1-q_1^2\right)-(2\beta_2+\theta)\widehat{q}(\widehat{q}-q_1)=0, \qquad (5.20)
\end{aligned}
$$

where $\theta=\frac{\xi_1+\xi_2}{\Delta\xi}$, $\widehat{\beta}=\frac{\beta_1+\beta_2}{2}$ and $K_{in}=\left(\frac{\widehat{\xi}}{\widehat{U}_e}\right)^{\frac{1}{2}}V$.

Derivatives with respect to η are discretised using second-order accurate finite-difference approximations as in Section 3.2, and the definite integrals are evaluated using the trapezoidal rule, denoted by $\sum''$, with the first and last terms halved. After making these substitutions and multiplying through by h^2 equation (5.20) has the following discretised form

$$
\begin{aligned}
&(\widehat{q}_{j+1} - 2\widehat{q}_j + \widehat{q}_{j-1})\left[1 + C_0\widehat{\xi}^{\frac{1-n}{2}}\left\{\widehat{\xi} + n\widehat{U}_e^3\left(\lambda\frac{\widehat{q}_{j+1} - \widehat{q}_{j-1}}{2h}\right)^2\right\}\left\{\widehat{\xi} + \widehat{U}_e^3\left(\lambda\frac{\widehat{q}_{j+1} - \widehat{q}_{j-1}}{2h}\right)^2\right\}^{\frac{n-3}{2}}\right] \\
&\quad + h^2\left[\frac{1}{2}(\beta_2 + 2\theta + 1)\sum_{r=0}^{j}{}''\widehat{q}_r + \frac{1}{4}(\beta_1 - \beta_2 - 4\theta)\sum_{r=0}^{j}{}'' q_{1,r} - K_{in}\right]\left(\frac{\widehat{q}_{j+1} - \widehat{q}_{j-1}}{2h}\right) \\
&\quad + h^2\left[\widehat{\beta}\left(1 - q_1^2\right)_j - (2\beta_2 + \theta)\widehat{q}_j(\widehat{q} - q_1)_j\right] = 0.
\end{aligned}
$$

The solution at the j^{th} mesh point involves the unknowns $\widehat{q}_1, \ldots, \widehat{q}_{j+1}$ and is found on a uniformly spaced mesh with points at $j = 1, \ldots, J$. The mesh point at $j = 0$ lies on the flat plate while $j = J+1$ is at the outer limit of the computational domain. The far-field boundary condition is satisfied by setting the $J + 1^{th}$ mesh point to a constant value, i.e. $\widehat{q}_{J+1} = 1$. This system of non-linear algebraic equations needs to be solved at each streamwise location. As the governing partial differential equations are parabolic, a marching scheme is used. At each streamwise location an iterative process based on Newton's method for non-linear systems of equations is used. Making use of the notation introduced in Section 3.2, the coordinate function f_j takes the following form

$$
\begin{aligned}
&f_j\left(\widehat{\mathbf{q}}^{(k)}\right) = \left(\widehat{q}_{j+1}^{(k)} - 2\widehat{q}_j^{(k)} + \widehat{q}_{j-1}^{(k)}\right) \times \\
&\left[1 + C_0\widehat{\xi}^{\frac{1-n}{2}}\left\{\widehat{\xi} + n\widehat{U}_e^3\left(\lambda\frac{\widehat{q}_{j+1}^{(k)} - \widehat{q}_{j-1}^{(k)}}{2h}\right)^2\right\}\left\{\widehat{\xi} + \widehat{U}_e^3\left(\lambda\frac{\widehat{q}_{j+1}^{(k)} - \widehat{q}_{j-1}^{(k)}}{2h}\right)^2\right\}^{\frac{n-3}{2}}\right] \\
&+ \left[\frac{h^3}{2}\left\{(\beta_2 + 2\theta + 1)\left(\widehat{q}_1^{(k)} + \ldots + \widehat{q}_{j-1}^{(k)} + \frac{1}{2}\widehat{q}_j^{(k)}\right)\right.\right. \\
&\qquad \left.\left. + \frac{1}{2}(\beta_1 - \beta_2 - 4\theta)\left(q_{1,1} + \ldots + q_{1,j-1} + \frac{1}{2}q_{1,j}\right)\right\} - h^2K_{in}\right]\left(\frac{\widehat{q}_{j+1}^{(k)} - \widehat{q}_{j-1}^{(k)}}{2h}\right) \\
&+ h^2\left[\widehat{\beta}\left(1 - q_1^2\right)_j - (2\beta_2 + \theta)\widehat{q}_j^{(k)}\left(\widehat{q}^{(k)} - q_1\right)_j\right]. \qquad (5.21)
\end{aligned}
$$

In the above equation, the trapezoidal sum has been expanded and the no-slip condition at $j = 0$ has been used. The superscript k is used to indicate which variables are being solved for in the iteration procedure as well as the iteration step.

The system of non-linear equations can be expressed as $\mathbf{F}(\widehat{\mathbf{q}}) = \mathbf{0}$. This system of equations will be solved using Newton iteration. The form of the Jacobian matrix that is required for the Newton iteration is described in Appendix C. We note that the Jacobian required for the solution of equation (5.21) has a sparse structure identical to that encountered in the solution procedure for power-law fluids.

For Falkner-Skan flows, having an external velocity given by $U_e(x) = x^m$, or, in the transformed variables $U_e(\xi) = \xi^m$, the equation at the j^{th} mesh point along with the Jacobian matrix can be simplified. The pressure gradient parameter β, defined by equation (5.10), becomes constant, i.e. $\beta_1 = \beta_2 = \beta$. In this case, the equations to be solved take the following simplified form

$$\begin{aligned}
f_j\left(\widehat{\mathbf{q}}^{(k)}\right) = {} & \left(\widehat{q}_{j+1}^{(k)} - 2\widehat{q}_j^{(k)} + \widehat{q}_{j-1}^{(k)}\right) \times \\
& \left[1 + C_0 \widehat{\xi}^{\frac{1-n}{2}} \left\{\widehat{\xi} + n\widehat{U}_e^3 \left(\lambda \frac{\widehat{q}_{j+1}^{(k)} - \widehat{q}_{j-1}^{(k)}}{2h}\right)^2\right\} \left\{\widehat{\xi} + \widehat{U}_e^3 \left(\lambda \frac{\widehat{q}_{j+1}^{(k)} - \widehat{q}_{j-1}^{(k)}}{2h}\right)^2\right\}^{\frac{n-3}{2}}\right] \\
& + \left[\frac{h^2}{2}\left\{(\beta + 2\theta + 1){\sum_{r=0}^{j}}'' \widehat{q}_r^{(k)} - 2\theta {\sum_{r=0}^{j}}'' q_{1,r}\right\} - h^2 K_{in}\right] \left(\frac{\widehat{q}_{j+1}^{(k)} - \widehat{q}_{j-1}^{(k)}}{2h}\right) \\
& + h^2 \left[\beta\left(1 - q_1^2\right)_j - (2\beta + \theta)\widehat{q}_j^{(k)} \left(\widehat{q}^{(k)} - q_1\right)_j\right],
\end{aligned} \tag{5.22}$$

The form of the Jacobian matrix that is required to solve equation (5.21) using Newton iteration is also described in Appendix C.

The parabolic nature of the governing equations requires a suitable initial condition to commence the numerical marching scheme. Such an initial condition is provided in the form of a prescribed velocity profile at a location ξ_0 from which the marching scheme starts. The calculation of the initial velocity profile is discussed next.

5.3.1 Initial Velocity Profile

We first consider the form of the initial velocity profile for a shear-thinning Carreau fluid. For shear-thinning fluids the numerical marching scheme can start at $\xi = 0$. Substituting $\xi = 0$ in equation (5.11) and simplifying further by assuming that the dimensionless stream function

$f(\xi,\eta)$ is independent of ξ results in

$$\frac{\mathrm{d}^3 f}{\mathrm{d}\eta^3} + \frac{1}{2}\left[\beta+1\right] f \frac{\mathrm{d}^2 f}{\mathrm{d}\eta^2} + \beta\left[1 - \left(\frac{\mathrm{d}f}{\mathrm{d}\eta}\right)^2\right] = 0. \tag{5.23a}$$

The boundary conditions for this third-order non-linear ordinary differential equation are

$$f = 0, \quad \frac{\mathrm{d}f}{\mathrm{d}\eta} = 0, \quad \text{on} \qquad \eta = 0, \tag{5.23b}$$

$$\frac{\mathrm{d}f}{\mathrm{d}\eta} \to 1 \quad \text{as} \qquad \eta \to \infty. \tag{5.23c}$$

Equation (5.23) is the classical Falkner-Skan equation. Solutions of equation (5.23) provide the self-similar velocity profiles within the boundary-layer of Falkner-Skan type flows. A suitable initial velocity profile for the numerical marching scheme for a shear-thinning Carreau fluid is, therefore, provided by the solution of the Falkner-Skan equation.

We recall that for power-law fluids the initial velocity profile was given by the self-similar solution of a Falkner-Skan-like ordinary differential equation that involved the fluid index n as a parameter. However, for shear-thinning Carreau fluids the initial velocity profile is provided by the solution of the classical Falkner-Skan equation with no dependence on the viscosity model parameters. Appropriate account of the pressure gradient parameter β needs to be taken when solving for the initial velocity profile.

The equations governing the boundary-layer flow of a Carreau fluid along a flat plate, as well as the numerical marching scheme, have the origin of the co-ordinate system located at the leading edge of the flat plate. An identical co-ordinate system was used in the case of power-law fluids. However, the boundary-layer approximation is not applicable in the near-vicinity of the leading edge. Additionally, the Falkner-Skan equation that provides the initial velocity profile is itself not applicable near the leading edge. Even-though the numerical marching scheme starts from the leading edge of the plate, we need to be aware that the solutions obtained are a reasonable indication of how the boundary layer is developing when we are some distance down-stream from the leading edge. In effect the boundary layer needs to be allowed to fully develop.

The Falkner-Skan equation (5.23a) and the boundary conditions (5.23b,c) form a two-point boundary-value problem that is solved numerically using a shooting method based on a fourth order Runge-Kutta quadrature scheme and Newton iteration for refining the guessed initial value. The solution that the shooting method converges to provides the initial velocity profile.

For shear-thickening Carreau fluids, it was noted in Section 5.1 that a mathematical singularity is present in equation (5.11) at $\xi = 0$. The approach presented above for calculating an initial velocity profile for shear-thinning fluids is not applicable to shear-thickening fluids. The numerical marching scheme for shear-thickening fluids will need to be started at a non-zero value of ξ. To solve equation (5.11) at such a value of ξ would, in effect, involve a single step of the numerical marching scheme which would require some form of an initial velocity profile itself.

The lack of a convenient means for calculating an initial velocity profile for a shear-thickening Carreau fluid can be circumvented by using the solution of the Falkner-Skan equation as the initial velocity profile. In doing so we are assuming that such an initial velocity profile is not too different from the true solution of equation (5.11) at the starting value of ξ. An alternative starting value can be found by exploiting suitable exponential function that resembles a boundary-layer velocity profile as an initial condition for the numerical scheme. We consider the effect of the initial profile on the flow development in Section 5.4.2

5.4 Numerical Results

The numerical method described in Section 5.3 for solving the partial differential equations governing the boundary-layer flow of a Carreau-model fluid was implemented as a Fortran computer program. Use was made of subroutine libraries such as LAPACK to solve the system of equations at each streamwise location.

Before the code could be used to investigate the non-similar solutions of equation (5.18a) it was considered necessary to validate the results produced by the program. By setting $C_0 = 0$ and $n = 1$ in equation (5.18a) we obtain the equation for the boundary-layer flow of a Newtonian fluid. The boundary-layer flow characteristics of Newtonian fluids are well understood. In the absence of mass transfer through the flat plate we expect the streamwise velocity profiles at various locations along the plate to be identical, i.e. exhibit self-similarity.

To validate the computer program the step-size, h, in the η-direction was set to 1.0×10^{-2} and the far-field, η_∞, was set to 10. The step-size, $\Delta\xi$, in the ξ-direction was set to 1.0×10^{-4} and the stopping location, ξ_{end}, was set to 1.0. The iteration stopping criterion at each marching location, $\Delta\widehat{\mathbf{q}}^{(k)}$, was set to 1.0×10^{-5}. Fluid injection at the surface was turned off and the external flow was uniform, i.e. $\beta = 0$. For β identically zero the Falkner-Skan equation that provides the initial velocity profile at $\xi = 0$ reduces to the classical Blasius equation.

Streamwise velocity profiles were captured at $\xi = 0.0, 0.1, \ldots, 1.0$ and examined. The velocity profiles were found to be identical to each other, or self-similar, as was expected. This simple test confirms the suitability of the code.

5.4.1 Shear-thinning Carreau Fluid

The numerical method described in Section 5.3 was used to investigate the boundary-layer flow of Carreau fluids with a fluid index in the range $0 < n < 1$. Carreau-model fluids with n in this range are commonly referred to as shear-thinning, or pseudoplastic.

When the mass transfer rate through the flat plate is zero and the external flow is uniform, i.e. $\beta = 0$, the boundary-layer flow of a power-law fluid develops into a self-similar form. The self-similar velocity profile is given by the solution of a Blasius-like equation. It has been shown in Section 5.2 that for Carreau fluids a self-similar boundary-layer flow exists for one specific value of β. Hence for any other values of the pressure gradient parameter β we expect the boundary-layer flow to be non-similar.

In the numerical investigations conducted, the various parameters were set as follows. The η step-size, h, was set to 2.0×10^{-2} and the far-field, η_∞, was set to 20. The ξ step-size, $\Delta\xi$, was set to 1.0×10^{-4} and the stopping location, ξ_{end}, was set to 3.0. The iteration stopping criterion at each marching location, $\Delta\widehat{\mathbf{q}}^{(k)}$, was set to 1.0×10^{-5}. The normalised viscosity ratio, C_0,

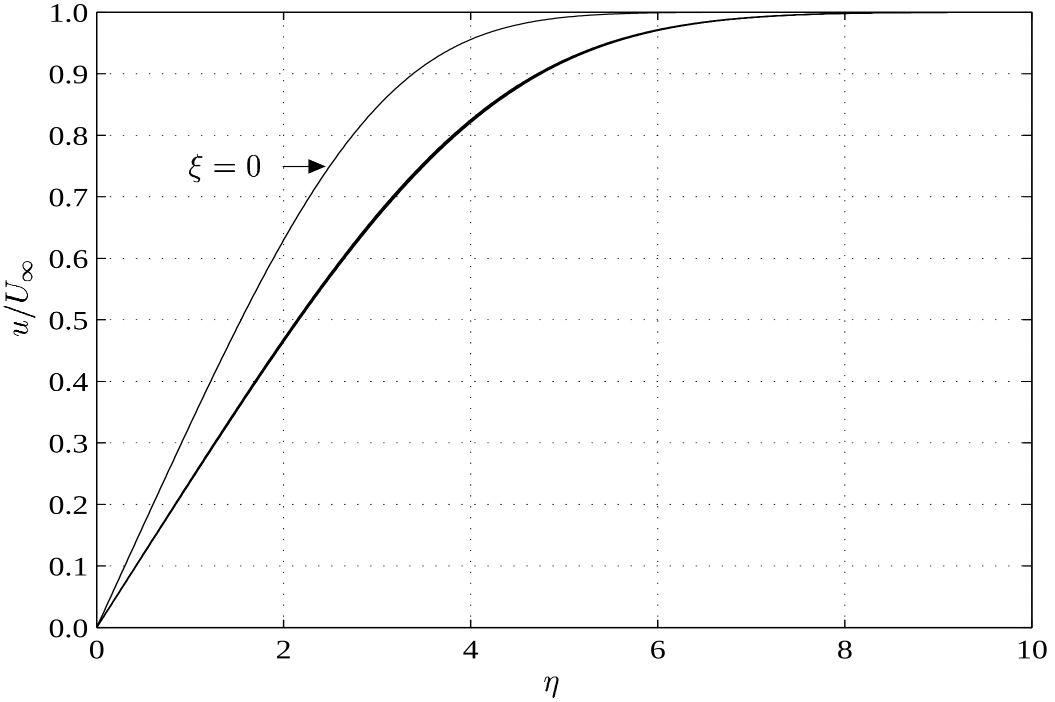

Figure 5.4: Velocity profiles for $n = 0.95$, $C_0 = 1$, $\lambda = 100$ at $\xi = 0, 0.5, \ldots, 3.0$

was set to 1.0, while the non-dimensional constant, λ, was set to a value of 100. The effect of the parameters in the Carreau viscosity model on the boundary-layer flow was investigated and is discussed later. The initial velocity profile for starting the numerical marching scheme was obtained by solving the Blasius equation.

Numerical solutions were obtained for different values of n, commencing at $n = 0.95$ and decreasing in steps of 0.05. Although sample velocity profiles were collected at $\xi = 0.0, 0.1, \ldots, 3.0$, the velocity profiles displayed in the figures below are from a selected subset of streamwise locations.

Velocity profiles for fluid index values $n = 0.95$, 0.75 and 0.50 are shown in Figures 5.4, 5.5 and 5.6 respectively. We see that the velocity profiles taken at various ξ locations differ from the initial Blasius velocity profile. This indicates that for a Carreau fluid the boundary-layer flow is non-similar for this choice of parameters. The boundary-layer equations governing the flow do not possess other similarity-type solutions apart from the one discussed previously. These plots indicate that for $n = 0.95$ the departure from the initial velocity profile occurs quite rapidly over a short distance from $\xi = 0$. The boundary layer can be considered to have

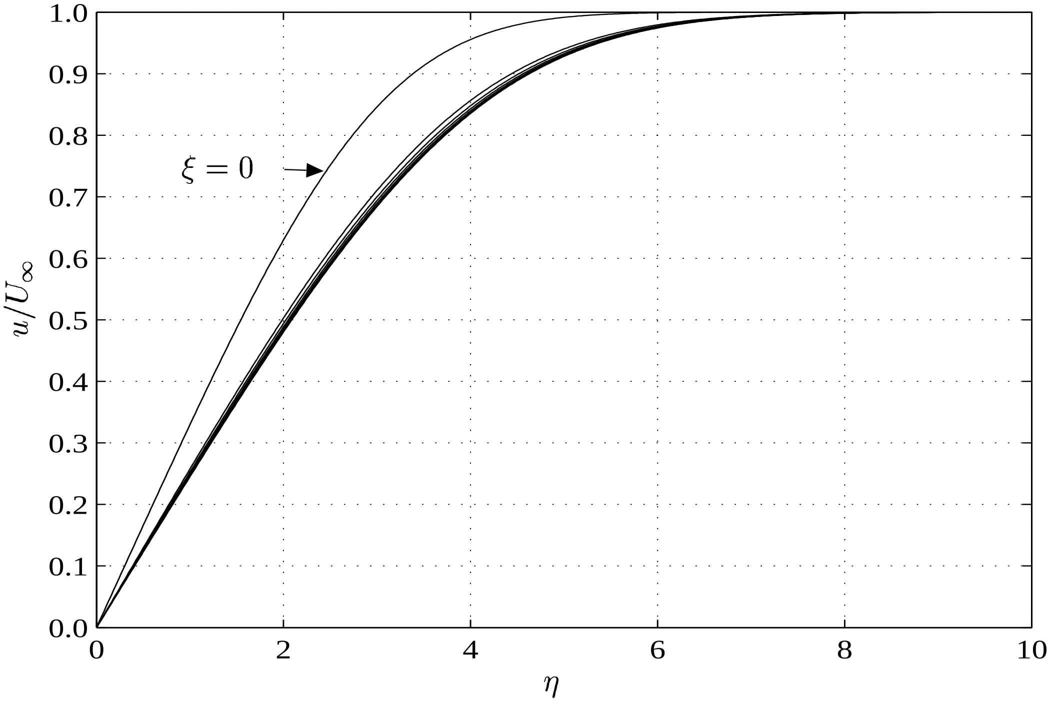

Figure 5.5: Velocity profiles for $n = 0.75$, $C_0 = 1$, $\lambda = 100$ at $\xi = 0, 0.5, \ldots, 3.0$

become fully developed after only a relatively short distance from the leading edge. However, for $n = 0.50$ the departure from the initial velocity profile is seen to be more gradual.

Such a rapid variation from the initial velocity profile is not unexpected as the boundary-layer approximation is not valid in the region $\xi = 0^+$. As the numerical solution proceeds a short distance past the leading edge of the plate, the boundary-layer is quickly developing into a form dictated by the governing equations as they become more physically appropriate. The rapid variation in velocity profiles can also be somewhat accounted for by the presence of the term $\xi^{\frac{1-n}{2}}$ in equation (5.18a). For a shear-thinning Carreau fluid, the exponent in this term is restricted to values between 0 and 0.5. When n is close to unity, the value of the exponent is close to 0. For the values of ξ in the solution domain this term results in values that are very close to unity and can be considered to be essentially constant. As n becomes small, the value of the exponent tends to 0.5. Hence the values that $\xi^{\frac{1-n}{2}}$ takes show more variability with the value of ξ. Thus there is a more noticeable change in the velocity profiles between different ξ locations.

The x-momentum equations (3.1b) and (5.8b) for power-law and Carreau fluids respectively

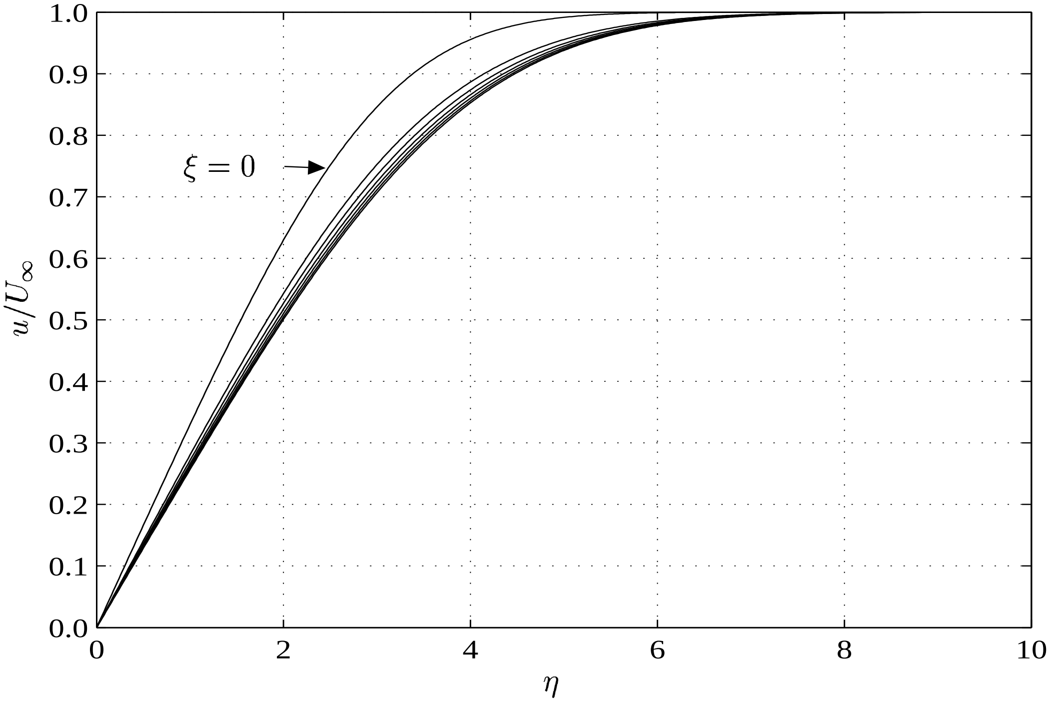

Figure 5.6: Velocity profiles for $n = 0.50$, $C_0 = 1$, $\lambda = 100$ at $\xi = 0, 0.5, \ldots, 3.0$

are alike except for the different viscosity terms. When the respective transformations to computational coordinates (ξ, η) are applied to both sets of governing equations we note that the viscosity term in equation (3.6a) for power-law fluids remains independent of streamwise location. However, the viscosity term in equation (5.18a) for Carreau fluids shows a dependence on ξ. The form of equation (5.18a) indicates that similarity-type solutions do not exist despite having used a similarity-type transformation for the computational variables. The non-similar nature of the streamwise velocity is supported by the numerical results described above.

The plots presented in Figures 5.4, 5.5 and 5.6 also reveal that the sequence of velocity profiles appear to converge to a final or asymptotic velocity profile. An inspection of the numerical values of the velocity profile at the last ξ location revealed them to be very much alike. Numerical calculations where the stopping location ξ_{end} was set to 10 were also carried out. The results obtained, while not displayed here, confirmed the presence of an asymptotic large-ξ form for the velocity profile. The large-ξ asymptotic form of the velocity profile is discussed in more detail in Section 5.5.

In the results described so far the dimensionless parameter λ has been set to a constant value

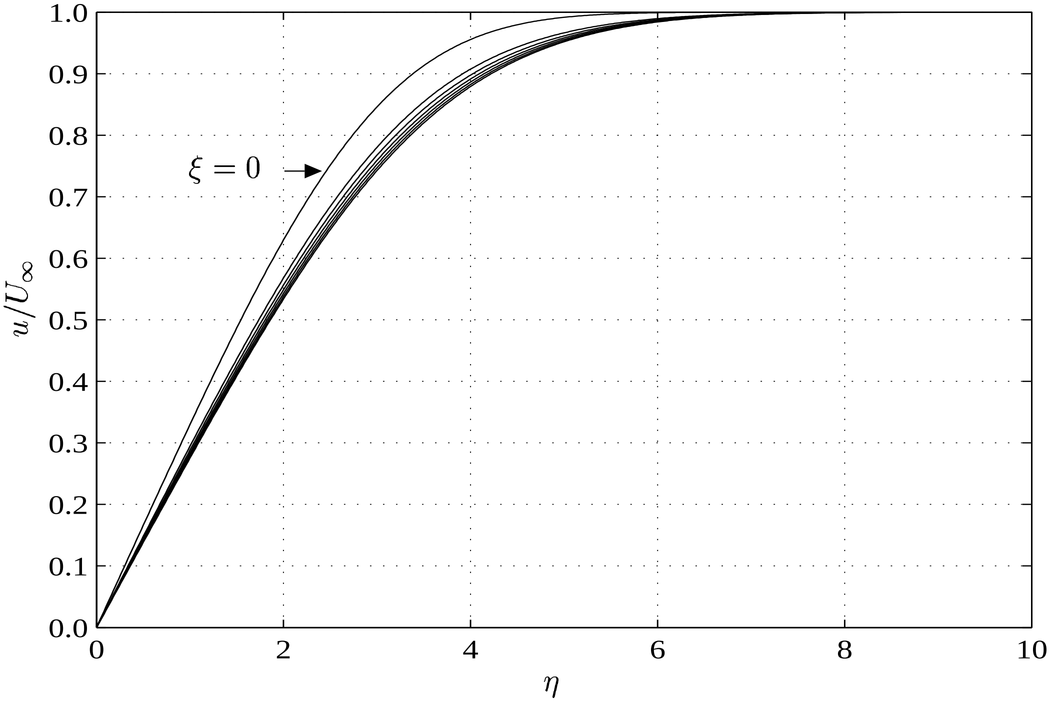

Figure 5.7: Velocity profiles for $n = 0.50$, $C_0 = 1$, $\lambda = 200$ at $\xi = 0, 0.5, \ldots, 3.0$

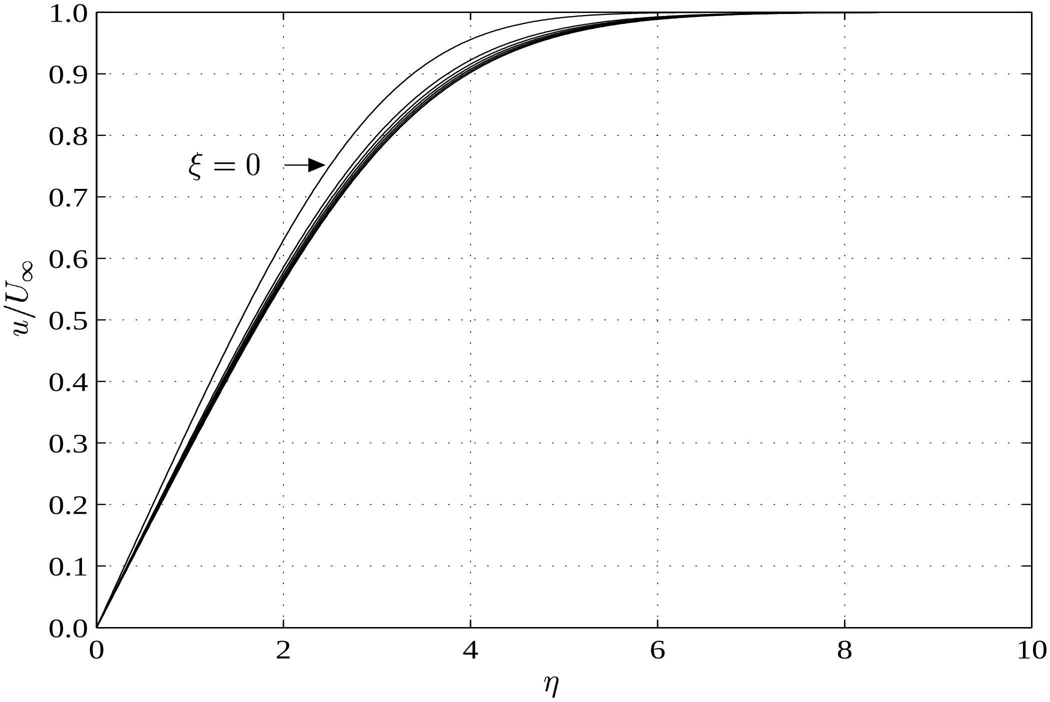

Figure 5.8: Velocity profiles for $n = 0.50$, $C_0 = 1$, $\lambda = 400$ at $\xi = 0, 0.5, \ldots, 3.0$

of 100. The effect that the value of λ has on the velocity profiles will now be considered. The fluid index was kept fixed at $n = 0.50$ and two additional values of λ were investigated, viz. 200 & 400. Figures 5.7 and 5.8 show streamwise velocity profiles for $\lambda = 200$ and $\lambda = 400$ respectively. The velocity profiles displayed are from the same streamwise locations in each case.

A comparison of Figures 5.6, 5.7 and 5.8 provides an indication of the effect that the parameter λ has on the velocity profiles. For relatively low values of λ there is a fairly rapid variation in the velocity profile away from the initial Blasius profile. This variation occurs early in the development of the flow and further changes in the velocity profiles are less dramatic as the flow moves along the plate. For larger values of λ the variation from the initial velocity profile to subsequent velocity profiles at down-stream locations is more gradual. An examination of the final velocity profiles reveals some small differences between them. Such variations suggest that the large-ξ asymptotic form of the velocity profile may be dependent on the value of λ.

5.4.2 Shear-thickening Carreau Fluid

The numerical scheme described in Section 5.3 was next used to investigate the boundary-layer flow of Carreau fluids with a fluid index in the range $1 < n < 2$. Carreau-model fluids with n in this range are commonly referred to as shear-thickening or dilatant.

For a zero mass-transfer rate through the plate and an external flow that is uniform, we expect the boundary-layer for shear-thickening Carreau fluids to be non-similar. In the numerical investigations conducted, the various parameters were set as follows. The η step-size, h, was set to 2.0×10^{-2} and the far-field, η_∞, was set to 20. The ξ step-size, $\Delta\xi$, was set to 1.0×10^{-4} and the stopping location, ξ_{end}, was set to 3.0. The iteration stopping criterion at each marching location, $\Delta\widehat{\mathbf{q}}^{(k)}$, was set to 1.0×10^{-5}. The normalised viscosity ratio, C_0, was set to 1.0, while the non-dimensional parameter, λ, was set to an arbitrary value of 100. The effect of the parameters in the Carreau viscosity model on the boundary-layer flow was also investigated and is discussed later.

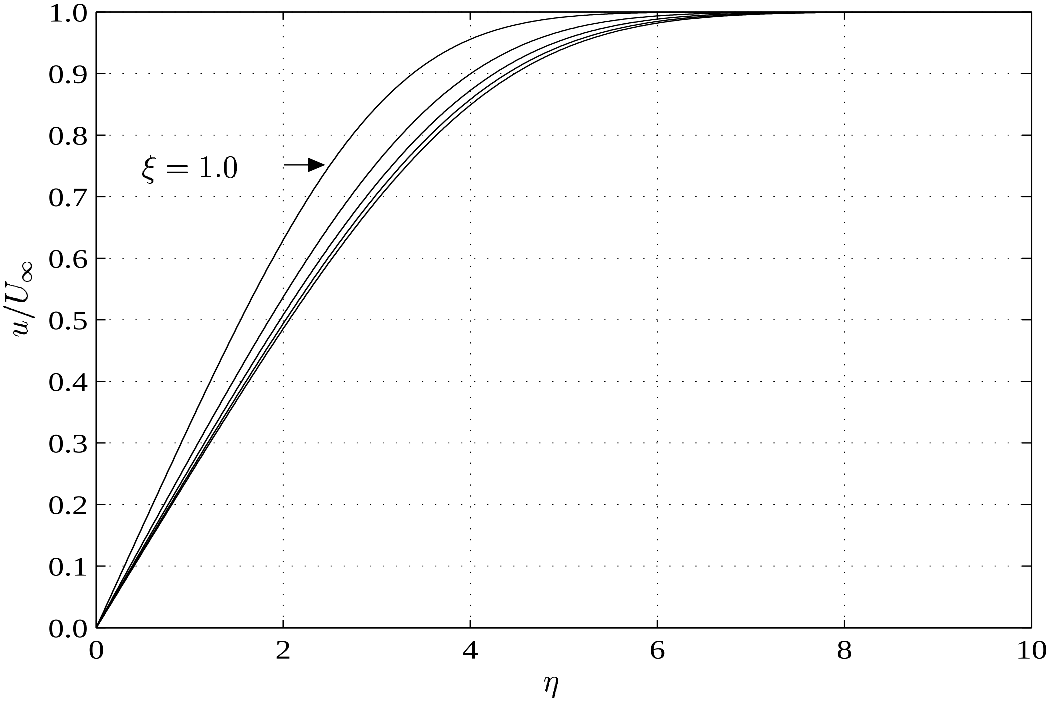

Figure 5.9: Velocity profiles for $n = 1.25$, $C_0 = 1$, $\lambda = 100$ at $\xi = 1.0, 1.5, \ldots, 3.0$

With the fluid index in the range $1 < n < 2$ for a shear-thickening Carreau fluid, equation (5.18a) possesses a mathematical singularity at $\xi = 0$. The presence of this singularity means that the numerical marching scheme needs to start from a non-zero value of ξ. A value of $\xi = 1.0$ was selected for the streamwise starting location. As was discussed in Section 5.3.1, the initial velocity profile will be provided by the solution to the classical Blasius equation.

Numerical solutions were obtained for different values of n, commencing at $n = 1.25$ and increasing in steps of 0.25. Although velocity profiles were captured at $\xi = 1.0, 1.1, \ldots, 3.0$, the velocity profiles from a selected subset of streamwise locations are displayed in the following figures.

Velocity profiles for fluid index values $n = 1.25$, 1.50 and 1.75 are shown in Figures 5.9, 5.10 and 5.11 respectively. We see that the velocity profiles taken at various ξ locations differ from the initial Blasius velocity profile. This confirms that for a shear-thickening Carreau fluid the solutions to the boundary-layer equation, and the streamwise velocity profiles within the boundary layer, are non-similar.

Furthermore, it can be seen that for $n = 1.25$ the variation from the initial velocity profile is

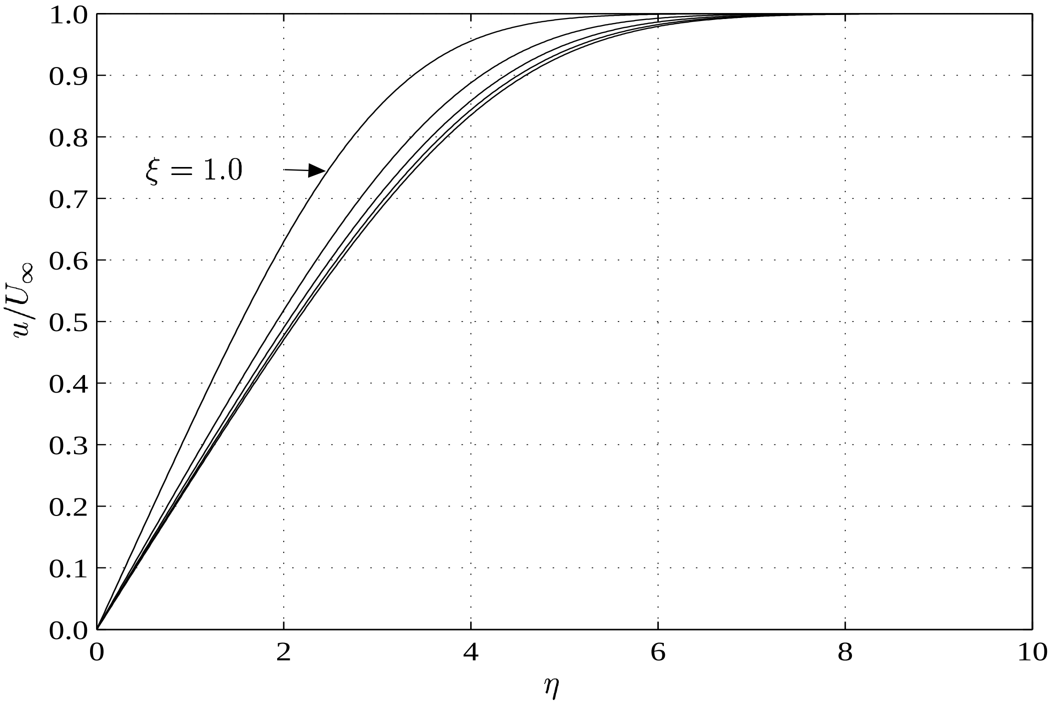

Figure 5.10: Velocity profiles for $n = 1.50$, $C_0 = 1$, $\lambda = 100$ at $\xi = 1.0, 1.5, \ldots, 3.0$

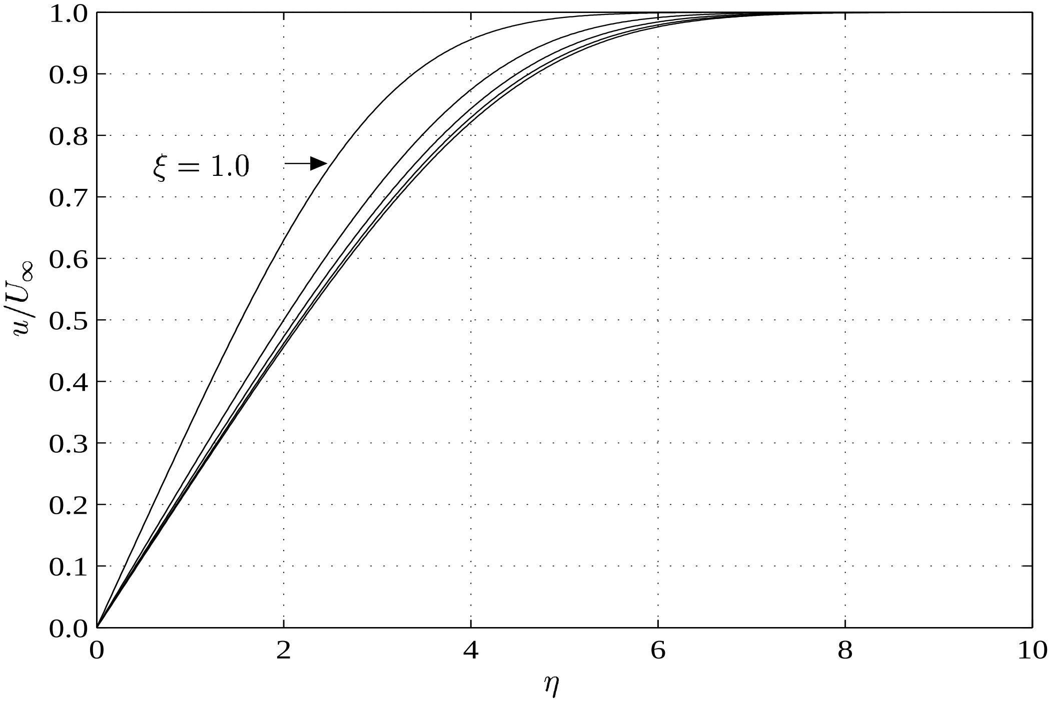

Figure 5.11: Velocity profiles for $n = 1.75$, $C_0 = 1$, $\lambda = 100$ at $\xi = 1.0, 1.5, \ldots, 3.0$

quite gradual, while for $n = 1.75$ the variation from the initial velocity profile is more rapid. As was described for shear-thinning Carreau fluids, this behaviour can be explained by the presence of the term $\xi^{\frac{1-n}{2}}$ in equation (5.18a). When n is slightly greater than unity the exponent in this term is close to zero and negative. For values of ξ in the solution domain this term takes values that are less than unity and show relatively slow variability. When n takes a value noticeably greater than unity, the values that this term takes show more rapid variability over ξ in the solution domain. Consequently there is a more rapid change in the velocity profiles between different ξ locations.

In the results described so far the dimensionless parameter λ has been set to a constant value of 100. The effect that the value of λ has on the velocity profiles of shear-thickening Carreau fluids will now be considered. The fluid index was kept fixed at $n = 1.75$ and two additional values of λ were investigated, viz. 200 & 400. The velocity profiles displayed are from the same streamwise locations in each case.

A comparison of Figures 5.11, 5.12 and 5.13 provides an indication of the effect that the parameter λ has on the velocity profiles. For relatively low values of λ there is a fairly rapid variation in the velocity profile away from the initial Blasius profile. This variation occurs early in the development of the flow and further changes in the velocity profiles are less dramatic as the flow proceeds along the plate. For larger values of λ the variation from the initial velocity profile is much more apparent and this variation occurs over a larger streamwise extent of the plate.

Effect of Different Starting Location

The results for shear-thickening Carreau fluids presented above were obtained by starting the numerical marching scheme at $\xi = 1.0$. Apart from avoiding $\xi = 0$, where the mathematical singularity is located, the choice of the ξ starting value for the numerical marching scheme is largely arbitrary. From equation (5.18a) it can be seen that the development of the non-similar boundary layer is explicitly dependent on the streamwise location ξ. It would not be unreasonable to expect that the choice of starting location for the numerical marching scheme

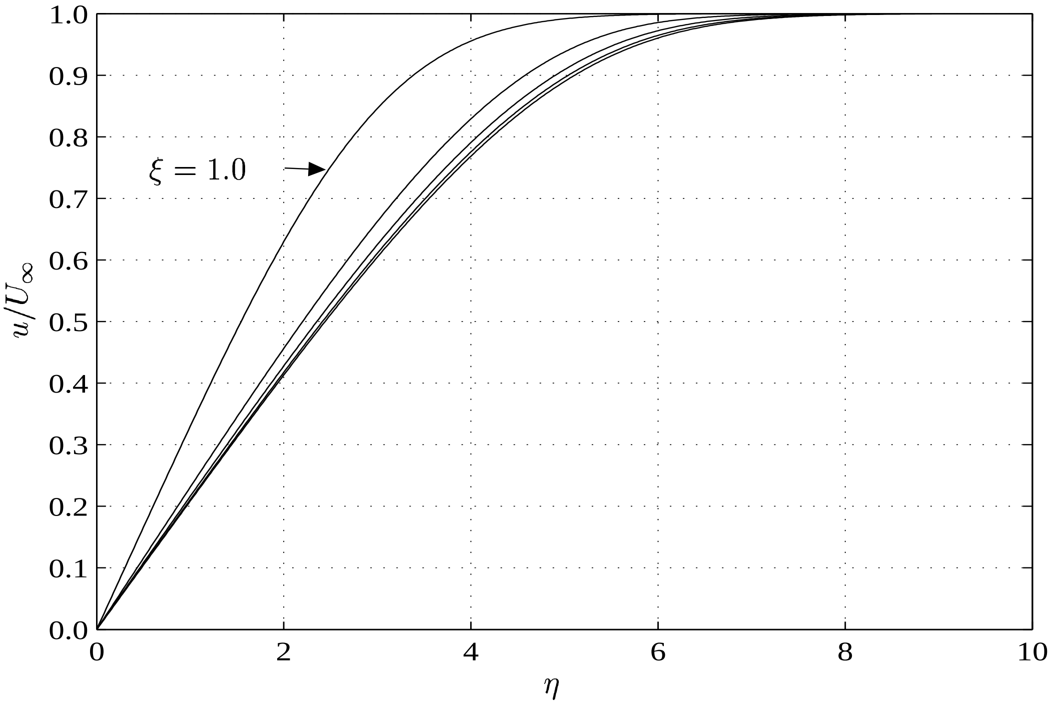

Figure 5.12: Velocity profiles for $n = 1.75$, $C_0 = 1$, $\lambda = 200$ at $\xi = 1.0, 1.5, \ldots, 3.0$

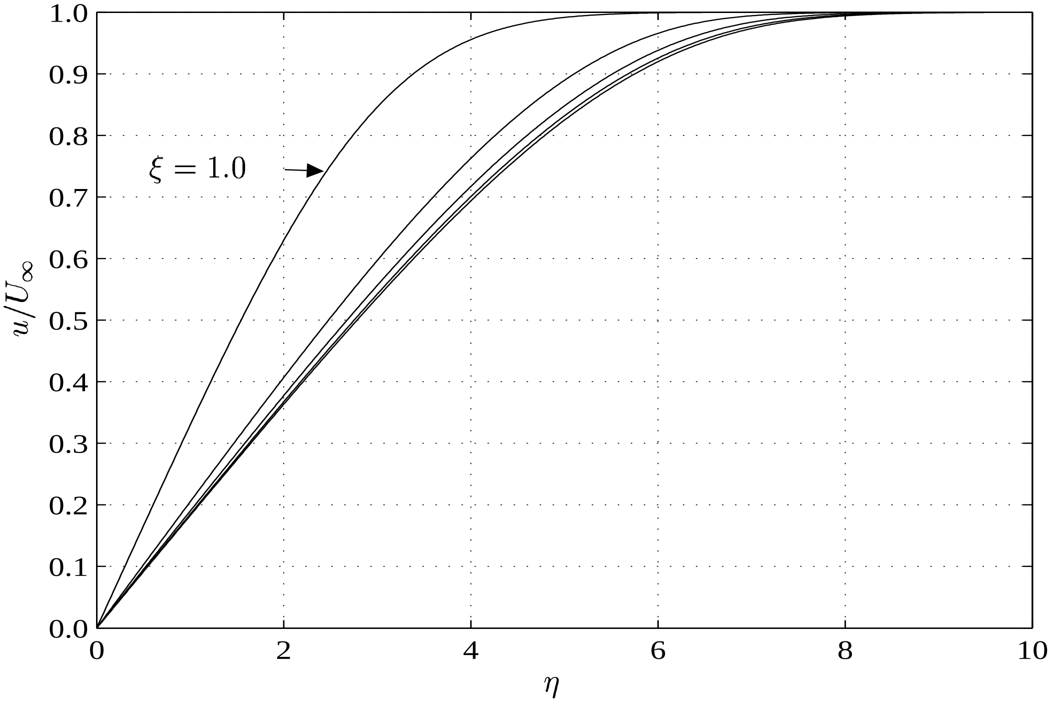

Figure 5.13: Velocity profiles for $n = 1.75$, $C_0 = 1$, $\lambda = 400$ at $\xi = 1.0, 1.5, \ldots, 3.0$

should have some effect on the manner in which the down-stream velocity profiles develop.

To investigate the effect of the starting location, a shear-thickening Carreau fluid with parameters $n = 1.50$, $C_0 = 1.0$ and $\lambda = 100$ was used. The numerical marching scheme was started at $\xi = 0.5$ and stopped at $\xi = 3.0$. The velocity profile at $\xi = 3.0$ was compared with the corresponding velocity profile obtained when $\xi = 1.0$ is used as the starting location. The two velocity profiles were found to be noticeably different from each other. Such a difference in velocity profiles may be due to the boundary layer not becoming fully developed when started at $\xi = 1.0$ and stopped at $\xi = 3.0$. Hence, the numerical calculation was repeated by starting at $\xi = 1.0$ and stopping at $\xi = 5.0$ so as to allow the boundary layer to develop more fully.

An examination of the difference between consecutively sampled velocity profiles provides an indication of how well the boundary layer has converged to a velocity profile that is considered to be invariant with respect to ξ. The maximum absolute difference between velocity values at $\xi = 2.9$ and $\xi = 3.0$ is 0.0014, whereas the value of $|u(5.0) - u(4.9)|_{max}$ is 2.5708×10^{-4}. These variations in velocity between successive ξ locations indicate that the boundary-layer velocity profile is still developing at $\xi = 3.0$. The numerical marching scheme is second-order accurate, so with an η step-size of 0.01 the fully converged solution should show no variation in the first 4 decimal places. However, even at $\xi = 5.0$ there are small variations between velocity profiles, which is taken to indicate that the boundary layer is still converging to a final 'steady-state' velocity profile.

For the calculation started at $\xi = 0.5$ and stopped at $\xi = 3.0$, the value of $|u(3.0) - u(2.9)|_{max}$ is 1.7081×10^{-4}. This very small difference between velocity profiles indicates that the boundary layer is almost fully developed at $\xi = 3.0$. The implication is that the boundary layer will be more fully developed and the velocity profile more closely converged to a final steady-state solution if the numerical marching scheme is started at a ξ location nearer to the leading edge rather than from further down-stream.

The observations about the effect of the starting location for the numerical marching scheme are not entirely unexpected. The boundary-layer flow of a Carreau fluid is governed by a system of partial differential equations that are parabolic. For such systems of equations, both the initial condition and its location will have an effect on the results down-stream in the solution domain.

Effect of Different Initial Velocity Profile

In Section 5.3.1 it was indicated that an initial velocity profile for a shear-thickening Carreau fluid could not be readily calculated. Hence, we have resorted to using the Blasius velocity profile to initiate the numerical calculations performed so far. For non-zero values of β the solution of the corresponding Falkner-Skan equation would be a suitable initial velocity profile. The question as to whether a different initial velocity profile could be used to start the numerical marching scheme is discussed briefly here.

The class of alternative initial velocity profiles considered is of the exponential type, i.e. $u(\eta) = 1 - e^{a\eta}$ where $a < 0$ is a constant. Since $u(0) = 0$ and $u(\infty) \to 1$, these exponential profiles meet the expected requirements of non-slip at the surface and matching onto the free-stream velocity.

To investigate the effect of the initial velocity profile, a shear-thickening Carreau fluid with parameters $n = 1.50$, $C_0 = 1.0$ and $\lambda = 100$ was used. The numerical marching scheme was started at $\xi = 1.0$ and stopped at $\xi = 3.0$. An initial velocity profile of the exponential type with $a = -0.9210$ was tried first. For this value of a the velocity is 0.99 of the normalised free-stream value at $\eta = 5$. The velocity profiles obtained at various ξ locations were referenced to corresponding velocity profiles obtained from an initial Blasius velocity profile. Using $u_{exp}(\xi)$ and $u_{Blas}(\xi)$ to denote the velocity profile at ξ resulting from an exponential and Blasius initial velocity profile respectively, we find that $|u_{Blas}(3) - u_{exp}(3)|_{max} = 0.0055$. This figure indicates quite good (2 decimal places) agreement between the velocity profiles. Additionally, $|u_{exp}(3.0) - u_{exp}(2.9)|_{max} = 0.0018$ indicates that the boundary-layer velocity profile is still converging to a 'steady-state' solution.

Next an initial velocity profile of the exponential type with $a = -0.4605$ was tried. For this value of a the velocity is 0.99 of the normalised free-stream value at $\eta = 10$. For this initial velocity profile we find that $|u_{Blas}(3) - u_{exp}(3)|_{max} = 0.0678$. This figure indicates quite poor (only 1 decimal place) agreement with the reference velocity profile. Furthermore, $|u_{exp}(3.0)-u_{exp}(2.9)|_{max} = 5.7029\times 10^{-4}$ indicates that in this case the boundary-layer velocity profile has largely converged to a 'steady-state' solution. Even when this velocity profile at $\xi = 3$ is compared with the more fully developed velocity profile at $\xi = 5$ started from an initial Blasius velocity profile, noticeable visible differences still exist. For this exponential initial velocity profile ($a = -0.4605$), the down-stream velocity profiles converge to a final velocity profile that is different from the 'steady-state' velocity profile that the first exponential ($a = -0.9210$) and Blasius initial velocity profiles converge to.

The choice of initial velocity profile certainly does have an effect on the nature of the solutions obtained at down-stream locations. The main difference between the exponential velocity profiles considered is their rate of approach to the free-stream velocity. The exponential velocity profile with $a = -0.9210$ approaches the free-stream velocity value at a rate that is not vastly different from that of the Blasius velocity profile. However, the rate of approach to the free-stream velocity of the second exponential velocity profile with $a = -0.4605$ is much more gradual. This difference between the exponential initial velocity profiles may be partly responsible for the results observed. We also need to remember that for a parabolic system of partial differential equations, the initial conditions play a significant role in the subsequent development of solutions.

5.5 The large-ξ limiting form

The results that are presented up to this point have been obtained using the numerical marching scheme which has progressed down-stream to the location $\xi = 3$. It has also been shown that the boundary-layer flow of a Carreau fluid is non-similar. However, a comparison of the velocity profiles at $\xi = 3$ from the Carreau fluids considered indicates the existence of an asymptotic form for the boundary-layer velocity profile at large ξ values. In this section we investigate in more detail the nature of this large-ξ asymptotic form for the streamwise velocity profile. We will firstly develop an asymptotic description for the velocity profile at large-ξ values and then check its validity by comparison with velocity profiles obtained from the numerical marching scheme.

To explore the asymptotic form of the velocity profile at large-ξ we choose ξ^{-1} as an *a posteriori* estimate for the perturbing parameter and expanding f using the perturbation expansion

$$f = g_0(\eta) + \frac{1}{\xi} g_1(\eta) + O(\xi^{-2}),$$

where g_0 is a leading order, or base, velocity function and g_1 is an order-ξ^{-1} correction function.

After substituting the above expression into equation (5.11) and collecting terms in equal powers of ξ, a hierarchy of ordinary differential equations for the functions g_0 and g_1 is obtained. The first two equations are as follows

$$(1 + C_0)\, g_0''' + \frac{1}{2} g_0\, g_0'' = 0, \tag{5.24a}$$

$$(1 + C_0)\, g_1''' + \frac{1}{2} g_0\, g_1'' + g_0'\, g_1' - \frac{1}{2} g_0''\, g_1 = -\frac{3(n-1)C_0\lambda^2}{2} \left(g_0''\right)^2 g_0'''. \tag{5.24b}$$

The appropriate boundary conditions for equations (5.24) are

$$g_0 = g_0' = 0 \quad \text{on} \quad \eta = 0, \qquad g_0' \to 1 \quad \text{as} \quad \eta \to \infty, \tag{5.24c}$$

$$g_1 = g_1' = 0 \quad \text{on} \quad \eta = 0, \qquad g_1' \to 0 \quad \text{as} \quad \eta \to \infty. \tag{5.24d}$$

We note that in deriving equations (5.24a,b) from equation (5.11) the pressure gradient parameter β has been set to zero and $U_e \equiv 1$. Equation (5.24a) is a scaled version of the classical Blasius equation, while equation (5.24b) is a non-homogeneous third order linear ordinary differential equation with variable coefficients. The two equations are coupled via the variable coefficients in the $O(\xi^{-1})$ equation which are the solution of the leading order equation. The coefficient of the non-homogeneous term captures the contribution that the Carreau viscosity model parameters make to the asymptotic form of the velocity profile. The above expressions can be extended to cater for a non-zero value of β.

Equations (5.24a,b) can be simplified further by defining a new independent variable $\widehat{\eta} =$

$\eta/\sqrt{1+C_0}$ and new dependent variables

$$g_0 = \sqrt{1+C_0}\,G_0,$$
$$g_1 = \frac{3(n-1)C_0\lambda^2}{2(1+C_0)^{3/2}}G_1.$$

Substituting these expressions into equations (5.24a,b) and simplifying gives

$$G_0''' + \frac{1}{2}G_0G_0'' = 0, \tag{5.25a}$$
$$G_1''' + \frac{1}{2}G_0G_1'' + G_0'G_1' - \frac{1}{2}G_0''G_1 = -(G_0'')^2G_0'''. \tag{5.25b}$$

The appropriate boundary conditions for equations (5.25) become

$$G_0 = G_0' = 0 \quad \text{on} \quad \widehat{\eta} = 0, \qquad G_0' \to 1 \quad \text{as} \quad \widehat{\eta} \to \infty, \tag{5.25c}$$
$$G_1 = G_1' = 0 \quad \text{on} \quad \widehat{\eta} = 0, \qquad G_1' \to 0 \quad \text{as} \quad \widehat{\eta} \to \infty. \tag{5.25d}$$

Hence, equation (5.25a) is now the classical Blasius equation and equation (5.25b) is independent of the Carreau fluid parameters.

A benefit offered by the set of equations (5.25a,b) and boundary conditions (5.25c,d) is that they need to be solved just once. Velocity profiles for various combinations of the Carreau fluid parameters can then be obtained by an appropriate rescaling of the solutions for G_0 and G_1. The nature of equations (5.25a,b) indicates that solutions for G_0 and G_1 need to be found numerically. The solution to this set of equations and the accompanying boundary conditions was found by recasting the problem as an initial-value problem with guesses for $G_0(0)$ and $G_1(0)$. Newton iteration was used to refine the guesses for $G_0(0)$ and $G_1(0)$ until the asymptotic boundary condition was satisfied. The initial-value problem solver employed an adaptive step-size Runge-Kutta quadrature scheme.

When the calculation of the streamwise velocity profile is from $\eta = 0$ to η_∞, then equations (5.25a,b) need to be solved from $\widehat{\eta} = 0$ to $\widehat{\eta}_\infty = \frac{\eta_\infty}{\sqrt{1+C_0}}$. This will ensure a correct mapping between the two independent variables used. The solutions will also need to be mapped to each other correctly, the mapping between the derivatives of the solutions g_0, g_1 and G_0, G_1 is

$$\begin{aligned}\frac{\mathrm{d}g_0}{\mathrm{d}\eta} &= \frac{\mathrm{d}G_0}{\mathrm{d}\widehat{\eta}},\\ \frac{\mathrm{d}g_1}{\mathrm{d}\eta} &= \frac{3(n-1)C_0\lambda^2}{2(1+C_0)^2}\frac{\mathrm{d}G_1}{\mathrm{d}\widehat{\eta}}.\end{aligned}$$

By setting the fluid index equal to unity, the Carreau viscosity model corresponds to a Newtonian fluid which is known to possess a self-similar velocity profile. The self-similar velocity profile is a solution of

$$(1+C_0)\,f''' + \frac{1}{2}f\,f'' = 0, \tag{5.26}$$

which is derived from equation (5.11) by firstly setting $n = 1$ and then setting $\xi = 0$ (with $\beta = 0$). Equation (5.11) is identical in form to equation (5.24a). We also note that equation (5.24b) becomes homogeneous when $n = 1$ and has the trivial solution $g_1 \equiv 0$. Hence, the velocity profile at large values of ξ along the plate is expected to approach g_0' with $g_1' \equiv 0$.

The $n = 1$ case also provides a convenient and known baseline against which the numerical implementation of the large-ξ asymptotic approximation can be verified. A numerical calculation was performed with Carreau fluid parameters $n = 1, C_0 = 1, \lambda = 100$ to a location of $\xi = 10$ along the plate. In the transverse direction to the plate the η step-size was 0.01, with $\eta_\infty = 15$ for the far-field. Also a solution for G_0 and G_1 was found using a step-size $\Delta\widehat{\eta} = \Delta\eta/\sqrt{2}$ and $\widehat{\eta}_\infty = \eta_\infty/\sqrt{2}$ since $C_0 = 1$. The solutions G_0', G_1' were then mapped to g_0', g_1' so as to be in agreement with the solution mesh used in the numerical calculation. We note that $g_1' \equiv 0$ as expected. The convergence rate of the numerical solution as well as the difference between g_0' and the numerical solution are summarised in Table 5.1.

In Table 5.1 we see that the velocity profile being calculated by the numerical marching scheme is converging to a limiting form, as indicated by the maximum absolute difference between consecutive selected ξ locations. The effect of the initial velocity profile on down-stream solutions is seen here in the value of $|u(\xi = 1) - u(\xi = 0)|_{max}$, as the numerical marching scheme uses a Blasius-type initial velocity profile while the actual velocity profile is given by the solution to equation (5.26). Next we see that the maximum absolute difference between the

ξ	$\|u(\xi_i) - u(\xi_{i-1})\|_{max}$	$\|g_0' - u(\xi_i)\|_{max}$
1.0	0.1874	
2.0	1.0717×10^{-6}	
3.0	3.5725×10^{-7}	
4.0	1.7863×10^{-7}	1.3203×10^{-6}
5.0	1.0718×10^{-7}	1.2191×10^{-6}
6.0	7.1454×10^{-8}	1.1519×10^{-6}
7.0	5.1039×10^{-8}	1.1045×10^{-6}
8.0	3.8279×10^{-8}	1.0701×10^{-6}
9.0	2.9773×10^{-8}	1.0434×10^{-6}
10.0	2.3818×10^{-8}	1.0220×10^{-6}

Table 5.1: Maximum absolute difference between velocity profiles at equi-spaced ξ values, and maximum absolute difference between velocity profiles and leading order asymptotic velocity profile.

asymptotic velocity profile g_0' and velocity profiles calculated at selected ξ locations, equivalent to g_1', is very small; to all intents zero. This set of results also demonstrates that $|g_0' - u(\xi_i)|_{max}$ decreases non-linearly with distance along the plate. Although not shown here, a graphical plot confirms that $|g_0' - u(\xi_i)|_{max}$ is proportional to $\frac{1}{\xi}$ as was assumed in the perturbation expansion.

The manner in which the non-similar velocity profile for a shear-thinning fluid approaches the large-ξ asymptotic velocity profile is considered next. The numerical marching scheme was used to calculate velocity profiles for Carreau fluids with fluid index values $n = 0.95, 0.75, 0.50$ and $C_0 = 1.0, \lambda = 100$. The η step-size was 0.01, with $\eta_\infty = 15$ for the far-field. The stopping location ξ_{end} was set to $\xi = 10, 20, 30$ for each respective value of n. Velocity profiles were sampled at the streamwise locations $\xi = 0.5k, k = 0, 1, \ldots,$ up to the appropriate value of ξ_{end}. The maximum absolute difference between consecutive sampled velocity profiles was found to decrease monotonically with increasing distance from the leading edge of the flat plate. Therefore the streamwise velocity in the boundary layer is seen to be converging onto an asymptotic velocity profile.

The maximum absolute difference between the sampled velocity profiles and the asymptotic velocity profile g_0' for the values of n considered is summarised in Table 5.2, at selected ξ locations.

n	$\xi = 5$	$\xi = 10$	$\xi = 15$	$\xi = 20$	$\xi = 25$	$\xi = 30$
0.95	0.0050	0.0033	0.0025	0.0021	–	–
0.75	0.0251	0.0167	–	–	–	–
0.50	0.0500	0.0336	0.0257	0.0210	0.0178	0.0156

Table 5.2: Maximum absolute difference between sampled velocity profiles and asymptotic velocity profile g_0' at selected ξ locations.

The results in Table 5.2 indicate that the velocity profiles are converging to an asymptotic velocity profile g_0'. We see that the rate of convergence is dependent on the fluid index n while other fluid parameters have been held fixed. The non-linear, i.e. inverse proportionality, dependence on the streamwise location ξ is evident from the non-uniform variation between consecutive values in Table 5.2. This convergence of the velocity profiles to an asymptotic profile is further illustrated in Figure 5.14 for fluid parameters $n = 0.50, C_0 = 1, \lambda = 100$.

The difference between the numerically calculated velocity profiles and the asymptotic velocity profile is approximated by the solution of equation (5.24) for g_1'. This is obtained by solving equation (5.25) for G_1 and applying the appropriate remapping to get g_1' for the Carreau fluid parameters of interest. For a Carreau fluid with parameters $n = 0.50, C_0 = 1, \lambda = 100$, the actual difference between the asymptotic velocity profile and the calculated velocity profile at $\xi = 30$, as well as g_1' representing the correction to the asymptotic velocity profile, are shown in Figure 5.15.

It can be seen from Figure 5.15 that the magnitude of g_1' is vastly greater than $g_0' - u(\xi = 30, \eta)$. This difference in the magnitudes of the two curves can be accounted for by the introduction of a suitable scaling constant. The perturbation expansion used did not introduce such a constant into the subsequent differential equations. This constant is quite likely to be dependent on some of the fluid parameters, though finding its specific form has not been pursued here.

There is also a slight difference in the η value at which the 'peaks' in the two curves are located. It has been observed that the peak in $g_0' - u(\xi, \eta)$ occurs at slightly different η values as the value of ξ increases. For the locations $\xi = 5, 10, \ldots, 30$ the peak in the difference between the asymptotic velocity profile and the calculated velocity profile occurs at $\eta = 2.80, 2.84, 2.87, 2.89, 2.91, 2.92$ respectively. The peak in g_1' is located at $\eta = 3.29$. These

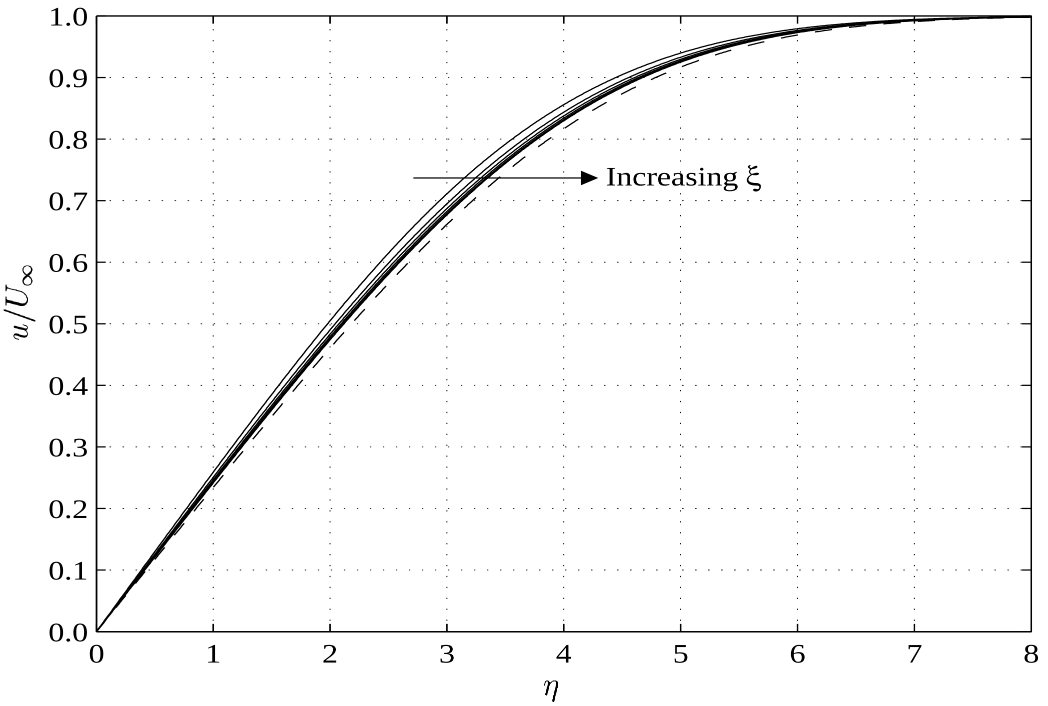

Figure 5.14: Velocity profiles at $\xi = 5, 10, 15, 20, 25, 30$ converging to asymptotic velocity profile g_0' (broken line) for a Carreau fluid with parameters $n = 0.50, C_0 = 1, \lambda = 100$.

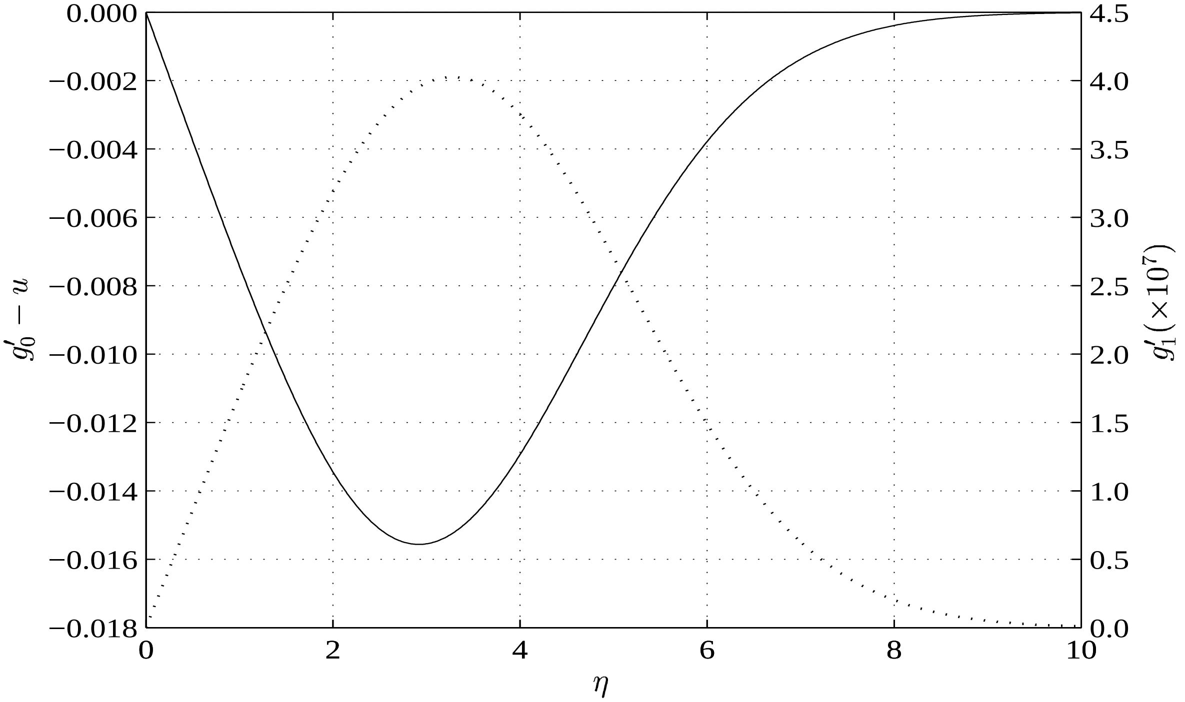

Figure 5.15: Difference between the asymptotic and the calculated velocity profile at $\xi = 30$ (solid line); along with g_1' representing the correction to the asymptotic velocity profile (dashed line) for a Carreau fluid with parameters $n = 0.50, C_0 = 1, \lambda = 100$.

n	$\xi = 2$	$\xi = 3$	$\xi = 5$	$\xi = 10$	$\xi = 15$	$\xi = 20$	$\xi = 30$
1.25	0.0524 0	0.0255 0	0.0096 0	0.0021 -0.0013	7.2×10^{-4} -0.0024	– –	– –
1.50	0.0280 0	0.0083 -0.0041	0.0013 -0.0136	4.4×10^{-5} -0.0149	2.6×10^{-6} -0.0131	2.8×10^{-7} -0.0115	4.2×10^{-9} -0.0092

Table 5.3: Maximum difference between non-similar velocity profile u and asymptotic velocity profile g_0' at selected ξ locations for shear-thickening Carreau fluids with $n = 1.25, 1.50$.

values indicate that the difference $g_0' - u(\xi, \eta)$ is slowly approaching the first correction term g_1'. Lower order terms in the perturbation expansion would also contribute to the rate at which $g_0' - u(\xi, \eta)$ converges to g_1'. Lastly we note that for shear-thinning Carreau fluids the numerically calculated velocity profile was always found to converge to the asymptotic velocity profile from above.

A corresponding investigation to examine the manner in which the non-similar velocity profile for a shear-thickening Carreau fluid approaches the large-ξ asymptotic velocity profile was also performed. The numerical marching scheme was used to calculate velocity profiles for Carreau fluids with $n = 1.25, 1.50$ and $C_0 = 1.0, \lambda = 100$. The η step-size was 0.01, with $\eta_\infty = 15$ for the far-field. The stopping location ξ_{end} was set to $\xi = 15, 30$ for each respective value of n. Velocity profiles were sampled at the streamwise locations $\xi = 0.5k, k = 0, 1, \ldots$, up to the appropriate value of ξ_{end}. For shear-thickening Carreau fluids it was found that that the manner in which the numerically calculated velocity profiles converged to the asymptotic velocity profile is different to that found for shear-thinning Carreau fluids. We proceed by calculating the difference $u - g_0'$, i.e. between the non-similar velocity profile and the asymptotic velocity profile, at selected ξ locations. Then the maximum and minimum values of $u - g_0'$ are found. These results are summarised in Table 5.3, where the upper and lower values correspond to the maximum and the minimum respectively of the difference $u - g_0'$.

For $n = 1.25$, the upper values in Table 5.3 indicate that the numerically calculated velocity profile is entirely 'above' the asymptotic velocity profile for the first few ξ locations shown. At $\xi = 15$ the numerically calculated velocity lies almost entirely 'below' the asymptotic velocity profile. The cross-over occurs between the locations $\xi = 7.0$ and 7.5. Though the numerical marching scheme stopped at $\xi = 15$ for this value of n, an examination of the minimum value

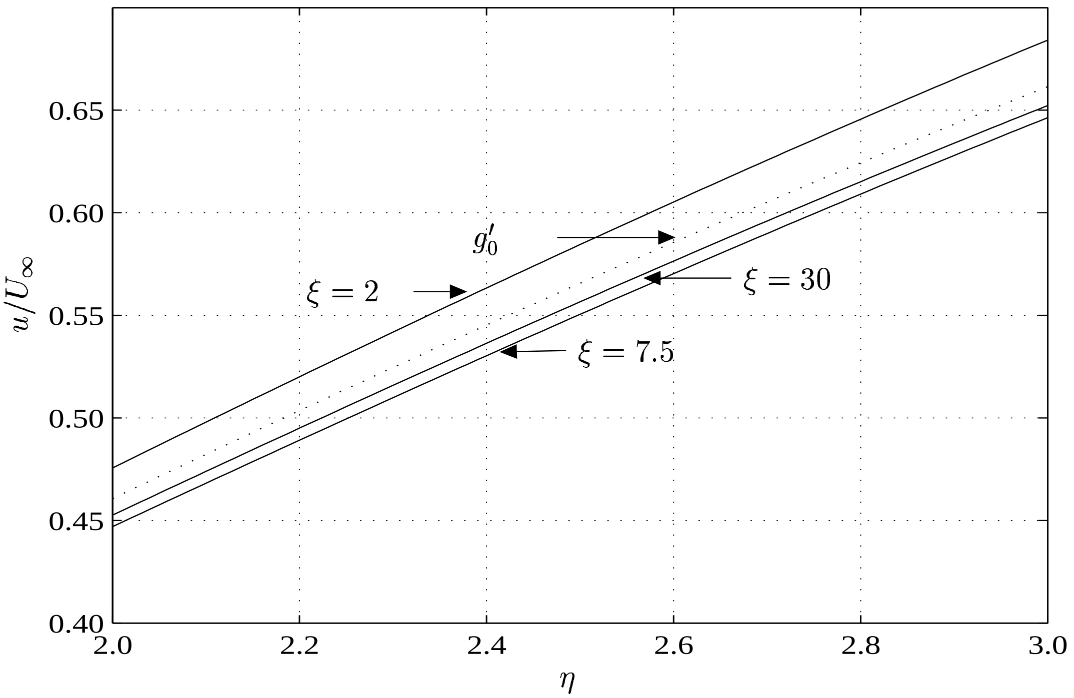

Figure 5.16: Velocity profiles at $\xi = 2, 7.5$, and 30 for a Carreau fluid with parameters $n = 1.50, C_0 = 1, \lambda = 100$ (solid lines). Also shown is the asymptotic velocity profile g_0' (dashed line).

of $u - g_0'$ at preceding ξ locations indicated that the rate of departure of u from g_0' was slowing down.

For $n = 1.50$ the numerical marching scheme stopped at $\xi = 30$. The values in Table 5.3 indicate that the cross-over of the calculated velocity profile occurs earlier than was the case for $n = 1.25$. Also the calculated velocity profile may be considered to be entirely 'below' the asymptotic velocity profile at $\xi = 15$. The results obtained indicate that the difference $u - g_0'$ is at its most negative value at a ξ location between 7.5 and 8. The calculated velocity profiles taken from ξ locations 2, 7.5 and 30, as well as g_0', are shown in Figure 5.16. The scale on the axes has been adjusted to highlight the described aspects of the velocity profiles.

Since the velocity profiles of shear-thinning Carreau fluids approach the asymptotic velocity profile from above, it is not unreasonable to expect that the velocity profiles of shear-thickening Carreau fluids should approach the asymptotic velocity profile from below. This expected behaviour of the calculated velocity profiles is seen after the shear-thickening Carreau fluid has been allowed to develop sufficiently far down the flat plate. The delay of this convergence

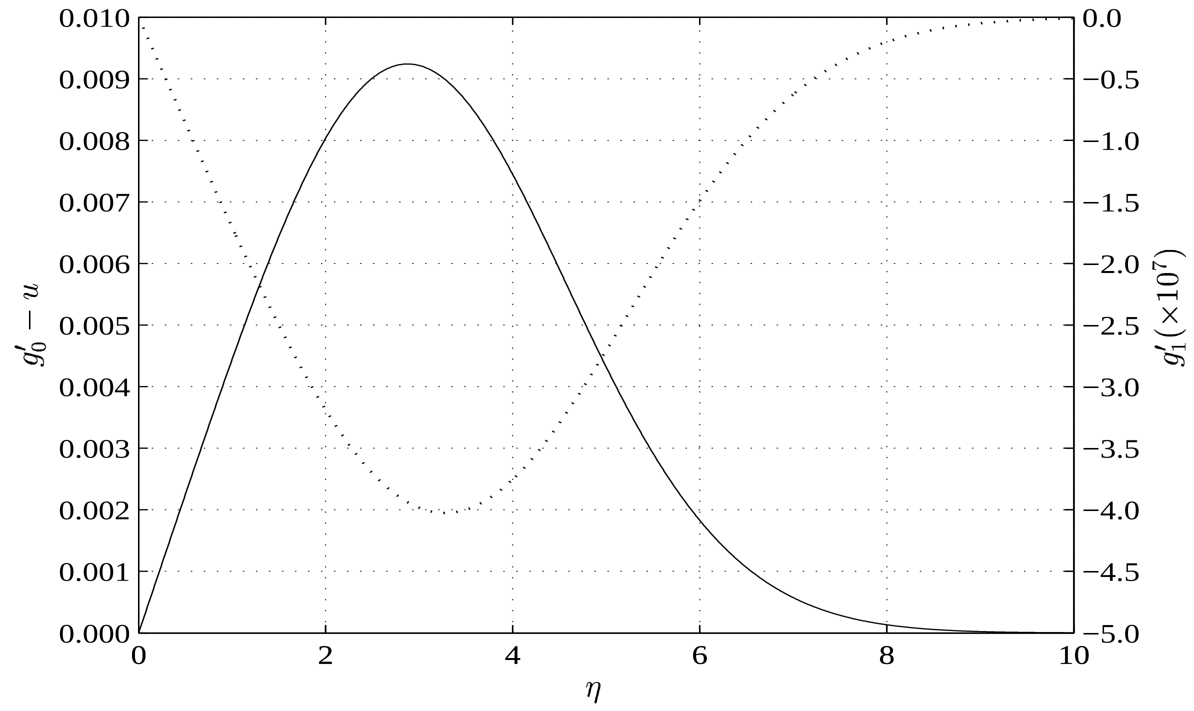

Figure 5.17: Difference between the asymptotic velocity profile and the calculated velocity profile at $\xi = 30$ (solid line), along with g_1' representing the correction to the asymptotic velocity profile (dashed line) for a Carreau fluid with parameters $n = 1.50, C_0 = 1, \lambda = 100$.

to g_0' can be attributed to the use of the Blasius velocity profile as the initial condition for shear-thickening Carreau fluids in the numerical marching scheme. A proper initial velocity profile for shear-thickening Carreau fluids could not be conveniently calculated due to the presence of a mathematical singularity in equation (5.18a) at $\xi = 0$. Though the numerical marching scheme was started with an inappropriate initial velocity profile for a shear-thickening fluid, the results obtained indicate that the correct numerical solution was eventually settled upon.

For a shear-thickening Carreau fluid, with parameters $n = 1.50, C_0 = 1, \lambda = 100$, the difference between the asymptotic velocity profile and the calculated velocity profile at $\xi = 30$ was compared with g_1' representing the correction to the asymptotic velocity profile. The results are shown in Figure 5.17. We note that these results are almost identical to those for a shear-thinning Carreau fluid shown in Figure 5.15, apart from a sign change.

As noted before, a suitable scaling constant needs to be introduced so that g_1' would align more closely with $g_0' - u(\xi, \eta)$. The difference in the η value at which the 'peaks' in the two curves are located can be seen again. Here too the peak in $g_0' - u(\xi, \eta)$ occurs at slightly different η values as the value of ξ increases. For the locations $\xi = 10, 15, \ldots, 30$ the peak in the difference between the asymptotic velocity profile and the calculated velocity profile occurs at $\eta = 2.80, 2.85, 2.87, 2.88, 2.89$ respectively. The peak in g_1' is located at $\eta = 3.29$. Hence, after the calculated velocity profile has re-oriented itself so as to lie below the asymptotic velocity profile, we see that the difference $g_0' - u(\xi, \eta)$ is slowly approaching the first correction term g_1'. Lower order terms in the perturbation expansion would also contribute to the rate at which $g_0' - u(\xi, \eta)$ converges to g_1'.

5.6 Chapter Summary

In this chapter we have introduced the Carreau viscosity model as an alternative to the power-law viscosity model. The Carreau viscosity model offers the advantage of being able to deal better with zero- and infinite-shear rates than does the power-law model. The system of partial differentiation equations governing the boundary-layer flow of a Carreau fluid have been derived and transformed to a set of computationally-preferred co-ordinates.

We have then shown the existence of a self-similar boundary-layer flow when the external free-stream flow is of a very specific form. This self-similar solution provides some very useful insight into the form and structure of the boundary-layer. Next a numerical marching scheme was described that allowed non-similar solutions to be calculated. It was shown that for shear-thinning Carreau fluids the numerical calculations can be started from the leading edge of the plate and that a suitable initial velocity profile is given by the solution of the Blasius equation. For shear-thickening Carreau fluids, however, a mathematical singularity exists at the leading edge of the plate and the numerical calculations need to start at some down-stream location. An explicit form the initial velocity profile is not available, so the Blasius velocity profile has been used instead.

The numerical calculation of non-similar boundary-layer flows for shear-thinning Carreau fluids indicate that the velocity profile tends to an asymptotic form. For shear-thickening Carreau fluids the velocity profile in the boundary layer also tends to an asymptotic form. However, the development of the velocity profile for shear-thickening fluids is affected by the choice of the starting location, as well as the initial velocity profile, for the numerical marching scheme.

We have also shown that the calculated velocity profile converges to an asymptotic velocity profile at large values of ξ. An examination of the structure of the asymptotic velocity profile revealed that it consists of a leading-order component that is the solution of a Blasius-like equation as well as a lower-order correction term. The lower-order correction term approximates the difference between the numerically calculated velocity profile and the asymptotic velocity profile quite well when the effect of a suitable scaling constant is taken into account.

Chapter 6

Boundary Layers for a Two-Fluid System

The study of two-fluid flows is of interest in a number of industrial and technological settings. The laminar boundary layer that develops in flows over turbine blades and airfoils or within channels and pipes is known to eventually become unstable with increasing flow speed. Yet, if the flow surface is coated with a thin liquid film of a fluid different from that in the main flow, then both the film and the main boundary layer exhibit complex flow patterns and non-linear behaviours that are different from those displayed by a single fluid.

An everyday example of a two-fluid flow is that of 'high-speed' air flowing over a rain-wetted panel of a car. A less well-known, though not of lesser interest, example of the boundary-layer flow of a two-fluid system is that of air flowing over an anti-icing liquid on an airplane wing. Further examples of two-fluid systems include pipeline lubrication using water-oil mixtures, visualisation experiments, thin films on bronchial passages and various industrial processes.

Two-fluid flow systems have been of interest to researchers for many years, with considerable effort being directed at the nature of instabilities of the fluid interface as well as the boundary-layer flow itself. Lock (1954) considered the problem of viscous flow along an interface between two immiscible fluids having different densities and viscosities in the context of water-wave generation by the wind. More recently Nelson et al. (1995) examined the boundary layer formed by air flowing over water on a flat plate. They show that the water film becomes asymptotically thin in comparison with the boundary layer with distance along the flat plate. Additionally it is shown that the velocity profile in the water film is linear, whereas the air flow takes the form of a Blasius-type flow. A two-fluid system consisting of the boundary-layer flow of a bulk fluid over a thin film along a flat plate was studied by Timoshin (1997) to investigate the nature of the instabilities in such a system. Both fluids were Newtonian and it was assumed that the velocity profile in the lower fluid was linear. Rothmayer et al. (2002) used an essentially identical two-fluid system to study the flow of air over a thin layer of water along rime ice[1] that has formed on an airfoil surface.

The number of studies of two-fluid systems involving non-Newtonian fluids as compared to Newtonian fluids have been fewer in the past, though this situation has been changing. An early investigation into two-fluid flows involving non-Newtonian fluids was conducted by Thompson and Snyder (1969), which considered the flow of a Newtonian fluid over an injected power-law fluid. They considered self-similar solutions to the two-fluid system, from which the form of the velocity profile in each fluid could be obtained along with the location of the fluid interface. More recently two-fluid systems with a non-Newtonian fluid have been used to investigate the behaviour of anti-icing liquids on an airplane wing. In Özgen (1995) and Özgen et al. (1998), the stability of the boundary layer in a two-fluid system where a power-law fluid in the lower layer represents an anti-icing liquid is studied. The upper Newtonian fluid is assumed to shear the lower fluid so that the velocity profile in the power-law fluid is regarded as being linear.

While the power-law model for a non-Newtonian fluid is popular and relatively straightforward to work with, it does possess some limitations that have been discussed in a previous chapter. The Carreau viscosity model has been proposed as providing a better description of a generalised Newtonian fluid than does the power-law model. While it has been assumed that a linear velocity profile in the power-law fluid of the lower layer is appropriate, for a Carreau fluid a similar assumption may not be entirely suitable. Hence, in this chapter we examine a two-fluid system with a Carreau fluid in the lower layer in an effort to understand the nature

---

[1] A rough, white icy covering; only formed from fog or vapour-bearing air.

of the boundary-layer flow and the shape of the velocity profile in both fluids. It should also be noted that fluid injection is taking place through the flat plate into the lower fluid.

We proceed by firstly deriving a set of coupled partial differential equations to describe the two-fluid system. The appropriate conditions at the material boundary between the two fluids are derived so that along with the conditions at the flat plate and the far-field the system of governing equations may be closed. Section 6.2 describes a transformation that is applied to the system of partial differential equations that results in a pair of coupled ordinary differential equations. A numerical scheme for solving these equations that yields self-similar velocity profiles is described. In Section 6.3 the results obtained are presented and discussed. An analysis of the small injection velocity limit is carried out in Section 6.4, along with a comparison of the analytic results with some of the available numerical results. Lastly in Section 6.5 we present some conclusions.

6.1 Governing Equations

We consider the flow of a fluid along a smooth surface that is coated by a thin film of a different fluid. The two fluids are incompressible and immiscible. We are particularly interested in the nature of the steady laminar boundary-layer that develops when the characteristic Reynolds number is assumed to be large. In a two-fluid system such as this there is also a strong coupling due to the continuity of the interfacial stresses and velocities.

The flow in each fluid is described by an equation for the conservation of mass and the steady Cauchy equations for momentum transport

$$\frac{\partial U_i}{\partial X} + \frac{\partial V_i}{\partial Y} = 0, \tag{6.1a}$$

$$\rho\left[U_i\frac{\partial U_i}{\partial X} + V_i\frac{\partial U_i}{\partial Y}\right] = -\frac{\partial P_i}{\partial X} - \left[\frac{\partial(\tau_{XX})_i}{\partial X} + \frac{\partial(\tau_{YX})_i}{\partial Y}\right], \tag{6.1b}$$

$$\rho\left[U_i\frac{\partial V_i}{\partial X} + V_i\frac{\partial V_i}{\partial Y}\right] = -\frac{\partial P_i}{\partial Y} - \left[\frac{\partial(\tau_{XY})_i}{\partial X} + \frac{\partial(\tau_{YY})_i}{\partial Y}\right], \tag{6.1c}$$

where the physical (dimensional) quantities are denoted in upper case and the subscript i

identifies the two different fluid regions. The lower fluid is indicated by $i = 1$ and the upper fluid is indicated by $i = 2$.

The upper fluid is a Newtonian fluid that is described by the constitutive relation

$$\boldsymbol{\tau}_2 = -\mu \dot{\boldsymbol{\gamma}},$$

in which μ is the constant viscosity and $\dot{\boldsymbol{\gamma}}$ is the rate-of-deformation tensor defined by $\boldsymbol{\nabla v} + (\boldsymbol{\nabla v})^T$ where $\boldsymbol{v}$ is the fluid velocity field. The lower fluid, or thin film, is a generalised Newtonian fluid described by the Carreau constitutive relation

$$\boldsymbol{\tau}_1 = -\left\{\mu_\infty + (\mu_0 - \mu_\infty)\left[1 + (K_1\dot{\gamma})^2\right]^{\frac{n-1}{2}}\right\}\dot{\boldsymbol{\gamma}},$$

introduced in Chapter 5. Here n is the fluid index, μ_0 is the zero-shear-rate viscosity, μ_∞ is the infinite-shear-rate viscosity and $\dot{\gamma}$ is the shear-rate. K_1 is a constant with the units of time.

The set of equations (6.1) are put into non-dimensional form by taking L as a typical length and U_∞ as the free-stream velocity. The non-dimensional equations are mapped to the boundary-layer scale by using the boundary-layer thickness of the upper fluid, ϵ_2, as the scale factor. The Reynolds number for the upper fluid is defined by $Re = \frac{\rho_2 U_\infty L}{\mu}$ and the boundary-layer thickness is given by $\epsilon_2 = O(Re^{-\frac{1}{2}})$. The Reynolds number for the Carreau fluid in the thin film has the same definition as the Reynolds number for the Newtonian fluid. Hence the scale factor ϵ_2 can be used to rescale the governing equations for the lower fluid as well. The subscript will not be used in subsequent references to ϵ.

Performing the non-dimensionalisation and rescaling the governing equations for the lower fluid results in

$$\frac{\partial u_1}{\partial x} + \frac{\partial v_1}{\partial y} = 0, \tag{6.2a}$$

$$u_1\frac{\partial u_1}{\partial x} + v_1\frac{\partial u_1}{\partial y} = -\frac{\partial p_1}{\partial x} + \left[1 + C_0\left\{1 + n\left(\lambda\frac{\partial u_1}{\partial y}\right)^2\right\}\left\{1 + \left(\lambda\frac{\partial u_1}{\partial y}\right)^2\right\}^{\frac{n-3}{2}}\right]\frac{\partial^2 u_1}{\partial y^2}, \tag{6.2b}$$

$$0 = -\frac{\partial p_1}{\partial y}, \tag{6.2c}$$

where $C_0 = \frac{\mu_0 - \mu_\infty}{\mu_\infty}$ is a viscosity ratio and λ is a dimensionless parameter defined by $\lambda^2 = \left(\frac{K_1 U_\infty}{\epsilon L}\right)^2$. Applying the same non-dimensionalisation and rescaling to the governing equations for the upper fluid results in

$$\frac{\partial u_2}{\partial x} + \frac{\partial v_2}{\partial y} = 0, \tag{6.3a}$$

$$u_2\frac{\partial u_2}{\partial x} + v_2\frac{\partial u_2}{\partial y} = -\frac{\partial p_2}{\partial x} + \frac{\partial^2 u_2}{\partial y^2}, \tag{6.3b}$$

$$0 = -\frac{\partial p_2}{\partial y}. \tag{6.3c}$$

To enable a solution to be found for this coupled system of partial differential equations, we need to specify some appropriate boundary conditions. The boundary conditions at the surface and in the far-field are given by

$$u_1 = 0, \qquad v_1 = v_{in} \qquad \text{at} \qquad y = 0, \tag{6.4a}$$

$$u_2 \to U_\infty \qquad \text{as} \qquad y \to \infty, \tag{6.4b}$$

where v_{in} is the injection rate of the lower fluid through the surface of the flat plate. The injection rate v_{in} needs not be a constant value, its value may depend on the streamwise location along the length of the flat plate. These boundary conditions reflect the physical requirement that the fluid flow satisfies the full viscous no-slip conditions at the surface of the plate and that the stream-wise velocity within the boundary layer of the upper fluid matches smoothly onto the free-stream, given by $U_\infty(x)$, at a large distance from the plate surface.

At the material boundary between the two fluids the matching conditions are supplied by the requirement to meet the dynamic and kinematic conditions there. The dynamic condition at the fluid interface is satisfied through continuity of both shear and normal stress. We note that the effect of surface tension at the fluid interface will be neglected as part of the derivation of the continuity of normal stresses between the two fluids. Variations in the thickness of the thin film are assumed to be very small in comparison to the streamwise scale, equivalently, the curvature of the fluid interface is very close to zero. Hence, the contribution of the surface tension to the continuity of normal stresses across the fluid interface is negligible (Timoshin (1997)). Firstly, continuity of shear stress, expressed in dimensional variables, is $(\tau_{XY})_1 = (\tau_{XY})_2$ where

$$\begin{aligned}(\tau_{XY})_1 &= \mu^*_{app}\left(\frac{\partial U_1}{\partial Y} + \frac{\partial V_1}{\partial X}\right),\\ (\tau_{XY})_2 &= \mu\left(\frac{\partial U_2}{\partial Y} + \frac{\partial V_2}{\partial X}\right),\end{aligned}$$

with μ^*_{app} denoting the non-constant viscosity of the Carreau fluid in the thin film. We proceed by non-dimensionalising and rescaling these expressions so that the resulting form of the continuity of shear stress at the fluid interface is given by

$$\frac{\partial u_2}{\partial y} = \left(\frac{\mu_\infty}{\mu}\right)\left[1 + C_0\left\{1 + \left(\lambda\frac{\partial u_1}{\partial y}\right)^2\right\}^{\frac{n-1}{2}}\right]\frac{\partial u_1}{\partial y}. \tag{6.5}$$

Secondly, we consider the continuity of normal stress at the fluid interface, expressed in dimensional variables, is $(\tau_{YY})_1 = (\tau_{YY})_2$ where

$$\begin{aligned}(\tau_{YY})_1 &= P_1 + \mu^*_{app}\left(2\frac{\partial V_1}{\partial Y}\right),\\ (\tau_{YY})_2 &= P_2 + \mu\left(2\frac{\partial V_2}{\partial Y}\right).\end{aligned}$$

Proceeding as before by non-dimensionalising and rescaling the expressions, we find that the continuity of normal stress at the fluid interface is given by

$$p_1 + 2\frac{\mu_\infty}{\rho_2 U_\infty L}\left[1 + C_0\left\{1 + \left(\lambda\frac{\partial u_1}{\partial y}\right)^2\right\}^{\frac{n-1}{2}}\right]\frac{\partial u_1}{\partial y} = p_2 + 2\frac{\mu}{\rho_2 U_\infty L}\frac{\partial v_2}{\partial y}.$$

Making use of the definition of the Reynolds number and letting $Re \to \infty$, simplifies the above expression to

$$p_1 = p_2. \tag{6.6}$$

The continuity of normal stress across the fluid interface is therefore equivalent to the requirement of continuity of pressure across the fluid interface.

Next, we consider the kinematic condition at the interface between the two fluids. Let the location of the fluid interface, expressed in dimensional variables, be given by $Y = Y^*(X,T)$. For convenience, we write the equation for the position of the fluid interface in the following equivalent form $F(X,Y,T) = Y - Y^*(X,T)$. The material derivative $\frac{\mathrm{D}F}{\mathrm{D}T}$ is set equal to 0 on the fluid interface and, hence, yields

$$0 = \frac{\partial F}{\partial T} + U_i \frac{\partial F}{\partial X} + V_i \frac{\partial F}{\partial Y} \quad \text{at} \quad Y = Y^*(X,T), \quad \text{for} \quad i = 1, 2.$$

Non-dimensionalisation and rescaling this expression results in

$$\frac{\partial y^*}{\partial t} + u_i \frac{\partial y^*}{\partial x} = v_i \quad \text{at} \quad y = y^*(x,t), \quad \text{for} \quad i = 1, 2.$$

The boundary-layer flow being considered here is steady, so the position of the fluid interface will also be steady in the absence of any interfacial instabilities. Hence, the interfacial velocity conditions are written as

$$u_1 = u_2, \tag{6.7a}$$

$$v_i = u_i \frac{\partial y^*}{\partial x} \quad \text{at} \quad y = y^*(x), \quad \text{for} \quad i = 1, 2. \tag{6.7b}$$

The governing equations (6.2) and (6.3) along with suitable boundary conditions can be used to model quite general flow regimes. Different classes of flow can be specified by the appropriate definition of the external free-stream, or potential, velocity function. For example, flows that are driven by a zero, adverse or favourable pressure gradient require that the free-stream velocity function, $U_\infty(x)$, is of suitable form. We note that in equations (6.2) and (6.3) the pressure is independent of the surface normal co-ordinate. Hence, in the free-stream flow we find that $\frac{\partial u_2}{\partial y} \to 0$ and $u_2(x, y) \to U_\infty(x)$. Using this far-field behaviour of the stream-wise velocity of the upper fluid in the x-momentum equation (6.3b) allows the pressure gradient to be expressed as

$$-\frac{\partial p_2}{\partial x} = U_\infty(x)\frac{\mathrm{d}U_\infty}{\mathrm{d}x}.$$

The continuity of normal stress across the fluid interface given by equation (6.6), which is equivalent to continuity of pressure, allows us to write the pressure gradient in the lower fluid as

$$-\frac{\partial p_1}{\partial x} = U_\infty(x)\frac{\mathrm{d}U_\infty}{\mathrm{d}x}.$$

Hence, the boundary-layer flow of a Newtonian fluid over a thin film of Carreau fluid is governed by the following coupled system of partial differential equations

$$\frac{\partial u_1}{\partial x} + \frac{\partial v_1}{\partial y} = 0, \tag{6.8a}$$

$$u_1\frac{\partial u_1}{\partial x} + v_1\frac{\partial u_1}{\partial y} = U_\infty\frac{\mathrm{d}U_\infty}{\mathrm{d}x} + \left[1 + C_0\left\{1 + n\left(\lambda\frac{\partial u_1}{\partial y}\right)^2\right\}\left\{1 + \left(\lambda\frac{\partial u_1}{\partial y}\right)^2\right\}^{\frac{n-3}{2}}\right]\frac{\partial^2 u_1}{\partial y^2}, \tag{6.8b}$$

and

$$\frac{\partial u_2}{\partial x} + \frac{\partial v_2}{\partial y} = 0, \tag{6.9a}$$

$$u_2\frac{\partial u_2}{\partial x} + v_2\frac{\partial u_2}{\partial y} = U_\infty\frac{\mathrm{d}U_\infty}{\mathrm{d}x} + \frac{\partial^2 u_2}{\partial y^2}. \tag{6.9b}$$

Equation (6.8) corresponds to the Carreau fluid in the thin film, while equation (6.9) corresponds to the upper Newtonian fluid. The boundary conditions on the flat plate and in the far-field are given by (6.4a) and (6.4b) respectively. The matching conditions at the material boundary between the two fluids are given by (6.5) and (6.7).

The matching condition (6.6), representing continuity of normal stress or continuity of pressure, has been used when the term $U_\infty\frac{\mathrm{d}U_\infty}{\mathrm{d}x}$ was introduced into the governing equations.

6.2 Numerical Scheme

The coupled system of equations governing the boundary-layer flow of a Newtonian fluid over a thin film of Carreau fluid does not admit an obvious closed form solution. However, we can obtain solutions using numerical methods. In this section we describe the transformation of the system of partial differential equations into a pair of ordinary differential equations which are then solved using a shooting method.

In Section 5.1 we showed that the 'apparent' Reynolds number for a Carreau fluid is identical to the Reynolds number for a classical Newtonian fluid. We also introduced a change of independent co-ordinates that transformed the governing equations for a Carreau fluid into a form that is amenable to solution by numerical methods. This change of co-ordinates is the same as that used for transforming the governing equations of Newtonian fluids. The new independent co-ordinates are defined by

$$\xi = x, \qquad \eta = y\left(\frac{U_\infty}{x}\right)^{\frac{1}{2}}. \tag{6.10}$$

We also introduce the stream function defined by $\psi(x,y) = (xU_\infty)^{\frac{1}{2}} f(\xi,\eta)$, where $f(\xi,\eta)$ is a non-dimensional stream function.

Applying this change of co-ordinates to the Carreau fluid in the thin film that is coating the flat plate results in

$$\begin{aligned}\frac{\partial^3 f_1}{\partial\eta^3}&\left[1 + C_0\xi^{\frac{1-n}{2}}\left\{\xi + nU_\infty^3\left(\lambda\frac{\partial^2 f_1}{\partial\eta^2}\right)^2\right\}\left\{\xi + U_\infty^3\left(\lambda\frac{\partial^2 f_1}{\partial\eta^2}\right)^2\right\}^{\frac{n-3}{2}}\right] + \frac{1}{2}\left[\beta+1\right]f_1\frac{\partial^2 f_1}{\partial\eta^2}\\ &+ \beta\left[1 - \left(\frac{\partial f_1}{\partial\eta}\right)^2\right] = \xi\left[\frac{\partial^2 f_1}{\partial\xi\partial\eta}\frac{\partial f_1}{\partial\eta} - \frac{\partial^2 f_1}{\partial\eta^2}\frac{\partial f_1}{\partial\xi}\right],\end{aligned} \tag{6.11}$$

where β is the external pressure gradient parameter and is defined as

$$\beta(\xi) = \frac{\xi}{U_\infty}\frac{\mathrm{d}U_\infty}{\mathrm{d}\xi}.$$

For the Newtonian fluid in the upper region of the two fluid system, after applying the same change of co-ordinates, we get

$$\frac{\mathrm{d}^3 f_2}{\mathrm{d}\eta^3} + \frac{1}{2}\left[\beta + 1\right] f_2 \frac{\mathrm{d}^2 f_2}{\mathrm{d}\eta^2} + \beta \left[1 - \left(\frac{\mathrm{d}f_2}{\mathrm{d}\eta}\right)^2\right] = 0. \tag{6.12}$$

The solution of equation (6.11) has been discussed in Chapter 5 and is accomplished via a numerical marching scheme. We also recall that equation (6.11) does not, in general, possess self-similar solutions. However, equation (6.12) is readily recognised as the Falkner-Skan equation and is known to possess self-similar solutions when β takes a constant value, these solutions are obtained by numerical methods. In principle, the numerical marching scheme could be used to provide a solution in the lower Carreau fluid at a given ξ location and in the η direction as far out as the location of the fluid interface. The boundary conditions on the interface would then be used to calculate a self-similar solution in the upper Newtonian fluid. This solution procedure is not very straightforward due to a dependence on the ξ location in the lower fluid, as well as the unknown position of the fluid interface. A simpler, or more direct, procedure for obtaining a solution to this pair of equations is preferable.

In Section 5.2 it was shown that a self-similar solution of equation (6.11) exists for a specific class of potential flow in the free-stream, viz. $U_\infty(x) = x^{\frac{1}{3}}$, or equivalently $U_\infty(\xi) = \xi^{\frac{1}{3}}$. Consequently, an understanding of how the flow of this two fluid system develops may be provided by a combination of self-similar solutions, each solution being applicable to each fluid. We proceed by substituting this specific form for the external flow U_∞, so that equation (6.11) for the lower Carreau fluid takes the form

$$\left[1 + C_0\left\{1 + n\left(\lambda f_1''\right)^2\right\}\left\{1 + \left(\lambda f_1''\right)^2\right\}^{\frac{n-3}{2}}\right] f_1''' + \frac{2}{3} f_1 f_1'' + \frac{1}{3}\left[1 - \left(f_1'\right)^2\right] = 0, \tag{6.13}$$

where the prime denotes differentiation with respect to η. Equation (6.12) for the upper Newtonian fluid becomes

$$f_2''' + \frac{2}{3} f_2 f_2'' + \frac{1}{3}\left[1 - \left(f_2'\right)^2\right] = 0. \tag{6.14}$$

The velocity components in each fluid are given by

$$u_i = \xi^{\frac{1}{3}} f_i'$$
$$v_i = -\frac{2}{3}\frac{1}{\xi^{\frac{1}{3}}}\left[f_i - \frac{\eta}{2} f_i'\right],$$

where $i = 1, 2$ corresponds to the lower and upper fluids respectively.

The boundary conditions on the surface and in the far-field take the following form

$$f_1 = -\frac{3}{2}\xi^{\frac{1}{3}} v_{in}, \qquad f_1' = 0 \qquad \text{at} \qquad \eta = 0, \tag{6.15a}$$

$$f_2' \to 1 \qquad \text{as} \qquad \eta \to \infty. \tag{6.15b}$$

We note that the expression for the injection rate v_{in} must be chosen so that $f_1(0)$ is constant. The continuity of shear stress condition at the fluid interface, given by equation (6.5), becomes

$$f_2'' = \left(\frac{\mu_\infty}{\mu}\right)\left[1 + C_0\left\{1 + (\lambda f_1'')^2\right\}^{\frac{n-1}{2}}\right] f_1'' \qquad \text{at} \qquad \eta = \eta^*. \tag{6.16}$$

The kinematic conditions at the interface between the two fluids are

$$f_1 = f_2, \tag{6.17a}$$

$$f_1' = f_2' \qquad \text{at} \qquad \eta = \eta^*. \tag{6.17b}$$

It is readily apparent that the success of the numerical scheme for solving equation (6.13) followed by equation (6.14) is very dependent on being able to determine the location of the fluid interface. We next describe the manner in which the location of the fluid interface is determined. We proceed by noting that for the free-stream flow that allows a self-similar solution, the independent co-ordinates defined by (6.10) become

$$\xi = x, \qquad \eta = \frac{y}{x^{\frac{1}{3}}},$$

and η is the familiar Falkner-Skan type similarity variable. Hence, the non-dimensional form for the location of the fluid interface $y^*(x)$ becomes

$$\eta^* = \frac{y^*}{x^{\frac{1}{3}}}.$$

As a result of this similarity transformation η^* is required to take a constant value, hence the location of the fluid interface can be expressed as

$$y^*(x) = \eta^* x^{\frac{1}{3}}.$$

Making use of this expression for $y^*(x)$, the non-dimensional form of the interfacial velocity condition (6.7) becomes

$$u\left(\frac{\eta^*}{3}\frac{x^{\frac{1}{3}}}{x}\right) = v.$$

Substituting expressions for the velocity components derived from the similarity transformation and simplifying gives

$$\frac{\eta^*}{3} f' \xi^{-\frac{1}{3}} = -\frac{2}{3}\xi^{-\frac{1}{3}}\left[f - \frac{\eta^*}{2} f'\right].$$

Simplifying further gives

$$f_1(\eta) = f_2(\eta) = 0 \quad \text{at} \quad \eta = \eta^*, \tag{6.18}$$

as the conditions that defines the location of the fluid interface.

The numerical scheme that is used to obtain self-similar solutions to this pair of ordinary differential equations is as follows. The shooting method is used to solve equation (6.13) for the lower Carreau fluid with initial conditions given by (6.15a) and an initial guess for $f_1''(0)$. The integration of equation (6.13) is carried out until the condition defining the location of the fluid interface is met, i.e. the value of f_1 changes sign from negative to positive. If a poor choice for the initial value of $f_1''(0)$ is made, then it is likely that the numerical solution will deviate away from the expected solution. Such behaviour of the numerical solution is indicated, and trapped, when f_1'' first becomes negative. The resulting value of η^* is still used as a crude, though incorrect, location for the fluid interface.

At the fluid interface, the matching conditions (6.16) and (6.17) are used to determine the initial conditions for equation (6.14) that governs the upper Newtonian fluid. The solution procedure continues with the integration of equation (6.14) being performed until either the far-field location η_∞ is reached or the numerical solution is found to be deviating away from the expected solution. As before, this behaviour is indicated when f_2'' first becomes negative. The solution at η_∞, the value of η where the integration has stopped, is used to 'predict' a new set of initial conditions for equation (6.14) at η^* using a Newton-Raphson correction. The 'predicted' value of $f_2''(\eta^*)$ is then back-propagated via equation (6.16) to provide an updated value for $f_1''(0)$ that is also determined using a Newton-Raphson correction.

This two-stage numerical solution procedure is iterated until convergence of the solution has been achieved to a suitable accuracy. The iteration process stopped when the change in the value of $f_1''(0)$ fell below a pre-defined tolerance. This tolerance was 1.0×10^{-7} for all calculations unless otherwise indicated.

This numerical scheme for finding a self-similar solution to the coupled system of equations (6.13) and (6.14) was implemented in MATLAB. The governing ordinary differential equation in each fluid region was solved using the `ode45` initial value problem solver based on the Runge-Kutta quadrature method.

6.3 Numerical Results

The numerical scheme described in Section 6.2 for obtaining similarity-type solutions of equations (6.13) and (6.14) has been used to investigate the effect of the parameters n, λ and C_0 in the Carreau viscosity model on the location of the fluid interface η^*. The fluid injection rate through the flat plate is another factor that affects the location of the fluid interface. The dependence of the fluid interface location on these parameters is described below.

We will proceed by considering the effect of each model parameter individually, while keeping the other parameters fixed at a representative value. The step-size $\Delta\eta$ in the wall-normal direction was set to 0.001 and the far-field η_∞, for matching to the asymptotic boundary condition, was set to 10.0.

Fluid Index (n)	0.30	0.40	0.50	0.60	0.70	0.80	0.90	1.00	-
η^*	0.756	0.770	0.786	0.803	0.823	0.844	0.867	0.890	-
Fluid Index (n)	1.10	1.20	1.30	1.40	1.50	1.60	1.70	1.80	1.90
η^*	0.914	0.939	0.963	0.988	1.012	1.036	1.058	1.081	1.102

Table 6.1: Location of fluid interface, η^*, for shear-thinning ($0 < n < 1$) and shear-thickening ($n > 1$) Carreau fluids with $\lambda = 10, C_0 = 1.0$ and the fluid injection rate $v_{in} = 0.1$.

6.3.1 Effect of Fluid Index (n)

We first consider the effect that the fluid index n has on the location of the interface between the two fluids and on the self-similar velocity profile. The other parameters in the Carreau viscosity model were set to $C_0 = 1$ and $\lambda = 10$. The fluid injection rate at the surface of the flat plate was set to $v_{in} = 0.1$. The fluid index values considered are in the range $n = 0.3, 0.4, \ldots, 1.9$.

The location of the fluid interface η^* between the lower Carreau fluid and the upper Newtonian fluid for each fluid index value was calculated and the results obtained are summarised in Table 6.1. The results for shear-thinning Carreau fluids are grouped separately from the results for shear-thickening Carreau fluids.

The results in Table 6.1 indicate that as the fluid index n increases, the location of the fluid interface η^* also increases. Hence the fluid interface moves further away from the the flat plate with an increase in n. The variation of η^* with fluid index n is also shown in Figure 6.1, where it can be seen that as the fluid index increases the interface between the two fluids is located at greater distances from the surface along which the lower Carreau fluid flows. The plot also shows that the curve representing the relationship between n and η^* is weakly non-linear. Performing a least squares fit of the data points to an exponential model yields $\eta^* = 0.697e^{0.2453n}$ with $R^2 = 0.9986$ being an indication of the residual. This relationship may be used to determine the position of the interface η^* for other values of the fluid index n.

The reduced skin friction or wall shear is also of interest when investigating boundary layer flows. The wall shear τ_w for the lower Carreau fluid along with the interfacial shear for the upper Newtonian fluid are shown in Figure 6.2.

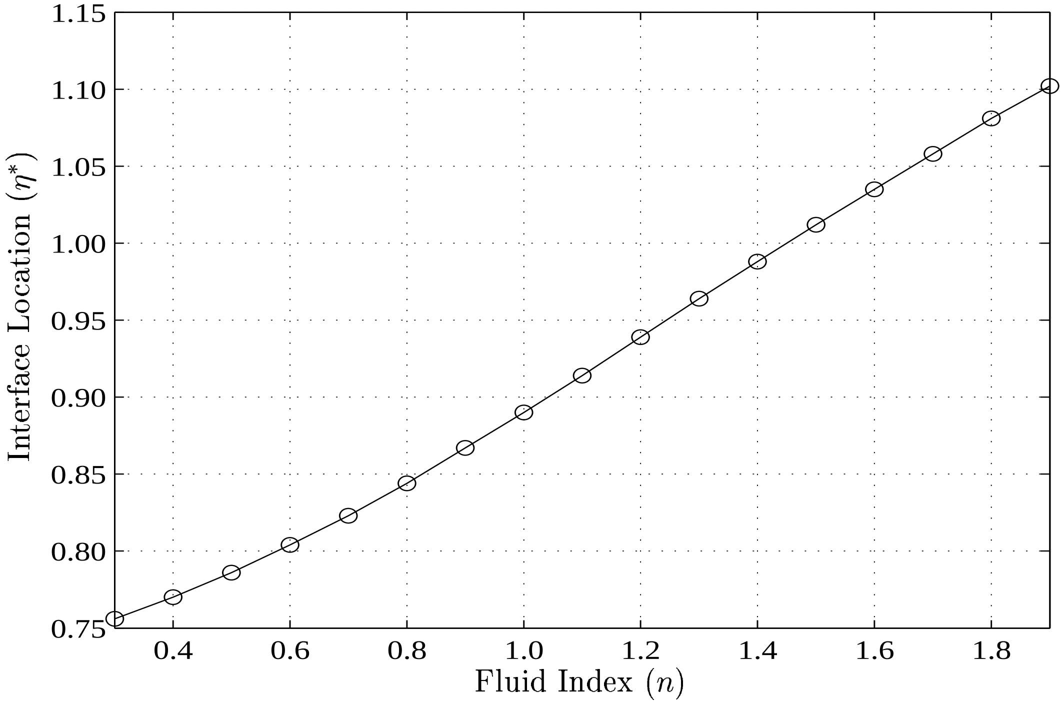

Figure 6.1: Location of fluid interface η^* for fluid index values $n = 0.3, 0.4, \ldots, 1.9$. Other Carreau viscosity model parameters set to $\lambda = 10, C_0 = 1.0$ and the fluid injection rate $v_{in} = 0.1$.

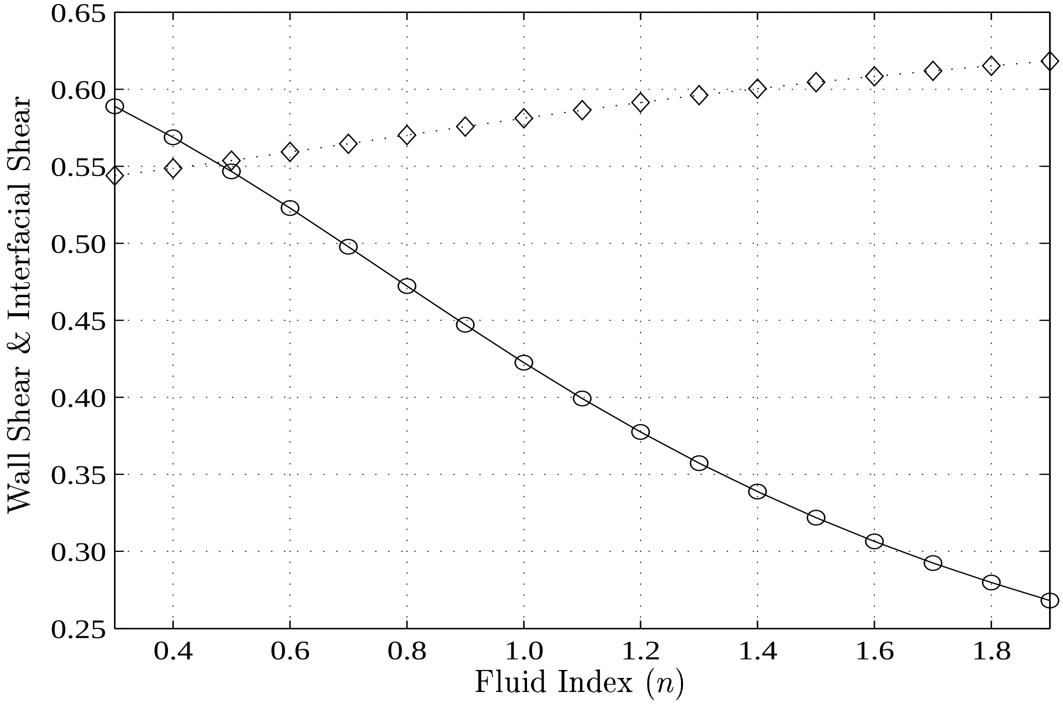

Figure 6.2: Wall shear for lower Carreau fluid (solid line) and interfacial shear for upper Newtonian fluid (dashed line) for fluid index values $n = 0.3, 0.4, \ldots, 1.9$. Other Carreau viscosity model parameters set to $\lambda = 10, C_0 = 1.0$ and the fluid injection rate $v_{in} = 0.1$.

The results plotted in Figure 6.2 indicate that as the fluid index n increases, the wall shear, given by $f''(0)$, decreases. The wall shear does not display a distinct asymptotic approach to a limiting value over the range of fluid index values n considered. It may be the case that for larger values of n the wall shear curve may flatten out somewhat, but fluid index values greater than 2 are considered physically unrealistic and hence have not been pursued with numerical calculations. The interfacial shear, given by $f''(\eta^*)$, shows a gradual monotonic increase in value as the fluid index n takes larger values.

The self-similar velocity profiles for $n = 0.50$, 1.0 and 1.50 are shown in Figure 6.3. The location of the fluid interface can be inferred from the 'kink' in the velocity profile. When the thin film is a shear-thinning Carreau fluid then the discontinuity in the velocity gradient across the fluid interface is less dramatic. For a thin film that is a shear-thickening Carreau fluid we see that this discontinuity in the velocity gradient across the fluid interface is quite sharp. For $n = 1.0$ the Carreau fluid in the thin film is not genuinely Newtonian like the upper fluid since $C_0 \neq 0$. With $C_0 = 1$ the Carreau fluid still has a non-constant viscosity that is different from the viscosity of the Newtonian fluid. For this combination of fluid parameters, the two fluids effectively have differing viscosities and hence a material interface is present.

The sharpness of the 'kink' in the velocity profile can be partly accounted for by the observation that for a shear-thinning thin film the velocity profile has a relatively high velocity gradient at the fluid interface. Hence, the shear in the Carreau fluid, indicated by the gradient of the velocity profile, in the vicinity of the fluid interface is a relatively large non-zero value. However, for a shear-thickening thin film the gradient of the velocity profile is smaller in magnitude as the fluid interface is approached. Thus the shear in the Carreau fluid in the vicinity of the fluid interface is a value close to zero. So the sharpness of the 'kink' in the velocity profile may, in part, be attributed to the difference between the interfacial shear and the shear in the lower fluid in the near vicinity of the fluid interface. This difference in fluid shear on either side of the fluid interface increases with n.

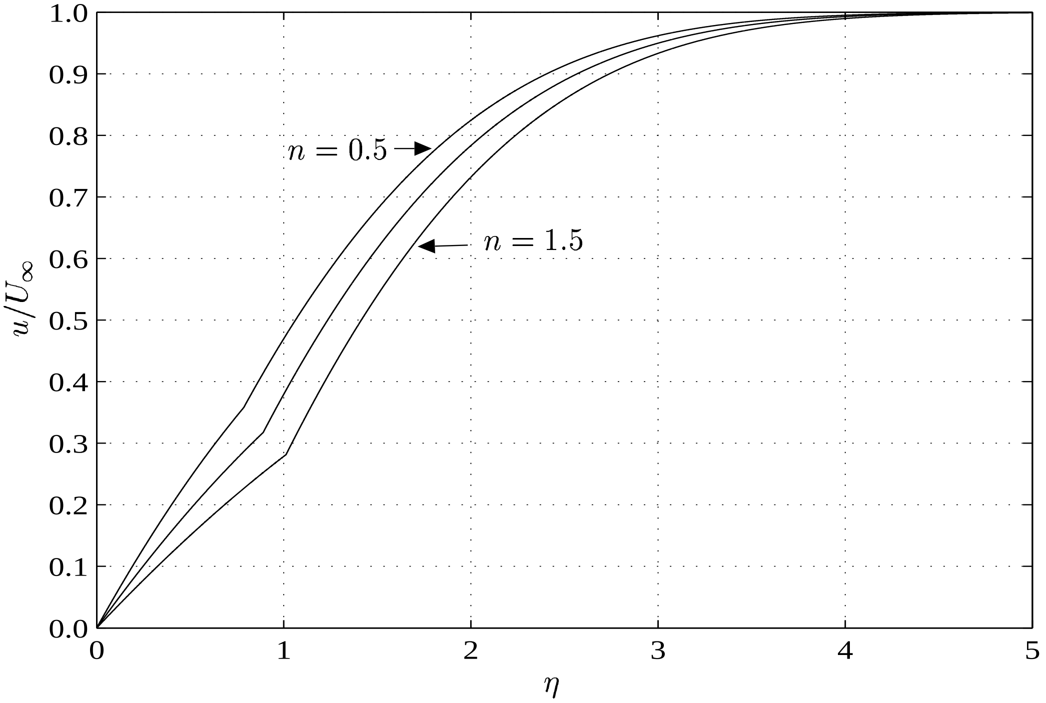

Figure 6.3: Self-similar velocity profiles for $n = 0.50$, 1.0 and 1.50. Other Carreau viscosity model parameters set to $\lambda = 10, C_0 = 1.0$ and the fluid injection rate $v_{in} = 0.1$.

6.3.2 Effect of Relaxation Parameter λ

The Carreau viscosity model has a so-called 'relaxation' parameter that takes the dimensions of time. This parameter is represented by λ in the non-dimensional form of the governing equations. To investigate the effect of this parameter on the location of the fluid interface, we first consider a shear-thinning fluid with $n = 0.90$ and the other parameters set to $C_0 = 1.0, v_{in} = 0.1$. The values of the relaxation parameter considered were $\lambda = 5, 10, 20, 100, 200, 400, 800$. The results obtained are summarised in Table 6.2.

Next we consider a shear-thickening fluid with $n = 1.10$ and the other parameters set to $C_0 = 1.0, v_{in} = 0.1$. The values of the relaxation parameter considered were as before. The results obtained are summarised in Table 6.3.

An examination of Tables 6.2 and 6.3 indicates that the location of the fluid interface is not significantly affected by the value of λ. While the value of λ has been varied by at least two orders of magnitude, the variation in the value of η^* has been less dramatic. However, we note that for the shear-thinning fluid the interface location moves toward the surface, while

λ	5	10	20	100	200	400	800
η^*	0.877	0.867	0.856	0.833	0.824	0.816	0.808

Table 6.2: Location of fluid interface for different values of λ and $n = 0.90, C_0 = 1.0, v_{in} = 0.1$.

λ	5	10	20	100	200	400	800
η^*	0.904	0.914	0.927	0.959	0.974	0.989	1.006

Table 6.3: Location of fluid interface for different values of λ and $n = 1.10, C_0 = 1.0, v_{in} = 0.1$.

for the shear-thickening fluid the location of the interface moves away from the surface as the value of λ is increased. Both the lack of sensitivity of η^* to the value of λ and the direction of movement of the fluid interface location may be accounted for by considering the role that λ plays in the Carreau viscosity model.

6.3.3 Effect of C_0

In the Carreau viscosity model the parameter C_0 is defined by $C_0 = \frac{\mu_0 - \mu_\infty}{\mu_\infty}$. This parameter represents the ratio of the difference between the zero-shear and infinite-shear viscosities with the infinite-shear viscosity. Hence $C_0 = 0$ corresponds to $\mu_0 = \mu_\infty$ (a Newtonian fluid), while other values of C_0 correspond to different ratios between μ_0 and μ_∞. To investigate the effect that this parameter has on the location of the fluid interface, the values of C_0 considered were $0.25, 0.50, \ldots, 1.50$, while the other fluid parameters were $\lambda = 10, v_{in} = 0.1$. For these calculations the η step-size was 0.01 and the calculations were repeated for $n = 0.50, 0.75, 1.00, 1.25, 1.50$. The family of curves for the location of the fluid interface are shown in Figure 6.4.

The results shown in Figure 6.4 indicate that the viscosity ratio C_0 has a noticeable effect on the location of the fluid interface η^*. It can be seen that for a given value of the fluid index n, the fluid interface moves further from the surface as the value of C_0 increases. When the value of C_0 is relatively low we see that the fluid interface is confined to a small range of values for the fluid index values considered. As the value of C_0 increases then so does the range of possible locations for the fluid interface. The relationship between C_0 and η^* is non-linear and this is made most apparent for larger values of the fluid index n.

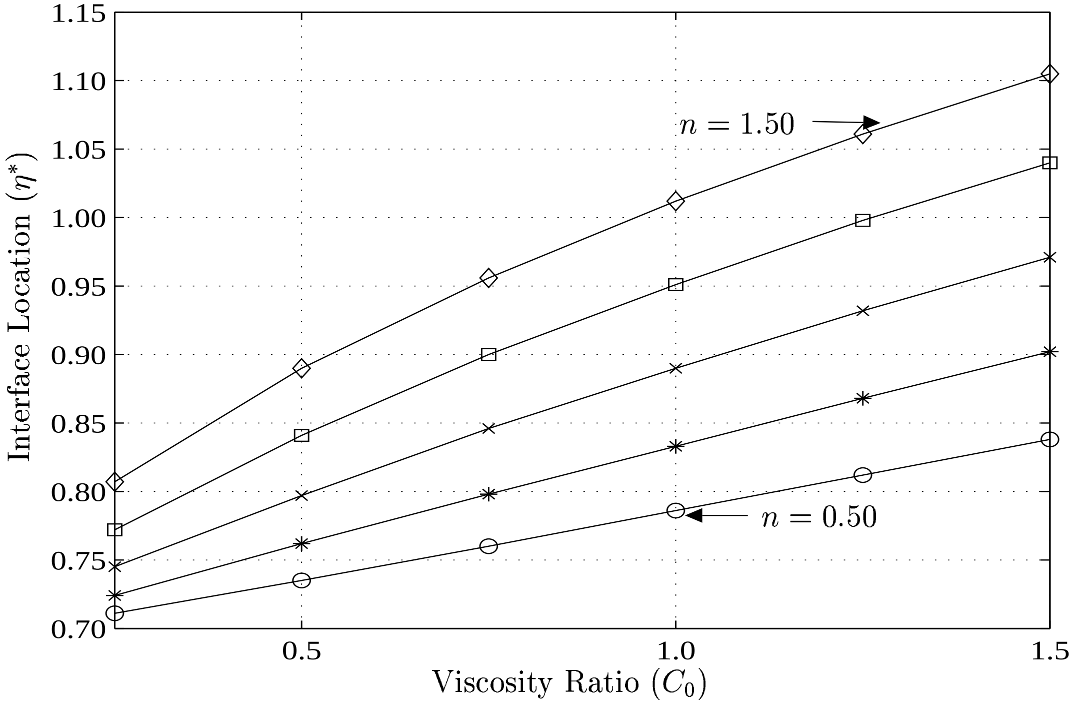

Figure 6.4: Location of fluid interface η^* for $n = 0.50, 0.75, \ldots, 1.50$ and viscosity ratio values $C_0 = 0.25, 0.50, \ldots, 1.50$. Relaxation time parameter $\lambda = 10$ and fluid injection rate $v_{in} = 0.1$.

6.3.4 Effect of Injection Rate (v_{in})

We expect that the fluid injection rate will have a direct effect on the location of the fluid interface and this was investigated next. Fluid index values $n = 0.50, 0.75, 1.25, 1.50$ were selected along with $v_{in} = 0.04, 0.05, \ldots, 0.10, 1.15, 1.20, 1.25$. The remaining fluid parameters were set to $\lambda = 10, C_0 = 1.0$ and the η step-size was set to 0.001. For each combination of n and v_{in} the numerical scheme was used to find a solution. The location of the fluid interface η^* as well as the wall shear $f_1''(0)$ and interfacial shear $f_2''(\eta^*)$ were recorded. Figure 6.5 shows plots of the location of the fluid interface η^* against the injection rate v_{in} for the selected values of the fluid index.

The results in Figure 6.5 indicate that as the fluid injection rate varies then so does the location of the fluid interface. We see that as the value of v_{in} is increased, then the fluid interface is located further from the surface for all values of n considered. Likewise, as the value of v_{in} is decreased, we see that the fluid interface location moves closer to the surface. These outcomes of the numerical investigations are in keeping with the intuitive expectation

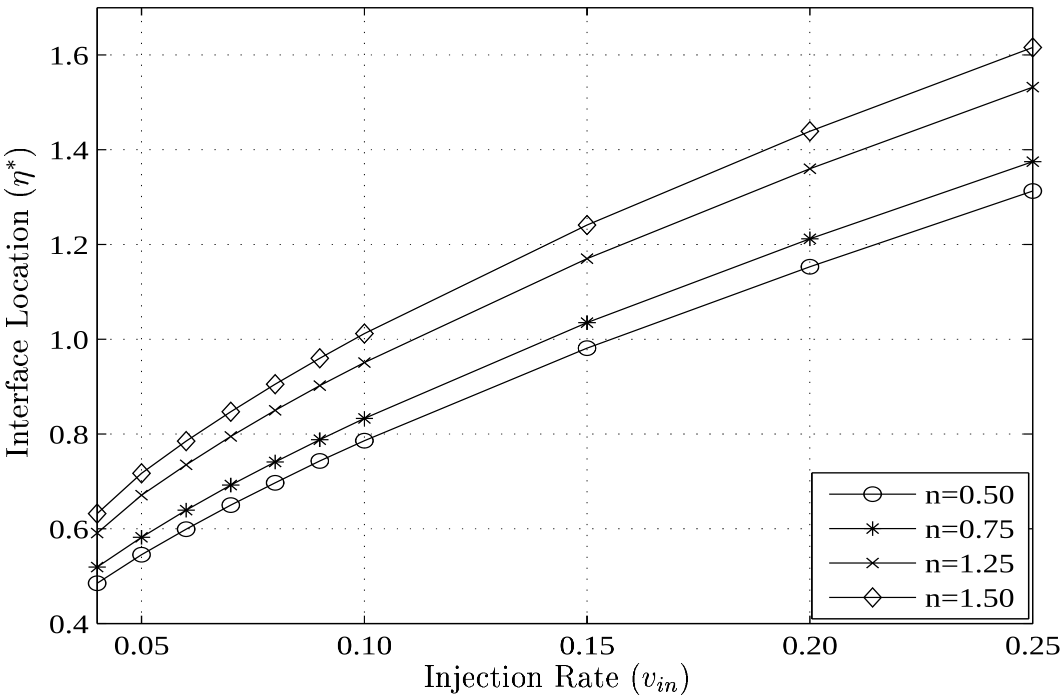

Figure 6.5: Location of fluid interface η^* for various injection rates and fluid index values $n = 0.50, 0.75, 1.25, 1.50$. Relaxation time parameter set to $\lambda = 10$ and viscosity ratio $C_0 = 1.0$.

that the magnitude of the injection rate will directly affect the distance of the fluid interface from the surface. The results also suggest that for relatively large fluid injection rates the location of the fluid interface varies in an almost linear manner. For smaller rates of fluid injection, the variation in the fluid interface location shows a more non-linear behaviour.

The results from this set of calculations also allows us to see how the wall shear $f_1''(0)$ behaves for different fluid injection rates. Figure 6.6 shows plots of the wall shear $f_1''(0)$ versus the injection rate v_{in} for the fluid index values investigated. The plots corresponding to the shear-thinning fluids considered indicate that the wall shear decreases as the injection rate increases. For the shear-thickening fluids considered the plots firstly indicate less variability in the value of the wall shear. Next, there is evidence of a slight increase in the value of $f_1''(0)$ as the injection rate increases, which is more apparent in the plot for fluid index $n = 1.50$. An examination of the numerical values obtained from the calculations indicates the presence of a maximum on each curve. This maximum value of wall shear occurs at a different value of v_{in} for each fluid index value considered. While performing these calculations, it was found that for some combinations of the fluid parameters and v_{in} the numerical scheme was unable

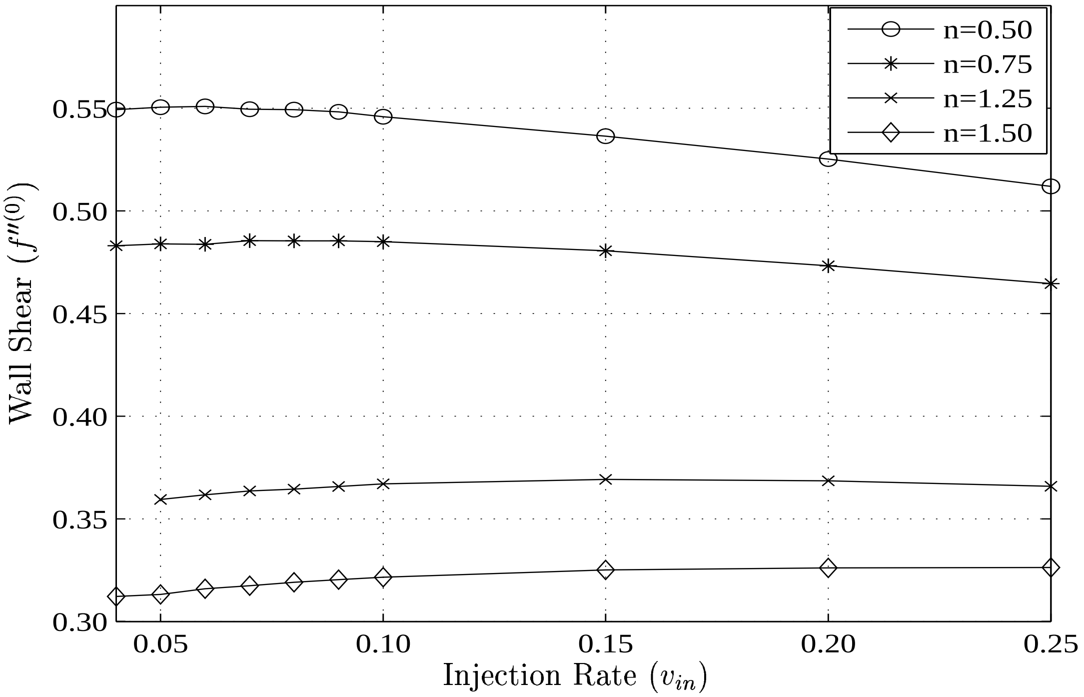

Figure 6.6: Wall shear $f_1''(0)$ for various injection rates and fluid index values $n = 0.50, 0.75, 1.25, 1.50$. Relaxation time parameter set to $\lambda = 10$ and viscosity ratio $C_0 = 1.0$.

to converge to a unique solution. The numerical scheme would either oscillate between two 'fixed-points' or exhibit divergent behaviour. Using a smaller η step-size did in some instances overcome these convergence problems and yield a solution.

A check of the shear at the fluid interface revealed that the values of $f_1''(\eta^*)$ remained in a finite range for the combinations of n and v_{in} considered. This indicates that the upper Newtonian fluid is remaining attached to the lower Carreau fluid, i.e. there is no evidence of boundary-layer-like detachment at the fluid interface.

For this two-fluid system in the presence of an external potential flow that allows the existence of self-similar solutions, these results suggest that the boundary-layer flow will remain attached to the surface over a 'reasonable' range of injection rates and fluid parameter values.

However, the nature of the boundary-layer flow in this two-fluid system when the injection rate is very small is still unclear and we examine this issue in more detail shortly.

6.4 Small Injection Velocity Limit

As has been noted previously, the numerical scheme used to solve equations (6.13) and (6.14) is unable to converge to a unique solution when the fluid injection rate is small ($<\approx 0.05$). We now consider the form of the solution, and hence the velocity profile, in the lower fluid when v_{in} takes small values.

Returning to the non-dimensional equations (6.2) and (6.3), the injection of fluid through the surface is given by

$$v_1(x) = v_{in}(x) \qquad \text{at} \qquad y = 0,$$

where the dependence on the streamwise variable has been made explicit. For convenience we write the injection rate as

$$v_1(x) = \frac{\epsilon}{x^{\frac{1}{3}}} \qquad \text{at} \qquad y = 0, \tag{6.19}$$

where $0 < \epsilon \ll 1$.

Applying the similarity transformation yields the ordinary differential equation (6.13) and the surface normal velocity is given by

$$v_1 = -\frac{2}{3}\frac{1}{\xi^{\frac{1}{3}}}\left[f_1 - \frac{\eta}{2}f_1'\right].$$

Making use of the no-slip condition at the surface, $f_1'(0) = 0$, allows the mass injection velocity through the surface to be written as

$$f_1 = -\frac{3}{2}\epsilon \qquad \text{at} \qquad \eta = 0, \tag{6.20}$$

where f_1 is the dimensionless stream function in the lower fluid.

We proceed by using ϵ to scale the velocity in the lower fluid as follows

$$f(\eta) = \epsilon g(\eta) \qquad \text{so that} \qquad f'(\eta) = \epsilon g'(\eta),$$

where the subscript 1 has been omitted for convenience.

For a small injection velocity, the fluid interface is located at $\eta^* \ll 1$, so that in the lower fluid the similarity variable η is also $\ll 1$. We now define $\eta = \epsilon^s z$ and substitute into $g(\eta)$ to give

$$f(\eta) = \epsilon g(\epsilon^s z).$$

Taking derivatives gives

$$\frac{\mathrm{d}f}{\mathrm{d}\eta} = \epsilon^{1-s}\frac{\mathrm{d}g}{\mathrm{d}z}$$
$$\text{and} \qquad \frac{\mathrm{d}^2 f}{\mathrm{d}\eta^2} = \epsilon^{1-2s}\frac{\mathrm{d}^2 g}{\mathrm{d}z^2}, \qquad \frac{\mathrm{d}^3 f}{\mathrm{d}\eta^3} = \epsilon^{1-3s}\frac{\mathrm{d}^3 g}{\mathrm{d}z^3}.$$

Substituting these expressions into equation (6.13), expanding and after some algebra we obtain

$$(1+C_0)\,\epsilon^{1-3s}\frac{\mathrm{d}^3 g}{\mathrm{d}z^3} + \left[C_0\left(n+\frac{n-3}{2}\right)\left(\lambda\epsilon^{1-2s}\frac{\mathrm{d}^2 g}{\mathrm{d}z^2}\right)^2 + \dots\right]\epsilon^{1-3s}\frac{\mathrm{d}^3 g}{\mathrm{d}z^3}$$
$$+ \frac{2}{3}\epsilon^{2-2s}\frac{\mathrm{d}^2 g}{\mathrm{d}z^2}g + \frac{1}{3}\left[1-\epsilon^{2-2s}\left(\frac{\mathrm{d}g}{\mathrm{d}z}\right)^2\right] = 0.$$

A balance of leading order ($O(1)$) terms is made possible by requiring $1-3s=0$, i.e. $s=\frac{1}{3}$. For this choice of s we get

$$(1+C_0)\,\frac{\mathrm{d}^3 g}{\mathrm{d}z^3} + \frac{1}{3} = 0.$$

This differential equation can be readily integrated to give

$$g(z) = -\frac{z^3}{18(1+C_0)} + \frac{k_1}{2}z^2 + k_2 z + k_3,$$

where k_1, k_2, k_3 are constants to be determined. Making the change of variable $z = \frac{\eta}{\epsilon^{\frac{1}{3}}}$, we have $f(\eta) = \epsilon g(\eta)$ where

$$g(\eta) = -\frac{\eta^3}{18\epsilon(1+C_0)} + \frac{k_1}{2\epsilon^{\frac{2}{3}}}\eta^2 + \frac{k_2}{\epsilon^{\frac{1}{3}}}\eta + k_3.$$

From the initial condition for the injection velocity at $\eta = 0$, i.e. $f(0) = -\frac{3}{2}\epsilon$, and $f(0) = \epsilon g(0)$

n	$0.50^{\dagger}$	0.75	1.25	1.50
Numerical	0.551451	0.481855	0.367334	0.319346
Predicted	0.535285	0.474332	0.376396	0.335543

Table 6.4: Comparison of $f_1''(0)$ values as determined by the numerical scheme with values predicted by equation (6.22) for different values values of n with $\lambda = 10, C_0 = 1.0, v_{in} = 0.04$; $\dagger v_{in} = 0.05$.

we find that $k_3 = -\frac{3}{2}$. The no-slip condition on the surface, $f'(0) = 0$, results in $k_2 = 0$. At the location of the fluid interface η^*, we require $f(\eta^*) = 0$, or equivalently $g(\eta^*) = 0$. Imposing this condition gives

$$\frac{k_1}{2\epsilon^{\frac{2}{3}}} = \frac{(\eta^*)^3 + 27\epsilon(1+C_0)}{18\epsilon(1+C_0)(\eta^*)^2}.$$

Hence we write $g(\eta)$ as

$$g(\eta) = -\frac{\eta^3}{18\epsilon(1+C_0)} + \frac{(\eta^*)^3 + 27\epsilon(1+C_0)}{18\epsilon(1+C_0)(\eta^*)^2}\eta^2 - \frac{3}{2}.$$

Based on the foregoing analysis, the self-similar velocity profile in the thin film composed of a Carreau fluid, in conjunction with a small injection rate, may be approximated by

$$f_1'(\eta) = -\frac{\eta^2}{6(1+C_0)} + \frac{(\eta^*)^3 + 27\epsilon(1+C_0)}{9(1+C_0)(\eta^*)^2}\eta. \tag{6.21}$$

Also, the auxiliary initial condition, $f''(0)$, that was obtained by Newton iteration in the numerical scheme is given directly by

$$f_1''(0) = \frac{(\eta^*)^3 + 27\epsilon(1+C_0)}{9(1+C_0)(\eta^*)^2}. \tag{6.22}$$

We can use equation (6.22) to ‘predict’ $f_1''(0)$ and then compare these values with the initial values found by the numerical scheme. The lowest injection velocity for which numerical solutions were obtained is 0.05 for $n = 0.5$ and 0.04 for the other values of n considered. The numerically calculated and predicted values of $f_1''(0)$ for these fluid index are shown in Table 6.4.

The results in Table 6.4 show quite good agreement between the predicted and numerically

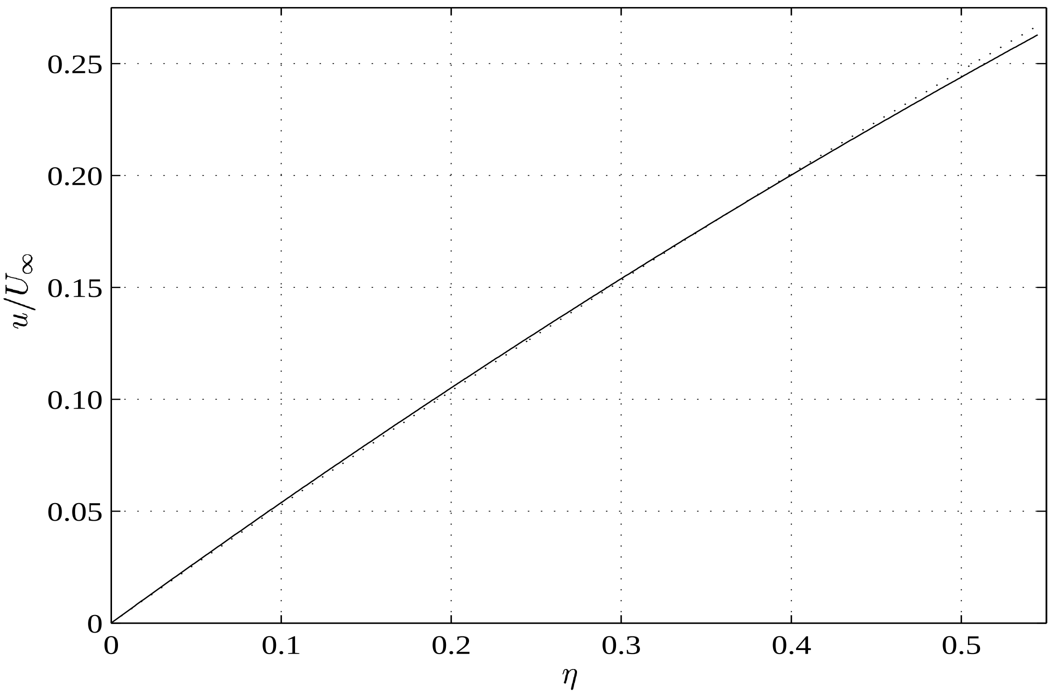

Figure 6.7: Numerically calculated (solid) and predicted (dashed) velocity profiles in lower Carreau fluid for $n = 0.50, \eta^* = 0.545, v_{in} = \epsilon = 0.05$.

calculated values of $f_1''(0)$. This indicates that equation (6.22) gives a good first approximation for $f_1''(0)$ to be used in a numerical scheme. We also note that the predicted values for shear-thinning fluids are greater than the actual values, with an opposite behaviour for shear-thickening fluids. It is possible that the inclusion of an additional correction term in the rescaling of $f_1(\eta)$ by ϵ may either correct or diminish this behaviour.

The velocity profile provided by equation (6.21) was compared with the velocity profile in the Carreau fluid that was obtained by the numerical scheme. For the comparison we selected $v_{in} = \epsilon = 0.05$ and $\eta^* = 0.545$, which corresponds to fluid index $n = 0.50$. The two velocity profiles are shown in Figure 6.7. From the results plotted in Figure 6.7 it can be seen that there is very good agreement between the two velocity profiles. Thus the velocity profile calculated by equation (6.21) will serve as a good approximation for the actual velocity profile in a thin film of Carreau fluid in the presence of a very small fluid injection rate.

6.5 Chapter Summary

In this chapter we have considered the boundary-layer flow of a Newtonian fluid over a thin film of a Carreau fluid. The set of coupled partial differential equations describing the flow has been derived. The boundary conditions along with appropriate conditions at the material interface between the two fluids have also been specified. This set of equations is quite formidable and would require the development of sophisticated numerical methods to obtain a solution. A self-similar solution exists for a particular instance of the potential flow in the free-stream. The coupled ordinary differential equations from which a self-similar solution is obtained have been given along with suitable boundary and material interface conditions. A numerical scheme for solving the pair of coupled ordinary differential equations has been described. This numerical method has been used to examine the effect of the Carreau fluid parameters and the fluid injection rate on the location of material interface between the two fluids.

The numerical solutions obtained indicate that the position of the fluid interface increases in a non-linear manner with increasing fluid index n. The fluid parameter λ was shown to have a minor effect on the location of the fluid interface; an increase in λ resulted in the fluid interface moving closer toward the flat plate for shear-thinning fluids and moving away from the flat plate for shear-thickening fluids. Increasing the viscosity ratio C_0 was found to result in the fluid interface being located further away from the flat plate. Decreasing C_0 had the opposite effect. Lastly, it was found that increasing (decreasing) the fluid injection rate through the flat plate resulted in the fluid interface moving away from (toward) the flat plate. Both the wall and interfacial shear were recorded during this investigation. It was found that the wall and interfacial shear values did not show any tendency toward zero, suggesting that separation of the boundary-layer from the flat plate was unlikely for the potential flow considered.

The numerical scheme was unable to converge to a unique numerical solution for small rates of fluid injection. A small injection velocity analysis yielded an approximate solution for the velocity profile in the thin film lower fluid along with the wall shear. Both the approximate velocity profile and the wall shear were found to be in good agreement with an available numerical solution for a 'small' injection velocity.

Chapter 7

Future Directions

The preceding chapters provide a description of some investigations into the nature of the boundary-layer flow of non-Newtonian fluids. The class of fluids considered are referred to as generalised Newtonian fluids, characterised by having a non-constant viscosity. The two non-Newtonian fluids examined are known as the power-law and Carreau fluids. Such an investigation cannot look at every conceivable aspect that may be of interest. However, during the course of carrying out this study and during deliberations about the various outcomes, a number of issues that may be of sufficient interest so as to warrant further investigation came to mind. In this chapter we summarise some of the areas where continued effort may be applied to further enhance our knowledge of the boundary-layer flow of non-Newtonian fluids.

In Chapter 3 the boundary-layer flow of a power-law fluid along with fluid injection through the surface was examined. The system of partial differential equations governing the flow is non-linear and a finite-difference scheme was developed to obtain a numerical solution. However, it was found that this numerical scheme did not converge to a solution for shear-thickening fluids. Certain limitations of the power-law constitutive relation were offered as explanations for this situation. A number of other re-arrangements of the terms in the governing partial differential equations were looked at and were found to lead to convergence-related problems in subsequent numerical schemes. The matter of whether a different re-arrangement of the terms, or an appropriate linearisation of the viscosity term, would yield a form of the governing partial differential equations for a shear-thickening fluid that would be amenable to numerical solution could be clarified, or even resolved, through some further effort. Also the structure of the boundary layer in the very near vicinity of the separation point could be investigated. Such an investigation could be approached in a manner similar to that used by Catherall et al. (1965) in their study of the boundary-layer flow of a Newtonian fluid along a flat plate in the presence of fluid injection.

The nature of the numerical results served to prompt an in-depth examination of the self-similar solutions that exist for the boundary-layer flow of a power-law fluid. The outcomes of this examination are presented in Chapter 4. For shear-thinning power-law fluids it was found that the self-similar velocity profile obtained using a numerical scheme based on simple shooting was quite acceptable. However, using the same numerical scheme for a shear-thickening power-law fluid results in a self-similar velocity profile that corresponds to a finite-width boundary-layer. While it is not uncommon for such a velocity profile to be ‘padded’ out to the far-field using free-stream velocity values, it has been shown that an intermediate layer exists that permits the velocity profile in the viscous sub-layer to match smoothly onto the free-stream velocity. Hence, there may be some merit in implementing this numerical method in a format that may be readily used to calculate the ‘correct’ self-similar velocity profile for a power-law fluid.

The study of the boundary-layer flow of a power-law fluid, specifically of the shear-thinning variety, produced some encouraging results as well as highlighting some deficiencies of the underlying model for the viscosity. The boundary-layer flow of fluids that are described by the Carreau viscosity model was selected for ongoing examination, as the Carreau viscosity model may be regarded as being a worthwhile improvement on the power-law viscosity model. The system of partial differential equations governing the boundary-layer flow of a Carreau fluid were derived and a numerical scheme to solve them was developed. It was also found that a self-similar solution was available for a single Falkner-Skan-type potential flow. The numerical scheme was used to examine how the boundary-layer flow developed with distance along the flat plate with zero fluid injection. It was found that the velocity profile of both shear-thinning and shear-thickening Carreau fluids tended to an asymptotic form far from the leading edge of the plate. A natural extension of the work that has been performed would be to consider the effect that fluid injection through the flat plate would have on the boundary-layer flow. Such an activity should be relatively easy to undertake using the existing numerical scheme with only a change to an appropriate boundary condition being needed.

The boundary-layer flow of a Newtonian fluid along a thin film of non-Newtonian fluid on a flat plate was also examined. The thin film was subject to fluid injection through the surface. The system of coupled partial differential equations was derived and self-similar velocity profiles within each fluid were found. This work could be continued by seeking solutions to the governing system of equations over a wider class of free-stream flow regimes. The numerical scheme would need to be generalised as these other flow regimes would yield non-self-similar velocity profiles. The small injection velocity analysis provided some useful insights into the form of the velocity profile within the thin film. However, *a priori* knowledge of the location of the fluid interface was required. Hence, a useful extension to this component of the investigations performed would be to remove the explicit need for the location of the fluid interface from the calculation of the velocity profile in the thin film. Scope also exists for investigating the stability of the flow in the boundary layer of such a two-fluid system.

Appendix A

Numerical method for power-law fluids - Jacobian matrix

The system of non-linear algebraic equations that needs to be solved to obtain the velocity profile in the boundary-layer flow of a shear-thinning power-law fluid along a flat plate with fluid injection is given by equation (3.12). This system of non-linear algebraic equations is solved with a Newton iteration method that requires the corresponding Jacobian matrix. For an arbitrary potential flow in the free-stream, the elements of the j^{th} row of the Jacobian matrix are given by

$$
\begin{aligned}
\frac{\partial f_j}{\partial \widehat{q}_s^{(k)}} &= \frac{h^3\left((2n-1)\beta_2 + n\theta + 1\right)}{n+1}\left(\frac{\widehat{q}_{j+1}^{(k)} - \widehat{q}_{j-1}^{(k)}}{2h}\right)^{2-n} \qquad s = 1, \ldots, j-2, \\
\frac{\partial f_j}{\partial \widehat{q}_{j-1}^{(k)}} &= 1 \\
&- \frac{2-n}{2h}\left\{h^3\left[\left(\frac{(2n-1)(\beta_1-\beta_2) - 2n\theta}{2(n+1)}\right)\left(q_{1,1} + \ldots + q_{1,j-1} + \frac{1}{2}q_{1,j}\right) + \right.\right. \\
&\left.\left.\left(\frac{(2n-1)\beta_2 + n\theta + 1}{n+1}\right)\left(\widehat{q}_1^{(k)} + \ldots + \widehat{q}_{j-1}^{(k)} + \frac{1}{2}\widehat{q}_j^{(k)}\right)\right] - K_{in}^*\right\}\left(\frac{\widehat{q}_{j+1}^{(k)} - \widehat{q}_{j-1}^{(k)}}{2h}\right)^{1-n} \\
&+ \frac{h^3\left((2n-1)\beta_2 + n\theta + 1\right)}{n+1}\left(\frac{\widehat{q}_{j+1}^{(k)} - \widehat{q}_{j-1}^{(k)}}{2h}\right)^{2-n}, \\
\frac{\partial f_j}{\partial \widehat{q}_j^{(k)}} &= -2 + \frac{1}{2}\frac{h^3\left((2n-1)\beta_2 + n\theta + 1\right)}{n+1}\left(\frac{\widehat{q}_{j+1}^{(k)} - \widehat{q}_{j-1}^{(k)}}{2h}\right)^{2-n}
\end{aligned}
$$

$$- h^2 \left\{ \left(2\beta_2 + \frac{n\theta}{n+1} \right) (2\widehat{q}^{(k)} - q_1)_j \right\} \left(\frac{\widehat{q}^{(k-1)}_{j+1} - \widehat{q}^{(k-1)}_{j-1}}{2h} \right)^{1-n},$$

$$\frac{\partial f_j}{\partial \widehat{q}^{(k)}_{j+1}} = 1$$

$$+ \frac{2-n}{2h} \left\{ h^3 \left[\left(\frac{(2n-1)(\beta_1 - \beta_2) - 2n\theta}{2(n+1)} \right) \left(q_{1,1} + \ldots + q_{1,j-1} + \frac{1}{2} q_{1,j} \right) + \right.\right.$$

$$\left.\left. \left(\frac{(2n-1)\beta_2 + n\theta + 1}{n+1} \right) \left(\widehat{q}^{(k)}_1 + \ldots + \widehat{q}^{(k)}_{j-1} + \frac{1}{2} \widehat{q}^{(k)}_j \right) \right] - K^*_{in} \right\} \left(\frac{\widehat{q}^{(k)}_{j+1} - \widehat{q}^{(k)}_{j-1}}{2h} \right)^{1-n}.$$

When the potential flow in the free-stream is from the Falkner-Skan family of flows, then the boundary-layer flow of a shear-thinning power-law fluid along a flat plate with fluid injection is given by equation (3.13). The elements of the j^{th} row of the corresponding Jacobian matrix take the following slightly simplified form

$$\frac{\partial f_j}{\partial \widehat{q}^{(k)}_s} = \frac{h^3\left((2n-1)\beta + n\theta + 1\right)}{n+1} \left(\frac{\widehat{q}^{(k)}_{j+1} - \widehat{q}^{(k)}_{j-1}}{2h} \right)^{2-n} \qquad s = 1, \ldots, j-2,$$

$$\frac{\partial f_j}{\partial \widehat{q}^{(k)}_{j-1}} = 1$$

$$- \frac{2-n}{2h} \left\{ h^3 \left[\left(\frac{(2n-1)\beta + n\theta + 1}{n+1} \right) \left(\widehat{q}^{(k)}_1 + \ldots + \widehat{q}^{(k)}_{j-1} + \frac{1}{2} \widehat{q}^{(k)}_j \right) - \right.\right.$$

$$\left.\left. \frac{n\theta}{n+1} \left(q_{1,1} + \ldots + q_{1,j-1} + \frac{1}{2} q_{1,j} \right) \right] - K^*_{in} \right\} \left(\frac{\widehat{q}^{(k)}_{j+1} - \widehat{q}^{(k)}_{j-1}}{2h} \right)^{1-n}$$

$$+ h^3 \left(\frac{(2n-1)\beta + n\theta + 1}{n+1} \right) \left(\frac{\widehat{q}^{(k)}_{j+1} - \widehat{q}^{(k)}_{j-1}}{2h} \right)^{2-n},$$

$$\frac{\partial f_j}{\partial \widehat{q}^{(k)}_j} = -2 + \frac{1}{2} \frac{h^3((2n-1)\beta + n\theta + 1)}{n+1} \left(\frac{\widehat{q}^{(k)}_{j+1} - \widehat{q}^{(k)}_{j-1}}{2h} \right)^{2-n}$$

$$- h^2 \left\{ \left(2\beta + \frac{n\theta}{n+1} \right) (2\widehat{q}^{(k)} - q_1)_j \right\} \left(\frac{\widehat{q}^{(k-1)}_{j+1} - \widehat{q}^{(k-1)}_{j-1}}{2h} \right)^{1-n},$$

$$\frac{\partial f_j}{\partial \widehat{q}^{(k)}_{j+1}} = 1$$

$$+ \frac{2-n}{2h} \left\{ h^3 \left[\left(\frac{(2n-1)\beta + n\theta + 1}{n+1} \right) \left(\widehat{q}^{(k)}_1 + \ldots + \widehat{q}^{(k)}_{j-1} + \frac{1}{2} \widehat{q}^{(k)}_j \right) - \right.\right.$$

$$\left.\left. \frac{n\theta}{n+1} \left(q_{1,1} + \ldots + q_{1,j-1} + \frac{1}{2} q_{1,j} \right) \right] - K^*_{in} \right\} \left(\frac{\widehat{q}^{(k)}_{j+1} - \widehat{q}^{(k)}_{j-1}}{2h} \right)^{1-n}.$$

The boundary-layer flow of a shear-thickening power-law fluid along a flat plate with fluid injection in the presence of a Falkner-Skan external flow is given by equation (3.16). The elements of the j^{th} row of the corresponding Jacobian matrix take the following form

$$\begin{aligned}
\frac{\partial f_j}{\partial \widehat{q}_s^{(k)}} &= \frac{h^3\left((2n-1)\beta+n\theta+1\right)}{n+1}\left(\frac{\widehat{q}_{j+1}^{(k)}-\widehat{q}_{j-1}^{(k)}}{2h}\right) \qquad s=1,\ldots,j-2,\\
\frac{\partial f_j}{\partial \widehat{q}_{j-1}^{(k)}} &= \left(\frac{\widehat{q}_{j+1}^{(k-1)}-\widehat{q}_{j-1}^{(k-1)}}{2h}\right)+h^3\left(\frac{(2n-1)\beta+n\theta+1}{n+1}\right)\left(\frac{\widehat{q}_{j+1}^{(k)}-\widehat{q}_{j-1}^{(k)}}{2h}\right)\\
&\quad -\frac{1}{2h}\left\{h^3\left[\left(\frac{(2n-1)\beta+n\theta+1}{n+1}\right)\left(\widehat{q}_1^{(k)}+\ldots+\widehat{q}_{j-1}^{(k)}+\frac{1}{2}\widehat{q}_j^{(k)}\right)-\right.\right.\\
&\qquad\qquad \left.\left.\frac{n\theta}{n+1}\left(q_{1,1}+\ldots+q_{1,j-1}+\frac{1}{2}q_{1,j}\right)\right]-K_{in}^*\right\},\\
\frac{\partial f_j}{\partial \widehat{q}_j^{(k)}} &= -2\left(\frac{\widehat{q}_{j+1}^{(k-1)}-\widehat{q}_{j-1}^{(k-1)}}{2h}\right)+\frac{1}{2}\frac{h^3((2n-1)\beta+n\theta+1)}{n+1}\left(\frac{\widehat{q}_{j+1}^{(k)}-\widehat{q}_{j-1}^{(k)}}{2h}\right)\\
&\quad -h^2\left(2\beta+\frac{n\theta}{n+1}\right)\left(2\widehat{q}^{(k)}-q_1\right)_j,\\
\frac{\partial f_j}{\partial \widehat{q}_{j+1}^{(k)}} &= \left(\frac{\widehat{q}_{j+1}^{(k-1)}-\widehat{q}_{j-1}^{(k-1)}}{2h}\right)\\
&\quad +\frac{1}{2h}\left\{h^3\left[\left(\frac{(2n-1)\beta+n\theta+1}{n+1}\right)\left(\widehat{q}_1^{(k)}+\ldots+\widehat{q}_{j-1}^{(k)}+\frac{1}{2}\widehat{q}_j^{(k)}\right)-\right.\right.\\
&\qquad\qquad \left.\left.\frac{n\theta}{n+1}\left(q_{1,1}+\ldots+q_{1,j-1}+\frac{1}{2}q_{1,j}\right)\right]-K_{in}^*\right\}.
\end{aligned}$$

Appendix B

Derivation of Similarity Transformation

We wish to find a similarity-type solution to equations (4.1a) and (4.1b). We use an approach along the lines described in Schlichting (1979).

First we introduce a stream function $\psi(x, y)$, where $u = \frac{\partial \psi}{\partial y}$ and $v = -\frac{\partial \psi}{\partial x}$, so as to satisfy continuity identically. Next we introduce new independent co-ordinates

$$\xi = x, \quad \text{and} \quad s = \frac{y}{g(x)},$$

where $g(x)$ is a scale factor. A normalised stream function is defined by

$$f(\xi, s) = \frac{\psi(x, y)}{U_e(x) g(x)},$$

or equivalently

$$\psi(x, y) = U_e(x) g(x) f(\xi, s).$$

The partial derivatives with respect to the original co-ordinates are now replaced by derivatives with respect to the new co-ordinates as follows

$$\begin{aligned}\frac{\partial}{\partial x} &= \frac{\partial}{\partial \xi} - y\frac{g_\xi}{g^2}\frac{\partial}{\partial s},\\ \frac{\partial}{\partial y} &= \frac{1}{g}\frac{\partial}{\partial s}.\end{aligned}$$

Utilising the new co-ordinates and the normalised stream function, existing variables can be replaced by the following

$$\begin{aligned}u &= U_e f',\\ \frac{\partial u}{\partial y} &= \frac{U_e}{g}f'',\\ \frac{\partial^2 u}{\partial y^2} &= \frac{U_e}{g^2}f''',\\ \frac{\partial u}{\partial x} &= U_{e\xi}f' + U_e\left(f'_\xi - y\frac{g_\xi}{g^2}f''\right),\\ -v &= U_{e\xi}gf + U_e g_\xi f + U_e g\left(f_\xi - y\frac{g_\xi}{g^2}f'\right),\end{aligned}$$

where

$$f' = \frac{\partial f(\xi, s)}{\partial s}.$$

By considering the behaviour of the momentum equation far from the boundary layer in the freestream, or more directly by using Bernoulli's equation, the pressure gradient can be expressed as

$$-\frac{\mathrm{d}p}{\mathrm{d}x} = U_e(x)\frac{\mathrm{d}U_e}{\mathrm{d}x},$$

or, in the new co-ordinates the pressure gradient becomes

$$-\frac{\mathrm{d}p}{\mathrm{d}\xi} = U_e(\xi)\frac{\mathrm{d}U_e}{\mathrm{d}\xi}.$$

The expressions obtained above can now be substituted into the momentum equation, which, after some simplification, becomes

$$\begin{aligned}((f'')^n)' &+ g^n {U_e}^{1-n}(g_\xi U_e + g U_{e\xi}) f'' f \\ &+ g^{n+1} {U_e}^{1-n} U_{e\xi}(1-(f')^2) = g^{n+1} {U_e}^{2-n}(f' f'_\xi - f'' f_\xi). \qquad \text{(B.1)}\end{aligned}$$

Similarity-type solutions exist when both f and f' along with the 'coefficient' terms on the LHS are independent of ξ. Hence, the above equation needs to take the following form for similarity solutions to be found

$$n f'''(f'')^{n-1} + \alpha f'' f + \beta(1-(f')^2) = 0, \qquad \text{(B.2)}$$

where

$$\begin{aligned}\alpha &= g^n g_\xi {U_e}^{2-n} + g^{n+1} {U_e}^{1-n} U_{e\xi}, \\ \beta &= g^{n+1} {U_e}^{1-n} U_{e\xi},\end{aligned}$$

with α, β constant.

We need to determine the form of the scale factor, $g(\xi)$, and the velocity distribution of the potential flow, $U_e(\xi)$, that will result in similarity-type solutions. Subtracting β from α gives

$$\begin{aligned}\alpha - \beta &= g^n g_\xi {U_e}^{2-n}, \\ (\alpha-\beta)\frac{U_{e\xi}}{U_e} &= g^{n+1} {U_e}^{1-n} U_{e\xi} \frac{g_\xi}{g}, \\ (\alpha-\beta)\frac{U_{e\xi}}{U_e} &= \beta \frac{g_\xi}{g}.\end{aligned}$$

Integrating the above expression yields

$${U_e}^{\alpha-\beta} = K_1 g^\beta \qquad \text{(B.3)}$$

where K_1 is a constant.

The constant α, as defined above, can be expressed as

$$\begin{aligned}\alpha &= (n+1)g^n g_\xi {U_e}^{2-n} + (2-n)g^{n+1}{U_e}^{1-n}U_{e\xi} - ng^n g_\xi {U_e}^{2-n} \\ &\quad + (n-1)g^{n+1}{U_e}^{1-n}U_{e\xi} \\ &= \frac{\mathrm{d}}{\mathrm{d}\xi}(g^{n+1}{U_e}^{2-n}) - n(\alpha-\beta) + (n-1)\beta.\end{aligned}$$

This expression simplifies to give

$$(n+1)\alpha - (2n-1)\beta = \frac{\mathrm{d}}{\mathrm{d}\xi}(g^{n+1}{U_e}^{2-n}).$$

Assuming that $(n+1)\alpha - (2n-1)\beta \neq 0$ and integrating once we get

$$g^{n+1}{U_e}^{2-n} = [(n+1)\alpha - (2n-1)\beta]\xi. \tag{B.4}$$

By eliminating g from A and B we get an expression for the velocity distribution of the potential flow

$$U_e(\xi) = K_2\left([(n+1)\alpha - (2n-1)\beta]\xi\right)^{\frac{\beta}{(n+1)\alpha-(2n-1)\beta}}$$

where $K_2 = K_1^{\frac{n+1}{(n+1)\alpha-(2n-1)\beta}}$. The scale factor is given by

$$g(\xi) = \left([(n+1)\alpha - (2n-1)\beta]\frac{\xi}{{U_e}^{2-n}}\right)^{\frac{1}{n+1}}.$$

As long as $\alpha \neq 0$, then, without loss of generality, it is permissible to put $\alpha = 1$. We also introduce a new constant m to replace β by putting

$$\begin{aligned} m &= \frac{\beta}{(n+1)-(2n-1)\beta}, \\ \text{or}\quad \beta &= \frac{(n+1)m}{(2n-1)m+1}.\end{aligned}$$

So with $\alpha = 1$, the velocity distribution of the potential flow and the scale factor, $g(x)$, for the ordinate become

$$U_e(x) = K_2\left[\frac{(n+1)x}{(2n-1)m+1}\right]^m,$$

$$g(x) = \left[\frac{(n+1)}{(2n-1)m+1}\frac{x}{{U_e}^{2-n}}\right]^{\frac{1}{n+1}}$$

Appendix C

Numerical method for Carreau fluids - Jacobian matrix

The system of non-linear algebraic equations that needs to be solved to obtain the velocity profile in the boundary-layer flow of a Carreau fluid along a flat plate is given by Equation (5.21). This system of non-linear algebraic equations is solved with a Newton iteration method that requires the corresponding Jacobian matrix. For an arbitrary potential flow in the free-stream, the elements of the j^{th} row of the Jacobian matrix are given by

$$
\begin{aligned}
\frac{\partial f_j}{\partial \widehat{q}_s^{(k)}} &= \frac{h^3}{2}\left(\beta_2+2\theta+1\right)\left(\frac{\widehat{q}_{j+1}^{(k)}-\widehat{q}_{j-1}^{(k)}}{2h}\right) \qquad\qquad s=1,\ldots,j-2,\\
\frac{\partial f_j}{\partial \widehat{q}_{j-1}^{(k)}} &= \left[1+C_0\widehat{\xi}^{\frac{1-n}{2}}\left\{\widehat{\xi}+n\widehat{U}_e^3\left(\lambda\frac{\widehat{q}_{j+1}^{(k)}-\widehat{q}_{j-1}^{(k)}}{2h}\right)^2\right\}\left\{\widehat{\xi}+\widehat{U}_e^3\left(\lambda\frac{\widehat{q}_{j+1}^{(k)}-\widehat{q}_{j-1}^{(k)}}{2h}\right)^2\right\}^{\frac{n-3}{2}}\right]\\
&\quad -\frac{C_0\lambda^2\widehat{U}_e^3\widehat{\xi}^{\frac{1-n}{2}}}{h}\left(\widehat{q}_{j+1}^{(k)}-2\widehat{q}_j^{(k)}+\widehat{q}_{j-1}^{(k)}\right)\left(\frac{\widehat{q}_{j+1}^{(k)}-\widehat{q}_{j-1}^{(k)}}{2h}\right)\times\\
&\quad \left\{\widehat{\xi}+\widehat{U}_e^3\left(\lambda\frac{\widehat{q}_{j+1}^{(k)}-\widehat{q}_{j-1}^{(k)}}{2h}\right)^2\right\}^{\frac{n-5}{2}}\left[n\left\{\widehat{\xi}+\widehat{U}_e^3\left(\lambda\frac{\widehat{q}_{j+1}^{(k)}-\widehat{q}_{j-1}^{(k)}}{2h}\right)^2\right\}+\right.\\
&\quad \left.\frac{n-3}{2}\left\{\widehat{\xi}+n\widehat{U}_e^3\left(\lambda\frac{\widehat{q}_{j+1}^{(k)}-\widehat{q}_{j-1}^{(k)}}{2h}\right)^2\right\}\right]\\
&\quad -\left[\frac{h^2}{2}\left\{\left(\beta_2+2\theta+1\right)\sum_{r=0}^{j}{}''\widehat{q}_r^{(k)}+\frac{1}{2}\left(\beta_1-\beta_2-4\theta\right)\sum_{r=0}^{j}{}''q_{1,r}\right\}-\frac{h}{2}K_{in}\right]
\end{aligned}
$$

$$+\frac{h^3}{2}\left(\beta_2+2\theta+1\right)\left(\frac{\widehat{q}^{(k)}_{j+1}-\widehat{q}^{(k)}_{j-1}}{2h}\right),$$

$$\frac{\partial f_j}{\partial \widehat{q}^{(k)}_j}=-2\left[1+C_0\widehat{\xi}^{\frac{1-n}{2}}\left\{\widehat{\xi}+n\widehat{U}_e^3\left(\lambda\frac{\widehat{q}^{(k)}_{j+1}-\widehat{q}^{(k)}_{j-1}}{2h}\right)^2\right\}\left\{\widehat{\xi}+\widehat{U}_e^3\left(\lambda\frac{\widehat{q}^{(k)}_{j+1}-\widehat{q}^{(k)}_{j-1}}{2h}\right)^2\right\}^{\frac{n-3}{2}}\right]$$

$$+\frac{1}{2}\frac{h^3}{2}\left(\beta_2+2\theta+1\right)\left(\frac{\widehat{q}^{(k)}_{j+1}-\widehat{q}^{(k)}_{j-1}}{2h}\right)-h^2(2\beta_2+\theta)\left[2\widehat{q}^{(k)}-q_1\right]_j,$$

$$\frac{\partial f_j}{\partial \widehat{q}^{(k)}_{j+1}}=\left[1+C_0\widehat{\xi}^{\frac{1-n}{2}}\left\{\widehat{\xi}+n\widehat{U}_e^3\left(\lambda\frac{\widehat{q}^{(k)}_{j+1}-\widehat{q}^{(k)}_{j-1}}{2h}\right)^2\right\}\left\{\widehat{\xi}+\widehat{U}_e^3\left(\lambda\frac{\widehat{q}^{(k)}_{j+1}-\widehat{q}^{(k)}_{j-1}}{2h}\right)^2\right\}^{\frac{n-3}{2}}\right]$$

$$+\frac{C_0\lambda^2\widehat{U}_e^3\widehat{\xi}^{\frac{1-n}{2}}}{h}\left(\widehat{q}^{(k)}_{j+1}-2\widehat{q}^{(k)}_j+\widehat{q}^{(k)}_{j-1}\right)\left(\frac{\widehat{q}^{(k)}_{j+1}-\widehat{q}^{(k)}_{j-1}}{2h}\right)\times$$

$$\left\{\widehat{\xi}+\widehat{U}_e^3\left(\lambda\frac{\widehat{q}^{(k)}_{j+1}-\widehat{q}^{(k)}_{j-1}}{2h}\right)^2\right\}^{\frac{n-5}{2}}\left[n\left\{\widehat{\xi}+\widehat{U}_e^3\left(\lambda\frac{\widehat{q}^{(k)}_{j+1}-\widehat{q}^{(k)}_{j-1}}{2h}\right)^2\right\}+\right.$$

$$\left.\frac{n-3}{2}\left\{\widehat{\xi}+n\widehat{U}_e^3\left(\lambda\frac{\widehat{q}^{(k)}_{j+1}-\widehat{q}^{(k)}_{j-1}}{2h}\right)^2\right\}\right]$$

$$+\left[\frac{h^2}{2}\left\{(\beta_2+2\theta+1)\sum_{r=0}^{j}{}''\widehat{q}^{(k)}_r+\frac{1}{2}(\beta_1-\beta_2-4\theta)\sum_{r=0}^{j}{}''q_{1,r}\right\}-\frac{h}{2}K_{in}\right].$$

The boundary-layer flow of a Carreau fluid along a flat plate in the presence of a Falkner-Skan external flow is given by Equation (5.22). The elements of the j^{th} row of the corresponding Jacobian matrix take the following form

$$\frac{\partial f_j}{\partial \widehat{q}^{(k)}_s}=\frac{h^3}{2}\left(\beta+2\theta+1\right)\left(\frac{\widehat{q}^{(k)}_{j+1}-\widehat{q}^{(k)}_{j-1}}{2h}\right)\qquad s=1,\ldots,j-2,$$

$$\frac{\partial f_j}{\partial \widehat{q}^{(k)}_{j-1}}=\left[1+C_0\widehat{\xi}^{\frac{1-n}{2}}\left\{\widehat{\xi}+n\widehat{U}_e^3\left(\lambda\frac{\widehat{q}^{(k)}_{j+1}-\widehat{q}^{(k)}_{j-1}}{2h}\right)^2\right\}\left\{\widehat{\xi}+\widehat{U}_e^3\left(\lambda\frac{\widehat{q}^{(k)}_{j+1}-\widehat{q}^{(k)}_{j-1}}{2h}\right)^2\right\}^{\frac{n-3}{2}}\right]$$

$$-\frac{C_0\lambda^2\widehat{U}_e^3\widehat{\xi}^{\frac{1-n}{2}}}{h}\left(\widehat{q}^{(k)}_{j+1}-2\widehat{q}^{(k)}_j+\widehat{q}^{(k)}_{j-1}\right)\left(\frac{\widehat{q}^{(k)}_{j+1}-\widehat{q}^{(k)}_{j-1}}{2h}\right)\times$$

$$\left\{\widehat{\xi}+\widehat{U}_e^3\left(\lambda\frac{\widehat{q}^{(k)}_{j+1}-\widehat{q}^{(k)}_{j-1}}{2h}\right)^2\right\}^{\frac{n-5}{2}}\left[n\left\{\widehat{\xi}+\widehat{U}_e^3\left(\lambda\frac{\widehat{q}^{(k)}_{j+1}-\widehat{q}^{(k)}_{j-1}}{2h}\right)^2\right\}+\right.$$

$$
\begin{aligned}
&\frac{n-3}{2}\left\{\widehat{\xi}+n\widehat{U}_e^3\left(\lambda\frac{\widehat{q}_{j+1}^{(k)}-\widehat{q}_{j-1}^{(k)}}{2h}\right)^2\right\}\Bigg]\Bigg]\\
&-\left[\frac{h^2}{2}\left\{(\beta+2\theta+1){\sum_{r=0}^{j}}''\widehat{q}_r^{(k)}-2\theta{\sum_{r=0}^{j}}''q_{1,r}\right\}-\frac{h}{2}K_{in}\right]\\
&+\frac{h^3}{2}(\beta+2\theta+1)\left(\frac{\widehat{q}_{j+1}^{(k)}-\widehat{q}_{j-1}^{(k)}}{2h}\right),
\end{aligned}
$$

$$
\begin{aligned}
\frac{\partial f_j}{\partial\widehat{q}_j^{(k)}}=&-2\left[1+C_0\widehat{\xi}^{\frac{1-n}{2}}\left\{\widehat{\xi}+n\widehat{U}_e^3\left(\lambda\frac{\widehat{q}_{j+1}^{(k)}-\widehat{q}_{j-1}^{(k)}}{2h}\right)^2\right\}\left\{\widehat{\xi}+\widehat{U}_e^3\left(\lambda\frac{\widehat{q}_{j+1}^{(k)}-\widehat{q}_{j-1}^{(k)}}{2h}\right)^2\right\}^{\frac{n-3}{2}}\right]\\
&+\frac{1}{2}\frac{h^3}{2}(\beta+2\theta+1)\left(\frac{\widehat{q}_{j+1}^{(k)}-\widehat{q}_{j-1}^{(k)}}{2h}\right)-h^2(2\beta+\theta)\left[2\widehat{q}^{(k)}-q_1\right]_j,
\end{aligned}
$$

$$
\begin{aligned}
\frac{\partial f_j}{\partial\widehat{q}_{j+1}^{(k)}}=&\left[1+C_0\widehat{\xi}^{\frac{1-n}{2}}\left\{\widehat{\xi}+n\widehat{U}_e^3\left(\lambda\frac{\widehat{q}_{j+1}^{(k)}-\widehat{q}_{j-1}^{(k)}}{2h}\right)^2\right\}\left\{\widehat{\xi}+\widehat{U}_e^3\left(\lambda\frac{\widehat{q}_{j+1}^{(k)}-\widehat{q}_{j-1}^{(k)}}{2h}\right)^2\right\}^{\frac{n-3}{2}}\right]\\
&+\frac{C_0\lambda^2\widehat{U}_e^3\widehat{\xi}^{\frac{1-n}{2}}}{h}\left(\widehat{q}_{j+1}^{(k)}-2\widehat{q}_j^{(k)}+\widehat{q}_{j-1}^{(k)}\right)\left(\frac{\widehat{q}_{j+1}^{(k)}-\widehat{q}_{j-1}^{(k)}}{2h}\right)\times\\
&\left\{\widehat{\xi}+\widehat{U}_e^3\left(\lambda\frac{\widehat{q}_{j+1}^{(k)}-\widehat{q}_{j-1}^{(k)}}{2h}\right)^2\right\}^{\frac{n-5}{2}}\Bigg[n\left\{\widehat{\xi}+\widehat{U}_e^3\left(\lambda\frac{\widehat{q}_{j+1}^{(k)}-\widehat{q}_{j-1}^{(k)}}{2h}\right)^2\right\}+\\
&\frac{n-3}{2}\left\{\widehat{\xi}+n\widehat{U}_e^3\left(\lambda\frac{\widehat{q}_{j+1}^{(k)}-\widehat{q}_{j-1}^{(k)}}{2h}\right)^2\right\}\Bigg]\Bigg]\\
&+\left[\frac{h^2}{2}\left\{(\beta+2\theta+1){\sum_{r=0}^{j}}''\widehat{q}_r^{(k)}-2\theta{\sum_{r=0}^{j}}''q_{1,r}\right\}-\frac{h}{2}K_{in}\right].
\end{aligned}
$$

Bibliography

A. Acrivos, M.J. Shah, and E.E. Peterson. Momentum and heat transfer in laminar boundary-layer flows of non-newtonian fluids past external surfaces. *AIChE Jl.*, 6:312–317, 1960.

H.I. Andersson. Comments on bvps in non-newtonian boundary-layer flow. *Appl. Math. Comput.*, 182:1714–1716, 2006.

H.I. Andersson and T.H. Toften. Numerical solution of the laminar boundary layer equations for power-law fluids. *J. Non-Newtonian Fluid Mech.*, 32:175–195, 1989.

H.A. Barnes, J.F. Hutton, and K. Walters. *An Introduction to Rheology.* Elsevier, 1989.

G. Bayada, L. Chupin, and S. Martin. Viscoelastic fluids in a thin domain. *Quarterly of Applied Mathematics*, 65:625–651, 2007.

R. Bellman. *Stability Theory of Differential Equations.* McGraw Hill, New York, 1953.

M. Benlahsen, M. Guedda, and R. Kersner. The generalized blasius equation revisited. *Mathematical and Computer Modelling*, 47:1063–1076, 2008.

R.B. Bird, O. Hassager, R.C. Armstrong, and C.F. Curtiss. *Dynamics of Polymeric Fluids*, volume 1. J. Wiley & Sons, 1977.

F.G. Blottner. Investigation of some finite-difference techniques for solving the boundary layer equations. *Computer Methods in Applied Mechanics and Engineering*, 6:1–30, 1975.

S.N. Brown and K. Stewartson. On similarity solutions of the boundary-layer equations with algebraic decay. *J. Fluid Mech.*, 23:673–687, 1965.

W.B. Bush. Hypersonic strong-interaction similarity solutions for flow past a flat plate. *J. Fluid Mech.*, 25:51, 1966.

D. Catherall, K. Stewartson, and P.G. Williams. Viscous flow past a flat plate with uniform injection. *Proc. R. Soc. Lond. A*, 256:370–396, 1965.

J.P. Denier and P.P. Dabrowski. On the boundary-layer equations of power-law fluids. *Proc. R. Soc. Lond A*, 460:3143–3158, 2004.

J.P. Denier and R.E. Hewitt. Asymptotic matching constraints for a boundary-layer flow of a power-law fluid. *J. Fluid Mech.*, 518:261–279, 2004.

M. Guedda and R. Kersner. Asymptotic behaviour of the unbounded solutions to some degenerate boundary layer equations revisited. *Archiv der Mathemtik*, 89:278–288, 2007.

D.R. Hartree. On an equation occurring in falkner and skan's approximate treatment of the equations of the boundary layer. *Proc. Camb. Phil. Soc.*, 33:223, 1937.

D.R. Hartree and J.R. Womersley. A method for the numerical or mechanical solution of certain types of partial differential equations. *Proc. R. Soc. Lond. A*, 101:353–366, 1937.

R.S. Lee and H.K. Cheng. On the outer-edge problem of a hypersonic boundary layer. *J. Fluid Mech.*, 38:161, 1969.

S.Y. Lee and W.F. Ames. Similarity solutions for non-newtonian fluids. *AIChE Jl.*, 12:700–708, 1966.

D.C.F. Leigh. The laminar boundary-layer equation: a method of solution by means of an automatic computer. *Proc. Camb. Phil. Soc.*, 51:320, 1955.

R.C. Lock. Hydrodynamic stability of the flow in the laminar boundary layer between parallel streams. *Proc. Camb. Phil. Soc*, 50:105–124, 1954.

V.V. Mikhailov, V.Ya. Neiland, and V.V. Sychev. The theory of hypersonic viscous flow. *A. Rev. Fluid Mech.*, 3:371, 1971.

M.M. Molla and L.S. Yao. Non-newtonian fluid flow on a flat plate part 2: Heat transfer. *Journal of Thermophysics and Heat Transfer*, 22:762–765, 2008.

M.M. Molla and L.S. Yao. Non-newtonian natural convection along a vertical heated wavy surface using a modified power-law viscosity model. *Journal of Heat Transfer-Transaction of the ASME*, 131, 2009a.

M.M. Molla and L.S. Yao. The flow of non-newtonian fluids on a flat plate with uniform heat flux. *Journal of Heat Transfer-Transaction of the ASME*, 131, 2009b.

M.M. Molla and L.S. Yao. Non-newtonian natural convection along a vertical plate with uniform surface heat fluxes. *Journal of Thermophysics and Heat Transfer*, 23:176–185, 2009c.

A. Nachman and A. Callegari. A nonlinear singular boundary value problem in the theory of pseudoplastic fluids. *SIAM J. Appl. Math.*, 38:275–281, 1980.

A. Nachman and S. Taliaferro. Mass transfer into boundary layers for power law fluids. *Proc. R. Soc. Lond. A*, 365:313–326, 1979.

J.J. Nelson, A.E. Alving, and D.D. Joseph. Boundary layer flow of air over water on a flat plate. *J. Fluid Mech.*, 284:159–169, 1995.

S. Özgen. Stability of parallel non-newtonian flows. *Project Report 1995-22, Von Kármán Institute*, 1995.

S. Özgen, G Degrez, and G.S.R. Sarma. Two-fluid boundary layer stability. *Phys. Fluids*, 10: 2746–2757, 1998.

K.V. Prasad, D. Pal, and P.S. Datti. Mhd power-law fluid flow and heat transfer over a non-isothermal stretching sheet. *Communications in Nonlinear Science and Numerical Simulation*, 14:2178–2189, 2009.

L. Rosenhead, editor. *Laminar Boundary Layers.* Oxford Clarendon Press, 1963.

A.P. Rothmayer, B.D. Matheis, and S.N. Timoshin. Thin liquid films flowing over external aerodynamic surfaces. *J. Engrg Math*, 42:341–357, 2002.

H. Schlichting. *Boundary-Layer Theory.* McGraw-Hill, 7^{th} edition, 1979.

W.R. Schowalter. The application boundary-layer theory to power-law pseudoplastic fluids: similar solutions. *AIChE Jl.*, 6:24–28, 1960.

A.M.O. Smith and D.W. Clutter. Solution of the incompressible laminar boundary-layer equations. *AIAA Journal*, 1:2062–2071, 1963.

R.M. Terrill. Laminar boundary-layer flow near separation with and without suction. *Proc. R. Soc. Lond. A*, 253:55–100, 1960.

E.R. Thompson and W.T. Snyder. Drag reduction of a non-newtonian fluid by fluid injection at the wall. *J. Hydronautics*, 2(4):177–180, 1968.

E.R. Thompson and W.T. Snyder. Laminar boundary-layer flows of newtonian fluids with non-newtonian fluid injectants. *J. Hydronautics*, 4(2):86–91, 1969.

S.N. Timoshin. Instabilities in a high-reynolds-number boundary layer on a film-coated surface. *J. Fluid Mech.*, 353:163–195, 1997.

J. Walker. Serious fun with polyox, silly putty, slime and other non-newtonian fluids. *Scientific American*, 239(5), November 1978.

J. Wu and M.C. Thompson. Non-newtonian shear-thinning flows past a flat plate. *J. Non-Newtonian Fluid Mech.*, 66:127–144, 1996.

L.S. Yao and M.M. Molla. Non-newtonian fluid flow on a flat plate part 1: Boundary layer. *Journal of Thermophysics and Heat Transfer*, 22:758–761, 2008.

A.D. Young. *Boundary Layers.* AIAA, 1989.

J.G. Zhao and R.E. Khayat. Spread of a non-newtonian liquid jet over a horizontal plate. *J. Fluid Mech.*, 613:411–443, 2008.